Curtin Medical School

The role of the microtubule manufacturing chaperone TBCD in neuronal development and brain disorders

Jordan Gareth David Rowlands

0000-0003-1925-3940

This thesis is presented for the Degree of

Doctor of Philosophy

of

Curtin University

March 2021

Thesis Declaration

To the best of my knowledge and belief this thesis contains no material previously published by any other person except where due acknowledgment has been made. This thesis contains no material which has been accepted for the award of any other degree or diploma in any university.

Animal Ethics The research presented and reported in this thesis was conducted in compliance with the National Health and Medical Research Council Australian code for the care and use of animals for scientific purposes 8th edition (2013). The proposed research study received animal ethics approval from the Curtin University Animal Ethics Committee, Approval Number #ARE2017-23

This thesis contains work that has been submitted and that is being prepared for publication.

Signature: …….

Date: ……..

Abstract

Microtubules (MT) are cytoskeletal proteins essential to the ability of cells to adopt their appropriate shape, to undergo cell division, as well as to maintain metabolic homeostasis. Mutations to genes encoding components of the MT cytoskeleton cause neurodevelopmental disorders, collectively referred to as tubulinopathies. Recently, homozygous missense mutations to the tubulin-specific chaperone D (*TBCD)* gene were reported to cause a severe, early-onset neurodegenerative condition in infants, characterised by secondary microcephaly and cortical atrophy, resulting in dystonia, intellectual disability, and seizures. TBCD, alone or in concert with Arl2 and TBCE are part of the molecular machinery required for the generation and destruction of the MT subunits αβ-tubulin, and are thus essential to MT dynamics. However, the functions of TBCD in the development of neurons and their viability within the brain tissue is poorly understood. In this thesis, a molecular model of TBCD and its interacting partners was developed to explore the structural and biophysical basis of the binding of the different β-tubulin isotypes, while both *in vivo* and *in vitro* approaches were undertaken to delineate the molecular mechanism for TBCD in cells of the developing nervous system. TBCD knockdown and rescue experiments demonstrate that perturbations to TBCD expression lead to cell cycle arrest in a cell-autonomous fashion. These changes are accompanied by altered glycolytic respiration, elevated mitochondrial respiration, elevated mitochondrial function, and elevated levels of reactive oxygen species, as well as enhanced expression of neurodifferentiation markers. Neuroanatomical defects were observed using a CRISPR-engineered mouse strain harbouring an A475T “knock-in” allele. Furthermore, due to the observed TBCD induced perturbations to metabolism, cell cycle and cell fate in both the *in vitro* and *in vivo* systems, a therapeutic agent able to alleviate these severe homeostatic imbalances arising from TBCD perturbations was identified. Chronic application of the Type 2 diabetic drug Exendin-4 - an analogue of the hormone glucagon-like peptide-1 (GLP-1) - alleviated cell cycle arrest, promoted metabolic reprogramming and restored the aberrant expression of neuronal differentiation markers caused by TBCD perturbations. Furthermore, utilising a CRISPR-engineered insulin-like growth factor 1 receptor (IGF1R) and insulin receptor (INSR) knockout cell line, it was determined that the cell cycle restoration induced by the GLP-1 analogue was IGF1R, but not INSR, dependent. These data also illustrate a unique role for the increasingly clinically utilised GLP-1 analogues and offer further support for its

usage in neurodegenerative diseases. Taken together, these data suggest that TBCD influences neuronal proliferation, while disease-associated mutations can lead to brain developmental defects. By delineating the molecular mechanisms of TBCD, these findings have enabled a deeper understanding for the role of TBCD in the developing mammalian brain and offer unique and valuable insights through which TBCD gene perturbations mediate neurodegenerative pathologies.

Table of Contents

Table of Contents

Authorship Declarations

I have obtained permission from the copyright owners to use any third-party copyright material reproduced in the thesis, or to use any of my own published work in which the copyright is held by another party.

Rowlands J., Heng J., Newsholme P., Carlessi R. Pleiotropic Effects of GLP-1 analogs on cell signalling, metabolism and function. *Frontiers in Endocrinology*. 2018, 9:672

Location in thesis: Chapter 5

Attribution statement:

	Conception and Design	**Acquisition of Data and Method**	**Data Conditioning and Manipulation**	**Analysis and Statistical method**	**Interpretation and Discussion**	**Final Approval**	**Total % Contribution**
Jordan Rowlands	50	N/A	N/A	N/A	50	25	42
Co Author Acknowledgment: I acknowledge that these represent my contribution to the above research output Signed							
Julian Heng	5	N/A	N/A	N/A	10	25	13
Co Author Acknowledgment: I acknowledge that these represent my contribution to the above research output Signed:							
Philip Newsholme	5	N/A	N/A	N/A	15	25	15
Co Author Acknowledgment: I acknowledge that these represent my contribution to the above research output Signed							
Rodrigo Carlessi	40	N/A	N/A	N/A	25	25	30
Co Author Acknowledgment: I acknowledge that these represent my contribution to the above research output Signed							
Total %	**100**	**100**	**100**	**100**	**100**	**100**	

Rowlands J., Cruzat V., Carlessi R., Newsholme P. Insulin and IGF-1 Receptor autocrine loops are not required for Exendin-4 induced changes to pancreatic β-cell bioenergetics and metabolism in BRIN-BD11 cells. *Peptides*.2018, 100:140–149.

Location in thesis: Appendix

Attribution statement:

	Conception and Design	**Acquisition of Data and Method**	**Data Conditioning and Manipulation**	**Analysis and Statistical method**	**Interpretation and Discussion**	**Final Approval**	**Total % Contribution**
Jordan Rowlands	30	80	40	50	50	25	46
Co Author Acknowledgment: I acknowledge that these represent my contribution to the above research output Signed							
Vinicius Cruzat	0	0	10	10	10	25	9
Co Author Acknowledgment: I acknowledge that these represent my contribution to the above research output Signed:							
Rodrigo Carlessi	40	20	30	30	25	25	28
Co Author Acknowledgment: I acknowledge that these represent my contribution to the above research output Signed							
Philip Newsholme	30	0	20	10	15	25	17
Co Author Acknowledgment: I acknowledge that these represent my contribution to the above research output Signed							
Total %	**100**	**100**	**100**	**100**	**100**	**100**	

Rowlands J*, Walz N*, Rowles JE*, Keane KN, Carlessi R, Newsholme P. Method Protocols for metabolic and functional analysis of the BRIN-BD11 **β**-cell line: a preclinical model for type 2 diabetes. *Pre-Clinical Models*, 2019, 329-340. **co-first*

Location in thesis: Appendix

Attribution statement:

	Conception and Design	**Acquisition of Data and Method**	**Data Conditioning and Manipulation**	**Analysis and Statistical method**	**Interpretation and Discussion**	**Final Approval**	**Total % Contribution**
Jordan Rowlands	15	25	23.3	23.3	20	16.6	20.5
Co Author Acknowledgment: I acknowledge that these represent my contribution to the above research output Signed							
Nikita Walz	15	25	23.3	23.3	20	16.6	20.5
Co Author Acknowledgment: I acknowledge that these represent my contribution to the above research output Signed:							
Joanne Rolwes	15	25	23.3	23.3	20	16.6	20.5
Co Author Acknowledgment: I acknowledge that these represent my contribution to the above research output Signed							
Kevin Keane	10	10	10	10	10	16.6	11.1
Co Author Acknowledgment: I acknowledge that these represent my contribution to the above research output Signed							
Rodrigo Carlessi	20	15	10	10	10	16.6	13.6
Co Author Acknowledgment: I acknowledge that these represent my contribution to the above research output Signed							
Philip Newsholme	25	0	10	10	20	16.6	13.6
Co Author Acknowledgment: I acknowledge that these represent my contribution to the above research output Signed							
Total %	**100**	**100**	**100**	**100**	**100**	**100**	

Acknowledgements

Firstly, I would like to express my sincere gratitude to my supervisors. I am very thankful to Associate Professor Julian Heng for his time, patience and support. Julian, your enthusiasm and belief in me, my ideas and the project have aided my development and I am truly grateful. Thank you also to Professor Philip Newsholme for accepting me into your lab very early in my research career, as well as providing guidance, encouragement and feedback. I am deeply grateful for Doctor Rodrigo Carlessi for his unwavering support, mentorship, friendship and honesty both in and out of the lab, for always finding time for me, and for making me want to strive to be better. I sincerely appreciate Doctor Mark Agostino for his supervision, guidance and patience with molecular modelling. I am very thankful to all of you for the advice, encouragement, support and feedback provided throughout my PhD.

I would also like to extend my appreciation to the past and present members of the Brain Growth & Disease Laboratory and the Laboratory of Diabetes and Metabolism.

Thank you to Mrs Martina Mariano, a fellow PhD student, for your never-ending tolerance, encouragement, and support, for working late nights and early mornings, for the joy you bring and the many coffees. I would also like to thank the former PhD and now Doctor, Isabel Hemming for her wisdom, encouragement and constant support. I am also grateful for the support, cooperation, fun, and constant encouragement provided by Joanne Rowles and Nikita Walz, fellow PhD students who have been with me since the beginning of my research journey. My sincere gratitude also goes to Dr Imran Khan from whom I have learnt many things and been incredibly supportive, passionate and kind.

I would also like to thank the following institutes Curtin Health Innovation Research Institute, Sarich Neuroscience Institute, and the Harry Perkins Institute of Medical Research, as well as the plethora of people at each, including: Dr Carl Mousley, Dr Danielle Dye, Professor Elizabeth Watkin, Dr Kevin Keane, Dr Rob Steuart, Dr Virginie Lam, Dr Gae Ellison, Dr Ross Graham, , Dr Christian Tjiam, Mrs Jeanne Edmands, Mr Riley Murphy, Mr Ratish Permala, Mr Sam Siem, Mrs Winny Pun, Mr Mark Beonowski, Ms Lamprini Baklous, Ms Aleesha Davis, Ms Amy Black, Mrs Zalitha Pieterse-Mulley, Ms Jessia Murray, Mr Thiru Sabapathy, Ms May Majimbi, Mr Terence McGonigle, Ms Lilian Toomey, Ms Aleksandra Gotz, Dr Oliver Clément,

Mr Aaron Muscat, Ms Hayley Cullen, Ms Gwen Pfleger, and Mr Sam Siem. The encouragement, support and passion provided by each and every person is immeasurable and has helped me complete this thesis.

Although it is impossible to list everyone who has made this thesis possible, my sincere gratitude also goes to Mr Jack Kent, Mr Kofi Stevens, Ms Sarah Chee, Ms Nishra Varsani, Mr Ben Bartlett, Mr Sean Anderson and Ms Shana Nichols without whom I would not be where I am today. I am also grateful for the love and support of Bridget, Lucy, Alex, Sox and Billy Visser, whose faith in me has been unwavering. Thank you as well to my friends who have been tolerant beyond belief and encouraging every step of the way, including; Mr Hayden Collet, Mr Adrian Coles, Mr Arzhang Sharafi, Mr Sasha Khlon, Ms Nicole Chudy, Mr Jason Hugh, Mr Matthe Cheeseman, Mr Avren Paul, Ms Stephanie Allen, Mr Adam Wong, Mr Robert Harvey, Mr Jared Nair, Mr Bryan McgGann, Mr Rory Franks, and Mr Nick Fimognari. Each of you has enabled me to complete this journey and I wish to express my deepest thanks for taking it with me.

The research described in this thesis was supported by an Australian Government Research Training Program (RTP) Scholarship and a Curtin Research Stipend Top Up Scholarship (CRS) for which I am very grateful.

Lastly, I am forever indebted to my parents and my siblings for providing the opportunities and experiences, as well as the skills to undertake this task. The unwavering love, help, patience and support, you have provided has made me who I am today. Thank you.

List of Abbreviations

γ-TuRC	γ-tubulin ring complex
AC	Adenyl Cyclase
APC/C	Anaphase-promoting complex/cyclosome
aRGs	Apical radial glia cells
Arl2	ADP ribosylation factor-like protein 2
BP	Basal progenitors
cAMP	Cyclic adenosine monophosphate
CCT	cytosolic group II chaperonin containing TCP-1
Cdks	Cyclin dependent kinases
CoxIV	Mitochondrial cytochrome c oxidase subunit IV
CP	Cortical plate
CRISPR	Clustered regularly-interspaced short palindromic repeat
Ctip2	COUP-TF-interacting protein (also known as Bcl11b)
DHE	Dihydroethidium
DMSO	Dimethyl sulfoxide
ETC	Electron transport chain
Drp1	Dynamin related protein 1
ECAR	Extracellular acidification rate
EPAC	Exchange protein directly activated by cAMP
E14.5	Embryonic day 14.5
E17.5	Embryonic day 17.5
FCCP	Carbonyl cyanide-4-(trifluoromethoxy)phenylhydrazone

FoxG1	Forkhead box G1
GAP	GTPase activating protein
GTP	Guanosine triphosphate
gRNA	guide RNA
GSK3b	Glycogen synthase kinase 3b
GLP-1	Glucagon-like peptide-1
GLP-1R	Glucagon-like peptide-1 receptor
G0	Gap 0 phase
G1	Gap phase 1
G2	Gap phase 2
HEAT	Huntingtin, elongation factor 3, PR65/A, TOR
hESC	Human embryonic stem cells
Het	Heterozygous
hESCs	Human embryonic stem cells
Hif-1α	Hypoxia-inducible factor 1-α
HK	Hexokinase
Hom	Homozygous
HRP	Horseradish peroxidase
INM	Interkinetic nuclear migration
IPs	Intermediate progenitor cells
iPSCs	Induced pluripotent stem cells
IZ	Intermediate zone
KD	Knock-down

KO	Knock-out
MAPs	Microtubule-associated proteins
MCDs	Malformations of cortical development
MD	Molecular dynamics
MM-GB(PB)/SA	Molecular mechanics-generalised Born (Poisson Boltzmann)/surface area
MTOCs	Microtubule organising centres
MT	Microtubule
mtROS	Mitochondrial superoxide
MZ	Marginal zone
NECs	Neuronal epithelial cells
NeuN	Neuronal Nuclei
NGS	Normal goat serum
NPCs	Neuronal progenitor cells
NRF1	Nuclear transcription factor 1
NSCs	Neuronal stem cells
OCR	Oxygen consumption rate
OCT	Optimal cutting temperature compound
OPA1	Optic atrophy gene 1
OXPHOS	Oxidative phosphorylation
Pax6	Paired-box 6 factors
PBS	Phosphate-buffered saline
PER	Proton efflux rate
PI3K	Phosphatidylinositol 3-Kinase

PFA	Paraformaldehyde
PFD	Prefoldin
PKA	Protein Kinase A
PKM1	Pyruvate kinase M-type 1
PKM2	Pyruvate kinase M-type 2
PP	Preplate
PTMs	Post-translational modifications
Rb	Retinoblastoma tumour suppressor protein
RGCs	Radial glial cells
ROS	Reactive oxygen species
shRNA	Short hairpin RNA
SDHA	Succinate dehydrogenase complex, subunit A
Sox2-	SRY (Sex determining region Y)- box 2
SP	Subplate
S phase	Synthesis phases
SVZ	Subventricular zone
TBCA	Tubulin binding chaperone A
TBCB	Tubulin binding chaperone B
TBCC	Tubulin binding chaperone C
TBCCD1	Tubulin binding chaperone C-domain containing 1
TBCD	Tubulin binding chaperone D
TBCE	Tubulin binding chaperone E
TBCs	Tubulin binding chaperones

Tbr1	T-box brain protein 1
Tbr2	T-box brain protein 2
TBS	Tris-buffered saline
T2D	Type 2 diabetes mellitus
+TIP	MT plus-end targeting proteins
UPR	Unfolded protein response
VDAC	Voltage-dependent anion channel protein
VZ	Ventricular zone
WT	Wildtype

Chapter 1 Literature Review

1.1 Background

The complex architectural arrangement of neurons in the nervous system is a result of a meticulously regulated process which is essential for the establishment of sophisticated neurocircuitry required for cognitive functioning. Brain development requires coordinated, spatiotemporal neural stem cell (NSC) proliferation, migration and terminal differentiation [5, 6]. These prerequisites for neuronal development are facilitated by the highly dynamic neuronal cytoskeleton [7-9]. The cytoarchitecture of neurons is achieved through the organisation, assembly and remodelling of the cytoskeleton proteins actin and microtubules (MTs), each playing crucial roles in neuronal development and maturation [10]. Both MTs and actin are involved in the formation of projections from the cell body, termed neurites, extension and branching of axons and dendrites, and facilitate postsynaptic receptor mobility and anchoring [11, 12]. Furthermore, these cytoskeletal elements are essential in a number of other cellular functions such as proliferation, migration, cell morphology, polarity, and intracellular trafficking [1, 13, 14]. It is therefore not surprising that defects in the cytoskeleton of developing neurons lead to a plethora of debilitating neurodevelopmental disorders and nervous system abnormalities [7, 8, 15]. Owing to their immense importance in neuronal development and disease, mechanisms which govern cytoskeleton dynamics are widely studied. This chapter will focus on the molecular dynamics of MTs assembly and reorganisation in relation to mammalian brain development.

MTs are hollow cylinders approximately 25 nm in diameter, and are composed of repeating α/β polypeptide subunits orientated in a head-to-tail fashion that laterally interact to form polar protofilaments (**Fig. 1.1**) [16, 17]. MTs are considered highly dynamic, as they constantly switch between phases of either growth (polymerisation) or shrinkage (depolymerisation) in a guanosine triphosphate (GTP) dependent manner [13, 18, 19]. This growth and shrinkage can occur at either the positive (+) end, where β-tubulin is exposed, or negative (-) end, where α-tubulin is exposed, of the MT. However, both catastrophe and rescue (depolymerisation and polymerisation respectively) occurs more often and rapidly at MT+ ends, as the negative ends are often anchored at the MT nucleation site [20-23]. Although the exact mechanisms underlying the stochastic nature of MTs remains unclear, it is this dynamic instability of MTs

that allows them to mediate a wide-range of cellular functions[24, 25]. For example, during mitosis, MTs segregate chromosomes, position divisional planes and facilitate abscission [26-28]. In post mitotic cells such as neurons, MTs are involved in synchronized changes in cell shape, axonal growth, dendritic spine morphology, synaptic plasticity and the transport of organelles and intracellular cargo [1, 23, 29-34]. The dynamic instability of MTs is regulated by various factors, including microtubule associated proteins (MAPs) and their upstream signalling events, mechanical forces, tubulin isotype presence, and the abundance of energy molecules, that all together lead to a precise orchestration of MTs polymerization and depolymerisation (reviewed in [35-40]).

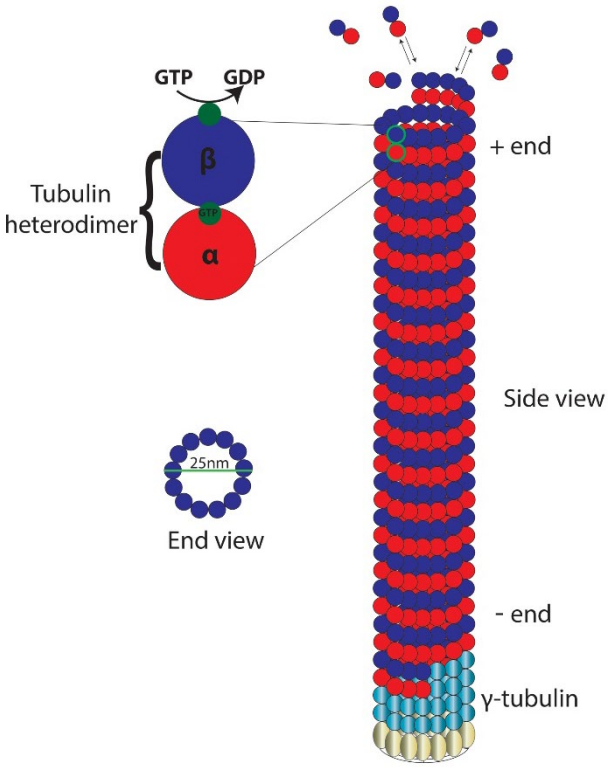

Figure 1.1. The microtubule lattice

The hollow microtubule cylinder, approximately 25 nm in diameter, composed of repeating α/β-tubulin heterodimers that laterally interact to form 13 polar protofilaments on a γ-tubulin ring complex. In order to be incorporated into the growing microtubule lattice the α/β-tubulin heterodimers must undergo hydrolysis of the β-tubulin bound GTP (adapted from [1])

The polymerisation and depolymerisation of MTs requires a multi-component molecular machine essential for the generation and destruction of the α/β tubulin subunits (**Fig. 1.2**). Nascent α and β tubulin polypeptides are stabilized and transferred by the hetero-hexametric chaperonin prefoldin (PFD), from the ribosome, directly to the cytosolic group II chaperonin CCT (chaperonin containing TCP-1 (CCT)) [1, 41-43]. The α- and β-tubulin subunits are bound and enclosed in the centre of CCT, then multiple rounds of ATP binding induce conformational changes in CCT, initiating the folding of the tubulin structure towards its native conformation [44-48]. Adoption of a quasi-native state enables the α and β-tubulin intermediates to be released from CCT to interact with the tubulin-specific chaperones A-E (also known as tubulin binding chaperones-TBCA, TBCB, TBCC, TBCD and TBCE). It should be noted that both α and β-tubulin are GTP-binding proteins, however α-tubulin does not exchange GTP, whilst β-tubulin does exchange GTP

which is utilised for both heterodimer formation and incorporation into the MT lattice [49-51]. Following the standard "linear model" of tubulin folding originally proposed by Tian, Huang et al. [52] (**Fig. 1.2**), α and β-tubulin are bound by TBCB and TBCA, which then transfer the tubulin subunits to TBCE and TBCD respectively. TBCD and TBCE, bound with their tubulin subunits, then interact with TBCC, which hydrolyses the β-tubulin GTP enabling the formation and release of the αβ-tubulin heterodimer. Additionally, TBCD and TBCE can dissociate the heterodimer back into monomers [4, 42, 45, 52-54].

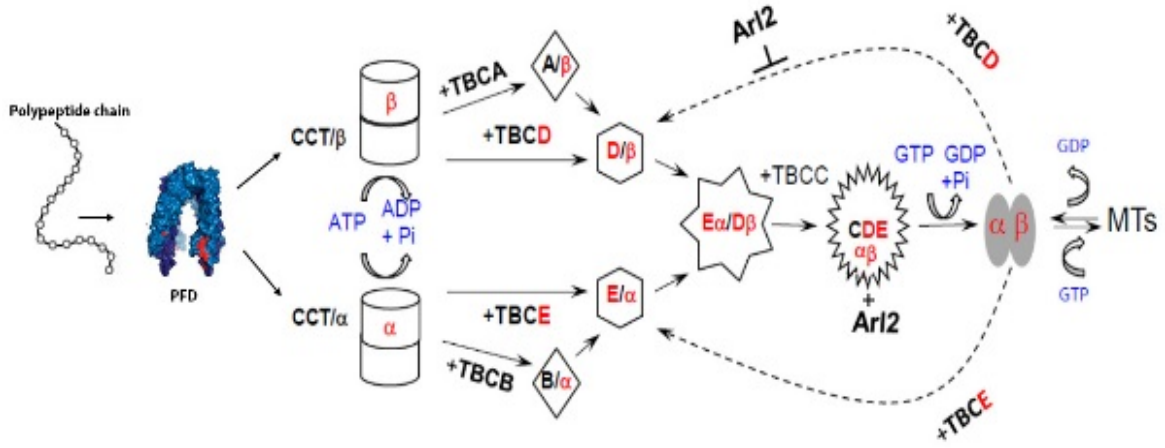

Figure 1.1. Microtubule synthesis pathway.

α and β-tubulin peptide monomers (A) are bound by prefoldin (PFD) (B), and transferred to chaperonin containing TCP-1 (CCT). Once bound by CCT, ATP driven conformational changes in CCT alter the tubulin monomer to a partially folded state (D). The now quasi-native α and β-tubulins are bound by TBCE/TBCB and TBCA/TBCD respectively (E). Both tubulins are eventually transferred to the TBCD-Arl2-TBCE superstructure (F). Tubulin binding to the superstructure induces conformational changes that enable TBCC to attach and stimulate the hydrolysis of GTP to GDP, catalysing the formation of the α/β-tubulin heterodimer and trigger its release (G). The released tubulin heterodimer undergoes an additional round of GTP hydrolysis to enable its incorporation into the MT lattice (H). Depolymerisation of the MT releases the tubulin heterodimers which are then bound and dissociated by TBCE/TBCB (I) and TBCD lacking ADP ribosylation factor-like protein 2 (Arl2) (J) (adapted from[4]).

Given the importance of the MTs to neural cell functions during development, such as proliferation, migration, and differentiation, it is perhaps unsurprising that mutations in genes that encode polypeptide products essential to its biosynthesis cause neurodevelopmental and central nervous system (CNS) abnormalities [55-60]. For example, recent studies have described mutations in the gene encoding the TBCD protein, to be responsible for severe infantile neurodegenerative pathologies including microcephaly, dystonia and cortical atrophy resulting in intellectual disability and seizures [4, 61-64]. In these studies, mutations

to the coding sequence of TBCD have been reported to perturb TBCD's critical role in polymerization and depolymerisation of MTs, consequently impacting neuronal function and development [4, 61-64]. Yet, the impact of missense variation on the molecular interactions between TBCD and MTs remains unknown. Therefore, by conducting a study of clinically relevant, disease associated TBCD missense mutations in cell and animal models it can improve our understanding of such molecular interactions.

1.2 Tubulin

Tubulins are characteristic key constituents of the cytoskeleton that support a diverse range of cellular processes, including cytoskeletal mediated chemotaxis, endo- and exocytosis, cell integrity, polarity, movement, organelle anchoring, and transport. [65]. Tubulins are globular protein monomers of ~50 kDa that polymerise to form protofilaments, 13 of which interact laterally to form the ~25 nm hollow MT cylinder [1, 13, 66]. In vertebrates, multiple genes encode the highly conserved tubulin polypeptide amino acid sequences. For example, humans possess 8 isotypes of α-tubulin, 9 β-tubulin, and 2 γ-tubulins with distinct isotype spatio-temporal expression pattern during development. Mice, however, possess 7 α, 8 β and 2 γ –tubulins [65, 67-69]. In the mammalian brain, the expression of the β-tubulin isotypes TUBB, TUBB2A, TUBB2B, TUBB3, TUBB4A and TUBB4B, and the α- tubulin isotypes TUBA1A, TUBA1B, TUBA1C, TUBA4A, TUBA4A, and TUBA8 have so far been identified [69-71]. This is important as various isotypes of tubulin can be incorporated into the growing MT lattice and contribute to the dynamic nature of MTs [36, 72, 73]. The ability of α and β-tubulin monomers to incorporate into the MT protofilaments, contribute to MT dynamics, and be dissociated relies upon their three different functional regions. Notably, the N-terminal region (residues 1-205) is responsible for nucleotide binding, and in the case of β-tubulin, hydrolysis of GTP for both dimer formation and MT incorporation [74, 75]. The intermediate region (residues 206-381) facilitates MT assembly via stabilisation of lateral protofilament interactions. Whilst the acidic and less conserved C-terminal region (382-440) facilitates the formation of tubulin dimers and involvement and interaction of MAPs with the MT [74, 75]. The total amount of available tubulin in the cell can further modulate MT dynamics and is mediated by tubulin biosynthesis and protein stability. The synthesis of tubulin, is modulated by the amount of nascent cellular tubulin in a negative feedback loop. Excessive tubulin monomers that are not bound by chaperones bind and destabilise tubulin mRNA - ribosome interactions, thereby

reducing tubulin production. This has been termed tubulin autoregulation [76-78]. Additional to monomer stabilisation, molecular chaperones are mediators of tubulin quality control, and ensure attainment of the correct quaternary assembly to facilitate heterodimer protofilament formation and MT assembly. Disruption of this intricate MT assembly process though mutations in tubulin proteins or chaperones leads to impairments in cell shape transitions that underlie division, migration and neuronal differentiation, leading to neurodevelopmental disorders collectively referred to as tubulinopathies [23, 53].

1.3 Mammalian neuronal development

The mammalian brain is derived from neural epithelial cells (NECs) that line the neural tube, the first well-defined neural structure. While the NECs in the most rostral region of the neural tube will give rise to the brain, the hindbrain and spinal cord arise from more caudally positioned cells [6, 79]. The formation of the neural tube, termed neurulation, is initiated as a result of epiblast cells migrating through the primitive streak of the embryo, followed by differentiation into the neuroectoderm [6, 79]. As development proceeds, the neuroectoderm extends its length whilst narrowing its width, transforming into the neural plate. The neural plate, then, invaginates anteriorly to give rise to the neural groove, which is flanked by neural folds [6, 79-81]. Finally, the neural folds fuse together in a zipper-like fashion caudally and cranially, with closure beginning near the hind brain's junction with the spinal cord, forming the neural tube, which will eventually give rise to the ventricular system of the brain (**Fig. 1.3**) [6, 82-84].

NECs lining the neural tube walls, contact both the basal (pial) and apical (ventricular) surfaces with their processes (cell body extensions), and undergo multiple rounds of symmetric division, at the ventricular surfaces, to form the proliferative region known as the ventricular zone (VZ), prior to the onset of neurogenesis [79, 85-87]. During each cell cycle, NECs move their nuclei between the apical and basal surfaces in a cell cycle-dependent manner, termed interkinetic nuclear migration (INM). This process utilises the cytoskeletal proteins, MTs and actin, to transport the nuclei of NECs from the apical-to-basal surface during (G1), and from the basal-to-apical surface during Synthesis phase (S-phase) and Gap phase 2 (G2), with mitosis taking place at the apical/ventricular surface (**Fig. 1.4A**) [87-89].

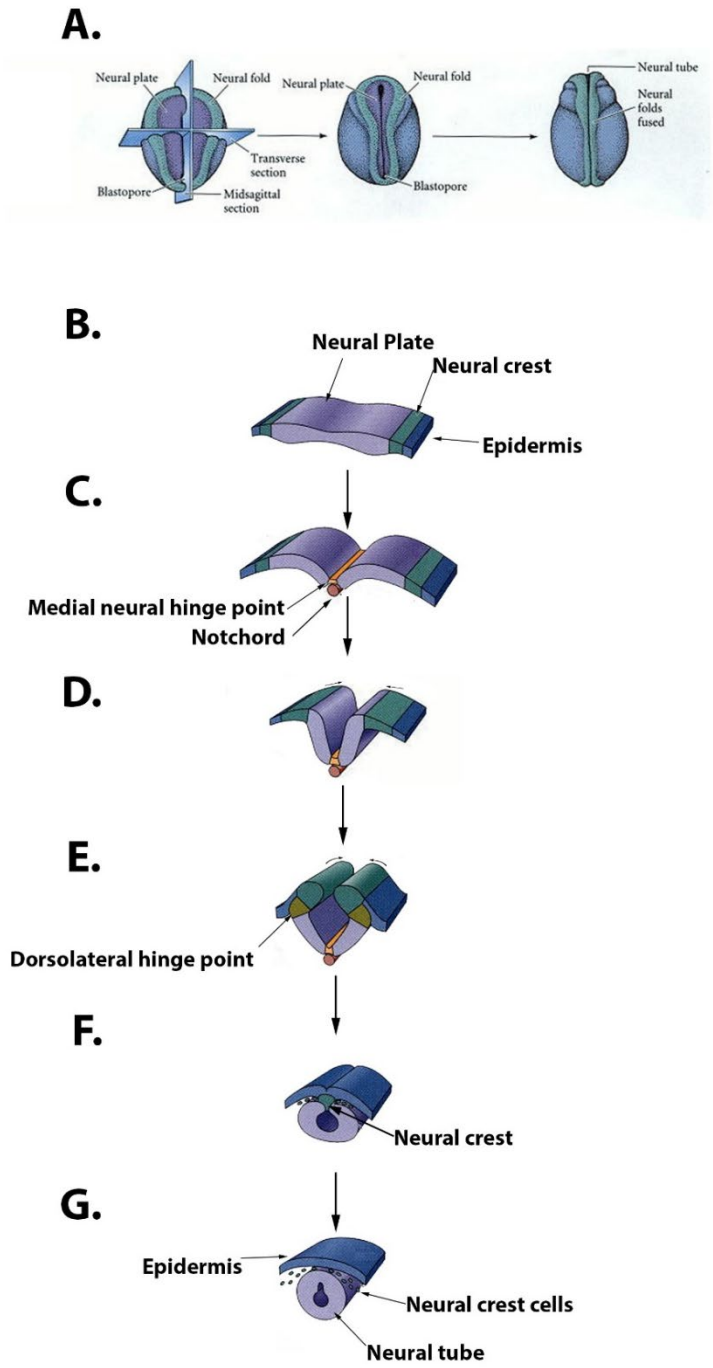

Figure 1.2 Neural tube formation.

(A) Early (left), middle (centre), and late (right) neurulation. (B) Dorsal region of ectoderm shows distinguishable neural plate cells. (C-E) Using medial neural hinge point cells anchored to the notchord, the neural plate then invaginates anteriorly to give rise to the neural groove, which is flanked by neural folds. (F and G) Neural folds fuse together in a zipper-like fashion caudally and cranially forming the neural tube. Neural crest cells initially linking the neural tube to epidermis prior to dispersion and separation of neural tube from epidermis (adapted from [2])

At the onset of neurogenesis, NECs in the VZ progressively adopt asymmetric modes of cell division over symmetric divisions. Asymmetrically dividing cells result in the daughter cells becoming one of the following, an NEC, an apical radial glial cell (aRG) (a highly related but distinct neural progenitor cell (NPC) type), a basal progenitor or a postmitotic neuron (**Fig. 1.4B**) [6, 79, 90]. It should be noted that the terms NPC and NSC are used interchangeably as they both describe the precursor cells that give rise to the various neuronal and glial cell types which will eventually populate CNS [79, 91, 92]. The classification for which type of progenitor cell arises from asymmetric NPC division is an ever expanding field of knowledge that is beyond the scope of this work and is reviewed in detail elsewhere [79, 87, 88]. A simple classification by Taverna et al (2014) however, utilises the following criteria to separate the NPCs progeny: location of mitosis, extent of cell polarity and the cells proliferative capacity. The full and diverse range of molecular mechanisms influencing the

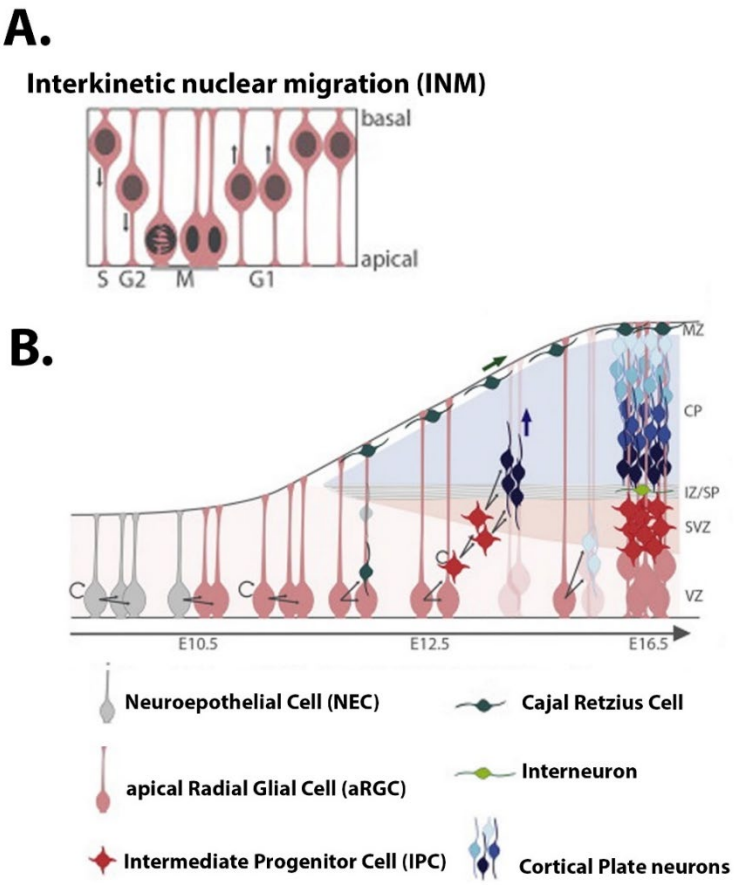

Figure 1.3. Neural progenitor cell subtypes during cortical development.

(A) Interkinetic nuclear migration (INM), in neuronal progenitor/epithelial cells (NPC/NECs) migrating between apical and basal in the ventricular zone (VZ) in a cell cycle dependent manner. (B) Schematic representation of NEC prolliferation, subsequent neurogenesis, differentiation and migration out of the VZ, forming the subventricular zone (SVZ), intermediate zone (IZ), subplate (SP), cortical plate (CP) and marginal zone (MZ) that will later become layers I-VI respectively (adapated from [3]).

onset of neurogenesis are vast and are yet to be fully elucidated, and thus are only touched upon in this work (reviewed in [90, 93-96]). Factors that are currently believed to influence the onset of neurogenesis, the switch to asymmetric cell division, fate acquisition and consequently terminal cell cycle exit include: cell cycle length/phases, cyclins/cyclin dependent kinases and other cell cycle regulators (sex determining region Y- box 2 (Sox2) [97-103], Geminin, retinoblastoma protein (Rb)), intracellular genetic signals (transcription factors, NeuroD), extracellular signals (Paired Box 6 (Pax6) [104, 105], Empty Spiracles Homeobox 2 (Emx2), Wnt, Notch) , reactive oxygen species (ROS) abundance [95, 96], and metabolic state [106-109].

As development progresses most NPCs migrate away from the proliferative region of the VZ to establish the neocortex [82, 110-114]. Integral to information and higher order processing the neocortex, also known as the cerebral cortex, is comprised of six histologically distinct layers (I-VI), formed in an inside-out pattern (discussed below) [79, 87, 88]. During the early stages of brain development, the earliest born neurons only traverse a relatively small distance from the germinal zone using a mode of migration referred to as somal translocation [114]. However, as the embryonic brain increases in size and volume, later born neurons rely on alternate methods of migration to position themselves within the developing cortex. Once

positioned in their appropriate cortical layer, the soon to be adult neuron undergoes morphological and physiological adaptations leading to the formation of axons and dendrites [115, 116]. Typically long and thin, axons conduct electrical signals from the cell body towards the distal axon terminals, stimulating the release of neurotransmitters from synaptic vesicles. Dendrites, however, are relatively short and branched projections emanating from the cell body, with small protruding membranous organelles (dendritic spines), containing neurotransmitter receptors, and the signalling systems essential for synaptic plasticity and function (reviewed in [1, 6, 79, 82, 117-119]). Coupling the importance of the cerebral cortex in information processing, feelings, sensations and actions with the observed cortical atrophy and associated neurodegenerative pathologies in patients harbouring TBCD mutations, the next section will describe development of cerebral cortex only to keep it in context of this dissertation [4, 6, 118].

Sitting atop the midbrain, brain stem, and pons, the cerebral cortex is the outermost layer of the cerebrum. One of the major information processing networks, the neocortex is responsible for higher order functions in mammals, notably marine mammals and great apes [120]. Comprised of specialised neurons, the neocortex is organised into six histologically distinct layers (I-VI), with each layer exhibiting unique afferent and efferent connections [121]. These layers form in an inside-out pattern, with the earliest migrating neurons forming the deepest layers of the cortex, layers V and VI, and later born neurons migrating past and forming more superficial layers [6, 82]. It should be noted that laminar identity and consequently axonal connectivity and function are intimately linked with neuronal birthdate [122-124]. One exception to the inside-out formation is the generation of the preplate by the first neurons to leave the proliferative zone, including Cajal-Rezius cells (transient cells that secrete reelin so as to instruct radial migration) (**Fig. 1.4B**) [125]. Following the completion of the preplate, the next wave of neurons to migrate will cause the preplate to split into two distinct regions termed the marginal zone (MZ) and subplate (SP) by generating a new region between them termed the cortical plate (CP). Neurons arriving in the CP are the cells that will form cortical layer VI, with subsequent migrating neurons forming the more superficial layers [6, 82]. Each neuronal layer contains neurons that share similar identities and connectivity patterns, with upper layer neurons (II-IV) tending to establish cortico-cortical connections that are contralateral or ipsilateral, whilst deep layer neurons (V and VI) connect

preferentially with subcortical structures [79]. Cortical neurons display striking diversity in their morphology, physiology and molecular phenotypes, which makes their systematic classification a challenging task [126]. Due to these terminological differences, neurons have been classified in a variety of ways, including; common morphological features; axonal projections, molecular identities, and cortical layer [126]. Therefore, in this work we will broadly categorise cortical neurons by their morphology and neurotransmitter properties into two main classes the GABAergic interneurons and excitatory/projection neurons. GABAergic interneurons (~20% of cortical neurons), only establish local connections as their axons do not extend into the white matter [121, 127]. Excitatory/projection neurons on the other hand, establish both short- and long-range connections by extending axons to subcortical and intercortical targets, and tend to possess a pyramidal morphology [128-131]. Both interneurons and projection neurons reside in most cortical layers and establish various and unique connections [117, 132].

In order to obtain their laminar fate however, NPCs must first migrate from the VZ up through the developing cortical layers of the cortex, respond to signalling molecules, such as Reelin, Netrins and Semaphorins, to reach their spatial cortical destination and finally establish the required neuronal circuitry [82, 133-135]. This migration can occur either radially, where neurons migrate perpendicularly to the ventral surface alongside radial glial fibres, or tangentially where neurons move parallel to the ventricular surface. Although it should be noted that tangentially migrating neurons may switch to radial migration to achieve their final laminar position [133, 136-138]. Once NPCs have reached their proper spatiotemporal position by following a variety of extracellular directional cues, they undergo terminal differentiation, forming synaptic connections via axons and dendrites, creating neural circuity and establishing neurotransmitter signalling pathways for information processing [139, 140].

1.3.1 Neuronal cytoskeleton

The characteristic proliferation, migration and differentiation of NPCs is contingent upon its highly dynamic cytoskeletal system. The cytoskeleton of neural cells represents an essential structural framework that underpins cellular integrity, cell division, organization and organelle transport. The cytoskeleton of cells is composed of three essential filaments, microtubules (MTs), actin and intermediate filaments, which differ in size, subunit composition and their specific function [13, 141-144]. Actin, the smallest filament, and MTs,

the largest filaments, are polymeric structures composed of actin and α/β tubulin, respectively. Actin and MT filament growth requires ATP and GTP, respectively, and utilises monomeric substrates presented by protein chaperones [12, 34, 145, 146]. In the developing brain, the complex yet dynamic architecture of the neuronal cytoskeleton is achieved through the organisation, assembly, disassembly and coordinated remodelling of both the actin and MTs cytoskeleton [10]. The functional contribution of both types of cytoskeleton proteins to cell physiology is significant and overlapping, with specific features documented in different cell types [11, 13, 34]. During prenatal brain growth, the regulation of cytoskeletal dynamics is essential to mediate proliferation, migration, and differentiation of NPCs. As they generate postmitotic neurons, disturbances of the cytoskeletal machinery can lead to cortical malformations [6, 8, 147, 148]. Both actin and MTs are integral to the physiology of all cells, however the primary focus of this thesis is to investigate the role of the neuronal MT cytoskeleton in neuronal proliferation, migration and differentiation during prenatal brain development. Thus, the following sections describe MT functions in neural cells during mammalian development.

1.3.2 Neural stem cell proliferation and MT dynamics

During embryonic development of the neocortex, neural progenitor cells (NPCs) undergo exponential symmetric cell divisions, with each mitotic division expanding the pool of available NPCs, and thus leading to expansion of both the lateral and the radial brain axes [6, 79]. Symmetric cell division leads to identical daughter cells that equally inherit the organelles of the mother cell, and requires both daughter cells inheriting the apical and basal epithelial structure/processes. Asymmetric NPC division however, is believed to initiate cortical neurogenesis and results in the production of a NPC, and either an intermediate progenitor/basal progenitor (IP/BP) or neuron [81, 86, 149]. It is believed that the daughter cell that inherits the entire apical epithelial structure becomes an NPC, whilst the daughter cell that segregates with the basal process becomes an IP or neuron (**Fig. 1.4**) [79, 134]. A critical molecular determinant of whether the cell divides symmetrically or asymmetrically is the plane of cell division. The plane of cell division is believed to be dictated by the central spindle, as well as astral MTs, which arise during mitosis [150-152].

Mitosis can be separated into 4 consecutive phases: prophase, metaphase, anaphase and telophase. Prophase is characterised by the condensation of chromatin, nuclear envelope

breakdown and the formation of the mitotic spindle. In metaphase, the spindle microtubules line the chromatids up at the cells equatorial plane; and is followed by anaphase, which is when centromeres divide, chromatids separate and move towards opposite poles [153, 154]. During telophase chromosomes reach opposite poles and decondense into chromatin, the central spindle microtubules dissociate from centrosomes, and the nuclear envelopes reform [153, 154]. Following telophase, cytokinesis, which begins immediately after the segregation of chromosomes in anaphase, is completed with the physical detachment of the two daughter cells [27, 155, 156]. In brief, the regulated control of division by MTs begins with the depolymerisation of interphase MTs, thereby providing tubulin subunits for mitotic MTs and enabling cellular reorganisation. Concomitantly, the centrosomes separate and each centriole is translocated to an opposite pole to facilitate MTs nucleation at the centrosomal microtubule organising centres (MTOC) [150, 157]. In addition to centrioles, a variety of non-centrosome MTOC are also involved in MT nucleation during cell division including, spindle microtubules, in the vicinity of chromatin, and kinetochores [157-161]. As mitosis progresses, the chromosomes are seen to align on the metaphase plate, and are connected to the mitotic spindle. The mitotic spindle is considered a supramolecular structure comprised of the components responsible for chromosomal segregation including kinetochore MTs, interpolar MTs, and astral MTs. Spindle orientation is essential in cell fate decisions as its orientation determines the axis of cell division and thus the symmetric or asymmetric division of the cell [151, 162-164]. Notably, TBCD is required for the organisation of the mitotic spindle, as well as spindle MT dynamics [28, 165]. In metaphase, the kinetochore MTs attach to the chromosomal kinetochores and are orientated via a specific subset of astral MTs that connect to the cell cortex (also called the actin cortex which is a specialised layer of cytoplasmic protein located at the inner leaflet of cell membrane)) [152]. Astral MTs bound at the cell cortex facilitate spindle orientation through interactions with the MAP dynein. Dynein is a MT- end directed motor protein, which is recruited to MTs via the heterotrimeric Gα, LGN and NuMA protein complex. Dynein promotes orientation by exerting pulling forces on the astral MTs [166]. In addition, actin facilitates MT orientation and separation, and has been described earlier [148]. Perturbations to astral MTs (such as altered MT dynamics and stability), and or spindle morphology (such as short spindles), can impact spindle orientation and consequently cell fate [85, 86, 167]. Once the mitotic spindle is oriented, the cell progresses from metaphase into anaphase, and is accompanied by poleward movement of

the chromatids, and the formation of the central spindle [27]. The central spindle is a bundled array of antiparallel MTs with interdigitating plus ends, which arises at the region between the two poles of the dividing cell called the midzone. The central spindle is believed to facilitate the positioning of the actomyosin -based contractile ring, a transient structure composed of filamentous actin and the motor protein myosin-2, which forms under the plasma membrane and constricts to create a cleavage furrow [26, 27, 167-172]. Cell division progression from late anaphase into telophase is marked by cleavage furrow ingression, which in turn stimulates the central spindle to condense into the structure known as the "midbody". From here on proteins associated with vesicular transport are concentrated at the midbody, which is followed by abscission and completion of cytokinesis [27, 173-175]. Depending on the plane of division, the completion of cytokinesis may result, as previously mentioned, in either two daughter cells, or one NPC and one IP/BP or neuron. Completion of mitosis is followed by interphase, which can in turn be subdivided into three different stages: G1, when the synthesis of proteins responsible for DNA replication takes place; S-phase, when replication of nuclear DNA is undertaken; and G2, wherein the proteins that are responsible for cell division are synthesised. Finally, cells can also be observed in Gap 0 phase (G0), a stage that occurs when cells have withdrawn from cell cycle, and is seen in most cells that have differentiated, such as neurons [27, 155, 156]. Cells who undergo terminal differentiation will migrate out of the VZ towards their prospective position in the neocortex [82].

1.3.2.1 Metabolism

Each stage of mitosis is an energy intensive process that requires substantial amounts of energy for DNA replication, organelle synthesis, and remodelling of the cytoskeletal network. Recently, studies have begun to recognise and investigate the role of metabolism in neurogenesis. Emerging evidence from these studies highlights that the metabolic pathways and metabolic states of NSC/NPCs can impact their decision to proliferate, become quiescent or begin differentiation [80, 108, 176-178]. It is therefore crucial to understand the interplay between mitochondrial dynamics (the coordinated cycles of fission and fusion), metabolism, cell cycle and MTs [reviewed in [106, 179-183]] and is outlined below.

Mitochondrial fission is the separation of a single mitochondrion into two or more daughter organelles. Whilst fusion is the formation of a single mitochondrion from previously independent and discrete structures [184-187]. Fission is essential for cellular proliferation as

mitochondria cannot be formed *de novo.* Fission is mediated in part by dynamin-like gene and fission 1 homolog protein (hFis1)/dynamin related protein 1 (Drp1) [188]. Mitochondrial fusion is able to rescue mitochondria from environmental damages and genetic mutation by mixing the contents of damaged mitochondria and is dependent on the pro-fusion proteins located in the outer mitochondrial membrane called mitofusins (Mfns), and the pro-fusion protein located in the inner mitochondrial membrane OPA1 (optic atrophy gene 1) [103, 186, 187]. Mitochondrial fusion and fission rates alter in response to metabolic demands, with an increase in fusion when mitochondria are forced to rely on oxidate phosphorylation (OXPHOS), and inhibition of fission during starvation [179, 181, 189, 190]. However, mitochondrial motility and dynamics are reliant upon an organised cytoskeleton, with mitochondria primarily traveling on MTs via the activity of motor proteins kinesin and dynein [reviewed in [103, 187]].

This is evident throughout the cell cycle, with mitochondria initially possessing a variety of morphologies in G1. At the G1-S transition however, mitochondria move along the MT cytoskeleton undergoing both fission and fusion events, to form a hyper fused giant tubular network [191, 192]. This fused network enables the mitochondria to stimulate OXPHOS in order to meet the metabolic requirements of the dividing cell and drive cell cycle progression [179, 183, 193]. Progression through S phase and towards G2 is marked by an increase in Drp1 and consequently mitochondrial fragmentation (fission) [172, 181, 182, 186, 194-198]. Of note, is that mitochondrial morphology and metabolic activity during the G1-S and G2/M phases can regulate and be regulated by cyclins and cyclin-dependent kinases (Cdks) [177, 183, 192, 199-201] (detailed below). This regulation is believed to enable OXPHOS to remain active even when mitochondria are fragmented [106, 192]. Mitochondrial fission throughout G2 and M phases enables the formation of multiple individual organelles spaced throughout the cell which, through their interactions with the MT network, are localised to the cleavage furrow where they have been proposed to aid in accurate mitochondrial inheritance and/or facilitate cytokinesis [103, 195]. Intriguingly, a recent study reported that in stem-like cells symmetric or asymmetric partitioning of mitochondria is important for the maintenance of stemness [202]. Katajisto *et al*. showed that daughter cells that inherited more old mitochondria differentiated, whilst cells with fewer old mitochondria retained their stemness

[202]. Upon re-entry into G1 mitochondria are observed to partially regain their elongated structure [195, 202, 203].

It has previously been recognised that whilst the highly proliferative NPCs are glycolytic, they undergo metabolic reprogramming during differentiation, characterised by an increase in mitochondrial mass/activity, OXPHOS, and presence of reactive oxygen species (ROS) [96, 108, 177, 203-205]. Recent reports have shown that although proliferating NPCs primarily exhibit prominent glycolysis, mediated by Hexokinase 2 (HK2), to meet their metabolic demands, interruption of electron transport chain (ETC) activity, and thus OXPHOS, can abolish NPC proliferation, leading to a significant increase in cell death, consequently decreasing neurogenesis and lineage progression [109, 205-208]. Furthermore, data obtained from *in vivo* and *in vitro* studies identified that reduced mitochondrial dynamics, and increased mitochondrial metabolism not only decreased NSC self-renewal, but enhanced cell fate/lineage commitment at the expense of self-renewal [107, 109, 205]. Findings from these studies demonstrated that mitochondrial metabolism and dynamics are able to act as an upstream regulator of neural stem/progenitor cell fate decisions, via ROS signalling, which in turn alters the transcriptional profile of NSCs [107, 109]. The increase to ROS levels observed in these studies are consistent with previous findings showing that ROS can influence a broad range of neural cell functions including neuronal plasticity, survival, cytoskeletal arrangement, proliferation and differentiation [reviewed in [95, 203, 204]]. Highly expressed in pluripotent NPCs, the transcription factor sex determining region Y- box 2 (Sox2) is down-regulated during the transition to a committed progenitor state and replaced by the expression of T-box brain protein 2 (Tbr2), an established marker of IPCs [103, 209, 210]. Interestingly, Khacho et al. observed that whilst the mitochondrial morphology of $Sox2^{+}$ cells exhibited an elongated morphology, $Tbr2^{+}$ cells possessed a more fragmented pool of mitochondria that regained their elongated phenotype once they became post-mitotic [109]. Disruption of mitochondrial dynamics, in this case through the increase in mitochondrial fragmentation, was demonstrated to decrease NSC self-renewal and increase fate commitment [109, 211]. Indeed, as mitochondrial number and morphology is tightly regulated by fission and fusion events, perturbations to this balance that result in excessive mitochondrial elongation or fragmentation, have been reported to be associated with severe neurodegenerative diseases, with features including; hearing loss [212], peripheral axonal neuropathies [213], and

dominant optic atrophy [214]. Taken together, these data highlight the importance of MTs, metabolism, and mitochondrial dynamics in NPC proliferation and fate decisions. This is further emphasised by the knowledge that there is cross talk between cellular metabolism and the cell cycle regulators/checkpoints.

1.3.2.2 Cell cycle regulation

Progression into and through each phase of the cell cycle is regulated by checkpoints that only allow a cell to progress if either internal or external conditions are suitable for progression. Factors influencing these decisions include, cell size, nutrient availability, extrinsic and intrinsic signalling, accurate replication and segregation of chromosomes, and or DNA integrity [215-219]. Persistent defects at such check point's results in apoptosis. Different types of checkpoints occur throughout the cell cycle, and are regulated by components of the Cdk/cyclin complexes (reviewed in [156, 219]).

NPC progression through proliferation and neurogenesis requires the concerted interactions of various factors such as the cytoskeleton, mitochondria and the cell cycle regulators cyclin and cyclin-dependent kinases (Cdks) [13, 79, 90, 109, 189, 199]. G1 is regulated by two check points with the first involved in sensing the availability of growth factors that suppress quiescent signalling and the second, occurring in late G1, assessing nutrient availability and if the cell is at an appropriate size for DNA replication. Cell cycle initiation and entry into G1 (Gap 1 phase) is stimulated by mitogens and growth factors activating D type cyclins (Cyclin D1, D2, and D3 in mammals). Cyclin D then activates and complexes with Cdk4/Cdk6 leading to the phosphorylation and inactivation of the retinoblastoma tumour suppressor protein (Rb) [220, 221]. Initial phosphorylation inhibits Rbs repression on the heterodimeric transcription factor E2F/DP, enabling initial transcriptional activation of Synthesis-phase genes (S-phase), such as cyclin E. Cyclin E then activates and binds Cdk2 (cyclin E/Cdk2 complex) and further phosphorylates Rb, thereby leading to the G1-S phase transition [221-225]. The checkpoint for S-phase is activated upon the detection of DNA damage that may have arisen during synthesis, or damaged DNA that was not repaired in the G1/S checkpoint [156, 219]. The cyclin E/Cdk2 complex can also inhibit Cdh1, a subunit of the anaphase-promoting complex (APC/C), blocking the degradation of S-phase cyclins and thereby facilitating an irreversible commitment to cell division [220, 225, 226]. Accompanying the G1-S transition, the mitochondria move along the MT cytoskeleton undergoing both fission and

fusion events, the separation and joining of two mitochondria respectively, to alter their morphology to form a hyper fused giant tubular network [191, 192]. This fused network enables the mitochondria to stimulate OXPHOS in order to meet the metabolic requirements of the dividing cell and drive cell cycle progression [179, 183, 193]. Progression through S-phase is promoted by the upregulation of cyclin A and its activation of Cdk2 and Cdk1. Similar to S phase, the G2 checkpoint helps maintain genomic stability by enabling the detection and repair of damaged DNA [227, 228] . The cyclin A/Cdk1/2 complex continues to accumulate into G2, during which it regulates the activation of the cyclin B1/Cdk1 complex required for prophase initiation and mitotic completion [153, 196, 199, 229]. Initiation of prophase and continuation into metaphase, anaphase and telophase requires significant cytoskeletal remodelling and is paralleled by further alterations to the mitochondrial morphology [34, 181]. The onset of mitosis has also been shown to be accompanied by mitochondrial fragmentation and MT dependent relocation to the cleavage furrow during anaphase. Mitochondrial fission in the G2/M transition occurs due to increased levels and activation of the large GTPase Drp1 [172, 181, 182, 186, 194-198]. The increase in Drp1 levels and its subsequent activation by the cyclin B/Cdk1 complexes arises as a result of inhibition of APC/C degradation of Drp1 during the G1/S transition [196, 229]. Finally, the APC/C is reactivated during the last phases of mitosis and cytokinesis in response Cdk activity. APC/C activation leads to the degradation of mitotic cyclins, mitotic exit and is accompanied by remodelling of the MT network to reform an elongated tubular network [192, 230]. In addition to cleavage plane orientation, it has recently been proposed that appropriate segregation of organelles, such as mitochondria, may be required for maintenance of stemness [202].

Interestingly, in addition to their role in regulating the cell cycle, various non-canonical functions of cyclins and Cdks have been reported (reviewed in [100, 231]). Emerging evidence from these studies indicates that Cyclins and Cdks can regulate neurogenic differentiation, the actin cytoskeleton and cell migration, and metabolism [95, 96, 100, 203, 231]. Of note, is the direct control of mitochondrial function by cyclin D1 alone or in concert with Cdk4. Several studies identified that these cell cycle regulators could impair metabolic activity by: repressing the nuclear transcription factor 1 (NRF1), thereby impairing mitochondrial respiration; binding to lipogenic enzymes and mitochondrial proteins; and preventing HK2 activation by binding to the voltage-dependent anion channel protein (VDAC) located in the outer

mitochondrial membrane [100, 231, 232]. Contrastingly, the cyclin B1/Cdk1 complex has been observed to localise to the mitochondrial matrix and increase mitochondrial respiration, which is proposed to coordinate the G2/M phase progression with mitochondrial respiration [100, 196]. Alterations to mitochondrial and/or cell cycle dynamics and their regulators, can lead to a plethora of interconnected downstream events impacting: cellular metabolism, cell cycle progression, cell fate and stemness [107, 109, 180, 181, 183, 190, 205, 211, 233]. Given that MTs are integral to these processes it is perhaps unsurprising that perturbations to MT regulators and dynamics can lead to a plethora of neurodevelopmental and neurodegenerative disorders [167, 168, 234, 235].

1.3.3 Migration-Locomotion

Unlike NSCs, IP and post mitotic neurons leave the proliferative zone and migrate to their appropriate laminar location in the developing neocortex. In order for neurons to move, migration or locomotion requires three synchronized steps. In the first step, the cell uses polarized cellular components to form a leading and a trailing process [236, 237]. The second phase of locomotion is movement of cell body and nucleus (nucleokinesis), and occurs through cytoplasmic swelling of the leading process, followed by the relocation of first the centrosome and then the organelles (including the nucleus) into the leading process region [111, 238]. To move the nucleus into the leading body during nucleokinesis, the nucleus is guided by a cage- or fork-like structure comprised of a MT network. This MT network links to the centrosome (which resides in the leading body), and pulls the nucleus toward the centrosome, by the MT molecular motor, dynein [5, 110, 239]. Actomyosin contraction at the rear of the cell retracts the trailing process to complete cellular locomotion. Several proteins are known to be essential for nucleokinesis including lissencephaly 1 (LIS1), doublecortin (DCX), and doublecortin-like kinase 1 (DCLK), and have been shown to associate with MTs promoting MT stability and polymerization [82, 112, 117, 130, 134]. The various mechanisms required to ensure the migrating neurons acquire their appropriate cortical positioning are precisely regulated and highly coordinated; and are yet to be fully elucidated. Currently, normal neuronal migration and laminar fate acquisition is believed to be influenced by neuron birth date (neurons born at similar time have similar laminar fate), neuronal cytoskeleton, and intra and extracellular cues including but not limited to Reelin, WNT, Pax6, Emx2, Fefz2 Ctip2, and Phosphatidylinositol 3-Kinase (PI3K) [82, 121, 124, 240-242].

1.3.4 Differentiation

Upon reaching their laminar position within the cortex, these post-migratory neurons undergo morphological and physiological changes to become integrated into the neural information processing network. The coordinated organisation and remodelling of the neuronal cytoskeleton is critical for the formation of the distinct cellular structures required for neurons to connect with other neural cells, and to function as cellular components of neural circuits. Working in concert with actin filaments (F-actin), the MT cytoskeleton provides mechanical forces that facilitate the establishment of axons and dendrites, as well as transporting organelles, secretory vesicles and protein complexes to specific sites across the cell, acting as local signalling platforms [13, 78, 243-245]. In addition to their morphological differences, the MTs in axons are oriented with their plus-end projecting away from the cell body, whilst dendrites have a mixed MT organisation. Furthermore, in axons and dendrites the differences between not only MT orientation, but their stability/dynamics, allows for selective cargo transport by specific MT molecular motors, with members of the plus-end directed family of Kinesin motors selectively transporting to the axon, and the minus-end directed family of dynein motors to the dendrites [33, 246]. Transport along the MT network is essential to neuronal functioning, as it enables cargo from the protein synthesis machinery, which is predominantly located in the cell body and proximal dendrites, to reach distant cellular locations. The importance of the MT to neuronal functions is reflected in the finding that perturbations to MT function, such as through disruptions to MT based transport or MT dynamics, can lead to a plethora of neuropathological conditions [246, 247].

The generation and formation of axons and dendrites begins with the breaking of the symmetry of the neuron by multiple protrusions from the cell body, termed neurites. Notably, enhanced actin dynamics, coupled with the mechanical forces provided by MT sliding, and an increase in MT bundles invading lamellipodia, are believed to stimulate neurite formation [13, 246, 248-250]. MT stabilization is recognised to be a key factor in determining the polarity of the developing neuron and the initial specification of the neurite to become the axon [247, 251, 252]. Recent findings have identified two MAPs, Tripartite Motif Containing 46 (TRIM46) and Calmodulin Regulated Spectrin Associated Protein Family Member 2 (CAMSAP2) that localise to future axon sites to be required for neuronal polarity and axon specification. TRIM46 has been observed to induce closely spaced MT bundles linked by thin cross bridges

and is required for the characteristic uniform orientation of MTs that drives polarized cargo transport in axons [251, 253]. Whereas CAMSAP2 protects MT- ends from depolymerisation and is believed to promote MT+ end outgrowth of MTs, by creating a local pool of non-centrosomal MTs at the first part of an axon [254, 255]. However, it should be noted that CAMSAP2 also has a role in dendritic branch formation, where it signals with γ-tubulin to form, organise and stabilize MT during dendritic development [254]. Additionally, MAPs such as Tau (MAP2) stabilises MT networks and are essential to axon specification and track determination for kinesin-mediate polarized trafficking of membranous organelles, cytosolic proteins and cytoskeletal proteins [29, 130, 256]. The transport of organelles is essential as the axon elongates, enabling the MT network to act in concert with adhesion complexes, actin, and MT plus-end targeting proteins (+TIPS) to aid in the formation and enlargement of the growth cone [257-259].

Further to its actions on axon development, the MT cytoskeleton interacts with F-actin, facilitating growth cone extension and steering in response to extracellular environmental cues, so as to guide the axon to its appropriate location for termination, and thus undergo branching and synapse formation [11, 13, 34, 260, 261]. During axon branching, F-actin accumulates to form axonal filopodia which are shortly thereafter invaded by dynamic MT bundles, whilst stable MTs are excluded. By invading the filopodia MTs provide cytoskeletal support and cargo delivery, thereby enabling the filopodium to mature into a branch [1, 139, 243, 258, 262]. The hexameric subfamily of ATPase's katanin and spastin, sever established MTs from their nucleation sites, such as the microtubule nucleation factor the γ-tubulin ring complex (γ –TuRC). This creates MT seeds/fragments which are believed to differentially promote branching formation [246, 263, 264]. In addition to its role in the axon, recent advances in visualization techniques have facilitated the elucidation of the essential role of MT dynamics in dendritic spine development [246, 261, 265, 266]. Assembled within the cell body, dynamic MTs interact with F-actin to transiently invade dendritic spines and contribute to spine morphology and synaptic plasticity via the transport of neurotransmitter receptors, postsynaptic proteins, organelles, mRNAs and cell signalling molecules [33, 261]. Remodelling and regulation of MT dynamics is essential to dendritic arborisation, axon formation, and neuronal functioning. Therefore, these are regulated by a large repertoire of MAPs, post-

translational modifications (PTMs), and cellular cues that are only briefly touched upon here (reviewed in [13, 33, 166, 267]).

In dendrites, MTs are regulated by the MAP CAMSAP2, as well as the +TIP end-binding protein Cytoplasmic Linker protein of 170kDa (CLIP-170) and the end-binding protein 3 (EB3). Knock down of these MAPs has been observed to alter dendritic morphology by reducing dendrite branching, complexity, as well spine morphology and plasticity [254, 260, 266, 268-270]. Interestingly, it was observed that spines undergoing large increases in F-actin, in response to increased synaptic calcium influx, were preferentially targeted for entry by MTs from proximal sites in the dendrite [260]. This calcium induced MT invasion into the dendritic spines was observed to be reliant upon the specific binding of the actin binding protein drebrinan A, which forms stable F-actin, with the MT +TIP EB3 in response to cyclin-dependent kinase 5 (Cdk5) activation [260, 271]. Although the orientation of MTs in dendrites are mixed, MTs invading spines grow with their plus-end towards spine end, and could therefore facilitate the trafficking of cargo and organelles into spines, aiding in synaptic plasticity [33, 272]. Indeed, the trafficking of mitochondria to synaptic regions supports the high metabolic requirement for such functions in neurons [273-277].

To meet the energetically demanding processes of neuronal differentiation and function, the cell must undergo a metabolic shift from glycolysis to OXPHOS. As aforementioned, the mitochondria undergo morphological changes during neuronal differentiation, transitioning from an elongated morphology to a fragmented state, then back again to an elongated state [182, 187, 278]. These morphological alterations reflect the metabolic OXPHOS shift in neuronal differentiation. The process is marked by increases in mitochondrial biogenesis/mass, ATP production, mitochondrial membrane potential, and ROS generation. In parallel, there is a downregulation in the expression of key glycolytic genes HK2, Lactose dehydrogenase A (LDHA), and an mRNA splicing shift from PKM2 to PKM1 [96, 107, 181, 189, 233]. By increasing ATP production, the mitochondria provide the energy to support various neuronal functions, including cytoskeletal remodelling, maintenance of mobilization of synaptic vesicles, generation of membrane potentials, and maintenance of Ca^{2+} homeostasis, thereby aiding neurotransmission and synaptic plasticity (reviewed in [273, 277-279]). In order to meet the rapidly changing high metabolic requirements of neurons, mitochondria travel along the MT network via the motor proteins dynein and kinesin, which in turn

cooperate with various adaptor proteins (such as Syntabulin, or Milton and Mitochondrial Rho GTPases (MIRO)) (reviewed in [33, 276]). Furthermore, several studies have shown that approximately two thirds of mitochondria in mature neurons are stationary in certain regions in order to provide a source of local ATP and Ca^{2+} buffering [280-282]. Recent studies have begun to identify the mitochondrial 'static anchors' and elucidate the mechanisms recruiting and retaining healthy mitochondria at areas of sustained synaptic activity, whilst transporting dysfunctional mitochondria back to the stoma [277]. Perturbations to mitochondrial distribution is known to lead to a range of neurological disorders including, motor neuron disease, type 2 Charcot-Marie-Tooth disease[147, 283], Alzheimer's disease [284], Parkinson's disease [285], Rett syndrome and Autism Spectrum Disorder (ASD) [211, 278]. Collectively, these studies further highlight the integral role of the MT cytoskeleton in the normal development and function of neurons.

However, the ability of the MAPs, mitochondria, and other elements to affect neuronal morphology and function is dependent upon the presence of a functional and dynamic MT network. Despite its seemingly simple components of repeating tubulin subunits, MTs display a remarkable diversity, with various tubulin isotypes introduced into the growing MT and contributing to their dynamic nature [65]. The synthesis and incorporation of tubulin isotypes into MTs require a complex interaction of specific molecular chaperones to achieve the dynamic MT instability essential for neuronal development and brain formation. Perturbations to the generation and maintenance of MTs and its regulatory elements can result in severe neurological disorders, such as tubulinopathies, and is outlined below [reviewed in [13, 34, 147, 286] with an emphasis on the TBCs in this pathway.

1.4 Tubulinopathies

A causal link between tubulin gene mutations and neurological disorders was described in a landmark study by Keays, Tian and colleagues [287] in 2007. These researchers identified mutations in the α1-tubulin isotype (aka TUBA3, TUBA1A) leading to lissencephaly and pachyrgria, shortly followed by two studies in 2009 identifying Class 2 β-tubulin mutations (TUBB2B) leading to polymicrogyria malformations [288] and, an α-tubulin isotype, tubulin alpha 8 mutation (TUBA8) resulting in polymicrogria with optic nerve hypoplasia [289]. Subsequently, mutations to other tubulin genes across three β-tubulin classes (I-III), as well as TUBA4A [290], and the γ-tubulin isotype, TUBG1 [extensively reviewed in [56, 60, 291],

were also documented. Clinical mutations in the tubulin isoforms are associated with a wide variety of brain malformations with overlapping pathologies and varying severity of symptoms. Common symptoms of tubulinopathies include ocular nerve hypoplasia, motor and intellectual disabilities, and epilepsy [60, 291]. A systematic analysis by Bahi-Buisson, Poirier [292] details five key phenotypic pathologies associated with tubulinopathies; microlissencephaly, polymicroglia-like cortical dysplasia, central pachygria, simplified gyral pattern, and a range of lissencephalies. Collective efforts to study the pleiotropic clinical presentation of tubulin mutations have enhanced our understanding of genotype-phenotype correlations. However, these studies altogether demonstrate that alterations to tubulin biosynthesis and incorporation into the MT cytoskeleton leads to a plethora of cortical malformations. As such, our understanding of genotype-phenotype correlations could be enhanced by investigating how each protein component of the MT biosynthetic pathway, the MT subunits, and their molecular chaperones influence the synthesis, subcellular-localisation, and dynamics of the MT cytoskeleton, as described further below.

1.5 Chaperones

Chaperones are proteins that assist in the conformational folding, unfolding and quality control of other proteins. During MT assembly molecular chaperones play key roles in tubulin formation and regulation (**Fig. 1.2**). Following ribosomal synthesis, tubulin monomers interact with the molecular chaperone prefoldin (PFD). PFD is a protein whose body is comprised of a double β-barrel connected to six alternate subunits each of which containing two helices, forming coiled coils assembled into an anti-parallel configuration that appear like appendages (each subunit is ~14-20kDa). These appendages immediately bind the tubulin sequence as it is released from the ribosomes [51, 293]. PFD selectively transfers the partially unfolded tubulin polypeptides in an ATP-independent manner to the highly specific group II chaperonin, CCT (chaperonin containing TCP-1 (aka: TCP1)) [43, 294]. This group II chaperonin contains two sets of eight different subunits stacked back-to-back. They perform the same function as the widely studied group I chaperonin GroES, although they differ in their structure, with group II chaperonins lacking a co-chaperone [295, 296]. Through multiple rounds of ATP binding and release, termed cycling, the polypeptide is released in a quasi-native state, this however, is only achieved with an efficiency rate of about 10-15%. These quasi-native α and β-tubulin proteins then rapidly interact with TBCB/E and TBCA/D,

respectively, to attain their functional-quaternary structure [53, 297]. The precise mechanism for the incorporation of monomers into TBCs is elusive, however recent evidence postulates that TBCB, and potentially other TBCs, directly binds to CCT, enabling tubulin to be released from the chaperonin already in a binary complex with the appropriate TBC [51, 298].

A widely recognised standard "linear model" of TBC folding established over two decades ago by Tian, Huang and colleagues [52], and since then expanded (**Fig. 1.2**), proposes that the α and β-tubulin monomers bound by TBCB and TBCA are subsequently transferred to TBCE and TBCD, respectively. In addition to the shuttling abilities of TBCs, it was observed that they serve as reservoirs for excess tubulin, thus contributing to the autoregulatory mechanism of tubulins, by binding, sequestering, and targeting the tubulin subunits for degradation [22, 54, 77, 147]. Once tubulin monomers are bound by TBCD and TBCE, they are able to form a super-complex, TBC-DE, that assembles the α and β-tubulin subunits into their unique heterodimeric conformation [51, 299]. Finally, the TBC-DE super-complex interacts with TBCC, which is believed to act as a GTPase activating protein (GAP). TBCC, stimulates hydrolysis of the β-tubulin bound GTP molecule that enables the dissociation of functional αβ-tubulin heterodimer from the super-complex [29, 34, 51, 54, 300]. This reaction has been proposed to take place at the end of the MT. Once released, the αβ-tubulin heterodimer, possesses a GTP molecule in N-site between the α-tubulin and β-tubulin that is non-exchangeable, and a GDP on the exchangeable or E-site of β-tubulin. There is then believed to be a free exchange of GDP to GTP at β-tubulins E-site. This GTP is then hydrolysed again into GDP, enabling the αβ-tubulin heterodimer to be incorporated into the growing end of the MT lattice [19, 51, 301].

During MT polymerization a stochastic switch can trigger MT depolymerisation. Upon depolymerisation, the αβ-tubulin heterodimer is bound and dissociated by TBCE/TBCB and TBCD, in a reaction that is the reverse to the assembly pathway (known as the back reaction), as detailed below. It is important to note however, that TBCD is regulated by ADP ribosylation factor-like protein 2 (Arl2), and disruption to this interaction can promote MT catastrophe by sequestering GTP-bound β-tubulin [302, 303]. Additionally, TBCE acts in concert with, and independently of, TBCB to dissociate the tubulin heterodimer through steric interactions at the αβ-tubulin interface mediated by its cytoskeleton-associated protein glycine rich (CAP-Gly) and Leucine rich-repeat (LRR) domains [304]. This energy-independent process enables

the formation of TBCB/TBCE complex with dissociated α tubulin (αEB) facilitating α-tubulin degradation by exposing the ubiquitin-like (UBL) domain to directly engage the proteasome [304].

Recent work by two groups has challenged the role/involvement of various components of the MT formation and dissociation in the standard 'linear model'. These studies propose TBCD as a central scaffold in the chaperone complex that is required for tubulin synthesis and degradation [301, 305]. In yeast, Nithan, Le and colleagues [301] et al. identified a cage-like structural complex comprising TBCD and TBCE, which interacts with Arl-2 (TBC-DEG) to form a stable chaperone that does not disassemble after each cycle of tubulin assembly and disassembly. In this proposed model, binding of α /β-tubulin to the TBC-DEG complex primes Arl2, allowing binding of TBCC. TBCC then interfaces with Arl2 and α and β-tubulin via its C-terminal β-helical domain to promote GTP hydrolysis, catalysing α/β tubulin heterodimer assembly and triggering its release from the supercomplex [301, 305]. In contrast, studies conducted in mammalian tissues identified several different complexes including, a novel trimer consisting of TBCD, α-tubulin and β-tubulin trimer, a tetramer of TBCD, TBCE, Arl2 and β-tubulin, and a TBCD, Arl2 and β-tubulin trimer. These three complexes were found to be in 1:1:1 ratio in most cells from a diverse array off tissues [299, 306]. Hydrogen/deuterium exchange mass spectrometric analysis, indicates that an interaction between β-tubulin and TBCD, alters the nucleotide binding properties of Arl2, to allosterically alter β-tubulin structure to promote α-tubulin binding [299, 306]. Nevertheless, these studies indicate a central and crucial role of TBCs in regulation of tubulin polymerisation and subsequent MTs formation. [13, 34]. To decipher the molecular underpinning of MT dynamics it is critical to understand the structural properties of TBCs. Such studies will enable us to decipher the structural implications of neurological disorder causing clinical mutations [51, 283, 291]. Structural characterisation of cofactors TBC- A, B, C and E have been deciphered. However, structural information of TBCD still needs to be determined [146, 307-309]. Here I discuss the chaperons TBC- A, B, C and E, but will mainly focus on TBCD and its recently characterised mutations.

1.5.1 TBCs

TBCA is a tubulin cofactor originally characterised as a 14kDA release factor involved in the folding of β-tubulin [310], and believed to be a co-chaperone for CCT [311]. More recently,

TBCA has also been recognized to interact with a folding intermediate of β-tubulin upon its release from CCT [22, 52, 312]. Human TBCA is rod-like shaped monomer consisting of a trimeric or coiled coil connected by short turns, and a proline induced kin in the second helix, with β-tubulin interacting via the three α-helical regions [313]. TBCA functions to not only shuttle β-tubulin to TBCD enhancing dimerization rate, but has also been shown to capture excess β-tubulin [313, 314]. Studies into TBCA homologues, such as the *Schizosaccaromyces pombe* Alp31, have indicated a role for TBCA in cytoplasmic MT integrity and the proper control of cell growth polarity [315]. Whilst loss or reduction of TBCA in mammalian tissues has been indicated to lead to alterations to the MT cytoskeleton contributing to cell cycle arrest and cell death [58, 146], the molecular actions of TBCA remains poorly characterised in mammals.

In the case of TBCC, the GAP activity for this protein is essential to stimulate the GTP-hydrolysis of β-tubulin units and subsequent tubulin heterodimer release from TBC-DEG super complex [52, 297, 316, 317]. The *N*-terminal domain structure of TBCC contains three helices that form a bundle, whilst its C-terminal domain fold is defined as a β-helix possessing a conserved arginine residue implicated to trigger hydrolysis of GTP-bound tubulin by acting as an arginine finger trigger [317-319]. Unsurprisingly, recent studies have indicated that alterations to TBCC levels alters cell cycle dynamics through perturbations to MT dynamics and centrosome disorganisation [320, 321]. Findings from one of these reports demonstrate that whilst overexpression of TBCC leads to an increase in G2/M cells, silencing of TBCC increases the percent of S phase cells, stemming from reduced MT growth, increased stabilisation, and increased pool of nonpolymerizable tubulins [320]. Further highlighting the importance of TBCC to the MT, was the identification of a TBCC related protein that is a key regulator of internal cell organization and centrosome positioning, termed TBCC-domain containing 1 protein (TBCCD1) [321].

Recent evidence has elucidated the tertiary structure of TBCB and TBCE, and their ability to dissociate tubulin dimers in an energy-independent process, thus allowing a deeper insight into their roles in MT dynamics. Both cofactors possess globular protein domains and a CAP-Gly, and UBL domain, that is connected by a short coiled coil region in TBCB, while TBCE's UBL lies adjacent to a LRR [304]. Although the CAP-Gly domain of TBCB has been demonstrated to interact with various microtubule binding proteins to alter MT dynamics, such as the neuron

specific anti-catastrophe factor dynactin subunit p150 Glued, its ability to dissociate the tubulin heterodimer requires the participation of TBCE [298, 322, 323]. TBCE however, can act in concert and independently of TBCB to dissociate the tubulin heterodimer through steric interactions between the α/β-tubulin interface derived from its Cap-Gly and LRR domains [304]. Mutations to *TBCB* and *TBCE* have been indicated in hypoparathyroidism facial dysmorphia and giant axonal neurophathy, resultant from impairments to MT cytoskeletal function [34, 112, 324].

1.5.2 TBCD

TBCD was first implicated in tubulin synthesis in a study published in 1992 [316]. Several overexpression studies implicated bovine TBCD and TBCE in MT destabilisation [302, 303]. However, it was only in 1996 that the purified ~120kDa protein was reported and deemed to be actively involved in the generation of tubulin heterodimers [52]. Lewi, Tian and colleagues [53], first reported the integral role of TBCD in MT dynamics in which TBCD disrupts α/β dimers and sequesters β-tubulin. However, it should be noted that the activity of Human TBCD is mediated by its interactions with Arl2 [165, 325]. In addition to its involvement in *de novo* tubulin dimer assembly and disassembly, TBCD has been implicated to facilitate the organization of the mitotic spindle, recruitment of γ –TuRC at centrosomes, and appropriate chromosomal segregation in various organisms [28, 302, 326-329]. Furthermore, genetic mutations to TBCD result in severe neuropathological disorders in children, with a recent study identifying two novel homozygous missense mutations in the *TBCD* gene, A475T and A586V (rs775014444), in two girls from two independent consanguineous families with infantile neurodegeneration [4]. These mutations were associated with a plethora of neuropathological disorders including microcephaly, epilepsy, dystonia, optic atrophy, nystagmus, hypotonia, generalized atrophy of white matter, thin corpus callosum, language deficits, and intellectual disability [4, 63]. These mutations result in a drastic reduction in the amount of TBCD protein in the fibroblasts of afflicted individuals. Further *in vitro* analysis revealed that while mutants were functionally capable of binding and discharging TBCD intermediates, they were comparatively less efficient than WT TBCD proteins at *de novo* assembly, and disassembly of heterodimers even when overexpressed. TBCD knockdown using short hairpin RNA (shRNA), *in vitro*, resulted in reduced proliferation and radial migration of cortical cells. These deleterious effects could be partially rescued by expressing

TBCD mutants and fully rescued by WT TBCD [4]. Consistent with these findings Pode-Shakked, Barash and colleagues [63] documented perturbed MT dynamics and reduction in TBCD levels from samples obtained from patients harbouring the A475T and A586V mutations, as well as documenting an increase in re-polymerization and a significant reduction in β-tubulin levels. Furthermore, by silencing *TBCD* in a Zebra fish model, Pode-Shakked, Barash and colleagues [63] observed a phenotype reminiscent of human neuropathological phenotype described in patients. In addition to these phenotypic changes, the authors also documented a reduced level of α and β-tubulin compared to control. Whilst the causes for a reduction in β-tubulin levels remains unclear, it has been attributed to an increased ubiquitination of TBCD bound β-tubulin or β-tubulin misfolding, or both [63].

Following from this work, two additional research groups identified a variety of heterozygous and homozygous mutations to *TBCD*, as well as a loss-of-function (deletion) allele [61, 62, 330]. Notably, a P1122L mutation was associated with a more severe phenotype when compared with others reported in these studies, as subjects were reported to exhibit the following features additional to well-documented TBCD pathological traits: growth failure, muscle weakness, early onset cortical atrophy, developmental delay, spastic tetraplegia, limited response to noise and delayed myelination as determined via magnetic resonance imaging [61]. Thus, these results could be interpreted to mean that TBCD is important not only in neuronal development but also in the development of multiple organs of the body. The mutations reported in studies by Flex, Niceta and colleagues [61], and by Miyake, Fukai and colleagues [62], displayed scenarios in which a reduced pool of soluble tubulin and accelerated rate of MT re-polymerization was observed for several cases of disease-associated variants, suggestive of a rapidly growing and potentially more stable MT population. On the other hand, Flex, Niceta and colleagues [61], were also able to identify a reduced binding of β-tubulin and impaired binding to TBCE and Arl2 in TBCD mutants.

1.6 Aims

Unlike the other TBCs, there is little functional molecular modelling or structural biological data on the protein to describe its structures relative to MT biosynthetic pathway complexes, leaving a gap in knowledge into the exact mechanisms of function and the alternate effect that mutations in this gene may encompass. However, the significant insights into genotype-phenotype relationships documented in abovementioned studies of the 15 *TBCD* mutations

already provide clues to suggest the importance for this chaperonin in MT folding and, hence, serve as motivation to clarify its mode of action.

In this thesis, the role of TBCD in neurogenesis and neurodevelopment is investigated. To achieve this, a combination of molecular modelling, cell culture and preclinical (mouse) models, was used. Firstly, the biophysical properties of TBCD as a protein complex with its binding partners TBCE, ARL2 and β-tubulin, essential to its role as a microtubule biosynthetic chaperone, were explored. Next, to understand the biological roles of TBCD in cells, the impact of TBCD gene disruption on cell cycle, cell viability, energy metabolism, mitochondrial function, and redox status was investigated. Finally, to understand the physiological impact of TBCD mutations on mammalian neuronal development and disease, a novel knock-in mouse model harbouring the TBCD clinical mutation (A475T) was characterised to understand the impact of this mutation in neurodevelopment and disease. Altogether, these studies delineate the molecular functions for TBCD in neural cells, and how disease-associated mutations directly influence mammalian nervous system development resulting in disease.

1.7 References

1. Conde, C. and A. Cáceres, *Microtubule assembly, organization and dynamics in axons and dendrites.* Nature Reviews Neuroscience, 2009. **10**(5): p. 319-332.
2. Gilbert, S.F., *Formation of the neural tube.* Developmental Biology, 2000.
3. Jiang, X. and J. Nardelli, *Cellular and molecular introduction to brain development.* Neurobiology of disease, 2016. **92**: p. 3-17.
4. Edvardson, S., et al., *Infantile neurodegenerative disorder associated with mutations in TBCD, an essential gene in the tubulin heterodimer assembly pathway.* Human Molecular Genetics, 2016. **25**(21): p. 4635-4648.
5. Rivas, R. and M. Hatten, *Motility and cytoskeletal organization of migrating cerebellar granule neurons.* The Journal of Neuroscience, 1995. **15**(2): p. 981-989.
6. Stiles, J. and T.L. Jernigan, *The Basics of Brain Development.* Neuropsychology Review, 2010. **20**(4): p. 327-348.
7. Jaglin, X.H. and J. Chelly, *Tubulin-related cortical dysgeneses: microtubule dysfunction underlying neuronal migration defects.* Trends Genet, 2009. **25**(12): p. 555-66.
8. Lundin, V.F., M.R. Leroux, and P.C. Stirling, *Quality control of cytoskeletal proteins and human disease.* Trends in biochemical sciences, 2010. **35**(5): p. 288-297.
9. Ngo, L., et al., *TUBB5 and its disease-associated mutations influence the terminal differentiation and dendritic spine densities of cerebral cortical neurons.* Human molecular genetics, 2014: p. ddu238.

10. Heng, J.I.-T., A. Chariot, and L. Nguyen, *Molecular layers underlying cytoskeletal remodelling during cortical development.* Trends in neurosciences, 2010. **33**(1): p. 38-47.
11. Cingolani, L.A. and Y. Goda, *Actin in action: the interplay between the actin cytoskeleton and synaptic efficacy.* Nature Reviews Neuroscience, 2008. **9**(5): p. 344-356.
12. Chhabra, E.S. and H.N. Higgs, *The many faces of actin: matching assembly factors with cellular structures.* Nature cell biology, 2007. **9**(10): p. 1110-1121.
13. Kapitein, Lukas C. and Casper C. Hoogenraad, *Building the Neuronal Microtubule Cytoskeleton.* Neuron, 2015. **87**(3): p. 492-506.
14. Breuss, M., et al., *Mutations in the β-tubulin gene TUBB5 cause microcephaly with structural brain abnormalities.* Cell reports, 2012. **2**(6): p. 1554-1562.
15. Boivin, M.J., et al., *Reducing neurodevelopmental disorders and disability through research and interventions.* Nature, 2015. **527**(7578): p. S155-S160.
16. Bretscher, A., *Microfilament structure and function in the cortical cytoskeleton.* Annual review of cell biology, 1991. **7**(1): p. 337-374.
17. Avila, J., *Microtubule functions.* Life Sciences, 1992. **50**(5): p. 327-334.
18. Howard, J. and A.A. Hyman, *Growth, fluctuation and switching at microtubule plus ends.* Nature Reviews Molecular Cell Biology, 2009. **10**(8): p. 569-574.
19. Alushin, G.M., et al., *High resolution microtubule structures reveal the structural transitions in αβ–tubulin upon GTP hydrolysis.* Cell, 2014. **157**(5): p. 1117-1129.
20. Mitchison, T. and M. Kirschner, *Dynamic instability of microtubule growth.* nature, 1984. **312**(5991): p. 237-242.
21. Tian, G. and N.J. Cowan, *Tubulin-specific chaperones: components of a molecular machine that assembles the α/β heterodimer.* Methods in cell biology, 2013. **115**: p. 155.
22. Szymanski, D., *Tubulin Folding Cofactors: Half a Dozen for a Dimer.* Current Biology, 2002. **12**(22): p. R767-R769.
23. Subramanian, R. and T.M. Kapoor, *Building complexity: insights into self-organized assembly of microtubule-based architectures.* Developmental cell, 2012. **23**(5): p. 874-885.
24. Ilan, Y., *Randomness in microtubule dynamics: an error that requires correction or an inherent plasticity required for normal cellular function?* Cell Biology International, 2019. **43**(7): p. 739-748.
25. Goodson, H.V. and E.M. Jonasson, *Microtubules and microtubule-associated proteins.* Cold Spring Harbor perspectives in biology, 2018. **10**(6): p. a022608.
26. Wittmann, T., A. Hyman, and A. Desai, *The spindle: a dynamic assembly of microtubules and motors.* Nat Cell Biol, 2001. **3**(1): p. E28-34.
27. Glotzer, M., *The 3Ms of central spindle assembly: microtubules, motors and MAPs.* Nat Rev Mol Cell Biol, 2009. **10**(1): p. 9-20.
28. Fanarraga, M.L., et al., *TBCD links centriologenesis, spindle microtubule dynamics, and midbody abscission in human cells.* PLoS One, 2010. **5**(1): p. e8846.
29. Amos, L.A. and D. Schlieper, *Microtubules and maps.* Advances in protein chemistry, 2005. **71**: p. 257-298.
30. Carazo-Salas, R.E. and P. Nurse, *Self-organization of interphase microtubule arrays in fission yeast.* Nat Cell Biol, 2006. **8**(10): p. 1102-1107.
31. Kaverina, I. and A. Straube, *Regulation of cell migration by dynamic microtubules.* Semin Cell Dev Biol, 2011. **22**(9): p. 968-74.
32. Jaworski, J., et al., *Dynamic microtubules regulate dendritic spine morphology and synaptic plasticity.* Neuron, 2009. **61**(1): p. 85-100.
33. Hirokawa, N., S. Niwa, and Y. Tanaka, *Molecular motors in neurons: transport mechanisms and roles in brain function, development, and disease.* Neuron, 2010. **68**(4): p. 610-638.
34. Poulain, F.E. and A. Sobel, *The microtubule network and neuronal morphogenesis: Dynamic and coordinated orchestration through multiple players.* Molecular and Cellular Neuroscience, 2010. **43**(1): p. 15-32.

35. Brouhard, G.J. and L.M. Rice, *Microtubule dynamics: an interplay of biochemistry and mechanics.* Nature reviews Molecular cell biology, 2018. **19**(7): p. 451-463.
36. Vemu, A., et al., *Tubulin isoform composition tunes microtubule dynamics.* Molecular biology of the cell, 2017. **28**(25): p. 3564-3572.
37. Janson, M.E., E. Mathilde, and M. Dogterom, *Dynamic instability of microtubules is regulated by force.* The Journal of cell biology, 2003. **161**(6): p. 1029-1034.
38. Howard, J. and A.A. Hyman, *Microtubule polymerases and depolymerases.* Curr Opin Cell Biol, 2007. **19**(1): p. 31-5.
39. Desai, A. and T.J. Mitchison, *Microtubule polymerization dynamics.* Annual review of cell and developmental biology, 1997. **13**(1): p. 83-117.
40. Valiron, O., N. Caudron, and D. Job, *Microtubule dynamics.* Cellular and Molecular Life Sciences CMLS, 2001. **58**(14): p. 2069-2084.
41. Vainberg, I.E., et al., *Prefoldin, a chaperone that delivers unfolded proteins to cytosolic chaperonin.* Cell, 1998. **93**(5): p. 863-873.
42. Llorca, O., et al., *Eukaryotic type II chaperonin CCT interacts with actin through specific subunits.* Nature, 1999. **402**(6762): p. 693-696.
43. Cowan, N.J. and S.A. Lewis, *Type II chaperonns, prefoldin, and the tubulin-specific chaperones.* Advances in protein chemistry, 2001. **59**: p. 73-104.
44. Valpuesta, J.M., et al., *Structure and function of a protein folding machine: the eukaryotic cytosolic chaperonin CCT.* FEBS letters, 2002. **529**(1): p. 11-16.
45. Llorca, O., et al., *Eukaryotic chaperonin CCT stabilizes actin and tubulin folding intermediates in open quasi-native conformations.* The EMBO journal, 2000. **19**(22): p. 5971-5979.
46. Llorca, O., et al., *Analysis of the interaction between the eukaryotic chaperonin CCT and its substrates actin and tubulin.* Journal of structural biology, 2001. **135**(2): p. 205-218.
47. Leitner, A., et al., *The molecular architecture of the eukaryotic chaperonin TRiC/CCT.* Structure, 2012. **20**(5): p. 814-825.
48. Llorca, O., et al., *The 'sequential allosteric ring'mechanism in the eukaryotic chaperonin-assisted folding of actin and tubulin.* The EMBO journal, 2001. **20**(15): p. 4065-4075.
49. Tian, G., et al., *Tubulin Folding Cofactors as GTPase-activating Proteins GTP HYDROLYSIS AND THE ASSEMBLY OF THE α/β-TUBULIN HETERODIMER.* Journal of Biological Chemistry, 1999. **274**(34): p. 24054-24058.
50. Holscher, C., *Incretin analogues that have been developed to treat type 2 diabetes hold promise as a novel treatment strategy for Alzheimer's disease.* Recent patents on CNS drug discovery, 2010. **5**(2): p. 109-117.
51. Serna, M. and J.C. Zabala, *Tubulin Folding and Degradation.* eLS, 2016.
52. Tian, G., et al., *Pathway Leading to Correctly Folded β-Tubulin.* Cell, 1996. **86**(2): p. 287-296.
53. Lewis, S.A., G. Tian, and N.J. Cowan, *The alpha- and beta-tubulin folding pathways.* Trends Cell Biol, 1997. **7**(12): p. 479-84.
54. Tian, G., et al., *Tubulin subunits exist in an activated conformational state generated and maintained by protein cofactors.* J Cell Biol, 1997. **138**(4): p. 821-32.
55. Brock, S., et al., *Tubulinopathies continued: refining the phenotypic spectrum associated with variants in TUBG1.* European journal of human genetics: EJHG, 2018.
56. Rees, M., et al., *Tubulinopathies in malformations of the cerebral cortex.* Journal of Neurology, Neurosurgery & Psychiatry, 2014. **85**(10): p. e4-e4.
57. Poirier, K., et al., *Mutations in the neuronal β-tubulin subunit TUBB3 result in malformation of cortical development and neuronal migration defects.* Human Molecular Genetics, 2010. **19**(22): p. 4462-4473.
58. Nolasco, S., et al., *Tubulin cofactor A gene silencing in mammalian cells induces changes in microtubule cytoskeleton, cell cycle arrest and cell death.* FEBS letters, 2005. **579**(17): p. 3515-3524.

59. Guerrini, R. and W.B. Dobyns, *Malformations of cortical development: clinical features and genetic causes.* The Lancet Neurology, 2014. **13**(7): p. 710-726.
60. Chang, B.S., *Tubulinopathies and Their Brain Malformation Syndromes: Every TUB on Its Own Bottom.* Epilepsy Currents, 2015. **15**(2): p. 65-67.
61. Flex, E., et al., *Biallelic Mutations in TBCD, Encoding the Tubulin Folding Cofactor D, Perturb Microtubule Dynamics and Cause Early-Onset Encephalopathy.* The American Journal of Human Genetics, 2016. **99**(4): p. 962-973.
62. Miyake, N., et al., *Biallelic TBCD mutations cause early-onset neurodegenerative encephalopathy.* The American Journal of Human Genetics, 2016. **99**(4): p. 950-961.
63. Pode-Shakked, B., et al., *Microcephaly, intractable seizures and developmental delay caused by biallelic variants in TBCD: Further delineation of a new chaperone-mediated tubulinopathy.* Clinical genetics, 2016.
64. Ikeda, T., et al., *TBCD may be a causal gene in progressive neurodegenerative encephalopathy with atypical infantile spinal muscular atrophy.* J Hum Genet, 2017. **62**(4): p. 473-480.
65. Janke, C., *The tubulin code: Molecular components, readout mechanisms, and functions.* The Journal of Cell Biology, 2014. **206**(4): p. 461-472.
66. Sato, M., et al., *Mechanical properties of brain tubulin and microtubules.* The Journal of cell biology, 1988. **106**(4): p. 1205-1211.
67. Sullivan, K.F., *Structure and utilization of tubulin isotypes.* Annual review of cell biology, 1988. **4**(1): p. 687-716.
68. Ludueña, R.F., *A hypothesis on the origin and evolution of tubulin*, in *International review of cell and molecular biology*. 2013, Elsevier. p. 41-185.
69. Cowan, N. and L. Dudley, *Tubulin isotypes and the multigene tubulin families.* International review of cytology, 1983. **85**: p. 147-173.
70. Lewis, S.A., W. Gu, and N.J. Cowan, *Free intermingling of mammalian β-tubulin isotypes among functionally distinct microtubules.* Cell, 1987. **49**(4): p. 539-548.
71. Minoura, I., *Towards an understanding of the isotype-specific functions of tubulin in neurons: Technical advances in tubulin expression and purification.* Neuroscience Research, 2017.
72. Honda, Y., et al., *Tubulin isotype substitution revealed that isotype combination modulates microtubule dynamics in C. elegans embryos.* J Cell Sci, 2017. **130**(9): p. 1652-1661.
73. Panda, D., et al., *Microtubule dynamics in vitro are regulated by the tubulin isotype composition.* Proceedings of the National Academy of Sciences, 1994. **91**(24): p. 11358-11362.
74. Chakraborti, S., et al., *The emerging role of the tubulin code: from the tubulin molecule to neuronal function and disease.* Cytoskeleton, 2016. **73**(10): p. 521-550.
75. Löwe, J., et al., *Refined structure of αβ-tubulin at 3.5 Å resolution.* Journal of molecular biology, 2001. **313**(5): p. 1045-1057.
76. Pachter, J.S., T.J. Yen, and D.W. Cleveland, *Autoregulation of tubulin expression is achieved through specific degradation of polysomal tubulin mRNAs.* Cell, 1987. **51**(2): p. 283-92.
77. Yen, T.J., P.S. Machlin, and D.W. Cleveland, *Autoregulated instability of β-tubulin mRNAs by recognition of the nascent amino terminus of βtubulin.* Nature, 1988. **334**(6183): p. 580-585.
78. Laferrière, N.B., T.H. MacRae, and D.L. Brown, *Tubulin synthesis and assembly in differentiating neurons.* Biochemistry and Cell Biology, 1997. **75**(2): p. 103-117.
79. Florio, M. and W.B. Huttner, *Neural progenitors, neurogenesis and the evolution of the neocortex.* Development, 2014. **141**(11): p. 2182-2194.
80. Homem, C.C., M. Repic, and J.A. Knoblich, *Proliferation control in neural stem and progenitor cells.* Nature Reviews Neuroscience, 2015. **16**(11): p. 647-659.
81. Matsuzaki, F. and A. Shitamukai, *Cell division modes and cleavage planes of neural progenitors during mammalian cortical development.* Cold Spring Harbor perspectives in biology, 2015. **7**(9): p. a015719.
82. Ayala, R., T. Shu, and L.-H. Tsai, *Trekking across the brain: the journey of neuronal migration.* Cell, 2007. **128**(1): p. 29-43.

83. Merkle, F.T. and A. Alvarez-Buylla, *Neural stem cells in mammalian development.* Current opinion in cell biology, 2006. **18**(6): p. 704-709.
84. Sadler, T. *Embryology of neural tube development*. in *American Journal of Medical Genetics Part C: Seminars in Medical Genetics*. 2005. Wiley Online Library.
85. Fietz, S.A. and W.B. Huttner, *Cortical progenitor expansion, self-renewal and neurogenesis—a polarized perspective.* Current opinion in neurobiology, 2011. **21**(1): p. 23-35.
86. Konno, D., et al., *Neuroepithelial progenitors undergo LGN-dependent planar divisions to maintain self-renewability during mammalian neurogenesis.* Nature cell biology, 2008. **10**(1): p. 93-101.
87. Paridaen, J.T. and W.B. Huttner, *Neurogenesis during development of the vertebrate central nervous system.* EMBO reports, 2014. **15**(4): p. 351-364.
88. Taverna, E., M. Götz, and W.B. Huttner, *The cell biology of neurogenesis: toward an understanding of the development and evolution of the neocortex.* Annual review of cell and developmental biology, 2014. **30**.
89. Del Bene, F., et al., *Regulation of neurogenesis by interkinetic nuclear migration through an apical-basal notch gradient.* Cell, 2008. **134**(6): p. 1055-1065.
90. Hardwick, L.J. and A. Philpott, *Nervous decision-making: to divide or differentiate.* Trends in Genetics, 2014. **30**(6): p. 254-261.
91. Martínez-Cerdeño, V. and S.C. Noctor, *Neural progenitor cell terminology.* Frontiers in Neuroanatomy, 2018. **12**: p. 104.
92. Morest, D.K. and J. Silver, *Precursors of neurons, neuroglia, and ependymal cells in the CNS: what are they? Where are they from? How do they get where they are going?* Glia, 2003. **43**(1): p. 6-18.
93. Cremisi, F., A. Philpott, and S.-i. Ohnuma, *Cell cycle and cell fate interactions in neural development.* Current opinion in neurobiology, 2003. **13**(1): p. 26-33.
94. Okano, H. and S. Temple, *Cell types to order: temporal specification of CNS stem cells.* Current opinion in neurobiology, 2009. **19**(2): p. 112-119.
95. Kennedy, K.A., et al., *Reactive oxygen species and the neuronal fate.* Cellular and Molecular Life Sciences, 2012. **69**(2): p. 215-221.
96. Tsatmali, M., et al., *Reactive oxygen species modulate the differentiation of neurons in clonal cortical cultures.* Molecular and Cellular Neuroscience, 2006. **33**(4): p. 345-357.
97. Lange, C., W.B. Huttner, and F. Calegari, *Cdk4/cyclinD1 overexpression in neural stem cells shortens G1, delays neurogenesis, and promotes the generation and expansion of basal progenitors.* Cell stem cell, 2009. **5**(3): p. 320-331.
98. Kranenburg, O., et al., *Inhibition of cyclin-dependent kinase activity triggers neuronal differentiation of mouse neuroblastoma cells.* J Cell Biol, 1995. **131**(1): p. 227-34.
99. Calegari, F. and W.B. Huttner, *An inhibition of cyclin-dependent kinases that lengthens, but does not arrest, neuroepithelial cell cycle induces premature neurogenesis.* Journal of Cell Science, 2003. **116**(24): p. 4947-4955.
100. Hydbring, P., M. Malumbres, and P. Sicinski, *Non-canonical functions of cell cycle cyclins and cyclin-dependent kinases.* Nature reviews Molecular cell biology, 2016. **17**(5): p. 280-292.
101. Bani-Yaghoub, M., et al., *Role of Sox2 in the development of the mouse neocortex.* Developmental biology, 2006. **295**(1): p. 52-66.
102. Ferri, A.L., et al., *Sox2 deficiency causes neurodegeneration and impaired neurogenesis in the adult mouse brain.* Development, 2004. **131**(15): p. 3805-3819.
103. Hutton, S.R. and L.H. Pevny, *SOX2 expression levels distinguish between neural progenitor populations of the developing dorsal telencephalon.* Developmental biology, 2011. **352**(1): p. 40-47.
104. Manuel, M.N., et al., *Regulation of cerebral cortical neurogenesis by the Pax6 transcription factor.* Frontiers in cellular neuroscience, 2015. **9**: p. 70.

105. Sansom, S.N., et al., *The level of the transcription factor Pax6 is essential for controlling the balance between neural stem cell self-renewal and neurogenesis.* PLoS genetics, 2009. **5**(6).
106. Kalucka, J., et al., *Metabolic control of the cell cycle.* Cell cycle (Georgetown, Tex.), 2015. **14**(21): p. 3379-3388.
107. Agostini, M., et al., *Metabolic reprogramming during neuronal differentiation.* Cell death and differentiation, 2016. **23**(9): p. 1502-1514.
108. Knobloch, M. and S. Jessberger, *Metabolism and neurogenesis.* Current opinion in neurobiology, 2017. **42**: p. 45-52.
109. Khacho, M., et al., *Mitochondrial dynamics impacts stem cell identity and fate decisions by regulating a nuclear transcriptional program.* Cell stem cell, 2016. **19**(2): p. 232-247.
110. Tsai, L.-H. and J.G. Gleeson, *Nucleokinesis in neuronal migration.* Neuron, 2005. **46**(3): p. 383-388.
111. Schaar, B.T. and S.K. McConnell, *Cytoskeletal coordination during neuronal migration.* Proceedings of the National Academy of Sciences of the United States of America, 2005. **102**(38): p. 13652-13657.
112. Guerrini, R. and E. Parrini, *Neuronal migration disorders.* Neurobiology of Disease, 2010. **38**(2): p. 154-166.
113. Cooper, J.A., *Mechanisms of cell migration in the nervous system.* The Journal of Cell Biology, 2013. **202**(5): p. 725-734.
114. Nadarajah, B. and J.G. Parnavelas, *Modes of neuronal migration in the developing cerebral cortex.* Nature Reviews Neuroscience, 2002. **3**(6): p. 423-432.
115. van Beuningen, S.F. and C.C. Hoogenraad, *Neuronal polarity: remodeling microtubule organization.* Current opinion in neurobiology, 2016. **39**: p. 1-7.
116. Lasser, M., J. Tiber, and L.A. Lowery, *The role of the microtubule cytoskeleton in neurodevelopmental disorders.* Frontiers in cellular neuroscience, 2018. **12**: p. 165.
117. Greig, L.C., et al., *Molecular logic of neocortical projection neuron specification, development and diversity.* Nature Reviews Neuroscience, 2013. **14**(11): p. 755-769.
118. DeFelipe, J., *The Evolution of the Brain, the Human Nature of Cortical Circuits, and Intellectual Creativity.* Frontiers in Neuroanatomy, 2011. **5**(29).
119. Arimura, N. and K. Kaibuchi, *Neuronal polarity: from extracellular signals to intracellular mechanisms.* Nat Rev Neurosci, 2007. **8**(3): p. 194-205.
120. Hofman, M.A., *Evolution of the human brain: when bigger is better.* Frontiers in neuroanatomy, 2014. **8**: p. 15.
121. Campbell, K., *Cortical neuron specification: it has its time and place.* Neuron, 2005. **46**(3): p. 373-376.
122. Franco, S.J. and U. Müller, *Shaping our minds: stem and progenitor cell diversity in the mammalian neocortex.* Neuron, 2013. **77**(1): p. 19-34.
123. Hirota, Y. and K. Nakajima, *Control of neuronal migration and aggregation by reelin signaling in the developing cerebral cortex.* Frontiers in Cell and Developmental Biology, 2017. **5**: p. 40.
124. Kwan, K.Y., N. Šestan, and E. Anton, *Transcriptional co-regulation of neuronal migration and laminar identity in the neocortex.* Development, 2012. **139**(9): p. 1535-1546.
125. Gil-Sanz, C., et al., *Cajal-Retzius cells instruct neuronal migration by coincidence signaling between secreted and contact-dependent guidance cues.* Neuron, 2013. **79**(3): p. 461-477.
126. DeFelipe, J., et al., *New insights into the classification and nomenclature of cortical GABAergic interneurons.* Nature Reviews Neuroscience, 2013. **14**(3): p. 202-216.
127. Molyneaux, B.J., et al., *Neuronal subtype specification in the cerebral cortex.* Nature reviews neuroscience, 2007. **8**(6): p. 427-437.
128. Hevner, R.F., et al., *Beyond laminar fate: toward a molecular classification of cortical projection/pyramidal neurons.* Developmental neuroscience, 2003. **25**(2-4): p. 139-151.
129. Markram, H., et al., *Interneurons of the neocortical inhibitory system.* Nat Rev Neurosci, 2004. **5**(10): p. 793-807.

130. Marin, O., et al., *Guiding neuronal cell migrations.* Cold Spring Harb Perspect Biol, 2010. **2**(2): p. a001834.
131. Rakic, P., *The radial edifice of cortical architecture: From neuronal silhouettes to genetic engineering.* Brain research reviews, 2007. **55**(2): p. 204-219.
132. Tremblay, R., S. Lee, and B. Rudy, *GABAergic interneurons in the neocortex: from cellular properties to circuits.* Neuron, 2016. **91**(2): p. 260-292.
133. Polleux, F., et al., *Control of cortical interneuron migration by neurotrophins and PI3-kinase signaling.* Development, 2002. **129**(13): p. 3147-60.
134. Métin, C., et al., *Cell and molecular mechanisms involved in the migration of cortical interneurons.* European Journal of Neuroscience, 2006. **23**(4): p. 894-900.
135. López-Bendito, G., et al., *Chemokine signaling controls intracortical migration and final distribution of GABAergic interneurons.* Journal of Neuroscience, 2008. **28**(7): p. 1613-1624.
136. Rakic, P., *Neurons in rhesus monkey visual cortex: systematic relation between time of origin and eventual disposition.* Science, 1974. **183**(4123): p. 425-427.
137. Lavdas, A.A., et al., *The medial ganglionic eminence gives rise to a population of early neurons in the developing cerebral cortex.* Journal of Neuroscience, 1999. **19**(18): p. 7881-7888.
138. Ang, E.S., et al., *Four-dimensional migratory coordinates of GABAergic interneurons in the developing mouse cortex.* Journal of Neuroscience, 2003. **23**(13): p. 5805-5815.
139. Dent, E.W., S.L. Gupton, and F.B. Gertler, *The growth cone cytoskeleton in axon outgrowth and guidance.* Cold Spring Harbor perspectives in biology, 2011. **3**(3): p. a001800.
140. Flynn, K.C., et al., *ADF/cofilin-mediated actin retrograde flow directs neurite formation in the developing brain.* Neuron, 2012. **76**(6): p. 1091-1107.
141. Mitchison, T.J. and L.P. Cramer, *Actin-Based Cell Motility and Cell Locomotion.* Cell, 1996. **84**(3): p. 371-379.
142. Stossel, T.P., *On the crawling of animal cells.* SCIENCE-NEW YORK THEN WASHINGTON-, 1993. **260**: p. 1086-1086.
143. Zigmond, S.H., *Signal transduction and actin filament organization.* Current Opinion in Cell Biology, 1996. **8**(1): p. 66-73.
144. Elson, E.L., *Cellular mechanics as an indicator of cytoskeletal structure and function.* Annual review of biophysics and biophysical chemistry, 1988. **17**(1): p. 397-430.
145. Herrmann, H., et al., *Intermediate filaments: primary determinants of cell architecture and plasticity.* J Clin Invest, 2009. **119**(7): p. 1772-83.
146. Zhang, P., et al., *Tubulin cofactor A functions as a novel positive regulator of ccRCC progression, invasion and metastasis.* Int J Cancer, 2013. **133**(12): p. 2801-11.
147. Breuss, M. and D.A. Keays, *Microtubules and neurodevelopmental disease: the movers and the makers.* Adv Exp Med Biol, 2014. **800**: p. 75-96.
148. Kunda, P. and B. Baum, *The actin cytoskeleton in spindle assembly and positioning.* Trends in cell biology, 2009. **19**(4): p. 174-179.
149. Shitamukai, A., D. Konno, and F. Matsuzaki, *Oblique radial glial divisions in the developing mouse neocortex induce self-renewing progenitors outside the germinal zone that resemble primate outer subventricular zone progenitors.* Journal of Neuroscience, 2011. **31**(10): p. 3683-3695.
150. Mora-Bermúdez, F. and W.B. Huttner, *Novel insights into mammalian embryonic neural stem cell division: focus on microtubules.* Molecular Biology of the Cell, 2015. **26**(24): p. 4302-4306.
151. di Pietro, F., A. Echard, and X. Morin, *Regulation of mitotic spindle orientation: an integrated view.* EMBO reports, 2016: p. e201642292.
152. Mora-Bermúdez, F., F. Matsuzaki, and W.B. Huttner, *Specific polar subpopulations of astral microtubules control spindle orientation and symmetric neural stem cell division.* eLife, 2014. **3**: p. e02875.
153. Gavet, O. and J. Pines, *Activation of cyclin B1–Cdk1 synchronizes events in the nucleus and the cytoplasm at mitosis.* Journal of Cell Biology, 2010. **189**(2): p. 247-259.

154. Syred, H.M., et al., *Cell cycle regulation of microtubule interactomes: multi-layered regulation is critical for the interphase/mitosis transition.* Molecular & Cellular Proteomics, 2013. **12**(11): p. 3135-3147.
155. D'Avino, P.P., M.G. Giansanti, and M. Petronczki, *Cytokinesis in animal cells.* Cold Spring Harbor perspectives in biology, 2015. **7**(4): p. a015834.
156. Frade, J.M. and M.C. Ovejero-Benito, *Neuronal cell cycle: the neuron itself and its circumstances.* Cell Cycle, 2015. **14**(5): p. 712-720.
157. Petry, S. and R.D. Vale, *Microtubule nucleation at the centrosome and beyond.* Nature cell biology, 2015. **17**(9): p. 1089-1093.
158. Mogensen, M. and J. Tucker, *Evidence for microtubule nucleation at plasma membrane-associated sites in Drosophila.* Journal of cell science, 1987. **88**(1): p. 95-107.
159. Janson, M.E., et al., *Efficient formation of bipolar microtubule bundles requires microtubule-bound γ-tubulin complexes.* The Journal of Cell Biology, 2005. **169**(2): p. 297-308.
160. Heald, R., et al., *Self-organization of microtubules into bipolar spindles around artificial chromosomes in Xenopus egg extracts.* Nature, 1996. **382**(6590): p. 420-425.
161. Chabin-Brion, K., et al., *The Golgi Complex Is a Microtubule-organizing Organelle.* Molecular Biology of the Cell, 2001. **12**(7): p. 2047-2060.
162. Laan, L., et al., *Cortical dynein controls microtubule dynamics to generate pulling forces that position microtubule asters.* Cell, 2012. **148**(3): p. 502-514.
163. Good, M.C., et al., *Cytoplasmic volume modulates spindle size during embryogenesis.* Science, 2013. **342**(6160): p. 856-860.
164. Théry, M., et al., *Experimental and theoretical study of mitotic spindle orientation.* Nature, 2007. **447**(7143): p. 493-496.
165. Cunningham, L.A. and R.A. Kahn, *Cofactor D functions as a centrosomal protein and is required for the recruitment of the gamma-tubulin ring complex at centrosomes and organization of the mitotic spindle.* J Biol Chem, 2008. **283**(11): p. 7155-65.
166. Kotak, S., C. Busso, and P. Gönczy, *Cortical dynein is critical for proper spindle positioning in human cells.* J Cell Biol, 2012. **199**(1): p. 97-110.
167. Lancaster, M.A. and J.A. Knoblich, *Spindle orientation in mammalian cerebral cortical development.* Current opinion in neurobiology, 2012. **22**(5): p. 737-746.
168. Feng, Y. and C.A. Walsh, *Mitotic spindle regulation by Nde1 controls cerebral cortical size.* Neuron, 2004. **44**(2): p. 279-293.
169. Inoue, Y.H., et al., *Mutations in orbit/mast reveal that the central spindle is comprised of two microtubule populations, those that initiate cleavage and those that propagate furrow ingression.* The Journal of cell biology, 2004. **166**(1): p. 49-60.
170. Dechant, R. and M. Glotzer, *Centrosome separation and central spindle assembly act in redundant pathways that regulate microtubule density and trigger cleavage furrow formation.* Developmental cell, 2003. **4**(3): p. 333-344.
171. Mishima, M., S. Kaitna, and M. Glotzer, *Central spindle assembly and cytokinesis require a kinesin-like protein/RhoGAP complex with microtubule bundling activity.* Developmental cell, 2002. **2**(1): p. 41-54.
172. Zhai, Y., et al., *Microtubule dynamics at the G2/M transition: abrupt breakdown of cytoplasmic microtubules at nuclear envelope breakdown and implications for spindle morphogenesis.* The Journal of Cell Biology, 1996. **135**(1): p. 201-214.
173. Jantsch-Plunger, V., et al., *CYK-4: A Rho family gtpase activating protein (GAP) required for central spindle formation and cytokinesis.* The Journal of cell biology, 2000. **149**(7): p. 1391-1404.
174. Saxton, W.M. and J.R. McIntosh, *Interzone microtubule behavior in late anaphase and telophase spindles.* The Journal of Cell Biology, 1987. **105**(2): p. 875-886.
175. Paweletz, N., *Walther Flemming: pioneer of mitosis research.* Nature reviews Molecular cell biology, 2001. **2**(1): p. 72-75.

176. Hindley, C. and A. Philpott, *Co-ordination of cell cycle and differentiation in the developing nervous system.* Biochemical Journal, 2012. **444**(3): p. 375-382.
177. Ito, K. and T. Suda, *Metabolic requirements for the maintenance of self-renewing stem cells.* Nature reviews Molecular cell biology, 2014. **15**(4): p. 243-256.
178. Van Blerkom, J. *Mitochondria in early mammalian development*. in *Seminars in cell & developmental biology*. 2009. Elsevier.
179. Mishra, P. and D.C. Chan, *Metabolic regulation of mitochondrial dynamics.* Journal of Cell Biology, 2016. **212**(4): p. 379-387.
180. Mishra, P. and D.C. Chan, *Mitochondrial dynamics and inheritance during cell division, development and disease.* Nature reviews Molecular cell biology, 2014. **15**(10): p. 634-646.
181. Moore, A.S. and E.L. Holzbaur, *Mitochondrial-cytoskeletal interactions: dynamic associations that facilitate network function and remodeling.* Current opinion in physiology, 2018. **3**: p. 94-100.
182. Anesti, V. and L. Scorrano, *The relationship between mitochondrial shape and function and the cytoskeleton.* Biochimica et Biophysica Acta (BBA)-Bioenergetics, 2006. **1757**(5-6): p. 692-699.
183. Antico Arciuch, V.G., et al., *Mitochondrial regulation of cell cycle and proliferation.* Antioxidants & redox signaling, 2012. **16**(10): p. 1150-1180.
184. Liu, X., et al., *Mitochondrial 'kiss-and-run': interplay between mitochondrial motility and fusion–fission dynamics.* The EMBO journal, 2009. **28**(20): p. 3074-3089.
185. Chan, D.C., *Mitochondrial fusion and fission in mammals.* Annu. Rev. Cell Dev. Biol., 2006. **22**: p. 79-99.
186. Youle, R.J. and A.M. Van Der Bliek, *Mitochondrial fission, fusion, and stress.* Science, 2012. **337**(6098): p. 1062-1065.
187. Brown, G.C., et al., *Mitochondrial fission and fusion.* Essays in biochemistry, 2010. **47**: p. 85-98.
188. Smirnova, E., et al., *Dynamin-related protein Drp1 is required for mitochondrial division in mammalian cells.* Molecular biology of the cell, 2001. **12**(8): p. 2245-2256.
189. Zheng, X., et al., *Metabolic reprogramming during neuronal differentiation from aerobic glycolysis to neuronal oxidative phosphorylation.* eLife, 2016. **5**: p. e13374.
190. Horbay, R. and R. Bilyy, *Mitochondrial dynamics during cell cycling.* Apoptosis, 2016. **21**(12): p. 1327-1335.
191. Mitra, K., et al., *A hyperfused mitochondrial state achieved at G1–S regulates cyclin E buildup and entry into S phase.* Proceedings of the National Academy of Sciences, 2009. **106**(29): p. 11960-11965.
192. Salazar-Roa, M. and M. Malumbres, *Fueling the Cell Division Cycle.* Trends Cell Biol, 2017. **27**(1): p. 69-81.
193. Melser, S., et al., *Rheb regulates mitophagy induced by mitochondrial energetic status.* Cell metabolism, 2013. **17**(5): p. 719-730.
194. Bartolák-Suki, E., et al., *Regulation of mitochondrial structure and dynamics by the cytoskeleton and mechanical factors.* International journal of molecular sciences, 2017. **18**(8): p. 1812.
195. Lawrence, E.J. and C.A. Mandato, *Mitochondria localize to the cleavage furrow in mammalian cytokinesis.* PLoS One, 2013. **8**(8): p. e72886.
196. Wang, Z., et al., *Cyclin B1/Cdk1 coordinates mitochondrial respiration for cell-cycle G2/M progression.* Developmental cell, 2014. **29**(2): p. 217-232.
197. Zunino, R., et al., *Translocation of SenP5 from the nucleoli to the mitochondria modulates DRP1-dependent fission during mitosis.* Journal of Biological Chemistry, 2009. **284**(26): p. 17783-17795.
198. Ferreira-da-Silva, A., et al., *Mitochondrial Dynamics Protein Drp1 Is Overexpressed in Oncocytic Thyroid Tumors and Regulates Cancer Cell Migration.* PLOS ONE, 2015. **10**(3): p. e0122308.

199. Miyazaki, T. and S. Arai, *Two distinct controls of mitotic cdk1/cyclin B1 activity requisite for cell growth prior to cell division.* Cell Cycle, 2007. **6**(12): p. 1418-1424.
200. Sakamaki, T., et al., *Cyclin D1 determines mitochondrial function in vivo.* Mol Cell Biol, 2006. **26**(14): p. 5449-69.
201. Marcussen, M. and P.J. Larsen, *Cell cycle-dependent regulation of cellular ATP concentration, and depolymerization of the interphase microtubular network induced by elevated cellular ATP concentration in whole fibroblasts.* Cell Motility, 1996. **35**(2): p. 94-99.
202. Katajisto, P., et al., *Asymmetric apportioning of aged mitochondria between daughter cells is required for stemness.* Science, 2015. **348**(6232): p. 340-343.
203. Sauer, H., M. Wartenberg, and J. Hescheler, *Reactive oxygen species as intracellular messengers during cell growth and differentiation.* Cellular physiology and biochemistry, 2001. **11**(4): p. 173-186.
204. Oswald, M.C., et al., *Regulation of neuronal development and function by ROS.* FEBS letters, 2018. **592**(5): p. 679-691.
205. Beckervordersandforth, R., et al., *Role of mitochondrial metabolism in the control of early lineage progression and aging phenotypes in adult hippocampal neurogenesis.* Neuron, 2017. **93**(3): p. 560-573. e6.
206. Cabello-Rivera, D., et al., *Mitochondrial complex I function is essential for neural stem/progenitor cells proliferation and differentiation.* Frontiers in neuroscience, 2019. **13**: p. 664.
207. Su, Y., et al., *STAT3 Regulates Mouse Neural Progenitor Proliferation and Differentiation by Promoting Mitochondrial Metabolism.* Frontiers in Cell and Developmental Biology, 2020. **8**.
208. van den Ameele, J. and A.H. Brand, *Neural stem cell temporal patterning and brain tumour growth rely on oxidative phosphorylation.* Elife, 2019. **8**: p. e47887.
209. Englund, C., et al., *Pax6, Tbr2, and Tbr1 are expressed sequentially by radial glia, intermediate progenitor cells, and postmitotic neurons in developing neocortex.* Journal of Neuroscience, 2005. **25**(1): p. 247-251.
210. Lv, X., et al., *TBR2 coordinates neurogenesis expansion and precise microcircuit organization via Protocadherin 19 in the mammalian cortex.* Nature communications, 2019. **10**(1): p. 1-15.
211. Khacho, M., et al., *Mitochondrial dysfunction underlies cognitive defects as a result of neural stem cell depletion and impaired neurogenesis.* Human molecular genetics, 2017. **26**(17): p. 3327-3341.
212. Mohr, J. and K. Mageröy, *Sex-linked deafness of a possibly new type.* Acta genetica et statistica medica, 1960: p. 54-62.
213. Züchner, S., et al., *Mutations in the mitochondrial GTPase mitofusin 2 cause Charcot-Marie-Tooth neuropathy type 2A.* Nature genetics, 2004. **36**(5): p. 449-451.
214. Thiselton, D.L., et al., *A frameshift mutation in exoná28 of the OPA1 gene explains the high prevalence of dominant optic atrophy in the Danish population: evidence for a founder effect.* Human genetics, 2001. **109**(5): p. 498-502.
215. Lukas, J., C. Lukas, and J. Bartek, *Mammalian cell cycle checkpoints: signalling pathways and their organization in space and time.* DNA repair, 2004. **3**(8-9): p. 997-1007.
216. Barnum, K.J. and M.J. O'Connell, *Cell cycle regulation by checkpoints*, in *Cell Cycle Control*. 2014, Springer. p. 29-40.
217. Gascón, S., et al., *Identification and successful negotiation of a metabolic checkpoint in direct neuronal reprogramming.* Cell stem cell, 2016. **18**(3): p. 396-409.
218. Stark, G.R. and W.R. Taylor, *Analyzing the G2/M checkpoint*, in *Checkpoint Controls and Cancer*. 2004, Springer. p. 51-82.
219. Sancar, A., et al., *Molecular mechanisms of mammalian DNA repair and the DNA damage checkpoints.* Annual review of biochemistry, 2004. **73**(1): p. 39-85.
220. Liu, L., et al., *The cell cycle in stem cell proliferation, pluripotency and differentiation.* Nature cell biology, 2019. **21**(9): p. 1060-1067.

221. Ruijtenberg, S. and S. van den Heuvel, *Coordinating cell proliferation and differentiation: Antagonism between cell cycle regulators and cell type-specific gene expression.* Cell cycle, 2016. **15**(2): p. 196-212.
222. Honda, R., et al., *The structure of cyclin E1/CDK2: implications for CDK2 activation and CDK2-independent roles.* The EMBO journal, 2005. **24**(3): p. 452-463.
223. Narasimha, A.M., et al., *Cyclin D activates the Rb tumor suppressor by mono-phosphorylation.* Elife, 2014. **3**: p. e02872.
224. Topacio, B.R., et al., *Cyclin D-Cdk4, 6 drives cell-cycle progression via the retinoblastoma protein's C-terminal helix.* Molecular cell, 2019. **74**(4): p. 758-770. e4.
225. Hardwick, L.J.A., et al., *Cell cycle regulation of proliferation versus differentiation in the central nervous system.* Cell and Tissue Research, 2015. **359**: p. 187-200.
226. Cappell, S.D., et al., *Irreversible APCCdh1 inactivation underlies the point of no return for cell-cycle entry.* Cell, 2016. **166**(1): p. 167-180.
227. Malumbres, M., *Cyclin-dependent kinases.* Genome biology, 2014. **15**(6): p. 1-10.
228. Malumbres, M. and M. Barbacid, *Mammalian cyclin-dependent kinases.* Trends in biochemical sciences, 2005. **30**(11): p. 630-641.
229. Gavet, O. and J. Pines, *Progressive activation of CyclinB1-Cdk1 coordinates entry to mitosis.* Developmental cell, 2010. **18**(4): p. 533-543.
230. Lee, S., et al., *Human mitochondrial Fis1 links to cell cycle regulators at G2/M transition.* Cellular and molecular life sciences, 2014. **71**(4): p. 711-725.
231. Kaplon, J., L. van Dam, and D. Peeper, *Two-way communication between the metabolic and cell cycle machineries: the molecular basis.* Cell Cycle, 2015. **14**(13): p. 2022-2032.
232. Tchakarska, G., et al., *Cyclin D1 inhibits mitochondrial activity in B cells.* Cancer research, 2011. **71**(5): p. 1690-1699.
233. Vega-Naredo, I., et al., *Mitochondrial metabolism directs stemness and differentiation in P19 embryonal carcinoma stem cells.* Cell Death & Differentiation, 2014. **21**(10): p. 1560-1574.
234. Godin, J.D., et al., *Huntingtin is required for mitotic spindle orientation and mammalian neurogenesis.* Neuron, 2010. **67**(3): p. 392-406.
235. Yingling, J., et al., *Neuroepithelial stem cell proliferation requires LIS1 for precise spindle orientation and symmetric division.* Cell, 2008. **132**(3): p. 474-486.
236. Sakakibara, A. and Y. Hatanaka, *Neuronal polarization in the developing cerebral cortex.* Frontiers in neuroscience, 2015. **9**: p. 116.
237. Evsyukova, I., C. Plestant, and E. Anton, *Integrative mechanisms of oriented neuronal migration in the developing brain.* Annual review of cell and developmental biology, 2013. **29**: p. 299-353.
238. Bellion, A., et al., *Nucleokinesis in tangentially migrating neurons comprises two alternating phases: forward migration of the Golgi/centrosome associated with centrosome splitting and myosin contraction at the rear.* Journal of Neuroscience, 2005. **25**(24): p. 5691-5699.
239. Xie, Z., et al., *Serine 732 phosphorylation of FAK by Cdk5 is important for microtubule organization, nuclear movement, and neuronal migration.* Cell, 2003. **114**(4): p. 469-482.
240. Hevner, R.F., et al., *Tbr1 regulates differentiation of the preplate and layer 6.* Neuron, 2001. **29**(2): p. 353-366.
241. Lennon, M.J., et al., *Bcl11b—A Critical Neurodevelopmental Transcription Factor—Roles in Health and Disease.* Frontiers in cellular neuroscience, 2017. **11**: p. 89.
242. Paul, V., et al., *Scratch2 modulates neurogenesis and cell migration through antagonism of bHLH proteins in the developing neocortex.* Cerebral Cortex, 2014. **24**(3): p. 754-772.
243. Ka, M. and W.Y. Kim, *Microtubule-Actin Crosslinking Factor 1 Is Required for Dendritic Arborization and Axon Outgrowth in the Developing Brain.* Mol Neurobiol, 2016. **53**(9): p. 6018-6032.

244. Sarma, T., et al., *Activation of microtubule dynamics increases neuronal growth via the nerve growth factor (NGF)-and Gαs-mediated signaling pathways.* Journal of Biological Chemistry, 2015. **290**(16): p. 10045-10056.
245. Gardiner, J., R. Overall, and J. Marc, *The microtubule cytoskeleton acts as a key downstream effector of neurotransmitter signaling.* Synapse, 2011. **65**(3): p. 249-256.
246. Maday, S., et al., *Axonal transport: cargo-specific mechanisms of motility and regulation.* Neuron, 2014. **84**(2): p. 292-309.
247. Millecamps, S. and J.-P. Julien, *Axonal transport deficits and neurodegenerative diseases.* Nature Reviews Neuroscience, 2013. **14**(3): p. 161-176.
248. Sainath, R. and G. Gallo, *Cytoskeletal and signaling mechanisms of neurite formation.* Cell and tissue research, 2015. **359**(1): p. 267-278.
249. Lu, W., et al., *Initial neurite outgrowth in Drosophila neurons is driven by kinesin-powered microtubule sliding.* Current Biology, 2013. **23**(11): p. 1018-1023.
250. Dehmelt, L., et al., *A microtubule-based, dynein-dependent force induces local cell protrusions: Implications for neurite initiation.* Brain cell biology, 2006. **35**(1): p. 39-56.
251. Kapitein, L.C. and C.C. Hoogenraad, *Which way to go? Cytoskeletal organization and polarized transport in neurons.* Molecular and Cellular Neuroscience, 2011. **46**(1): p. 9-20.
252. Witte, H., D. Neukirchen, and F. Bradke, *Microtubule stabilization specifies initial neuronal polarization.* Journal of cell biology, 2008. **180**(3): p. 619-632.
253. van Beuningen, S.F., et al., *TRIM46 controls neuronal polarity and axon specification by driving the formation of parallel microtubule arrays.* Neuron, 2015. **88**(6): p. 1208-1226.
254. Yau, K.W., et al., *Microtubule minus-end binding protein CAMSAP2 controls axon specification and dendrite development.* Neuron, 2014. **82**(5): p. 1058-1073.
255. Jiang, K., et al., *Microtubule minus-end stabilization by polymerization-driven CAMSAP deposition.* Developmental cell, 2014. **28**(3): p. 295-309.
256. Dehmelt, L. and S. Halpain, *The MAP2/Tau family of microtubule-associated proteins.* Genome biology, 2004. **6**(1): p. 204.
257. Hoogenraad, C.C. and F. Bradke, *Control of neuronal polarity and plasticity–a renaissance for microtubules?* Trends in cell biology, 2009. **19**(12): p. 669-676.
258. Suter, D.M. and K.E. Miller, *The emerging role of forces in axonal elongation.* Progress in neurobiology, 2011. **94**(2): p. 91-101.
259. Akhmanova, A. and M.O. Steinmetz, *Microtubule +TIPs at a glance.* Journal of Cell Science, 2010. **123**(20): p. 3415-3419.
260. Merriam, E.B., et al., *Synaptic regulation of microtubule dynamics in dendritic spines by calcium, F-actin, and drebrin.* Journal of Neuroscience, 2013. **33**(42): p. 16471-16482.
261. Jaworski, J., et al., *Dynamic microtubules regulate dendritic spine morphology and synaptic plasticity.* Neuron, 2009. **61**(1): p. 85-100.
262. Hirai, S.-i., et al., *Axon formation in neocortical neurons depends on stage-specific regulation of microtubule stability by the dual leucine zipper kinase–c-jun N-terminal kinase pathway.* Journal of Neuroscience, 2011. **31**(17): p. 6468-6480.
263. Armijo-Weingart, L. and G. Gallo, *It takes a village to raise a branch: cellular mechanisms of the initiation of axon collateral branches.* Molecular and Cellular Neuroscience, 2017. **84**: p. 36-47.
264. Yu, W., et al., *The microtubule-severing proteins spastin and katanin participate differently in the formation of axonal branches.* Molecular biology of the cell, 2008. **19**(4): p. 1485-1498.
265. Dent, E.W., *Of microtubules and memory: implications for microtubule dynamics in dendrites and spines.* Molecular biology of the cell, 2017. **28**(1): p. 1-8.
266. Yau, K.W., et al., *Dendrites in vitro and in vivo contain microtubules of opposite polarity and axon formation correlates with uniform plus-end-out microtubule orientation.* Journal of Neuroscience, 2016. **36**(4): p. 1071-1085.

267. Twelvetrees, Alison E., et al., *The Dynamic Localization of Cytoplasmic Dynein in Neurons Is Driven by Kinesin-1.* Neuron, 2016. **90**(5): p. 1000-1015.
268. Gu, J., B.L. Firestein, and J.Q. Zheng, *Microtubules in dendritic spine development.* Journal of Neuroscience, 2008. **28**(46): p. 12120-12124.
269. Swiech, L., et al., *CLIP-170 and IQGAP1 cooperatively regulate dendrite morphology.* Journal of Neuroscience, 2011. **31**(12): p. 4555-4568.
270. Stepanova, T., et al., *Visualization of microtubule growth in cultured neurons via the use of EB3-GFP (end-binding protein 3-green fluorescent protein).* Journal of Neuroscience, 2003. **23**(7): p. 2655-2664.
271. Gordon-Weeks, P.R., *The role of the drebrin/EB3/Cdk5 pathway in dendritic spine plasticity, implications for Alzheimer's disease.* Brain research bulletin, 2016. **126**: p. 293-299.
272. McVicker, D.P., et al., *Transport of a kinesin-cargo pair along microtubules into dendritic spines undergoing synaptic plasticity.* Nature communications, 2016. **7**(1): p. 1-13.
273. Li, Z., et al., *The importance of dendritic mitochondria in the morphogenesis and plasticity of spines and synapses.* Cell, 2004. **119**(6): p. 873-887.
274. Miller, K.E. and M.P. Sheetz, *Axonal mitochondrial transport and potential are correlated.* Journal of cell science, 2004. **117**(13): p. 2791-2804.
275. Morris, R. and P. Hollenbeck, *Axonal transport of mitochondria along microtubules and F-actin in living vertebrate neurons.* The Journal of cell biology, 1995. **131**(5): p. 1315-1326.
276. MacAskill, A.F. and J.T. Kittler, *Control of mitochondrial transport and localization in neurons.* Trends in cell biology, 2010. **20**(2): p. 102-112.
277. Sheng, Z.-H. and Q. Cai, *Mitochondrial transport in neurons: impact on synaptic homeostasis and neurodegeneration.* Nature Reviews Neuroscience, 2012. **13**(2): p. 77-93.
278. Son, G. and J. Han, *Roles of mitochondria in neuronal development.* BMB reports, 2018. **51**(11): p. 549.
279. Lin, M.-Y. and Z.-H. Sheng, *Regulation of mitochondrial transport in neurons.* Experimental cell research, 2015. **334**(1): p. 35-44.
280. Chada, S.R. and P.J. Hollenbeck, *Nerve growth factor signaling regulates motility and docking of axonal mitochondria.* Current Biology, 2004. **14**(14): p. 1272-1276.
281. Chen, Y.-M., C. Gerwin, and Z.-H. Sheng, *Dynein light chain LC8 regulates syntaphilin-mediated mitochondrial docking in axons.* Journal of Neuroscience, 2009. **29**(30): p. 9429-9438.
282. Kang, J.-S., et al., *Docking of axonal mitochondria by syntaphilin controls their mobility and affects short-term facilitation.* Cell, 2008. **132**(1): p. 137-148.
283. Karaca, E., et al., *Genes that Affect Brain Structure and Function Identified by Rare Variant Analyses of Mendelian Neurologic Disease.* Neuron, 2015. **88**(3): p. 499-513.
284. Castellani, R., et al., *Role of mitochondrial dysfunction in Alzheimer's disease.* Journal of neuroscience research, 2002. **70**(3): p. 357-360.
285. Dawson, T.M. and V.L. Dawson, *Molecular pathways of neurodegeneration in Parkinson's disease.* Science, 2003. **302**(5646): p. 819-822.
286. Baas, P.W., et al., *Stability properties of neuronal microtubules.* Cytoskeleton, 2016.
287. Keays, D.A., et al., *Mutations in α-tubulin cause abnormal neuronal migration in mice and lissencephaly in humans.* Cell, 2007. **128**(1): p. 45-57.
288. Jaglin, X.H., et al., *Mutations in the β-tubulin gene TUBB2B result in asymmetrical polymicrogyria.* Nature genetics, 2009. **41**(6): p. 746-752.
289. Abdollahi, M.R., et al., *Mutation of the variant alpha-tubulin TUBA8 results in polymicrogyria with optic nerve hypoplasia.* Am J Hum Genet, 2009. **85**(5): p. 737-44.
290. Pizzino, A., et al., *TUBB4A de novo mutations cause isolated hypomyelination.* Neurology, 2014. **83**(10): p. 898-902.
291. Bahi-Buisson, N. and M. Cavallin, *Tubulinopathies overview.* 2016.
292. Bahi-Buisson, N., et al., *The wide spectrum of tubulinopathies: what are the key features for the diagnosis?* Brain, 2014. **137**(Pt 6): p. 1676-700.

293. Martín-Benito, J., et al., *Structure of eukaryotic prefoldin and of its complexes with unfolded actin and the cytosolic chaperonin CCT.* The EMBO journal, 2002. **21**(23): p. 6377-6386.
294. Dekker, C., et al., *The interaction network of the chaperonin CCT.* Embo j, 2008. **27**(13): p. 1827-39.
295. Muñoz, I.G., et al., *Crystal structure of the open conformation of the mammalian chaperonin CCT in complex with tubulin.* Nature structural & molecular biology, 2011. **18**(1): p. 14-19.
296. Reissmann, S., et al., *A gradient of ATP affinities generates an asymmetric power stroke driving the chaperonin TRIC/CCT folding cycle.* Cell Rep, 2012. **2**(4): p. 866-77.
297. Lopez-Fanarraga, M., et al., *Review: postchaperonin tubulin folding cofactors and their role in microtubule dynamics.* Journal of structural biology, 2001. **135**(2): p. 219-229.
298. Carranza, G., et al., *Autoinhibition of TBCB regulates EB1-mediated microtubule dynamics.* Cellular and Molecular Life Sciences, 2013. **70**(2): p. 357-371.
299. Francis, J.W., et al., *A Trimer Consisting of the Tubulin-specific Chaperone D (TBCD), Regulatory GTPase ARL2, and β-Tubulin Is Required for Maintaining the Microtubule Network.* Journal of Biological Chemistry, 2017. **292**(10): p. 4336-4349.
300. Gardner, M.K., M. Zanic, and J. Howard, *Microtubule Catastrophe and Rescue.* Current opinion in cell biology, 2013. **25**(1): p. 14-22.
301. Nithianantham, S., et al., *Tubulin cofactors and Arl2 are cage-like chaperones that regulate the soluble αβ-tubulin pool for microtubule dynamics.* Elife, 2015. **4**: p. e08811.
302. Bhamidipati, A., S.A. Lewis, and N.J. Cowan, *ADP ribosylation factor-like protein 2 (Arl2) regulates the interaction of tubulin-folding cofactor D with native tubulin.* J Cell Biol, 2000. **149**(5): p. 1087-96.
303. Martín, L., et al., *Tubulin folding cofactor D is a microtubule destabilizing protein.* FEBS letters, 2000. **470**(1): p. 93-95.
304. Serna, M., et al., *The structure of the complex between α-tubulin, TBCE and TBCB reveals a tubulin dimer dissociation mechanism.* J Cell Sci, 2015. **128**(9): p. 1824-1834.
305. Chen, K., et al., *Arl2-and Msps-dependent microtubule growth governs asymmetric division.* J Cell Biol, 2016. **212**(6): p. 661-676.
306. Francis, J.W., et al., *Nucleotide Binding to ARL2 in the TBCD·ARL2·β-Tubulin Complex Drives Conformational Changes in β-Tubulin.* Journal of Molecular Biology, 2017. **429**(23): p. 3696-3716.
307. Parvari, R., et al., *Mutation of TBCE causes hypoparathyroidism–retardation–dysmorphism and autosomal recessive Kenny–Caffey syndrome.* Nature genetics, 2002. **32**(3): p. 448-452.
308. Wang, W., et al., *Gigaxonin Interacts with Tubulin Folding Cofactor B and Controls Its Degradation through the Ubiquitin-Proteasome Pathway.* Current Biology, 2005. **15**(22): p. 2050-2055.
309. Bartolini, F., et al., *Functional overlap between retinitis pigmentosa 2 protein and the tubulin-specific chaperone cofactor C.* J Biol Chem, 2002. **277**(17): p. 14629-34.
310. Campo, R., et al., *A 14 kDa release factor is involved in GTP-dependent β-tubulin folding.* FEBS Letters, 1994. **353**(2): p. 162-166.
311. Gao, Y., et al., *A novel cochaperonin that modulates the ATPase activity of cytoplasmic chaperonin.* Journal of Cell Biology, 1994. **125**(5): p. 989-996.
312. Melki, R., et al., *Cofactor A is a molecular chaperone required for beta-tubulin folding: functional and structural characterization.* Biochemistry, 1996. **35**(32): p. 10422-35.
313. Guasch, A., et al., *Three-dimensional structure of human tubulin chaperone cofactor A.* J Mol Biol, 2002. **318**(4): p. 1139-49.
314. Fanarraga, M., et al., *Regulated expression of p14 (cofactor A) during spermatogenesis.* Cytoskeleton, 1999. **43**(3): p. 243-254.
315. Radcliffe, P.A., M.A. Garcia, and T. Toda, *The cofactor-dependent pathways for alpha- and beta-tubulins in microtubule biogenesis are functionally different in fission yeast.* Genetics, 2000. **156**(1): p. 93-103.

316. Zabala, J.C. and N.J. Cowan, *Tubulin dimer formation via the release of alpha- and beta-tubulin monomers from multimolecular complexes.* Cell Motil Cytoskeleton, 1992. **23**(3): p. 222-30.
317. Garcia-Mayoral, M.F., et al., *The solution structure of the N-terminal domain of human tubulin binding cofactor C reveals a platform for tubulin interaction.* PLoS One, 2011. **6**(10): p. e25912.
318. Scheffzek, K., et al., *The Ras-RasGAP complex: structural basis for GTPase activation and its loss in oncogenic Ras mutants.* Science, 1997. **277**(5324): p. 333-8.
319. Barrack, K.L., et al., *Crystal structure of the C-terminal domain of tubulin-binding cofactor C from Leishmania major.* Molecular and Biochemical Parasitology, 2015. **201**(1): p. 26-30.
320. Hage-Sleiman, R., et al., *Tubulin binding cofactor C (TBCC) suppresses tumor growth and enhances chemosensitivity in human breast cancer cells.* BMC Cancer, 2010. **10**: p. 135.
321. Goncalves, J., et al., *TBCCD1, a new centrosomal protein, is required for centrosome and Golgi apparatus positioning.* EMBO Rep, 2010. **11**(3): p. 194-200.
322. Steinmetz, M.O. and A. Akhmanova, *Capturing protein tails by CAP-Gly domains.* Trends in biochemical sciences, 2008. **33**(11): p. 535-545.
323. Kuh, G.F., et al., *Tubulin-binding cofactor B is a direct interaction partner of the dynactin subunit p150Glued.* Cell and tissue research, 2012. **350**(1): p. 13-26.
324. Kortazar, D., et al., *Role of cofactors B (TBCB) and E (TBCE) in tubulin heterodimer dissociation.* Experimental cell research, 2007. **313**(3): p. 425-436.
325. Tian, G., S. Thomas, and N.J. Cowan, *Effect of TBCD and its regulatory interactor Arl2 on tubulin and microtubule integrity.* Cytoskeleton, 2010. **67**(11): p. 706-714.
326. Shern, J.F., et al., *Cytosolic Arl2 is complexed with cofactor D and protein phosphatase 2A.* Journal of Biological Chemistry, 2003. **278**(42): p. 40829-40836.
327. Fedyanina, O.S., et al., *Chromosome segregation in fission yeast with mutations in the tubulin folding cofactor D.* Current genetics, 2006. **50**(5): p. 281-294.
328. Mayer, U., et al., *Mutations in the pilz group genes disrupt the microtubule cytoskeleton and uncouple cell cycle progression from cell division in Arabidopsis embryo and endosperm.* European journal of cell biology, 1999. **78**(2): p. 100-108.
329. Grishchuk, E.L., J.L. Howe, and J.R. McIntosh, *A screen for genes involved in the anaphase proteolytic pathway identifies tsm1+, a novel Schizosaccharomyces pombe gene important for microtubule integrity.* Genetics, 1998. **149**(3): p. 1251-1264.
330. Ikeda, T., et al., *TBCD may be a causal gene in progressive neurodegenerative encephalopathy with atypical infantile spinal muscular atrophy.* Journal of Human Genetics, 2016.

Chapter 2 General Materials and Methods

2.1 Reagents

All chemicals, reagents and media were purchased from Sigma-Aldrich, unless indicated otherwise. Primary antibodies to αβ-Tubulin, β-actin, Ki67, cyclin D1, p70S6K and Total S6, as well as a Glycolysis Antibody Sampler Kit to detect Pkm1/2, Pkm2, Hexokinase 1, Hexokinase 2 and GAPDH were all obtained from Cell Signalling Technology, (Beverly, MA, USA). Additionally, rabbit anti-Sox2, anti-Synapsin I and mouse anti-NeuN were obtained from Merck Millipore (Burlington, MA, USA), while rabbit anti-Pax6 and anti-TBCD were obtained from BioLegened (San Diego, CA, USA) and Protein Tech (Chicago, IL, USA) respectively. Secondary antibodies consisted of horseradish peroxidase conjugated goat anti-mouse or anti-rabbit antibodies (Dako Cytomation, Carpinteria, CA, USA). Mammalian expression plasmid constructs encoding either full-length human wild type (WT) or mutant TBCD cDNA, and shRNAs containing a GFP cassette, that were consisting of either scrambled shRNA or the TBCD shRNA3 (denoted sh3) (5' CAGGCTTGTCACAGACTATCTGGATGAGA 3') that had been previously validated in the pcDNA3 vector (Invitrogen, Inc.) [1] were obtained and re-sequenced. Stock solutions of 100μM Exendin-4 (E7144) were prepared by pre-dilution in sterile water and stored at -20°C.

2.2 Plasmid preparation and isolation

Transformation of competent *Escherichia coli* (C3040H), obtained from New England Biolabs (Ipswich, MA, USA), was carried out by adding 1-2μL of the plasmid DNA (at a concentration of 100pg-100ng) to 50μL of cells in pre-chilled tubes, and carefully flicked to mix. Cells were incubated on ice for 30 minutes prior to incubation for 45 seconds in a 42°C water bath and then rested on ice for a further 2 minutes. Following this 250μL of Lysogeny broth (LB) (1% (w/v) Tryptone, 0.5% (w/v) Yeast Extract, 1% (w/v) NaCl, pH 7.5 (NaOH), 1.5% (w/v) bacteriological agar) media without antibiotics, mixed and gently spread onto LB agar plates supplemented with ampicillin (100ug/ml ampicillin) and incubated overnight (O/N) at 37°C. After O/N incubation single colonies were placed in 5-10mL of LB supplemented with ampicillin, and incubated on a shaker at 200 revolutions per minute (rpm) at 37°C for 12-16 hours. Cells were then harvested at 10,000g's for 1 minute and Plasmid DNA extracted using the Qiagen Plasmid Mini Kit (12125) (Hilden, Germany) according to the manufacturer's

instructions. Following extraction, the DNA was eluted in 50µL of elution buffer. For long term storage of plasmids transformed *E.coli* were grown O/N in the presence of antibiotics, spun down at 3,000 rpm for 10 minutes, resuspended and gently mixed in culture media containing 20% (v/v) sterile glycerol prior to snap freezing in liquid nitrogen and storage at -80°C.

2.3 Cell culture

The P19 Embryonic Carcinoma (P19ECs) cell line was seeded and cultured overnight in different formats according to the requirement for subsequent measurements. Cells were maintained in Dulbecco's modified Eagle's medium (DMEM) high glucose media (4500mg/L), with 1% v/v L-Glutamine, supplemented with 5% (v/v) Foetal bovine serum (FBS) (Sigma-Aldrich USA), at 37^0C in a humidified atmosphere of 95% air and 5% CO_2 in accordance with previous findings [2, 3]. For splitting, seeding and sub-culturing, P19ECs were required to be at ~75% confluency. Cells were then washed with phosphate buffer saline (PBS), without calcium, magnesium, and phenol red, and incubated at 37°C for 4-5 minutes in 0.25% Trypsin with EDTA 0.53mM (pre warmed at 37°C). Complete media, with a volume equal to or greater than the volume of trypsin, was added to stop the enzymatic activity of trypsin, and the cells transferred to a 15mL tube for a 5 minutes centrifugation at 300 x *g* at room temperature. Next, the supernatant was discarded and the cells were resuspended in a fresh volume of complete media, and aliquots taken for counting using the 0.4% Trypan Blue dye exclusion test. Cells were cultured overnight in various densities and plate formats, in accordance with the subsequent measurements.

Cells were then co-transfected with shRNA or sh3, and a mammalian expression plasmid construct encoding either a full-length human WT, A475T or A586V mutant TBCD. Transfections were performed using Lipofectamine 2000 (Thermo Fisher Scientific San Jose, CA, USA) in accordance with the manufacturer's protocol, with equal quantities of expression plasmids for each condition and collected 48 hours post-transfection to measure various functional parameters. In some experiments, transfected cells were treated in the presence or absence of 50nM Exendin-4 for 18 hours prior to assessment, in standard culture media as previously outlined [4, 5].

2.4 Flow Cytometry

After 48 hours, transfected cells, pre-conditioned in the presence or absence of 50nM Exendin-4 for 18 hours, were washed with PBS, collected by trypsinization and resuspended in complete media. Cells were then processed for flow Cytometry sorting utilising either the FACS Jazz or LSRFortessa (BD Biosciences, Heidelberg, Germany) and subject to assessment via various assays outlined below.

2.4.1 Cell Cycle Analysis

P19ECs were seeded at a density of $2.0x10^4$ in a 24-well plate format, cultured overnight, transfected, and pre-treated in the presence or absence of 50nM Exendin-4 for 18 hours as outlined. Following transfection, 48 hours later, cells were collected and subject to paraformaldehyde (PFA) fixation, ethanol permeabilization and stained with FxCycle Propidium iodide/RNAse staining solution (Thermo Fisher Scientific San Jose, CA, USA). To achieve this, transfected cells were collected by trypsinization and subsequently washed with PBS. Cells were then spun down at 300xg and resuspended in 500µL of ice cold PBS and 500µL of 4% Paraformaldehyde (PFA) (to achieve a 2% PFA final concentration), and incubated at 4°C for ~30 minutes. Fixed cells then underwent another ice cold PBS wash prior to permeabilization with -20°C 70% ethanol for ~30 minutes. Cells were then washed a final time with ice cold PBS, followed by treatment with 500µL of FxCycle per $1x10^6$ cells, and incubated for ~15 minutes at room temperature in the dark, in accordance with company's protocol. After incubation the cells were filtered through a 40µm cell strainer. Unlabelled control cells were generated by preparing cells as described above, however in the absence of GFP and or FxCycle. Cells stained with GFP (FITC) and PI (FxCycle) were analysed (blue-488 nm and yellow green-561 nm lasers) using FACS LSR Fortessa flow cytometer (BD Biosciences, Heidelberg, Germany). GFP and PI signals were measured upon excitation by the lasers using 530/30 nm and 610/20 nm bandpass filters respectively. A minimum of ten thousand GFP+ cells were selected and data was analysed using the FlowLogic FCS analysis software (Inivai Technologies, Melbourne, Australia). Cell debris was excluded from analysis by pulse processing side scatter area (SSC-A) and forward scatter area (FSC-A). After gating for GFP negative cells, GFP positive cells were identified and their median fluorescence intensities (MFI) for FxCycle, SSC and FSC fluorescence were obtained.

2.4.2 Mitotracker Deep Red, DHE and MitoSOX Red assays

Mitochondrial membrane potential of P19ECs was determined using the Mitotracker DeepRed assay (Thermo Fisher Scientific San Jose, CA, USA). Cells were seeded at a density of $2.0x10^4$ in a 24-well plate format, cultured overnight, transfected and pre-treated in the presence or absence of 50nM Exendin-4 for 18 hours as previously outlined. After 48 hours cells were incubated in the presence or absence of 5nM Mitotracker DeepRed, in the dark, at 37°C for 30 minutes in complete media. Cells were then detached with trypsin, washed in PBS, resuspended in 120µl of PBS and kept at 4°C prior to sorting. Unlabelled control cells were generated by preparing cells as described above, however in the absence of GFP and/or Mitotracker DeepRed. Cells stained with GFP (blue-488 nm), Mitotracker DeepRed (red-640 nm), dihydroethidium (DHE) (yellow-green-561 nm) and MitoSOX Red (yellow-green-561 nm) were analysed using FACS LSR Fortessa flow cytometer (BD Biosciences, Heidelberg, Germany). GFP, DHE, MitoSOX Red and Mitotracker DeepRed signals were measured upon excitation by lasers using 530/30 nm, 610/20 nm, 575/26 nm, and 670/14 nm bandpass filters respectively. A threshold of ten thousand cells co-labelled with Mitotracker DeepRed and GFP, was set for collection and analysis on the LSR Fortessa (BD Biosciences, Heidelberg, Germany).Data was analysed using the FlowLogic FCS analysis software (Inivai Technologies, Melbourne, Australia). Median Mitochondrial fluorescence was obtained after gating for single GFP positive cells. In order to estimate cellular reactive oxygen species (ROS) and mitochondrial superoxide respectively, DHE and MitoSOX Red Mitochondrial Superoxide indicator assays (Thermo Fisher Scientific San Jose, CA, USA) were performed. Following experimental treatments, cells were incubated with either 5µM DHE, in serum-free DMEM media, or 5nM MitoSOX Red, in PBS, at 37°C in the dark for 15 minutes and median fluorescence intensities immediately assessed by flow cytometry as described above.

2.5 Immunoblotting

Cells were GFP positively sorted following indicated treatments, washed in PBS at 4°C and lysed in 1x RIPA buffer (Astral Scientific, Sydney, Australia) containing protease and phosphatase inhibitors cocktail (1x) (Cell Signalling Technology, Beverly, MA, USA). Whole brains were collected from mice, put on ice, and weighed. Next, the whole brains were placed in a 2mL tube with Tris-buffered saline (TBS) and protease and phosphatase inhibitors cocktail (2x) at a 1:1.5 weight-to-volume ratio (brain weight: TBS and inhibitor 2x) prior to several

rounds of vortexing to homogenise the tissue. Once homogenised RIPA buffer was added, creating 1:3 weight-to-volume ratio, following which homogenates were incubated for 1 hour at 4°C and agitated to mix (spinning wheel). Following this, GFP+ sorted cells and whole brain homogenates were subject to multiple rounds of sonication at 4°C, ensuring complete lysis, spun down at 14,000 x *g* for 10 minutes, and the supernatant transferred to a new tube. Total protein concentrations were determined using Pierce BCA protein assay kit (Life Technologies, Gaithersburg, MD, USA) and a colorimetric capable plate reader (Enspire Multimode Plate Reader, PerkinElmer, USA). Cells were diluted in Bolt™ Sample Reducing agent (1x) and Bolt™ LDS Sample Buffer (1X) (Thermo Fisher Scientific, San Jose, CA, USA). Equal amounts of protein extracts were separated by SDS-PAGE Electrophoresis using Bolt™ 4–12% Bis-Tris precast gels in Bolt™ MES SDS Running Buffer at 120 volts for ~1 hour. Following migration gels were prepared for transfer onto 0.45µm nitrocellulose membranes (Bio-Rad Laboratories, Hercules, CA, USA) by soaking both in transfer buffer (25mM Tris Base, 192mM Glycine, 20% (v/v) methanol). To ensure an even transfer, a "sandwich" consisting of two foam pads, filter paper, the gel being transferred, filter paper, and two more foam pads was prepared, all of which were pre-soaked in transfer buffer prior to construction of the sandwich. The sandwich then had all air pockets removed using a roller and was placed with gel adjacent to the cathode in a Bio-Rad Mini Trans-Blot® Cell transfer tank and run at 150mA for 2 hours at 4°C.

After transfer, membranes were placed in a blocking solution (3% (w/v) of dry bovine serum albumin (BSA) dissolved in 1x TBS with Tween 20 (TBST) (Tris 20mM (pH 7.4), NaCl 140mM. 0.01% (v/v) Tween-20 detergent) for a minimum of 30 minutes, gently rocking at room temperature. Transfer efficiency was checked prior to blocking using Ponceau stain. Primary antibodies were diluted in blocking buffer with 0.02% sodium azide, for long term storage, and are listed in Supplementary Data Table 1. Membranes were incubated overnight at 4 °C with primary antibodies as indicated, and were subsequently subject to 4 TBST washes using the SNAP i.d. quick immunoblot vacuum system (Millipore, MA, USA) prior to incubations with the appropriate secondary antibody. Secondary antibodies (horse radish peroxidase conjugated) were diluted in blocking solution, and incubated on the membrane for a minimum of 1 hour at room temperature, which was then removed and membrane washed again with TBST 4 times. Following the final wash membranes were removed and incubated

in Clarity Western ECL substrate (Bio-Rad Laboratories, Hercules, CA, USA) to develop bands. Band visualization was performed using the Chemiluminescent protocol of a BioRad Chemidoc and quantitative densitometry analysis performed with BioRad Image Lab Software 6.1. Total S6 protein expression was used as a normalisation marker to avoid any possible confounding factors.

2.6 Extracellular Flux analysis and total ATP measurements

XFe96 Extracellular Flux Analyser (Agilent Technologies, USA) was used to determine bioenergetics parameters including mitochondrial electron transport and glycolytic flux of transfected cells. Following indicated treatments, single GFP positive cells were obtained, after gating for unlabelled GFP negative control cells, using the FACS Jazz (BD Biosciences, Heidelberg, Germany). GFP positive sorted cells were then washed in Serum-free DMEM, counted, seeded at a density of $\sim$2.0x10^4 per well in a 96 well Seahorse plate, and rested for 1 hour at 37 °C in a CO2-free atmosphere. Following this the basal extracellular acidification rate (ECAR), and oxygen consumption rate (OCR), indicators of glycolysis and/or lactate production and mitochondrial respiration respectively, were determined, as previously described [6] using Agilent Seahorse Wave software. Additionally, use of the Seahorse XF Glycolytic Rate Assay was undertaken in order to obtain a more accurate indication of the rate of glycolysis by accounting for the mitochondrial CO_2 contribution to extracellular acidification. To achieve this, cells were prepared similar to above, with the exception that they were washed in Serum-Free DMEM without phenol red. Cells were then placed in the XFe96 Extracellular Flux Analyser, and exposed to sequential injections of a combination of rotenone (1µM) and antimycin A (1µM), and 2-deoxy-D-glucose (2-DG) to determine the poton efflux rate (PER). Five two-minute cycles of mix and measurement following each injection were used to measure OCR, ECAR and PER. Cells were then lysed with RIPA buffer (Astral Scientific, Sydney, Australia) and total DNA was quantified using Quanti-iT PicoGreen (Life Technologies, Gaithersburg, MD, USA) according to manufactures instructions. Analysis of treated cells bioenergetics was performed using Agilent Seahorse XF Report Generators (Agilent Technologies, USA), as described in [7], and results were normalized by total DNA content. For Total ATP content measurements, P19ECs cells were treated and GFP sorted as outlined above. Next, 1.0x10^3 cells per well in a white 96-well plate were lysed with CellTiter-Glo® Reagent (Promega Corporation, Madison, WI, USA) and total ATP determined on a

luminescent capable plate reader (Enspire Multimode Plate Reader, PerkinElmer, USA) according to manufacturer's instructions.

2.7 Animals

Animals were maintained within the animal research laboratories of the Animal Resources Centre (ARC) on a 12:12 light: dark cycle with food available ad libitum. All procedures were performed in accordance with existing animal licenses and guidelines (ARE2017-23).

2.7.1 Generation of CRISPR-engineered Tbcd A475T mice cloning, rederivation and back-crossing

TBCD A475T knock-in CRISPR-CAS9 engineered mice were generated and genetically screened by M.M at the Transgenic Service Department at the Institute of Molecular Pathology (IMP) and Institute of Molecular Biotechnology (IMBA) in Vienna, Austria, following which they were imported to the ARC in Perth, Western Australia. Following quarantine, mice underwent standard rederivation in order to establish clean and healthy breeding colonies into the appropriate background strain (C57B/6J). Tbcd A475T transgenic mice were backcrossed for several generations prior to analysis, described below.

2.7.2 Sample preparation for histological analysis.

Mouse brains were collected at embryonic day 14.5 and E17.5, and postnatal day 5 (E14.5, E17.5 and P5) after culling the pregnant mothers in accordance with animal ethics (ARE2017-23). Day 0 of pregnancy was determined as the day that the vaginal plug was found. After opening of the mesometrium, individual embryos were isolated from the uterus and placed in a Petri dish containing ice cold TBS. Brains were then dissected under stereotactic microscope. Using sterile fine scissors the cranium of the pups was opened by cutting from caudal to rostral, until the nose was reached. Removing the meninges layer carefully, the embryonic brain, including the olfactory bulbs, was isolated and transferred to a 2 mL Eppendorf tube of ice cold 4% paraformaldehyde (PFA) diluted in PBS for overnight fixation at 4°C. In addition, a small tail sample form each embryo was collected for genotyping. Following overnight fixation, to remove excess PFA, brains were washed 3 times for 5 minute in PBS at 4° (with gentle agitation), and subsequently incubated in 30% sucrose and 0.2% sodium azide in PBS for 3 days for cryoprotection. Tissues were then embedded in Optimal cutting temperature compound (OCT), snap frozen, and stored at -80°C. OCT embedded

tissue was then sectioned using Leica CM-3050S cryostate and 16 µm thick coronal sections were collected onto SuperFrost Ultra Plus Adhesion slides (Thermo Fisher Scientific). Sectioned slides were stored at -80°C until histological analysis was performed.

2.7.3 Size and weight measurements of the brains.

Prior to incubation with cryoprotectant, brains were weighed on an analytical balance, placed on a laminated sheet of 1 mm square graph paper, and imaged. Using the ImageJ software, measurements were taken from the caudal end of the olfactory bulb to the caudal end of each cortical hemisphere for left and right cortical length. Values from each cortices were averaged to obtain average cortical length of each sample. The thickness of each hemisphere was similarly measured, averaged and used to determine the average cortical thickness of each sample.

2.7.4 Immunohistochemistry and Nissl-staining

Sectioned slides were dried in a fume hood for 45 minutes and then washed for 5 minutes in PBS whilst being gently agitated on an orbital shaker. Following this primary wash, slides were washed 2 more times in PBS 0.1% Triton whilst on shaker. Slides were then blocked with the appropriate blocking serum (same species as secondary antibody). Blocking serum was diluted to 10% with PBS 0.1% Triton and 190µL added to the slide, after which slides were covered with parafilm- to prevent evaporation, and incubated in an Immunohistochemistry Microscope Slides Humid chamber for 30 minutes at room temperature (RT). Primary antibodies were diluted to the appropriate concentration (as detailed in Supplementary Material Table S1.) with PBS 0.1% Triton, and 100µL was added to each slide which was then covered again with parafilm, and incubated in Humid slides chamber at 4°C overnight. Following overnight incubation, slides were washed in PBS 0.1% Triton 3 times for 5minutes on shaker. Appropriate secondary antibodies were diluted in PB1 0.1% Triton and 100µL added to each slide. Slides were then covered with parafilm and incubated for 2 hours at RT in Humid slides chamber. After incubation, slides were washed 3 times for 5 minutes in PBS 0.1% whilst minimising exposure to light. In order to visualize cell nuclei, slides were incubated with 300µL of DAPI (4’6-Diamidino-2-Phenylindole) for 15 minutes at RT. Slides were then subjected to another 3x 5 minute PBS 0.1% Triton washes. Glass cover slips were mounted with DAKO mounting media and left to dry in the dark for 24 hours. Images were

captured on a fluorescence microscope (BX51, Olympus) equipped with a CCD camera (Nikon, Japan).

Initially, cresyl violet staining (aka Nissl-staining) stock solution was prepared by mixing 0.2g of 150mL of distilled water and stirred for 20 minutes by magnetic stirrer and filtered with blotting paper. Cresyl violet staining solution was then prepared by mixing 30mL of cresyl violet stock with a 300mL buffer solution containing, 282mL of 0.1M acetic acid, and 18 mL of 0.1M sodium acetate. Prior to staining sectioned slides were equilibrated to RT. Slides were then stained as follows: 5 minute immersion in Xylene, followed by immersion in 95% ethanol and 70 % ethanol for 3 minutes each, after which excess ethanol was removed with a dry paper towel, slides were then immersed in deionised water for 3 minutes, followed by immersion in cresyl violet staining solution for 11 minutes. After removing excess cresyl violet staining solution with dry paper towel, slides were washed again in a second deionised water for another 3 minutes. Slides were then immersed in: 70% ethanol for 3 minutes, followed by immersion in 95% ethanol for 1 minute, then immersed in 100% ethanol twice (two dips), following which slides were immersed for 5 minutes in xylene, and then for another 5 minutes in a new xylene solution. Glass cover slips were mounted with DAKO mounting media and left to dry overnight. Nissl-stained sections were imaged on an Olympus IX-51 using CellSens standard software. For each marker, a representative coronal section from the rostral, medial and caudal regions of the brain was selected for imaging and analysis. For each coronal section a representative field of 300 pixels was selected, wherein cell density and orientation, as visualised by DAPI positive cells, was used to identify subdivisions of embryonic (ventricular zone (VZ), sub-ventricular zone (SVZ), intermediate zone (IZ), cortical plate (CP), marginal zone (MZ) and corpus callosum) and postnatal brains (layers I-VI). For each marker, the thickness of each immunostained layer was measured and compared to the thickness of the respective DAPI positive layer to determine total and relative immunostained layer thickness. Measurements of cortical layer thickness, corpus callosum thickness, and positive cell number count were performed blind to the condition on representative fields of randomized stained sections using ImageJ software.

2.8 Generation of CRISPR IGF-1R and INSR stable knockout cell lines

Two independent optimal gRNA sequences to target mouse Igf1r and Insr were taken from https://www.genscript.com/gRNA-database.html?src=leftbar (Supplementary material Table S2).

Each gRNA sequence was designed along with flanking BamHI and HindIII restriction sites, a U6 promoter and a gRNA scaffold sequence, then synthesised as a block with Integrated DNA Technologies (IDT) (**Fig. 2.1**).

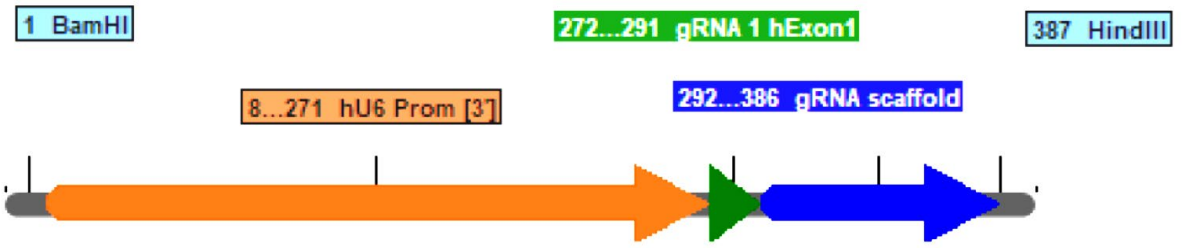

Figure 2.1. gRNA expression cassette.

This synthesised cassette was cloned into Plasmid B, a vector already containing a mammalian expression cassette for tdTomato to generate two gRNA vectors (gRNA1 and gRNA2) for each target gene, Igf1r and Insr. These gRNA vectors were co-transfected with pSpCas9(BB)-2A-GFP (Addgene Plasmid #48138), an expression vector containing Cas9 from *S. pyogenes* with 2A-EGFP, into P19ECs to disrupt the coding sequences of Igf1r and Insr. The molecular cloning, transfection and cell cloning procedures are described in detail below.

Plasmid B, a pUC19 derived vector containing a tdTomato expression cassette followed by a multiple cloning site was prepared via mini-prep, and digested with BamHI and HindIII, then quick CIP added. Product run on 0.8% agarose 40 minutes at 130V. Top band 4069bp was cut and purified leaving 120µL of ~100ng/µL of linearized plasmid DNA. gRNA cassettes (gBlocks from IDT, above) were resuspended in 50µL H2O (final 10ng/ µL), then 10µL of each (100ng) were digested with BamHI and HindIII for 30min. Products were purified by PCR clean up kit, and eluted in 10µL (concentrations ranged around 15ng/ µL). Ligation reactions were done in 10µL (50ng vector + 1.5 µL inserts + 0.5µL T4 ligase) overnight at 16°C (Vector: insert molar ratio ~1:4). Following this, 2µL of the ligation products were transformed into 20µL of NEB competent cells. Cells were left to recover for 1 hour at 37°C in 400µL SOC, then 150µL were plated in LB Amp plates. All plasmids were confirmed correct by digestion with BamHI and HindIII, (donor plasmid #B should release a fragment of 760bp and Igf1r and Insr gRNA plasmids release a fragment of 392bp). Plasmids were transformed into competent cells and plated on ampicillin plates for selection. Bacteria were then grown in LB with ampicillin for 12-16 hours and miniprep conducted, as previously outlined. P19ECs were co-transfected

with pSpCas9(BB)-2A-GFP alone or in combination with Igf1r or Insr gRNA plasmids for 48 hours as previously described. Following transfection, cells were subject to single cell sort via FACS Jazz (BD Biosciences, Heidelberg, Germany), with GFP+ and tdTomato+ single cells sorted into individual wells in a 96-well plate, and purities obtained. Single cell colonies were cultured in DMEM, high glucose media (4500mg/L), with 1% v/v L-glutamine, supplemented with 5% (v/v) FBS and 100 U/mL penicillin and 0.1 mg/mL streptomycin, pH 7.4, at 37^0C in a humidified atmosphere of 95% air and 5% CO_2. Cells reaching ~75% confluency were split and re-seeded, as previously outlined, in a larger receptacle until the appropriate cell numbers were reached. Knockouts were confirmed via immunoblot assay for IGF1R and INSR, and validated colonies were frozen down as stocks and/or used for further experiments.

2.9 Statistical analysis

All analyses were performed using GraphPad Prism 6 software (GraphPad, San Diego, CA, USA). Variables are reported as ± SEM. For variables that were normally distributed, ANOVA with a Tukey post hoc test was used when more than two experimental groups were compared, and Student's t-test when only two experimental groups were compared to evaluate statistical significance. For non-normally distributed variables the non-parametric equivalents were used, namely Kruskal-Wallis and Mann Whitney tests. Statistical significance was set at $P < 0.05$ (two-tailed). All graphs were generated using GraphPad Prism 6 software (GP Prism, San Diego, CA, USA).

2.10 References

1. Edvardson, S., et al., *Infantile neurodegenerative disorder associated with mutations in TBCD, an essential gene in the tubulin heterodimer assembly pathway.* Human Molecular Genetics, 2016. **25**(21): p. 4635-4648.
2. Li, S.S., et al., *The HSA21 gene EURL/C21ORF91 controls neurogenesis within the cerebral cortex and is implicated in the pathogenesis of Down Syndrome.* Scientific reports, 2016. **6**(1): p. 1-14.
3. Leszczyński, P., et al., *Neurogenesis Using P19 Embryonal Carcinoma Cells.* JoVE (Journal of Visualized Experiments), 2019(146): p. e58225.
4. Rowlands, J., et al., *Insulin and IGF-1 receptor autocrine loops are not required for Exendin-4 induced changes to pancreatic β-cell bioenergetic parameters and metabolism in BRIN-BD11 cells.* Peptides, 2018. **100**: p. 140-149.
5. Carlessi, R., et al., *GLP-1 receptor signalling promotes beta-cell glucose metabolism via mTOR-dependent HIF-1alpha activation.* Sci Rep, 2017. **7**(1): p. 2661.

6. Rowlands, J., et al., *Method Protocols for Metabolic and Functional Analysis of the BRIN-BD11 β-Cell Line: A Preclinical Model for Type 2 Diabetes*, in *Pre-Clinical Models: Techniques and Protocols*, P.C. Guest, Editor. 2019, Springer New York: New York, NY. p. 329-340.
7. Calton, E.K., et al., *Prevailing vitamin D status influences mitochondrial and glycolytic bioenergetics in peripheral blood mononuclear cells obtained from adults.* Redox Biology, 2016. **10**: p. 243-250.

Chapter 3 TBCD influences cell cycle and metabolic homeostasis *in vitro*

3.1 Introduction

Nervous system formation and function relies upon the coordinated, spatiotemporal proliferation, migration and differentiation of neuronal stem/progenitor cells (NSC/NPCs). These processes require the organisation, disassembly, assembly and coordinated remodelling of the highly dynamic neuronal cytoskeleton [1-3]. The structural framework of the cell, the neuronal cytoskeleton is composed of three essential filaments, microtubules (MTs), actin and intermediate filaments. During brain development, the organisation and dynamic remodelling of the actin and MT cytoskeleton is crucial for appropriate neuronal development and maturation [4-6]. The largest of the filaments, MTs are composed of repeating αβ-tubulin subunits, and are considered dynamically unstable due to their rapid stochastic switching between phases of polymerisation and depolymerisation in a guanosine triphosphate (GTP)-dependent manner [2, 5-8]. It is this dynamic instability that allows MTs, acting in concert with actin filaments, to mediate the wide-range of cellular functions required for appropriate neuronal development and nervous system formation, including proliferation, migration, axon and dendrite formation, establishment of cellular polarity and intracellular trafficking [2, 9-12]. Unsurprisingly, cytoskeletal defects in developing neurons lead to a plethora of debilitating neurodevelopmental disorders and nervous system abnormalities [5, 9, 13]. Recently, several studies have identified mutations in the gene encoding the tubulin-specific chaperone D (TBCD) protein to be responsible for the observed severe infantile neurodegenerative pathologies including; microcephaly, cortical atrophy and dystonia, resulting in intellectual disability and seizures [14-18]. These mutations have been reported to perturb TBCD's critical role in the in the polymerisation and depolymerisation of MTs, consequently impacting neuronal function and development.

The dynamic nature of MTs are regulated by specific molecular chaperones influencing synthesis, subcellular-localisation and protein stability of the α and β-tubulin subunits, as previously described. Briefly, the α and β-tubulin polypeptide sequences are taken from the ribosome by the chaperonin prefoldin (PFD) and transferred to the chaperonin containing TCP-1 (CCT) [19-21]. CCT then encloses the tubulin subunits in its centre, following which

multiple rounds of ATP-dependent binding drive conformational changes in CCT and consequently tubulin, resulting in tubulin to dissociate in a more native conformation [2, 20, 22-26]. Of note, both α and β-tubulin are GTP-binding proteins, with α-tubulin binding GTP nonexchangeably, whilst β-tubulin requires an exchangeable GTP for both heterodimer formation and incorporation into the MT lattice [22, 27, 28]. Released in a quasi-native, α and β-tubulin can then be bound by the tubulin binding cofactors B and A (TBCB and TBCA) respectively. Once bound, TBCA and TBCB transfer the bound tubulins to the TBCD-TBCE-Arl2 (TBC-DEG) superstructure, which in turn promotes the association of TBCC and its subsequent hydrolysis of the β –tubulin bound GTP [7, 29, 30]. This enables the dissociation of TBCC and the αβ- heterodimer from the super-complex, with the latter now able to be incorporated into the growing MT lattice. Additionally, TBCD and TBCE are able to participate in the destruction of heterodimers, with α-tubulin being bound by TBCE, alone or in concert with TBCB, and β-tubulin being sequestered by TBCD in the absence of Arl2 [31-33]. Perturbations to either the subunits or molecular chaperones in this system are known to lead to a plethora of cortical malformations, often stemming from impaired NPC proliferation, migration and differentiation [14-17, 32, 34, 35].

The first of these studies, by Edvardson, Tian and colleagues identified two novel homozygous missense mutations in *TBCD*, A475T and A586V (rs775014444), with reduced abundance in patient fibroblasts [14]. Whilst able to participate in heterodimer assembly, the mutant variants were reported to be less efficient in dimer disassembly, they also lead to an increase in MT stability, and were indicated to compromise neuroprogenitor proliferation and migration [14]. Additionally, three other research groups reported on a range of heterozygous and homozygous mutations to *TBCD*, as well as a loss-of-function (deletion) allele, with phenotypes of varying severity [15, 16, 36]. Findings from Flex, Niceta and colleagues [15], reported that while there was no significant alterations to the rate of proliferation in patient derived fibroblasts harbouring a mutant TBCD, the cells displayed aberrant mitotic MTs, enlarged centrosomes and enhanced γ-tubulin signalling. In addition to its involvement in *de novo* tubulin dimer assembly, TBCD has been implicated to facilitate the organization of the mitotic spindle and recruitment of γ –TuRC at centrosomes [33, 37]. Interestingly, histological examination of a morpholino-mediated TBCD silencing in Zebrafish by Pode-Shakked, Barrash and colleagues [17], revealed that either loss of or overexpression of TBCD resulted

in brain atrophy, decreased neural density, thin neuronal layering, defective retinal lamination and myocyte disorganization. Further extending these findings, Miyake et al. [16], hypothesized that disrupted mitochondrial transport in neuronal cells, resultant from TBCD perturbations, may underlie the cactus and somatic sprout formations observed in the Purkinje cells of the cerebellum in the autopsied brain from one individual. Consistent among these studies however, was the finding that perturbations to TBCD disrupted MT dynamics in several ways, including, accelerating the rate of MT re-polymerisation, altering tubulin expression levels, and impacting the binding and release of tubulin, all of which thereby result in an increase in MT stability [14-16, 36]. Taken together, data from these studies indicate that disease-associated TBCD mutations influence the polymerisation and depolymerisation of MTs, and such mutations could directly impact proliferation, neuronal differentiation and metabolic homeostasis during brain development. However, the functions for TBCD in neuronal homeostasis and cell proliferation remain poorly characterised. Furthermore, due to its large size and insolubility when not bound to interacting partners, a crystallographic structure of TBCD either alone or in complex with its binding partners has yet to be obtained. Although a low resolution structure of the TBC-DEG super complex (from a yeast homolog) has recently been obtained by electron microscopy, work conducted by Francis et al. has identified a different predominant form of TBCD and its binding partners in mammalian cells [32, 38]. Taken together, these findings provide a biologically relevant complex in which to assess the impact and interaction of the various β-tubulin isoforms with the TBC-DEG supercomplex.

In this chapter, atomistic models of the TBC-DEG supercomplex bound to β-tubulin isoforms were developed by fitting predicted and experimentally determined structures of the supercomplex components into the previously determined electron microscopy structure (accession EMDB-6390), refining these by a range of molecular dynamics-based approaches, followed by docking of a representative β-tubulin to the refined supercomplex and an estimation of the associated binding energy of all β-tubulin isoforms with the supercomplex. The function of TBCD on neuronal cell viability, cell cycle, energy metabolism, mitochondrial function and redox status was also investigated, achieved by shRNA-mediated silencing of TBCD coupled with expression rescue with wildtype TBCD or disease-associated missense variants (A475T and A586V) using the P19 embryonic carcinoma (P19EC) cell line. These data

demonstrate that TBCD and its disease-associated variants influence cell cycling, neurodifferentiation, as well as parameters of cellular metabolism in different ways.

3.2 Specific Methods

3.2.1 Prediction of TBCD-Arl2 complex structure

The sequence of human TBCD was obtained from UniProt (accession Q9BTW9). The secondary structure of TBCD was predicted using PSIPRED [39], and based on this, the TBCD sequence was divided into a series of overlapping fragments (**Fig. S1 and Table S4**), each comprising approximately 400 amino acids and containing four helix-loop-helix regions. The sequence of each fragment was submitted to the NeBcon server to predict likely residue-residue contacts in the fragments [40]. The predicted residue-residue contacts, along with the fragment sequences, were submitted to the C-QUARK server [41], yielding five potential structures for each fragment. These structures were further refined by energy minimisation using Prime (Schrodinger Suite). The full length TBCD structure was assembled by aligning the fragments to the Kap95p-RanGDP complex (PDB 3EA5) [42], as well as by overlaying the overlapping portions of adjacent TBCD fragments. The structure of Arl2 (PDB 3DOE) [43] was overlaid to RanGDP in the Kap95p-RanGDP complex to yield a TBCD-Arl2, and this complex was refined by energy minimisation in Prime. The complex was further refined via adiabatic biased molecular dynamics (ABMD) [44] to yield a more compact assembly. The complex was parameterised for simulation in AmberTools [45] using the AMBER *ff14SB* force field [46], converted to GROMACS format using *acpype* [47], and subsequently solvated in TIP3P water [48], charge neutralised, and sodium chloride added to 0.1 M using GROMACS 2018.3, with all subsequent steps performed in GROMACS [49]. GTP and magnesium were parameterised using previously published parameters [50, 51]. The prepared system was energy minimised, and short equilibrations in the NVT and NPT ensembles (0.1 ns each) with harmonic position restraints on heavy atoms (1000 kJ/(mol nm^2)) were carried out. Following NVT and NPT equilibration, an ABMD simulation was conducted, biasing on the radius of gyration (Rg) of a portion of TBCD (residues 1-837) and the complete Arl2. The bias force was set to 50,000 kJ/(mol nm^2), and target Rg set to 3.0 nm, corresponding with the most compact portion of the Kap95p-RanGDP complex (residues 1-861 of Kap95p, and the entire RanGDP).

3.2.2 Prediction of TBCE structure

A similar approach to modelling TBCD was employed to predict the TBCE structure. Due to its substantially smaller size, only two fragments were defined and modelled. The first fragment comprised the N-terminal CAP-Gly domain and the leucine-rich repeat region, while the second fragment comprised the leucine-rich repeat region and the ubiquitin-like domain. The full-length structure was assembled by overlaying the leucine-rich repeat regions of the generated fragment structures. The structure of the CAP-Gly domain was predicted by standard comparative modelling approaches in Prime and the C-QUARK prediction for this region replaced by the homology modelled structure. The structure of the TBCB CAP-Gly domain (PDB 4B6M) [52]provided the template for modelling the TBCE CAP-Gly domain; the corresponding sequence alignment is shown in Supplementary Figure 2. The structure of the ubiquitin-like domain was obtained from PDB 4ICV [53] and the C-QUARK prediction for this domain replaced by the experimental structure.

3.2.3 Assembly and refinement of the TBC-DEG complex

The EM structure of the TBC-DEG complex was obtained from the EMDatabank (accession EMD-6390) and imported into UCSF Chimera [38]. Five potential TBC-DEG complexes were generated by semi-manual fitting of the refined TBCD-Arl2 complex and the TBCE structure, using a combination of manual translation and rotation into the EM volume and Chimera's volume fitting tools. The complexes were then refined using Molecular Dynamics Flexible Fitting (MDFF) [54], facilitated by VMD [55] and NAMD [56]. System parameterisation and simulation setup followed that detailed in the MDFF tutorial and as previously published [57, 58]. MDFF simulations were performed for 75ns. The degree of fit of TBCD-Arl2 and TBCE to the volume was assessed over the simulation time course by determining the cross-correlation coefficient, with complexes further manually inspected to verify the compactness of the resulting assemblies over the course of the MDFF. The complex yielding the best fit to the volume and the most compact assembly was subject to a further 50ns unbiased simulation in GROMACS to verify the stability of the resulting complex.

3.2.4 Prediction of β-tubulin binding to the TBC-DEG complex

β-tubulin isoform TUBB2B was used as a representative β-tubulin for docking studies, being perhaps the most frequently characterised β-tubulin in the Protein Data Bank. The β-tubulin TUBB2B structure was obtained from the tubulin complex with zampanolide (PDB 4I4T) [59]

– representing the highest resolution structure of any β-tubulin available at the time the work was performed – and prepared using the Protein Preparation Wizard in Schrodinger Suite to ensure completeness. GDP co-crystallised with GTP was manually modified with the addition of a phosphate group, and neighbouring residues energy minimised. A previously developed docking and scoring procedure was utilised to predict β-tubulin binding to the TBC-DEG complex [60]. Briefly, ZDOCK 3.0.2 [61] was used to dock β-tubulin to TBC-DEG, employing dense sampling and retaining all 54000 poses. pyDockRST was used to filter prospective poses [62], eliminating those that substantially utilised α-tubulin-binding interfaces of β-tubulin to bind TBC-DEG, and favouring the selection of poses contacting TBCD residues known to be sites of pathogenic variation [63, 64]. The filtered poses were rescored using a variety of scoring functions in CCharPPI [65], covering atomic-level potentials [66], residue-level potentials [67], and shape-fitting functions [68]. The top 20 poses from the rescoring were subject to molecular dynamics simulations and a final round of rescoring using the molecular mechanics-generalized Born/surface area (MM-GB/SA) approach, as previously described [69]. Complexes were set up and equilibrated for simulations in AmberTools and GROMACS as described earlier, and a production run of 50ns carried out. The final 10ns of the simulation was used for MM-GB/SA calculations, and the poses re-ranked by the determined binding energy estimate. MM-GB/SA calculations were conducted using the *MMPBSA.py* tool of AmberTools [70], using the Onufriev-Bashford-Case GB model (*igb* = 5) [71]. The pose giving the best MM-GB/SA binding energy was used for subsequent modelling of remaining β-tubulin isoforms with the TBC-DEG supercomplex.

3.2.5 Binding energy estimation for β-tubulin isoforms to the TBC-DEG supercomplex

The structures of β-tubulin isoforms in complex with GTP-Mg were prepared by multi-template homology modelling against PDBs 4I4T and 1Z5V (γ-tubulin bound to GTP-Mg) using Prime (Schrodinger Suite). The majority of the β-tubulin structures were predicted based on PDB 4I4T, while GTP-Mg and residues likely to be within 4 Å of this predicted based on PDB 1Z5V (**Fig. S3**) [59, 72]. The β-tubulin isoform structures were overlaid to β-tubulin 2B in the derived TBC-DEG-β-tubulin 2B complex, prepared for simulation, and up to five simulations of each complex were performed and MM-GB/SA calculations performed as previously described. The three simulations affording the most stable complexes during the final 10ns of

the simulation were selected for MM-GB/SA calculations, with the calculated energy determined from considered frames from each of the three simulations.

3.3 Results

3.3.1 Molecular modelling of TBCD and the interactions of different β-tubulin isotypes

Of the five TBC-DEG assemblies prepared by manually fitting the atomic structures of the components to the EM volume, only one yielded a visibly tight complex with a reasonable fit to the volume following molecular dynamics flexible fitting at 75 ns (**Fig. 3.1A-F**). Further molecular dynamics simulation in explicit solvation and without the constraint of the EM volume revealed the stability of this assembly (**Fig. 3.1G-I**). Molecular docking of β-tubulin to this assembly was then carried out, following by contact-based filtering and rescoring, from which the top 20 poses obtained were subject to further rescoring by MM-GB/SA (Table 1); the top-ranked pose following MM-GB/SA rescoring – ranked 4th by the docking, filtering and rescoring procedure – was used as the basis for preparing complexes of the remaining β-tubulin isoforms with TBC-DEG. In the selected pose, the C-terminal domain of β-tubulin binds to the C terminus and leucine-rich repeat domains of TBCE. Additionally, the TBCE CAP-Gly domain residues near the C terminus of Arl2, which nestles in the core of TBCD, and close to the N-terminus of TBCD. The C terminus of TBCD binds to the α-helices of β-tubulin (residues 213-282) (**Fig. 3.2**). Molecular dynamics simulations and MM-GB/SA calculations performed on all β-tubulin isoforms bound to TBC-DEG revealed that TUBB2A and TUBB2B formed energetically favourable interactions with the TBC-DEG complex, whereas TUBB and TUBB4A, and TUBB8 exhibited less favourable binding to the

Table 1. Binding energy for the top 20 TBC-DEG complex poses re-ranked

Docking rank	MM-GB/SA ΔG_{Bind} (kcal/mol)
1	-34.4
2	-57.8
3	-6.9
4	-78.6
5	-44.9
6	-39.3
7	-25.0
8	-62.2
9	-2.5
10	-29.8
11	+7.6
12	-35.5
13	-40.8
14	+13.9
15	-34.3
16	-68.4
17	-20.9
18	-16.9
19	-26.6
20	-2.4

Table 2. Binding energy for each β-tubulin isoform interacting with the TBC-DEG super complex

β-Tubulin variant	ΔG_{Bind} (kcal/mol)
TUBB	-39.5±0.4
TUBB1	-49.9±0.3
TUBB2A	-65.5±0.3
TUBB2B	-66.7±0.4
TUBB3	-49.3±0.5
TUBB4A	-31.2±0.6
TUBB4B	-52.4±0.5
TUBB6	-48.9±0.3
TUBB8	-42.4±0.5

TBC-DEG complex (Table 2). The β-tubulin isoforms TUBB1, TUBB3, TUBB4B, and TUBB6 bound the TBC-DEG complex with a similar binding energy to one another. Extending these findings, per-residue decomposition of the MM-GB/SA-derived binding energies was undertaken to understand the interactions in each complex in finer detail (Table 3). Structural examination of the TBCD interface with TBCE and the various β-tubulin isoforms illuminated the particular intermolecular interactions associated with residues affording substantial contributions to the binding energies (**Fig. 3.2**). The β-tubulin residues Arg213, Tyr281, Arg282, and Arg390, the TBCD residues Tyr1133, Val1152, and Asp1157, and the TBCE residue Arg480 were found to be consistent contributors to the binding of the TBC-DEG complex with the majority of β-tubulin isoforms (**Table 3 and Figs. 3.2A and B, S5-9**).

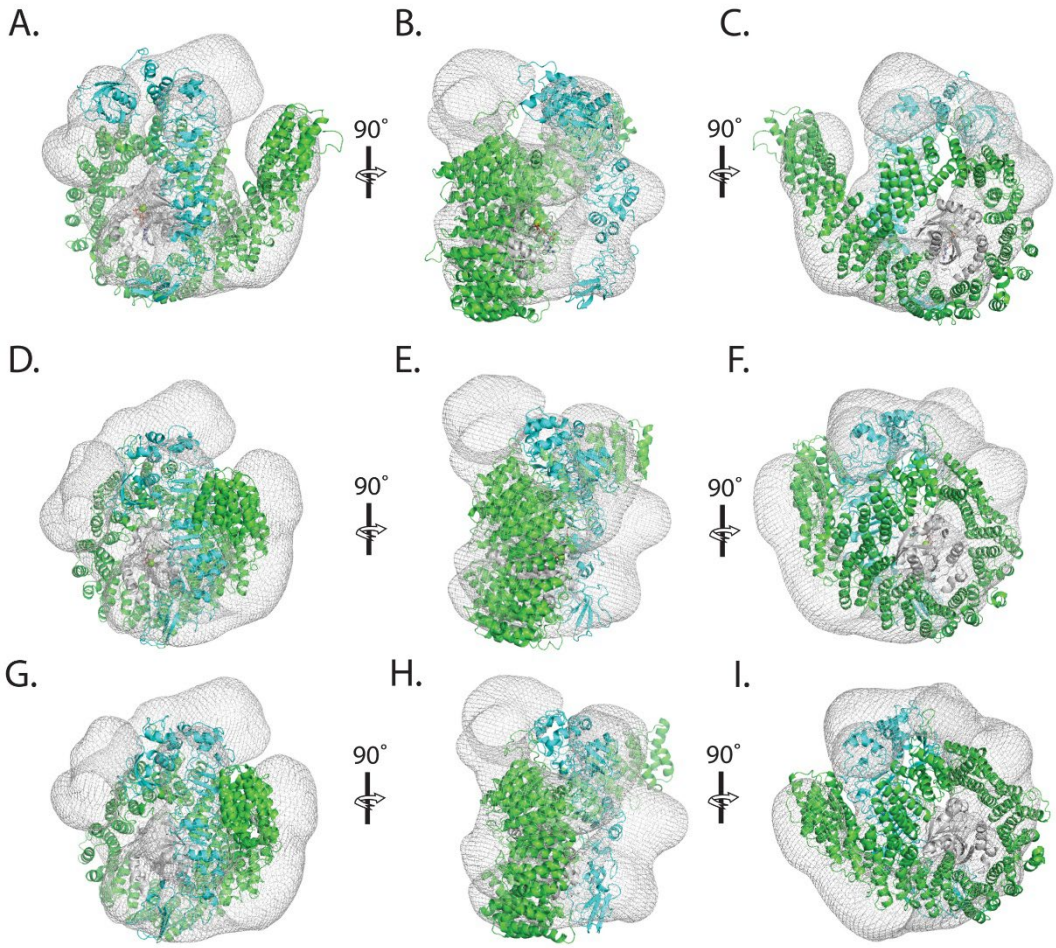

Figure 3.1. TBC-DEG assembly from Cryo-EM (volume)

(A-C) All-atom TBC-DEG complex fitted inside single particle reconstruction of TBC-DEG negative-stain EM data EMD-6390, shown in three different orientations. (D-F) TBC-DEG complex following 75ns molecular dynamics flexible fitting. in EMD-6390 volume. (G-I) TBC-DEG complex following 50 ns molecular dynamics simulation and prior to β-tubulin docking. In all models, the proteins are coloured as follows TBCD- green; TBCE- cyan; ARL2- grey.

Table 3. Binding energy decomposition for selected residues in TBC-DEG/β-tubulin isoform complexes

Protein	Residue	TUBB	TUBB1	TUBB2A	TUBB2B	TUBB3	TUBB4A	TUBB4B	TUBB6	TUBB8
β-Tubulin	Arg213	**-3.47**	**-5.96**	**-7.16**	**-5.85**	**-5.39**	**-6.58**	**-5.50**	**-3.19**	-0.18
β-Tubulin	Phe260	-1.12	-1.79	-2.16	-1.82	-1.64	-1.78	**-2.84**	-1.03	-2.14
β-Tubulin	Tyr281	**-2.84**	**-2.64**	**-3.77**	**-3.06**	**-3.20**	**-2.93**	-1.68	-2.11	**-2.96**
β-Tubulin	Arg282	**-3.77**	**-11.96**	**-8.52**	**-8.06**	**-11.45**	**-3.78**	**-6.82**	**-10.74**	**-9.67**
β-Tubulin	Trp344	**-3.58**	-1.79	-2.02	**-2.85**	-0.79	-0.64	-1.49	-0.21	-1.19
β-Tubulin	Phe389	-0.49	-1.00	-0.96	-1.56	-0.53	-1.13	**-2.59**	**-2.98**	-1.08
β-Tubulin	Arg390	**-5.64**	-1.02	**-2.73**	-0.82	**-2.63**	**-4.31**	**-5.42**	**-3.52**	-1.88
β-Tubulin	Gly409	-0.91	-0.46	-1.71	-1.06	-0.80	-0.79	-1.16	-1.59	**-2.51**
β-Tubulin	Ser420	0.28	**-2.73**	**-5.39**	-2.39	-0.27	-0.04	-1.59	-2.00	-1.44
β-Tubulin	Gln423	-0.27	-0.33	**-3.66**	-0.10	-0.84	-0.16	-0.17	-1.57	0.31
β-Tubulin	Phe425	-0.23	-0.37	**-2.71**	-1.59	-1.22	-0.99	-0.62	-0.15	**-2.50**
TBCD	Tyr1133	**-2.92**	**-2.76**	-2.22	**-3.26**	-2.01	**-4.63**	-2.23	**-2.76**	**-2.95**
TBCD	Val1152	**-2.60**	-2.13	**-3.03**	**-3.55**	-1.49	**-3.01**	-2.16	**-2.73**	**-2.57**
TBCD	Ser1156	-1.60	-0.76	-1.42	-1.32	-0.28	**-2.61**	-0.70	-1.47	0.09
TBCD	Asp1157	**-2.78**	**-3.01**	**-2.73**	**-2.61**	**-2.75**	-2.38	-1.40	**-3.32**	**-3.28**
TBCE	Lys192	-1.23	-0.23	0.07	-1.13	-0.38	-1.65	**-4.00**	-0.20	-1.73
TBCE	Pro194	-1.95	-1.51	-2.25	-2.45	-2.45	-1.01	**-4.99**	**-2.64**	**-2.53**
TBCE	Ser195	-0.32	-0.95	0.16	-0.87	-1.61	-1.66	-2.22	**-3.08**	**-2.52**
TBCE	Asn268	-0.14	0.42	**-4.19**	-0.02	0.00	0.34	-0.69	0.42	0.50
TBCE	Gln269	-1.58	-1.92	-1.41	-1.00	**-2.68**	-0.51	-1.64	-1.87	-0.79
TBCE	Tyr271	**-3.18**	-0.54	-1.79	**-3.56**	-1.03	-1.79	**-3.26**	-2.24	-1.81
TBCE	Lys473	**-4.96**	-0.98	-2.22	-1.04	**-2.98**	-1.52	-1.38	0.00	-2.46
TBCE	Arg480	**-3.76**	-0.42	**-5.86**	**-7.77**	**-7.75**	**-3.23**	**-3.47**	**-5.92**	**-6.52**
TBCE	Pro485	**-2.50**	-1.57	**-2.63**	-2.09	**-2.53**	-2.17	-1.73	-0.86	**-2.73**

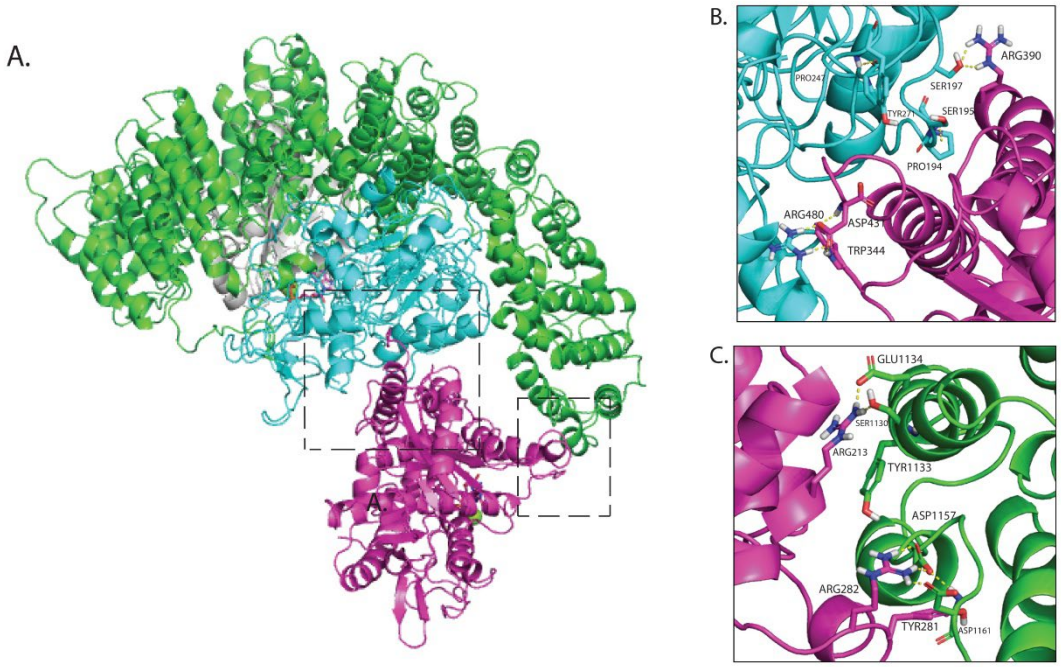

Figure 3.2. Model of TBC-DEG interactions with β-tubulin isoform TUBB2B

Representative images of TBC-DEG complex docked with the β-tubulin isoform TUBB2B. (A-C) Representative images of close up views for each TBC-DEG complex highlighting energetic contribution of selected residues between TUBB2B and TBCE (B), and TBCD (C). Favourable intermolecular interactions are represented as dashed yellow lines. In all models, the proteins are coloured as follows TBCD- green; TBCE- cyan; ARL2- grey; β-tubulin- magenta; magnesium- green sphere.

3.3.2 TBCD alterations impact cell cycle dynamics

In the developing neocortex, cortical expansion relies upon the exponential expansion of the NPC population, their appropriate exit from cell cycle, migration and consequent differentiation [1, 3]. Due to the crucial role of MT dynamics in each of these processes, coupled with previous findings that TBCD is linked with centriologenesis, cell abscission and mitotic spindle organisation [5, 32, 73], I sought to determine how alterations to TBCD may be influencing neuronal cell cycle using the well characterized P19 mouse embryonal carcinoma cell line (P19ECs) (**Fig. 3.3**). Euploid pluripotent cells, P19ECs can be induced to differentiate into neurons and glia, or cardiac and skeletal muscle with retinoic acid (RA) or dimethyl sulfoxide (DMSO) respectively [74-77]. Additionally, the functional and morphological changes during neuronal differentiation from neuroepithelial-like cells to postmitotic neurons in P19ECs closely resembles that of the mammalian central nervous system (CNS), making them an invaluable and suitable tool to analyse the regulation of

proliferation and neurogenesis [74-79]. To delineate the role TBCD plays in regards to NPC proliferation, silencing, overexpression and expression rescue experiments were conducted. Cells were co-transfected using either the previously generated and characterized TBCD targeting short hairpin RNA (TBCD shRNA) or scrambled shRNA (SCR shRNA), cloned in a vector containing a green fluorescent protein (GFP) expression cassette, in a balanced stoichiometry with mammalian expression vectors containing either wild-type human TBCD (WT), the A475T or the A586V TBCD mutation [14]. Following transfection, GFP+ single cells were sorted and processed for cell cycle and immunoblot analysis (**Fig. 3.3**). Initially, immunoblot was used to validate the silencing, overexpression and rescue of TBCD. Confirming TBCD silencing and rescue, assessment of TBCD protein expression in silenced and overexpressed cells was reduced and increased by ~70% for both groups ($p < 0.0001$), whilst no significant differences were observed in TBCD WT, A475T or A586V rescued cells compared to scrambled control (**Fig. 3.3D and E**). Additionally, the impact of TBCD perturbations on expression on the cytoskeletal subunits' actin and αβ-tubulin was assessed. Interestingly, cells expressing the A475T mutant variant trended towards a decreased expression of both total αβ-tubulin and actin. The expression of total actin was also observed to be significantly reduced in cells rescued with the A586V variant compared to control ($p < 0.05$) (**Fig. 3.3A, C and D**).

Next, cell cycle analysis was conducted on GFP+ sorted cells (**Fig. 3.3E-H**). Using FxCycle Propidium Iodide/RNAse staining solution (Thermo Fisher Scientific, San Jose, CA, USA) it was observed that either alterations to TBCD level (silenced or overexpressed), or structure (A475T and A586V variants) impacted cell cycle dynamics characterized by a significant increase to the percent of cells in G2 (**Fig. 3.3E-H**). TBCD silenced cells rescued with WT TBCD however, did not display any difference in cell cycle dynamics compared to control cells. Cell cycle analysis also revealed significant increases in the percent of TBCD silenced (~10%, $p < 0.0001$), overexpressed (~5%), A475T rescued (~14%, $p < 0.0001$) and A586V rescued (~7%, $p<0.05$) cells in G2 compared to scrambled control (**Fig. 3.3H**). Furthermore, there was a significant decrease in the percentage of S-phase cells rescued with either TBCD A475T (~7%, $p<0.01$) or A586V (~8%, $p<0.01$) compared to control (**Fig. 3.3G**). Whilst no significant differences were observed for any group in G1 compared to scrambled control, there was a

significant increase in the percentage of TBCD A586V cells compared to TBCD silenced cells (~35%, $p < 0.05$) (**Fig. 3.3F**).

In order to confirm this G2 delay, the protein expression levels of cyclin D1 (CD1), a regulatory subunit of the Cdk4/Cdk6 complex and a marker for cell cycle progression, was assessed [80, 81]. Highly expressed during G1, CD1 is reduced to low levels during S phase and must be upregulated by the Ras/extracellular-signal-regulated kinase (ERK) pathway during late G2/M to promote continued proliferation and re-entry into G1 [80, 82-84]. Validating the observed G2 delay, immunoblot and band densitometry analysis showed a drastic reduction in CD1 protein expression in both the A475T (~65%, $p < 0.01$) and A586V (~50%, $p < 0.01$) TBCD rescued cells, and to a lesser extent in TBCD silenced (~20%) cells. No differences were observed in either TBCD overexpressed or WT rescued cells (**Fig. 3.3I and J**). Taken together, these findings strongly support the notion that disruptions to TBCD expression levels or function perturb MT dynamics, consequently impacting appropriate cell cycle dynamics.

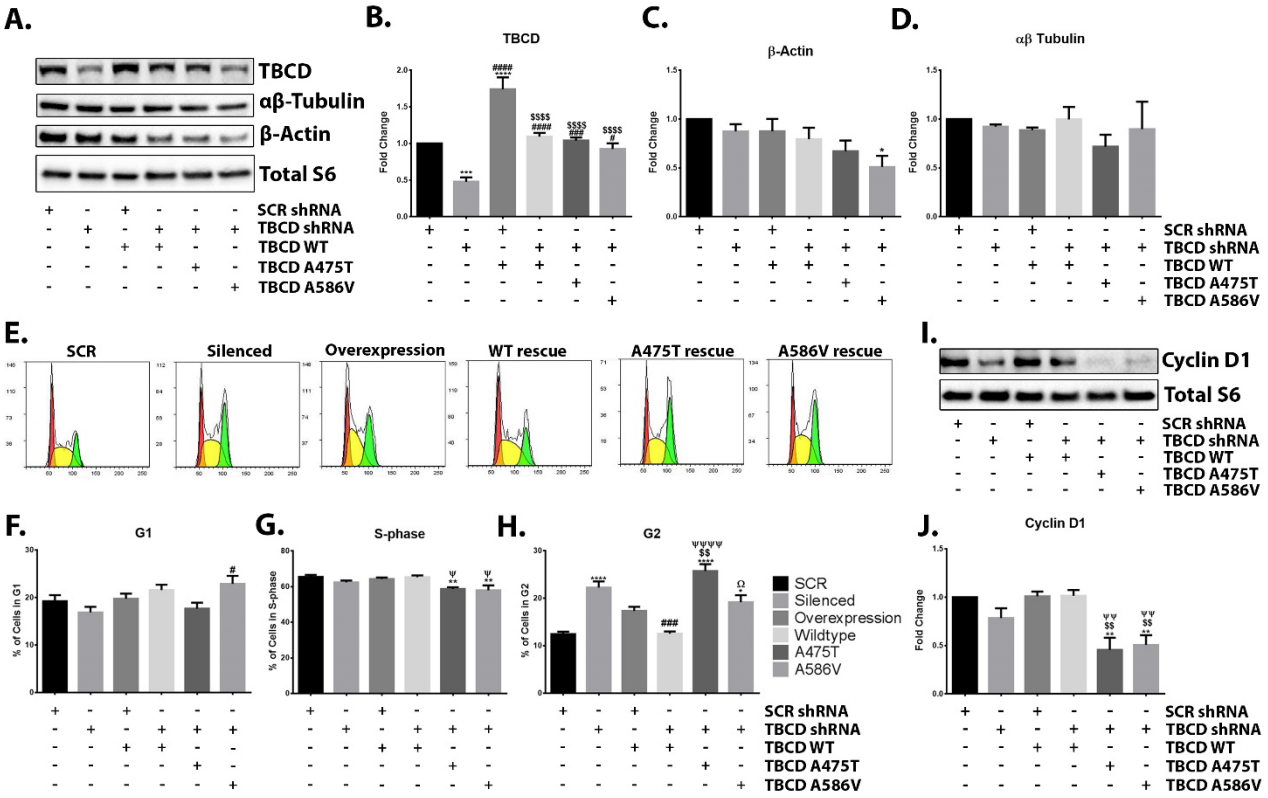

Figure 3.3. TBCD influences cell cycle dynamics

Cell cycle analysis, immunoblot and band densitometry analysis of GFP positive (GFP+) P19 cells co-transfected with shRNA vectors and TBCD expression constructs, as indicated. Transfected cells were processed for cell cycle, and GFP+ cells analysed by flow cytometry. (A-D) Band densitometry analysis of TBCD, αβ-tubulin and β-Actin. (E) Cell cycle profile of GFP+ transfected cells red for G1, yellow for S-phase and green for G2. (F-H) Cell cycle analysis of co-transfected GFP+ P19 cells, assessing percentage of cells in G1 (F), S-phase (G) and G2 (H) as determined by Dean-Jett fox algorithm. (I and J) Immunoblot and band densitometry analysis of Cyclin D1. Data represents mean ± SEM. n≥ 5 independent experiments. * represents comparisons against scrambled control cells. Ψ represents comparisons against TBCD WT rescue cells. # represents comparisons against TBCD silenced cells. $ represents comparisons against TBCD overexpressing cells. Ω represents comparisons against TBCD A475T rescued cells. *P < 0.05, **P < 0.01, ***P < 0.001, ****P < 0.0001. ΨP < 0.05, ΨΨP < 0.01, ΨΨΨ P < 0.001. #P < 0.05, ##P < 0.01, ###P < 0.001, ####P < 0.0001. $P <0.05, $$P < 0.01, $$$P < 0.001, $$$$P < 0.0001. &P <0.05, &&P < 0.01, &&&P < 0.001, &&&&P < 0.0001. ΩP <0.05, ΩΩP < 0.01.

3.3.3 Perturbations to TBCD impact glycolytic flux and mitochondrial bioenergetics

Progression through cell cycle checkpoints, G1/S and G2/M, is an energy-intensive process, requiring the co-ordinated action of mitochondria, cell cycle regulators and MTs [85-89]. Coupling this with the knowledge that both CD1 and MTs can alter mitochondrial dynamics/activity prompted the investigation of TBCD's impact on cellular metabolism [79, 80, 87, 90-94]. In order to determine whether perturbations to TBCD altered metabolism, the XF Seahorse flux analyser was utilised to assess transfected GFP+ sorted cells. Here, I undertook oxygen consumption (OCR), and extracellular acidification rate (ECAR) measurements to determine the impact of TBCD alterations on mitochondrial respiration and

glycolytic flux respectively (**Figs. 3.4 and 3.5**). OCR measurements were collected pre and post injection of 25 mM glucose followed by sequential injections of compounds that target different elements of the electron transport chain (ETC), (oligomycin A, FCCP, and rotenone/antimycin A) as specified in Materials and Methods section and the Mito stress test (Agilent Technologies, USA). Calculations from these OCR measurements demonstrated that, similar to above, TBCD WT rescued cells did not differ in OCR measurements when compared to scrambled control cells. However, when compared to control cells, TBCD A475T and A586V rescued cells possessed a significantly enhanced basal respiration (~3.5-fold, $p < 0.0001$ and ~3.2-fold, $p < 0.0001$), maximal respiration (~5-fold, $p < 0.0001$, and ~4-fold, $p < 0.0001$) and ATP production (~4.5-fold, $p < 0.0001$, and ~3.8-fold, $p < 0.0001$) (**Fig. 3.4A-D**). A similar response was seen when comparing WT TBCD rescued cells to TBCD A475T and A586V rescued cells with an average increase of approximately 3.9-fold and 3.3-fold respectively, for all of the above mentioned parameters ($p < 0.0001$) (**Fig. 3.4.A-D**). Additionally, an increase was observed for TBCD overexpressing cells in these parameters when compared to scrambled control or TBCD WT rescued cells, whilst no statistically significant differences were observed in TBCD silenced cells compared to WT TBCD rescued cells or control (**Fig. 3.4A-D**). In order to confirm the observed increase in ATP production, assessment of total cellular content via the ATP luciferase assay was undertaken. Analysis of these data revealed significant increases in the TBCD WT, A475T and A586V rescued cells when compared to control (~1.1-fold, $p < 0.0001$, ~1.2-fold, $p < 0.0001$, and ~1.15-fold, $p < 0.0001$ respectively), and in the clinical A475T variant against WT TBCD rescued cells (~1.15-fold, $p < 0.001$) (**Fig. 3.4E**). Taken together, these results suggest that TBCD perturbations induce an increase in either mitochondrial mass and/or function. Thus, assessment of the protein levels of succinate dehydrogenase complex, subunit A (SDHA), a key enzyme in the ETC was undertaken. Findings from immunoblot and band densitometry analysis demonstrated an increased trend in SDHA expression in all groups compared to scrambled control, which only reached significance in A475T expressing cells (~2.8-fold, $p < 0.05$), indicating an increase in cellular mitochondrial function and mass (**Fig. 3.4F and G**) [95]. Extending these findings, Mitotracker Deep Red analysis revealed that compared to both control and TBCD WT rescued cells, there was an increased fluorescence intensity in the TBCD overexpressing cells (~1.4-fold), the TBCD A475T (~2-fold, $p < 0.001$), and the TBCD A586V rescued cells (~1.9-fold, $p < 0.001$) (**Fig. 3.4H and I**). Mitotracker Deep Red staining is a measure of mitochondrial

membrane potential [96], which when at high levels is a significant producer of ROS. Sustained excessive high membrane potential however, can potentially lead to an excessive and damaging ROS production [97-99].

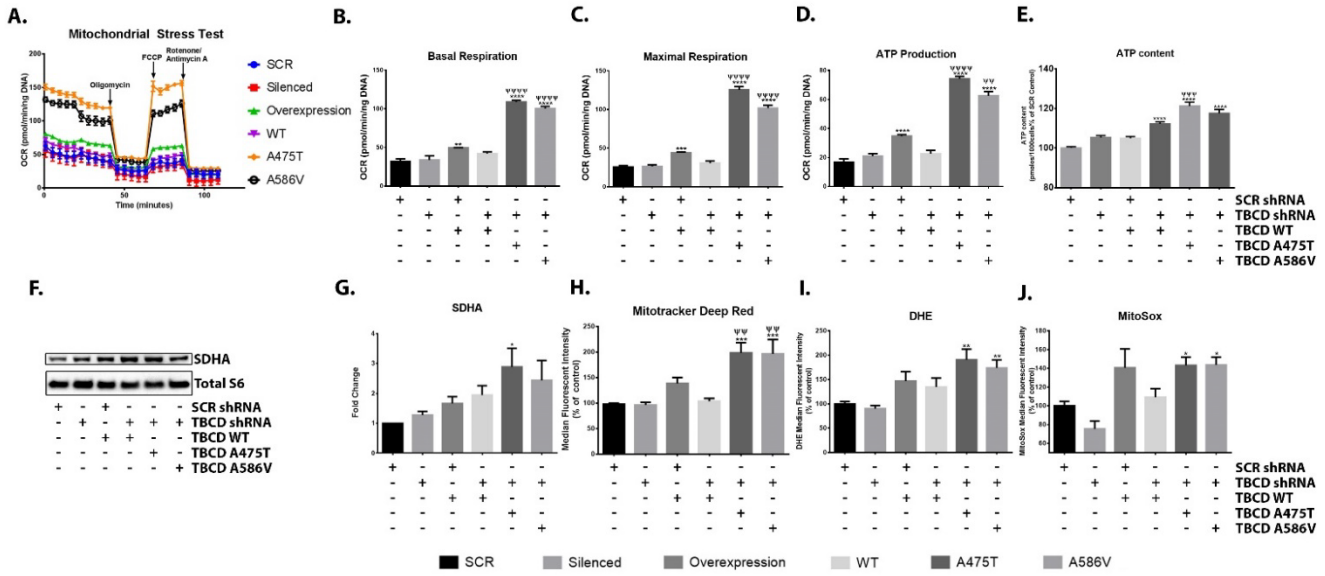

Figure 3.4. TBCD influences mitochondrial metabolism in a cell autonomous manner

Extracellular flux analysis, flow cytometry, immunoblot and band densitometry analysis of GFP positive (GFP+) sorted P19 cells co-transfected with or without TBCD shRNA vectors and TBCD expression as indicated. (A-E) Sequential injections of 25mM glucose, 2µM of oligomycin, 0.3µM FCCP and 1µM each of rotenone and antimycin A, enabled the generation of an Oxygen consumption rate (OCR)/mitochondrial stress test profile. (B-D) Mitochondrial parameters, were calculated from OCR profile using Mito Stress Test Agilent Seahorse XF Report Generator (Agilent Technologies, USA). (E) Assessment of ATP content from GFP+ sorted cells by Luciferase assay. (F and G) Immunoblot and band densitometry analysis of succinate dehydrogenase complex subunit A (SDHA). Flow cytometry analysis of median fluorescence intensities (MFI) of (H) MitoTracker Deep Red, (I) dihydroethidium (DHE), and (J) mitochondrial superoxide (MitoSox). Data represents mean ± SEM. n ≥ 3 independent experiments. Each point, n=5 technical replicates. * represents comparisons against scrambled control. Ψ represents comparisons against TBCD WT rescued cells. *P < 0.05, **P < 0.01, ***P < 0.001, ****P < 0.0001. Ψ P < 0.05, ΨΨ P < 0.01, ΨΨΨ P < 0.001, ΨΨΨΨ P < 0.0001.

In support of this, measurements of total ROS and mitochondrial superoxide levels, from dihydroethidium (DHE) and Mitosox respectively, displayed the expected increase associated with elevated mitochondrial membrane potential, as well as enhanced mitochondrial mass and/or function (**Fig. 3.4I and J**). These data revealed a significant increase in TBCD A475T and A586V rescued cells compared to both DHE (~1.9-fold, $p < 0.01$, and ~1.7-fold, $p < 0.01$ respectively) and MitoSox (~1.4-fold, $p < 0.05$ for both) (**Fig. 3.4I and J**). No significant differences were observed between control and TBCD silenced cells, however they did trend towards a decrease in both measurements. Similar to the clinical TBCD mutant rescued cells, TBCD overexpressing cells displayed a non-significant increase in DHE and MitoSox when compared to control (~1.4-fold for both measurements), and in DHE for TBCD WT rescued

cells compared to control (~1.3-fold). Taken together, this data indicates that the enhanced OCR observed in the TBCD clinical mutations is accompanied by an increased mitochondrial function and levels of ROS.

Next, ECAR measurements were performed to further analyse the impact of TBCD disruptions on cell metabolism. Calculations obtained from ECAR measurements demonstrated an increase in glycolysis, glycolytic capacity, and glycolytic reserve in the A475T rescued cells when compared to either scrambled or WT TBCD rescued cells (~1.8-fold, $p < 0.0001$, ~2.3-fold, $p < 0.0001$, and ~4.2-fold, $p < 0.0001$, against both groups) (**Fig. 3.5A-D**). Furthermore, TBCD A475T rescued cells displayed an increased glycolytic capacity and glycolytic reserve when compared to TBCD A586V rescued cells (~1.15-fold, $p < 0.01$, and ~1.3-fold, $p < 0.01$ respectively) (**Fig. 3.5C and D**). A similar increase, although to a lesser extent, was observed in the TBCD A586V rescued cells compared to either scrambled or WT TBCD rescued cells ~1.6fold, $p < 0.0001$, ~2.0-fold, $p < 0.0001$, and ~3.2-fold, $p < 0.0001$, against both groups) (**Fig. 3.5A-D**). TBCD silenced cells did not significantly differ from control cells in any measurement, whilst only the glycolytic capacity of TBCD overexpressed cells was significantly increased from scrambled control (~1.25-fold, $p < 0.05$) (**Fig. 3.5A-D**). No differences were observed in WT TBCD rescued cells compared to control.

In order to better understand these data, the Seahorse Glycolytic Rate Assay was used to assess the extracellular proton efflux in the absence of mitochondrial-derived CO_2 extracellular acidification. Glycolytic rate measurements obtained from the glycolytic-derived proton efflux rate (PER) profiles, showed a decrease in the % of PER from glycolysis and an increase in acidification from mitochondrial-derived CO_2 in the TBCD A475T (~4%, $p < 0.01$, and ~1.6-fold, $p < 0.01$ respectively) and A586V mutant rescued cells (~4%, $p=0.06$, and ~1.5-fold) (**Fig. 3.5E-G**). These data indicate that the increased ECAR and PER measured from TBCD A475T and A586V rescued cells is resultant from CO_2 acidification derived from their enhanced mitochondrial respiration.

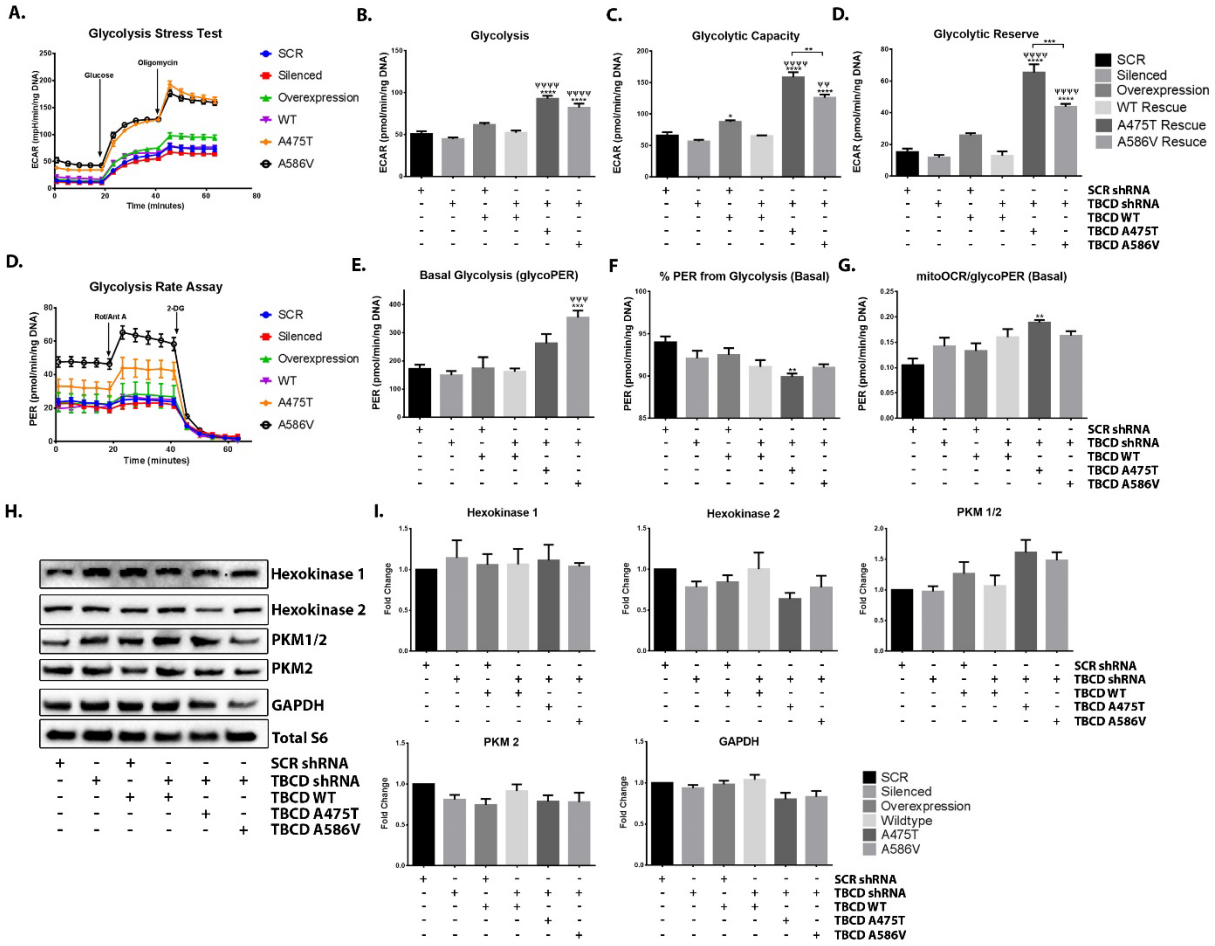

Figure 3.5. Metabolic adaptations arise from TBCD mutants

Glycolytic capacity of the P19 cell line was assessed following transfection and GFP+ cell sorting as previously outlined. (A) Extracellular acidification rate (ECAR) profiles were generated after sequential injection of 25mM glucose and 2µM oligomycin for GFP+ sorted cells. (B) Glycolysis, glycolytic capacity (C) and glycolytic reserve (D) were calculated from the ECAR profile using the Glycolysis stress tests report generator (Agilent Technologies, USA). (E) Glycolytic-derived proton efflux rate (PER) profiles of transfected cells were generated following sequential injections as indicated. (F-H) Basal glycolysis, the rate of protons extruded into the extracellular medium during glycolysis (% PER from glycolysis), and the rate of acidification due to mitochondrial metabolism (mitoOCR/glycoPER) were calculated from PER profile. (H and I) Protein expression of Hexokinase 1, Hexokinase 2, Pyruvate kinase isozymes 1/2 (PKm1/2), PKM2 and Glyceraldehyde 3-phosphate dehydrogenase (GAPDH) were quantified by immunoblot and band densitometry analysis. Data represents mean ± SEM. n ≥ 3 independent experiments. Each point, n=5 technical replicates. * represents comparisons against scrambled control. Ψ represents comparisons against TBCD WT rescued cells. *P < 0.05, **P < 0.01, ***P < 0.001, ****P < 0.0001. Ψ P < 0.05, ΨΨ P < 0.01, ΨΨΨ P < 0.001, ΨΨΨΨ P < 0.0001.

Consistent with this inference, cells rescued with either TBCD mutant variant exhibited decreased expression of glycolytic enzymes. Band densitometry analysis of P19ECs identified a trend towards an increase in Hexokinase 1 (HK1) and Pyruvate kinase isozymes 1 and 2 (PKM1/2) protein expression, and a similar decreased trend in Hexokinase 2 (HK2), PKM2 and Glyceraldehyde 3-phosphate dehydrogenase (GAPDH) expression in TBCD A475T rescued

cells compared to control (~1.1-fold, ~1.6-fold, ~40%, and ~22% respectively) (**Fig. 3.5H and I**). A similar response, but to a lesser extent, was observed in A586V expressing cells, TBCD silenced, and TBCD overexpressing cells, with an increase in HK1 (~1.05-fold, ~1.1-fold, and 1.05-fold respectively), PKM1/2 (~1.5-fold, N/A, and ~1.26-fold respectively), a decrease in HK2 (~23%, ~22%, and ~20% respectively), as well as PKM2 (~20% for all groups) (**Fig. 3.5H and I**). No differences were observed in WT TBCD rescued cells compared to control.

Recent reports have identified a similar metabolic phenotype in P19ECs and NPCs undergoing terminal cell cycle exit and differentiation [79, 91, 92, 100-104]. Findings from these studies show that terminal cell cycle exit and differentiation is accompanied by remodelling of the mitochondrial network, increased mitochondrial function/respiration, an increased membrane potential, elevated level of ROS, and a decreased expression of the glycolytic enzymes HK2 and PKM2 [79, 91, 92, 100-104]. These metabolic alterations were paralleled by a loss of pluripotency markers, such as sex determining region Y-box 2 (Sox2), and an increase in differentiation markers, such as Neuronal Nuclei (NeuN), β-III tubulin (Tuj1), Synapsin I and Forkhead Box G1 (FoxG1) [77, 79, 92, 105-107]. Therefore, I sought to assess the expression of different differentiation markers and pluripotency markers in this model. Corroborating these findings, a significant decrease was observed in the expression of the pluripotency marker Sox2 in A475T and A586V rescued cells (~41%, p<0.01 and ~44%, p=0.06 respectively) (**Fig. 3.6A and B**).

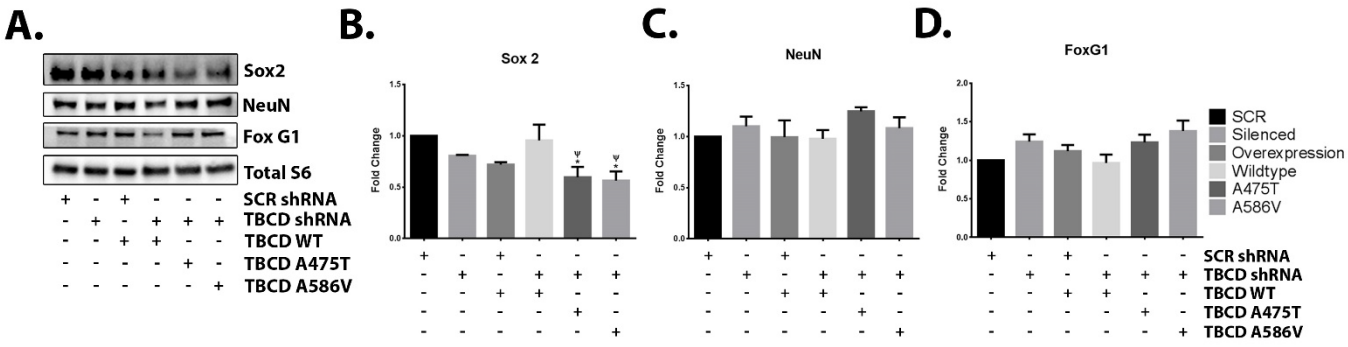

Figure 3.6. TBCD perturbations impact the expression of differentiation and pluripotency markers

GFP+ sorted P19 cells were assessed by immunoblot and band densitometry analysis. (A-D) Protein expression of the differentiation markers Sex determining region Y-box 2 (Sox2), Neuronal Nuclei (NeuN) and Forkhead Box G1 (FoxG1) in P19 transfected cells lysates. Data represents mean ± SEM. n≥ 3 independent experiments. * represents comparisons against scrambled control. ψ represents comparisons against TBCD WT rescued cells. *P < 0.05, **P < 0.01, ***P < 0.001, ****P < 0.0001. ψ P < 0.05.

Whilst no differences were observed in the TBCD WT rescue group, a decrease in Sox2 expression was also observed in the TBCD silenced and overexpressing cells (~21% and 28% respectively). This was paralleled by an increased expression of the neuronal marker, neuronal nuclei (NeuN), in the A475T and A586V rescued cells (~1.25 and ~1.1-fold respectively) (**Fig. 3.6A and B**), although this did not reach statistical significance. Similar, although less pronounced, responses were observed in the TBCD silenced and overexpressed groups but not TBCD WT rescued cells (**Fig. 3.6**). Interestingly, an increase was also observed in the transcription factor FoxG1, in the TBCD A475T and A586V rescued cells, and to a lesser extent in the TBCD silenced cells (~1.3-fold, ~1.3-fold, and ~1.2-fold respectively). FoxG1 has a dynamic expression during cortical development, thereby enabling it to play a central role in progenitor proliferation, differentiation, and metabolism, and is further detailed in the discussion [105, 108-112]. Taken together, these findings suggest that TBCD may influence the pluripotency and stemness of P19ECs [79, 90, 92, 105, 113-115].

3.4 Discussion

TBCD, a key regulator of MT dynamics, is essential to the synthesis of tubulin heterodimers, as well as their dynamic assembly and disassembly. TBCD is involved in neuronal morphogenesis, cell adhesion and signalling, and appropriate cell cycle progression [73, 87, 116, 117]. Highly expressed during foetal development in the brain and spinal cord, TBCD expression levels are maintained in a precise and delicate balance, with disruptions to this equilibrium impacting various aspects of neuronal development [5, 9, 14-17]. The importance of TBCD in human neuronal development is further supported by findings from recent studies identifying mutations in the *TBCD* gene to be causative for a severe, early onset neurodegenerative condition in infants [14, 17]. Beginning with the initial identification of the novel homozygous missense mutations in the *TBCD* gene, A475T and A586V, and recapitulated throughout each subsequent study, is the finding that the mutations identified in TBCD perturb MT dynamics and stability, leading to the associated plethora of neuropathological symptoms including; secondary microcephaly, dystonia, cortical atrophy, seizures, language deficits, and intellectual disability [14-17, 36]. Given the extensive MT organisation and remodelling required during NPC proliferation and neurogenesis, the perturbed dynamics and increased stability of the MT network incurred from TBCD mutations

may be relevant to the molecular mechanism through which it influences NPC proliferation, migration and differentiation essential to the formation of the brain [3, 5, 118].

Due to the lack of an atomic structure of the TBC-DEG assembly, a molecular model of this complex was prepared by fitting predicted structures of the TBCD bound to Arl2 and TBCE to the previously determined cryoEM structure of this assembly [38]. The approach undertaken to exploring both TBCD structure and the TBC-DEG assembly differs from previous studies. The TBCD structure was generated *ab initio*, whereas previous studies have utilised sequence homology-based strategies [15-17]. As TBCD affords less than 20% sequence identity to the nearest structurally characterised protein and likely has a simplistic fold consisting of a series of helix-loop repeats, template-based approaches (both sequence homology-based and fold recognition-based) are likely to be unsuitable for generating a structural model of TBCD capable of yielding meaningful interpretations of biological phenomena. Similarly, the TBCE leucine-rich repeat region shares limited sequence identity to proteins with known structure, with this region generated by *ab initio* means in this study, and the full-length structure predicted by combining this with crystallographic knowledge of the ubiquitin-like domain and a homology model of the CAP-Gly domain. In the study describing the determination of the TBC-DEG complex by cryoEM, a pseudoatomic structure based mostly on the nearest homologues of the protein components was prepared to illustrate the potential assembly, rather than using models of the protein components themselves [38]. The protein components were also individually fit to the cryoEM volume, without considering how particular protein-protein interactions between similar types of proteins occur. Both of these issues have been at least partially addressed in this study, wherein structures of the assembly proteins have been predicted by alternative means besides comparative modelling, and a TBCD-Arl2 complex developed based upon comparison to a crystallographic complex of a HEAT repeat-containing protein bound to a GTPase and specifically used for fitting [119]. In particular, by incorporating knowledge of how at least one protein-protein interface within the assembly is likely to occur, the complexity of the fitting is reduced, as that complex effectively functions as a single protein unit throughout the process. In addition to the development of this *in silico* model, it was observed that the β-tubulin isoforms TUBB2A and TUBB2B had the most energetically favourable interactions with the TBC-DEG complex, whilst TUBB, TUBB4A and TUBB8 exhibited less favourable binding, suggesting that the TBC-DEG

complex shows preference for binding to distinct β-tubulin isoforms. Notably, recent studies have demonstrated that tubulin isoforms have different dynamic properties, and can strongly impact the structural and dynamic features of MTs and MT motors [120-123]. Coupling this knowledge with the observations that TBC-DEG preferentially binds distinct β-tubulin isoforms, it would be beneficial for future studies to explore the impact of TBCD, alone or in complex, on binding the various β-tubulin isoforms and its effect on MT dynamics. Further, incorporating knowledge of such assemblies (and maintaining those assemblies throughout refinement) is likely to achieve more realistic results. The models derived in this study provide unprecedented detail into the TBC-DEG assembly, and may be beneficial to future studies exploring the impact of TBCD variation on MT biosynthesis.

Considering the important and interconnected role of MT dynamics, mitochondria and cell cycle dynamics [79, 87, 124, 125], it was hypothesised that perturbations to TBCD may impair appropriate cell cycle progression and cell fate. Data presented herein supports this notion, as well as identifies a unique mechanism wherein TBCD A475T and A586V mutant variants impact not only cell cycle dynamics, but also alter cellular bioenergetics, and likely affect fate determination and pluripotency (as evidenced by expression of pluripotency and neuronal markers). Here evidence is provided, through shRNA silencing and rescue experiments, that TBCD mutations and to a lesser extent TBCD expression levels, impairs cell cycle dynamics leading to an increase of P19ECs at the G2 checkpoint. This is concluded from evidence provided by cell cycle analysis and immunoblot assay of CD1 - a key component of CDK4 and 6 which regulates progression into and through G1 (**Fig. 3.3**). The expression of CD1, which is downregulated in S phase, will only be upregulated by Ras in G2 if conditions are conducive for continued proliferation [80, 94, 126-129]. However, failure for CD1 to accumulate during G2 has previously been shown to prevent entry into subsequent rounds of cellular division [83, 94, 126]. Consistent with these findings, in this model a significant reduction in CD1 was observed when cells express either the TBCD A475T or A586V mutant variants, and is thus strongly indicative of cells stuck in G2 and/or undergoing terminal cell cycle exit.

Progression through G2 is an energy-intensive phase, with an increased energy demand as cells compensate for the doubling of cellular contents, segregation of chromosomes and nuclear envelope breakdown [88, 91, 92, 130]. In order to meet this enhanced energy demand, the cell adapts the mitochondria into a more polarized tubular network during the

G1-S transition, modifying their respiratory super complexes, thereby driving mitochondrial OXPHOS and increased generation of ATP [88, 125]. As the cell progresses into G2 the mitochondria become fragmented but OXPHOS still remains active, most likely as a result of Cdk-dependent activation, and the reduced expression of CD1 [88, 91]. Due to the G2 arrest and decreased CD1 expression observed in this model, coupled with MTs role in mitochondrial dynamics, I sought to assess whether the perturbations to TBCD were altering the metabolic state of the transfected cells [86, 131-133]. Through the use of the Seahorse XF flux analyser, flow cytometry and immunoblot assay, it was determined that the TBCD mutants, but not TBCD silenced or overexpressing cells, possessed a significantly enhanced: oxidative respiratory capacity, levels of ATP, mitochondrial activity and ROS presence (**Fig. 3.4**). These increases were accompanied by a significantly increased rate of glycolysis in the TBCD A475T and A586V cells, however through the use of the Glycolytic Rate assay, this was observed to be attributable to extracellular acidification from mitochondrial derived CO_2 production (Agilent Technologies, USA) (**Fig. 3.5**).

Whilst these data support the energy demands required in G2, the severe phenotype observed in the OCR profile of the A475T and A586V mutants is reminiscent of the enhanced mitochondrial metabolism and metabolic profile observed in both embryonic stem cells (ESCs) and NSCs previously reported to be undergoing terminal differentiation [79, 92, 130]. Findings from both *in vivo* and *in vitro* studies reported that ESCs and NSCs undergoing differentiation, switch from a primarily glycolytic to a more oxidative metabolism and possess profound changes in mitochondrial morphology and activity [79, 87, 88, 91-93, 130, 134]. These changes to metabolic signalling have been shown to influence cell fate determination. In this model, increased mitochondrial fission and activity can influence stem cell fate decision by acting as an upstream regulator of developmental gene expression and physiological ROS levels [79, 130]. Increased mitochondrial activity, demonstrated by an increase in OCR and ATP production, then leads to an increase in both cytoplasmic ROS and mitochondrial superoxide (mtROS) [79, 92, 107]. This increase in ROS, in turn, is believed to signal a series of downstream events leading to stabilization of the master redox regulator, nuclear respiratory factor 2 (NRF2). Finally, stabilised NRF2 is then translocated to the nucleus where it mediates the transcriptional up-regulation of genes required to suppress self-renewal and activate differentiation [79, 106, 107]. Concurrent with changes in mitochondrial dynamics,

the loss of stemness and initiation of differentiation, several changes occur in glycolytic metabolism including: reduced expression of the enzymes hexokinase HK2 and lactate dehydrogenase (LDH), as well as an mRNA splicing shift from PKM2 to PKM1 [113]. However, it should be noted that it is believed the expression of PKM1, not the loss of PKM2, impairs progression through the cell cycle. This impediment to cell cycle is not associated with cell differentiation however, rather it is believed to promote a metabolic state in which DNA synthesis is not supported [135]. Indeed, similar changes were observed in mitochondrial metabolism in this work, as well as alterations in the glycolytic enzymes HK and PKMs. Consistent with the altered trajectory of neurodifferentiation, the data revealed a reduced expression of the pluripotency and proliferation markers Sox2 and CD1 respectively, as well as an increasing expression of the recognised neuronal differentiation marker NeuN [3, 81, 113, 136, 137] (**Fig. 3.6**). In addition to its role in cell cycle, several non-canonical functions of CD1 have also been recognised including: the targeting and inhibiting differentiation factors, such as neurogenic differentiation factor 1 (NEUROD1), as well as inhibiting mitochondrial respiration and biogenesis, such as through the repression of NRF1 and 2 [81, 90, 125, 131, 132, 138]. Therefore, these results altogether indicate that the reduced CD1 expression observed in this study reflects the increased mitochondrial activity and decreased proliferative capacity, which may increase cellular differentiation. It is noteworthy to mention, that the transcription factor FoxG1 is dynamically expressed during cortical development and plays a central role in progenitor proliferation. However, various studies identify contrasting results in FoxG1 expression, with some studies indicating that loss of FoxG1 induces neurodifferentiation, and others that overexpression of FoxG1 induces premature differentiation, all of which can differ depending on the cellular compartment, such as VZ compared to sub-VZ [105, 108-112]. FoxG1 has also been proposed to localise to the mitochondria, enhancing mitochondrial dynamics, increasing mitochondrial membrane potential and promoting neuronal differentiation [105]. Furthermore, it has been shown that overexpression of FoxG1 is able to restrict differentiation and even trigger dedifferentiation returning the cell to a proliferative NSC fate [139]. Combined with the observations that FoxG1 expression is increased in the TBCD A475T and A586V expressing cells', it is attractive to hypothesise that the upregulation of FoxG1 is resultant from both the cells enhanced state of differentiation and increased mitochondrial activity. Further investigation of the variable expression of FoxG1 however, is necessary before a definitive conclusion can be drawn.

In summary, a novel action of TBCD in the development of P19ECs which delays cell-cycle progression, and stimulates metabolic/bioenergetics reprogramming resulting in a primarily OXHPOS phenotype has been demonstrated. Altogether, this work points to a "double hit" scenario, whereby the TBCD mutations induced perturbations to MT dynamics, leading to cell cycle delay and metabolic reprogramming, which can act synergistically to promote both cell cycle exit and differentiation. These data provide evidence for the role of TBCD in cell cycle and metabolism, and offer unique insights into the neurodegenerative phenotype observed in patients, and a molecular mechanism for further elucidation through *in vivo* models.

3.5 References

1. Stiles, J. and T.L. Jernigan, *The Basics of Brain Development.* Neuropsychology Review, 2010. **20**(4): p. 327-348.
2. Kapitein, Lukas C. and Casper C. Hoogenraad, *Building the Neuronal Microtubule Cytoskeleton.* Neuron, 2015. **87**(3): p. 492-506.
3. Florio, M. and W.B. Huttner, *Neural progenitors, neurogenesis and the evolution of the neocortex.* Development, 2014. **141**(11): p. 2182-2194.
4. Schaar, B.T. and S.K. McConnell, *Cytoskeletal coordination during neuronal migration.* Proceedings of the National Academy of Sciences of the United States of America, 2005. **102**(38): p. 13652-13657.
5. Lundin, V.F., M.R. Leroux, and P.C. Stirling, *Quality control of cytoskeletal proteins and human disease.* Trends in biochemical sciences, 2010. **35**(5): p. 288-297.
6. Ayala, R., T. Shu, and L.-H. Tsai, *Trekking across the brain: the journey of neuronal migration.* Cell, 2007. **128**(1): p. 29-43.
7. Szymanski, D., *Tubulin Folding Cofactors: Half a Dozen for a Dimer.* Current Biology, 2002. **12**(22): p. R767-R769.
8. Greig, L.C., et al., *Molecular logic of neocortical projection neuron specification, development and diversity.* Nature Reviews Neuroscience, 2013. **14**(11): p. 755-769.
9. Jaglin, X.H. and J. Chelly, *Tubulin-related cortical dysgeneses: microtubule dysfunction underlying neuronal migration defects.* Trends Genet, 2009. **25**(12): p. 555-66.
10. Tian, G. and N.J. Cowan, *Tubulin-specific chaperones: components of a molecular machine that assembles the alpha/beta heterodimer.* Methods Cell Biol, 2013. **115**: p. 155-71.
11. Conde, C. and A. Cáceres, *Microtubule assembly, organization and dynamics in axons and dendrites.* Nature Reviews Neuroscience, 2009. **10**(5): p. 319-332.
12. Heng, J.I.-T., A. Chariot, and L. Nguyen, *Molecular layers underlying cytoskeletal remodelling during cortical development.* Trends in neurosciences, 2010. **33**(1): p. 38-47.
13. Boivin, M.J., et al., *Reducing neurodevelopmental disorders and disability through research and interventions.* Nature, 2015. **527**(7578): p. S155-S160.
14. Edvardson, S., et al., *Infantile neurodegenerative disorder associated with mutations in TBCD, an essential gene in the tubulin heterodimer assembly pathway.* Human Molecular Genetics, 2016. **25**(21): p. 4635-4648.
15. Flex, E., et al., *Biallelic Mutations in TBCD, Encoding the Tubulin Folding Cofactor D, Perturb Microtubule Dynamics and Cause Early-Onset Encephalopathy.* The American Journal of Human Genetics, 2016. **99**(4): p. 962-973.

16. Miyake, N., et al., *Biallelic TBCD mutations cause early-onset neurodegenerative encephalopathy.* The American Journal of Human Genetics, 2016. **99**(4): p. 950-961.
17. Pode-Shakked, B., et al., *Microcephaly, intractable seizures and developmental delay caused by biallelic variants in TBCD: Further delineation of a new chaperone-mediated tubulinopathy.* Clinical genetics, 2016.
18. Ikeda, T., et al., *TBCD may be a causal gene in progressive neurodegenerative encephalopathy with atypical infantile spinal muscular atrophy.* J Hum Genet, 2017. **62**(4): p. 473-480.
19. Vainberg, I.E., et al., *Prefoldin, a chaperone that delivers unfolded proteins to cytosolic chaperonin.* Cell, 1998. **93**(5): p. 863-873.
20. Janke, C., *The tubulin code: Molecular components, readout mechanisms, and functions.* The Journal of Cell Biology, 2014. **206**(4): p. 461-472.
21. Cowan, N.J. and S.A. Lewis, *Type II chaperonns, prefoldin, and the tubulin-specific chaperones.* Advances in protein chemistry, 2001. **59**: p. 73-104.
22. Serna, M. and J.C. Zabala, *Tubulin Folding and Degradation.* eLS, 2016.
23. Sakakibara, A., et al., *Microtubule dynamics in neuronal morphogenesis.* Open biology, 2013. **3**(7): p. 130061.
24. Amos, L.A., *Tubulin and microtubules.* eLS, 2004.
25. Al-Bassam, J., *Revisiting the tubulin cofactors and Arl2 in the regulation of soluble αβ-tubulin pools and their effect on microtubule dynamics.* Molecular Biology of the Cell, 2017. **28**(3): p. 359-363.
26. Francis, J.W., et al., *Nucleotide Binding to ARL2 in the TBCD·ARL2·β-Tubulin Complex Drives Conformational Changes in β-Tubulin.* Journal of Molecular Biology, 2017. **429**(23): p. 3696-3716.
27. Tian, G., et al., *Tubulin Folding Cofactors as GTPase-activating Proteins GTP HYDROLYSIS AND THE ASSEMBLY OF THE α/β-TUBULIN HETERODIMER.* Journal of Biological Chemistry, 1999. **274**(34): p. 24054-24058.
28. Holscher, C., *Incretin analogues that have been developed to treat type 2 diabetes hold promise as a novel treatment strategy for Alzheimer's disease.* Recent patents on CNS drug discovery, 2010. **5**(2): p. 109-117.
29. Tian, G. and N.J. Cowan, *Tubulin-specific chaperones: components of a molecular machine that assembles the α/β heterodimer.* Methods in cell biology, 2013. **115**: p. 155.
30. Leitner, A., et al., *The molecular architecture of the eukaryotic chaperonin TRiC/CCT.* Structure, 2012. **20**(5): p. 814-825.
31. Kortazar, D., et al., *Role of cofactors B (TBCB) and E (TBCE) in tubulin heterodimer dissociation.* Experimental cell research, 2007. **313**(3): p. 425-436.
32. Francis, J.W., et al., *A Trimer Consisting of the Tubulin-specific Chaperone D (TBCD), Regulatory GTPase ARL2, and β-Tubulin Is Required for Maintaining the Microtubule Network.* Journal of Biological Chemistry, 2017. **292**(10): p. 4336-4349.
33. Bhamidipati, A., S.A. Lewis, and N.J. Cowan, *ADP ribosylation factor-like protein 2 (Arl2) regulates the interaction of tubulin-folding cofactor D with native tubulin.* J Cell Biol, 2000. **149**(5): p. 1087-96.
34. Rees, M., et al., *Tubulinopathies in malformations of the cerebral cortex.* Journal of Neurology, Neurosurgery & Psychiatry, 2014. **85**(10): p. e4-e4.
35. Chang, B.S., *Tubulinopathies and Their Brain Malformation Syndromes: Every TUB on Its Own Bottom.* Epilepsy Currents, 2015. **15**(2): p. 65-67.
36. Ikeda, T., et al., *TBCD may be a causal gene in progressive neurodegenerative encephalopathy with atypical infantile spinal muscular atrophy.* Journal of Human Genetics, 2016.
37. Shern, J.F., et al., *Cytosolic Arl2 is complexed with cofactor D and protein phosphatase 2A.* Journal of Biological Chemistry, 2003. **278**(42): p. 40829-40836.
38. Nithianantham, S., et al., *Tubulin cofactors and Arl2 are cage-like chaperones that regulate the soluble αβ-tubulin pool for microtubule dynamics.* Elife, 2015. **4**: p. e08811.

39. Jones, D.T., *Protein secondary structure prediction based on position-specific scoring matrices.* J Mol Biol, 1999. **292**(2): p. 195-202.
40. He, B., et al., *NeBcon: protein contact map prediction using neural network training coupled with naïve Bayes classifiers.* Bioinformatics, 2017. **33**(15): p. 2296-2306.
41. Zheng, W., et al., *Deep-learning contact-map guided protein structure prediction in CASP13.* Proteins, 2019. **87**(12): p. 1149-1164.
42. Forwood, J.K., et al., *Kap95p binding induces the switch loops of RanGDP to adopt the GTP-bound conformation: implications for nuclear import complex assembly dynamics.* J Mol Biol, 2008. **383**(4): p. 772-82.
43. Zhang, T., et al., *Crystal structure of the ARL2-GTP-BART complex reveals a novel recognition and binding mode of small GTPase with effector.* Structure, 2009. **17**(4): p. 602-610.
44. Marchi, M. and P. Ballone, *Adiabatic bias molecular dynamics: A method to navigate the conformational space of complex molecular systems.* J Chem Phys, 1999. **110**(8): p. 3697-3702.
45. Salomon-Ferrer, R., D.A. Case, and R.C. Walker, *An overview of the Amber biomolecular simulation package.* WIREs Comput Mol Sci, 2013. **3**(2): p. 198-210.
46. Maier, J.A., et al., *ff14SB: Improving the Accuracy of Protein Side Chain and Backbone Parameters from ff99SB.* J Chem Theory Comput, 2015. **11**(8): p. 3696-3713.
47. Sousa da Silva, A.W. and W.F. Vranken, *ACPYPE - AnteChamber PYthon Parser interfacE.* BMC Research Notes, 2012. **5**(1): p. 367.
48. Jorgensen, W.L., et al., *Comparison of simple potential functions for simulating liquid water.* The Journal of chemical physics, 1983. **79**(2): p. 926-935.
49. Abraham, M.J., et al., *GROMACS: High performance molecular simulations through multi-level parallelism from laptops to supercomputers.* SoftwareX, 2015. **1-2**: p. 19-25.
50. Meagher, K.L., L.T. Redman, and H.A. Carlson, *Development of polyphosphate parameters for use with the AMBER force field.* J Comput Chem, 2003. **24**(9): p. 1016-25.
51. Li, P., et al., *Rational Design of Particle Mesh Ewald Compatible Lennard-Jones Parameters for +2 Metal Cations in Explicit Solvent.* Journal of chemical theory and computation, 2013. **9**(6): p. 2733-2748.
52. Fleming, J.R., et al., *The architecture of T rypanosoma brucei tubulin-binding cofactor B and implications for function.* The FEBS journal, 2013. **280**(14): p. 3270-3280.
53. Serna, M., et al., *The structure of the complex between α-tubulin, TBCE and TBCB reveals a tubulin dimer dissociation mechanism.* Journal of cell science, 2015. **128**(9): p. 1824-1834.
54. Trabuco, L.G., et al., *Molecular dynamics flexible fitting: A practical guide to combine cryo-electron microscopy and X-ray crystallography.* Methods, 2009. **49**(2): p. 174-180.
55. Humphrey, W., A. Dalke, and K. Schulten, *VMD: visual molecular dynamics.* J Mol Graph, 1996. **14**(1): p. 33-8, 27-8.
56. Phillips, J.C., et al., *Scalable molecular dynamics with NAMD.* Journal of Computational Chemistry, 2005. **26**(16): p. 1781-1802.
57. Yu, W., et al., *Extension of the CHARMM general force field to sulfonyl-containing compounds and its utility in biomolecular simulations.* Journal of computational chemistry, 2012. **33**(31): p. 2451-2468.
58. Vanommeslaeghe, K., et al., *CHARMM general force field: A force field for drug-like molecules compatible with the CHARMM all-atom additive biological force fields.* Journal of computational chemistry, 2010. **31**(4): p. 671-690.
59. Prota, A.E., et al., *Molecular mechanism of action of microtubule-stabilizing anticancer agents.* Science, 2013. **339**(6119): p. 587-590.
60. Agostino, M., et al., *Optimization of protein-protein docking for predicting Fc-protein interactions.* J. Mol. Recognit., 2016. **29**: p. 555-568.
61. Pierce, B.G., Y. Hourai, and Z. Weng, *Accelerating protein docking in ZDOCK using an advanced 3D convolution library.* PLoS One, 2011. **6**(9): p. e24657.

62. Chelliah, V., T.L. Blundell, and J. Fernández-Recio, *Efficient Restraints for Protein–Protein Docking by Comparison of Observed Amino Acid Substitution Patterns with those Predicted from Local Environment.* Journal of Molecular Biology, 2006. **357**(5): p. 1669-1682.
63. Pode-Shakked, B., et al., *Microcephaly, intractable seizures and developmental delay caused by biallelic variants in TBCD: further delineation of a new chaperone-mediated tubulinopathy.* Clin Genet, 2017. **91**(5): p. 725-738.
64. Flex, E., et al., *Biallelic Mutations in TBCD, Encoding the Tubulin Folding Cofactor D, Perturb Microtubule Dynamics and Cause Early-Onset Encephalopathy.* Am J Hum Genet, 2016. **99**(4): p. 962-973.
65. Moal, I.H., B. Jiménez-García, and J. Fernandez-Recio, *CCharPPI web server: computational characterisation of protein-protein interactions from structure.* Bioinformatics, 2015. **31**: p. 123-125.
66. Tobi, D., *Designing coarse grained-and atom based-potentials for protein-protein docking.* BMC structural biology, 2010. **10**(1): p. 1-11.
67. Feliu, E., P. Aloy, and B. Oliva, *On the analysis of protein–protein interactions via knowledge-based potentials for the prediction of protein–protein docking.* Protein Science, 2011. **20**(3): p. 529-541.
68. Mitra, P. and D. Pal, *New measures for estimating surface complementarity and packing at protein–protein interfaces.* FEBS letters, 2010. **584**(6): p. 1163-1168.
69. Hemming, I.A., et al., *Disease-associated missense variants in ZBTB18 disrupt DNA binding and impair the development of neurons within the embryonic cerebral cortex.* Human Mutation, 2019. **40**(10): p. 1841-1855.
70. Miller, B.R., et al., *MMPBSA.py: An Efficient Program for End-State Free Energy Calculations.* Journal of Chemical Theory and Computation, 2012. **8**(9): p. 3314-3321.
71. Onufriev, A., D. Bashford, and D.A. Case, *Exploring protein native states and large-scale conformational changes with a modified generalized born model.* Proteins: Structure, Function, and Bioinformatics, 2004. **55**(2): p. 383-394.
72. Aldaz, H., et al., *Insights into microtubule nucleation from the crystal structure of human γ-tubulin.* Nature, 2005. **435**(7041): p. 523-527.
73. Fanarraga, M.L., et al., *TBCD links centriologenesis, spindle microtubule dynamics, and midbody abscission in human cells.* PLoS One, 2010. **5**(1): p. e8846.
74. McBurney, M.W., et al., *Differentiation and maturation of embryonal carcinoma-derived neurons in cell culture.* Journal of Neuroscience, 1988. **8**(3): p. 1063-1073.
75. McBurney, M., *P19 embryonal carcinoma cells.* International Journal of Developmental Biology, 2003. **37**(1): p. 135-140.
76. Bain, G., et al., *From embryonal carcinoma cells to neurons: the P19 pathway.* Bioessays, 1994. **16**(5): p. 343-348.
77. Monzo, H.J., et al., *A method for generating high-yield enriched neuronal cultures from P19 embryonal carcinoma cells.* Journal of neuroscience methods, 2012. **204**(1): p. 87-103.
78. Konopka, R., et al., *Alternation of retinoic acid induced neural differentiation of P19 embryonal carcinoma cells by reduction of reactive oxygen species intracellular production.* Neuroendocrinology Letters, 2008. **29**(5): p. 770.
79. Vega-Naredo, I., et al., *Mitochondrial metabolism directs stemness and differentiation in P19 embryonal carcinoma stem cells.* Cell Death & Differentiation, 2014. **21**(10): p. 1560-1574.
80. Yang, K., M. Hitomi, and D.W. Stacey, *Variations in cyclin D1 levels through the cell cycle determine the proliferative fate of a cell.* Cell division, 2006. **1**(1): p. 32.
81. Ruijtenberg, S. and S. van den Heuvel, *Coordinating cell proliferation and differentiation: Antagonism between cell cycle regulators and cell type-specific gene expression.* Cell cycle, 2016. **15**(2): p. 196-212.
82. Stacey, D.W., *Cyclin D1 serves as a cell cycle regulatory switch in actively proliferating cells.* Curr Opin Cell Biol, 2003. **15**(2): p. 158-63.

83. Hitomi, M. and D.W. Stacey, *Ras-dependent cell cycle commitment during G2 phase.* FEBS Letters, 2001. **490**(3): p. 123-131.
84. Liu, X., et al., *Extracellular signal-regulated Kinases (ERKs) phosphorylate Lin28a protein to modulate P19 cell proliferation and differentiation.* Journal of Biological Chemistry, 2017. **292**(10): p. 3970-3976.
85. Bartolák-Suki, E., et al., *Regulation of mitochondrial structure and dynamics by the cytoskeleton and mechanical factors.* International journal of molecular sciences, 2017. **18**(8): p. 1812.
86. Liu, X., et al., *Mitochondrial 'kiss-and-run': interplay between mitochondrial motility and fusion–fission dynamics.* The EMBO journal, 2009. **28**(20): p. 3074-3089.
87. Moore, A.S. and E.L. Holzbaur, *Mitochondrial-cytoskeletal interactions: dynamic associations that facilitate network function and remodeling.* Current opinion in physiology, 2018. **3**: p. 94-100.
88. Salazar-Roa, M. and M. Malumbres, *Fueling the Cell Division Cycle.* Trends Cell Biol, 2017. **27**(1): p. 69-81.
89. Syred, H.M., et al., *Cell cycle regulation of microtubule interactomes: multi-layered regulation is critical for the interphase/mitosis transition.* Molecular & Cellular Proteomics, 2013. **12**(11): p. 3135-3147.
90. Sakamaki, T., et al., *Cyclin D1 determines mitochondrial function in vivo.* Mol Cell Biol, 2006. **26**(14): p. 5449-69.
91. Kalucka, J., et al., *Metabolic control of the cell cycle.* Cell cycle (Georgetown, Tex.), 2015. **14**(21): p. 3379-3388.
92. Agostini, M., et al., *Metabolic reprogramming during neuronal differentiation.* Cell death and differentiation, 2016. **23**(9): p. 1502-1514.
93. Wang, Z., et al., *Cyclin B1/Cdk1 coordinates mitochondrial respiration for cell-cycle G2/M progression.* Developmental cell, 2014. **29**(2): p. 217-232.
94. Stacey, D.W., *Cyclin D1 serves as a cell cycle regulatory switch in actively proliferating cells.* Current Opinion in Cell Biology, 2003. **15**(2): p. 158-163.
95. Stevens, D.A., et al., *Parkin loss leads to PARIS-dependent declines in mitochondrial mass and respiration.* Proc Natl Acad Sci U S A, 2015. **112**(37): p. 11696-701.
96. Xiao, B., et al., *Flow cytometry-based assessment of mitophagy using MitoTracker.* Frontiers in cellular neuroscience, 2016. **10**: p. 76.
97. Scialò, F., D.J. Fernández-Ayala, and A. Sanz, *Role of mitochondrial reverse electron transport in ROS signaling: potential roles in health and disease.* Frontiers in physiology, 2017. **8**: p. 428.
98. Lee, I., E. Bender, and B. Kadenbach, *Control of mitochondrial membrane potential and ROS formation by reversible phosphorylation of cytochrome c oxidase.* Molecular and cellular biochemistry, 2002. **234**(1): p. 63-70.
99. Zorova, L.D., et al., *Mitochondrial membrane potential.* Analytical biochemistry, 2018. **552**: p. 50-59.
100. Su, Y., et al., *STAT3 Regulates Mouse Neural Progenitor Proliferation and Differentiation by Promoting Mitochondrial Metabolism.* Frontiers in Cell and Developmental Biology, 2020. **8**.
101. Ito, K. and T. Suda, *Metabolic requirements for the maintenance of self-renewing stem cells.* Nature reviews Molecular cell biology, 2014. **15**(4): p. 243-256.
102. Knobloch, M. and S. Jessberger, *Metabolism and neurogenesis.* Current opinion in neurobiology, 2017. **42**: p. 45-52.
103. Karsten, S.L., et al., *Global analysis of gene expression in neural progenitors reveals specific cell-cycle, signaling, and metabolic networks.* Developmental biology, 2003. **261**(1): p. 165-182.
104. Beckervordersandforth, R., et al., *Role of mitochondrial metabolism in the control of early lineage progression and aging phenotypes in adult hippocampal neurogenesis.* Neuron, 2017. **93**(3): p. 560-573. e6.

105. Pancrazi, L., et al., *Foxg1 localizes to mitochondria and coordinates cell differentiation and bioenergetics.* Proceedings of the National Academy of Sciences, 2015. **112**(45): p. 13910-13915.
106. Khacho, M., et al., *Mitochondrial dysfunction underlies cognitive defects as a result of neural stem cell depletion and impaired neurogenesis.* Human molecular genetics, 2017. **26**(17): p. 3327-3341.
107. Khacho, M., et al., *Mitochondrial dynamics impacts stem cell identity and fate decisions by regulating a nuclear transcriptional program.* Cell stem cell, 2016. **19**(2): p. 232-247.
108. Brunetti-Pierri, N., et al., *Duplications of FOXG1 in 14q12 are associated with developmental epilepsy, mental retardation, and severe speech impairment.* European Journal of Human Genetics, 2011. **19**(1): p. 102-107.
109. Mariani, J., et al., *FOXG1-dependent dysregulation of GABA/glutamate neuron differentiation in autism spectrum disorders.* Cell, 2015. **162**(2): p. 375-390.
110. Hanashima, C., et al., *Foxg1 suppresses early cortical cell fate.* Science, 2004. **303**(5654): p. 56-59.
111. Martynoga, B., et al., *Foxg1 is required for specification of ventral telencephalon and region-specific regulation of dorsal telencephalic precursor proliferation and apoptosis.* Developmental biology, 2005. **283**(1): p. 113-127.
112. Brancaccio, M., et al., *Emx2 and Foxg1 inhibit gliogenesis and promote neuronogenesis.* Stem Cells, 2010. **28**(7): p. 1206-1218.
113. Zheng, X., et al., *Metabolic reprogramming during neuronal differentiation from aerobic glycolysis to neuronal oxidative phosphorylation.* eLife, 2016. **5**: p. e13374.
114. Zhang, S. and W. Cui, *Sox2, a key factor in the regulation of pluripotency and neural differentiation.* World Journal of Stem Cells, 2014. **6**(3): p. 305-311.
115. Li, Z., M.H. Theus, and L. Wei, *Role of ERK 1/2 signaling in neuronal differentiation of cultured embryonic stem cells.* Dev Growth Differ, 2006. **48**(8): p. 513-23.
116. Cunningham, L.A. and R.A. Kahn, *Cofactor D functions as a centrosomal protein and is required for the recruitment of the gamma-tubulin ring complex at centrosomes and organization of the mitotic spindle.* J Biol Chem, 2008. **283**(11): p. 7155-65.
117. Okumura, M., et al., *Linking cell surface receptors to microtubules: tubulin folding cofactor D mediates Dscam functions during neuronal morphogenesis.* Journal of Neuroscience, 2015. **35**(5): p. 1979-1990.
118. Poulain, F.E. and A. Sobel, *The microtubule network and neuronal morphogenesis: Dynamic and coordinated orchestration through multiple players.* Molecular and Cellular Neuroscience, 2010. **43**(1): p. 15-32.
119. Forwood, J.K., et al., *Kap95p binding induces the switch loops of RanGDP to adopt the GTP-bound conformation: implications for nuclear import complex assembly dynamics.* Journal of molecular biology, 2008. **383**(4): p. 772-782.
120. Sirajuddin, M., L.M. Rice, and R.D. Vale, *Regulation of microtubule motors by tubulin isotypes and post-translational modifications.* Nature cell biology, 2014. **16**(4): p. 335-344.
121. Vemu, A., et al., *Tubulin isoform composition tunes microtubule dynamics.* Molecular biology of the cell, 2017. **28**(25): p. 3564-3572.
122. Pamula, M.C., S.-C. Ti, and T.M. Kapoor, *The structured core of human β tubulin confers isotype-specific polymerization properties.* Journal of Cell Biology, 2016. **213**(4): p. 425-433.
123. Janke, C. and M.M. Magiera, *The tubulin code and its role in controlling microtubule properties and functions.* Nature Reviews Molecular Cell Biology, 2020. **21**(6): p. 307-326.
124. Sheng, Z.-H. and Q. Cai, *Mitochondrial transport in neurons: impact on synaptic homeostasis and neurodegeneration.* Nature Reviews Neuroscience, 2012. **13**(2): p. 77-93.
125. Lopez-Mejia, I.C. and L. Fajas, *Cell cycle regulation of mitochondrial function.* Current opinion in cell biology, 2015. **33**: p. 19-25.

126. Gabrielli, B.G., et al., *A cyclin D-Cdk4 activity required for G2 phase cell cycle progression is inhibited in ultraviolet radiation-induced G2 phase delay.* J Biol Chem, 1999. **274**(20): p. 13961-9.
127. Alao, J.P., *The regulation of cyclin D1 degradation: roles in cancer development and the potential for therapeutic invention.* Molecular cancer, 2007. **6**: p. 24-24.
128. Bunz, F., et al., *Requirement for p53 and p21 to Sustain G₂ Arrest After DNA Damage.* Science, 1998. **282**(5393): p. 1497-1501.
129. Gire, V. and V. Dulić, *Senescence from G2 arrest, revisited.* Cell Cycle, 2015. **14**(3): p. 297-304.
130. Khacho, M., et al., *Mitochondrial Dynamics Impacts Stem Cell Identity and Fate Decisions by Regulating a Nuclear Transcriptional Program.* Cell Stem Cell, 2016. **19**(2): p. 232-247.
131. Bienvenu, F., et al., *Transcriptional role of cyclin D1 in development revealed by a genetic–proteomic screen.* Nature, 2010. **463**(7279): p. 374-378.
132. Hydbring, P., M. Malumbres, and P. Sicinski, *Non-canonical functions of cell cycle cyclins and cyclin-dependent kinases.* Nature reviews Molecular cell biology, 2016. **17**(5): p. 280-292.
133. Horbay, R. and R. Bilyy, *Mitochondrial dynamics during cell cycling.* Apoptosis, 2016. **21**(12): p. 1327-1335.
134. Marcussen, M. and P.J. Larsen, *Cell cycle-dependent regulation of cellular ATP concentration, and depolymerization of the interphase microtubular network induced by elevated cellular ATP concentration in whole fibroblasts.* Cell Motility, 1996. **35**(2): p. 94-99.
135. Lunt, S.Y., et al., *Pyruvate kinase isoform expression alters nucleotide synthesis to impact cell proliferation.* Mol Cell, 2015. **57**(1): p. 95-107.
136. Bani-Yaghoub, M., et al., *Role of Sox2 in the development of the mouse neocortex.* Developmental biology, 2006. **295**(1): p. 52-66.
137. Sikorska, M., et al., *Epigenetic modifications of SOX2 enhancers, SRR1 and SRR2, correlate with in vitro neural differentiation.* Journal of neuroscience research, 2008. **86**(8): p. 1680-1693.
138. Ratineau, C., et al., *Cyclin D1 represses the basic helix-loop-helix transcription factor, BETA2/NeuroD.* Journal of Biological Chemistry, 2002. **277**(11): p. 8847-8853.
139. Bulstrode, H., et al., *Elevated FOXG1 and SOX2 in glioblastoma enforces neural stem cell identity through transcriptional control of cell cycle and epigenetic regulators.* Genes & development, 2017. **31**(8): p. 757-773.

Chapter 4 Characterisation of a TBCD A475T CRISPR Mouse Line

4.1 Introduction

The cerebral cortex (also called the neocortex) constitutes the major information processing network of the mammalian brain responsible for higher order functions, including sensorimotor planning, language, and learning [1-5]. The cerebral cortex is the outermost layer of the cerebrum and is comprised of specialled neurons organised into six histologically distinct layers (I-VI) that arise in an inside-out pattern along the ventrodorsal axis of the developing brain [6-11]. The earliest migrating neurons form the deepest layers of the cortex (V and VI), whilst the later migrating neurons sequentially form more superficial layers. Each cortical layer contains neurons that can be broadly categorised by their morphology and neurotransmitter properties into two distinct groups: interneurons (INs) and projection neurons (PNs) [6, 7, 10-13]. Whilst both are essential for information processing and distribution, INs establish local connections, whereas PNs can establish both short and long-range connections by extending their axons to subcortical and intercortical targets [14-18]. Establishment of these neurons in their appropriate locations is crucial for appropriate neuronal development and function [19-23].

Neocortical development is mediated by actions of the highly dynamic neuronal cytoskeleton within neural cells. Cytoskeleton organisation, assembly, disassembly, and coordinated remodelling facilitates neuronal proliferation, migration and terminal differentiation in order to establish cortical layers [9, 24, 25]. Dysregulation of neuronal cytoskeleton dynamics (for example due to clinical mutations) leads to neurodevelopmental disorders such as microcephaly [26], which is characterised by severe intellectual disability and microcephaly (small brain). Microcephaly is a consequence of impaired brain development and maturation resulting in a head circumference more than three standard deviations below the norm for a given age [22, 23, 26, 27]. Primary microcephaly (also known as microcephaly vera) is a foetal neurodevelopmental disorder and presents with microcephaly at birth. Primary microcephaly is characterised by molecular perturbations in neuronal proliferation during embryonic development. Some of these molecular perturbations are attributed to disruptions to MT cytoskeleton dynamics [20, 26, 28, 29]. Secondary microcephaly is characterised by post-natal microcephaly, and can arise due to disruptions to neuronal migration and/or increased

degeneration/death of neurons resulting in microcephaly. In contrast to primary microcephaly, majority of secondary microcephaly cases are not associated with disruptions of the MT cytoskeleton dynamics [26, 30-32]. Recently however, several studies have reported clinical mutations in the key MT biosynthesis chaperone tubulin folding co-factor D (TBCD) that compromise the dynamic behaviour of the neuronal cytoskeleton, leading to an infantile neurodegenerative disorder characterized by global developmental delay, dystonia, seizures, and acquired microcephaly (also known as secondary microcephaly) [33-37].

TBCD acts as a scaffold for the assembly of several co-factors involved in the assembly and disassembly of αβ-tubulin heterodimers, and is essential to the polymerization and depolymerisation of MTs [25, 38-42]. TBCD acts in concert with ADP ribosylation factor-like protein 2 (Arl2), TBCE and TBCC to catalyse the formation of the αβ-tubulin dimers from the individual monomeric subunits. The αβ-tubulin heterodimers can then be incorporated into the growing MT lattice in a GTP-dependent manner. Acting in reverse, TBCE can bind the αβ-heterodimers, dissociating α-tubulin and subsequently mediating its proteolytic degradation alone or in concert with TBCB [9, 43-45]. Similarly, TBCD binds, dissociates and sequesters β-tubulin in the absence of Arl2. Overexpression of either TBCE or TBCD leads to the rapid and unregulated destruction of the cells MT network. In addition, TBCD has been implicated in mitosis, spindle morphology and cell abscission in various organisms [41, 46-51].

Recent studies have identified clinical mutations in the *TBCD* gene that perturb the critical role of TBCD in MT dynamics, leading to severe infantile neurodegenerative pathologies, like cortical atrophy and acquired microcephaly, resulting in intellectual disability, seizures, and dystonia [33, 34, 36, 37, 52]. Two of the recent case studies have identified the homozygous missense mutations A475T and A586V, resulting in reduced expression of TBCD [33, 37]. Additionally, A475T and A586V mutant TBCD proteins were found to be functionally less efficient in αβ-tubulin heterodimer disassembly. Nevertheless the mutant TBCD proteins partially restored neural progenitor proliferation and radial migration in TBCD knockout cells [33, 37]. Several other studies have identified a further 13 clinical mutations in the TBCD gene, each of which perturbed MT dynamics resulting in increased MT stability [33, 34, 36, 37, 52]. Although TBCD clinical mutations have indicated a critical role for TBCD in MT cytoskeleton formation and neuronal development, the exact molecular mechanism underlying this process is not yet fully understood. A detailed analysis of the previously identified clinical

mutations may offer new and unique insights into molecular mechanisms of TBCD's mode of action and its role in brain development and diseases.

In this chapter, a transgenic TBCD clinical mutation A475T knock-in mouse model was characterised. The results demonstrate that this mutation leads to prenatal aberrations in NSCs proliferation, migration and identity. Postnatally, mice with a TBCD A475T mutation showed evidence of cortical malformation, observed as disruptions in cortical lamination, significantly reduced cortical thickness, weight, and length. These data suggest that TBCD mutations influence the proliferation, migration and development of NSCs, and the mouse model may be useful to understand disease progression *in vivo*.

4.2 Results

4.2.1 CRISPR-engineered TBCD$^{A475T/A475T}$ mice have perturbed brain anatomy

To investigate the pathogenesis of the TBCD Alanine to Threonine (TBCD^{A475T}) amino acid substitution detected in patients diagnosed with secondary microcephaly, I used a recently generated CRISPR-Cas9 knock in mouse model carrying the corresponding patient single nucleotide variant in homozygous and heterozygous mice (*Homo sapiens,* TBCD gene, Chr 17: NM_005993, c.G1423A, p.A475T, *Mus musculus,* TBCD gene, Chr 11: NM_029878.4, c.G1429A, p.A477T) [33, 37]. To achieve this, the mouse model was assessed by examining, at different embryonic time points, the gross brain morphology of the heterozygous and homozygous A475T mutations, from now on referred to as TBCD$^{A475T/WT}$ and TBCD$^{A475T/A475T}$ respectively, compared to their wild-type (WT) littermates (**Fig. 4.1**)

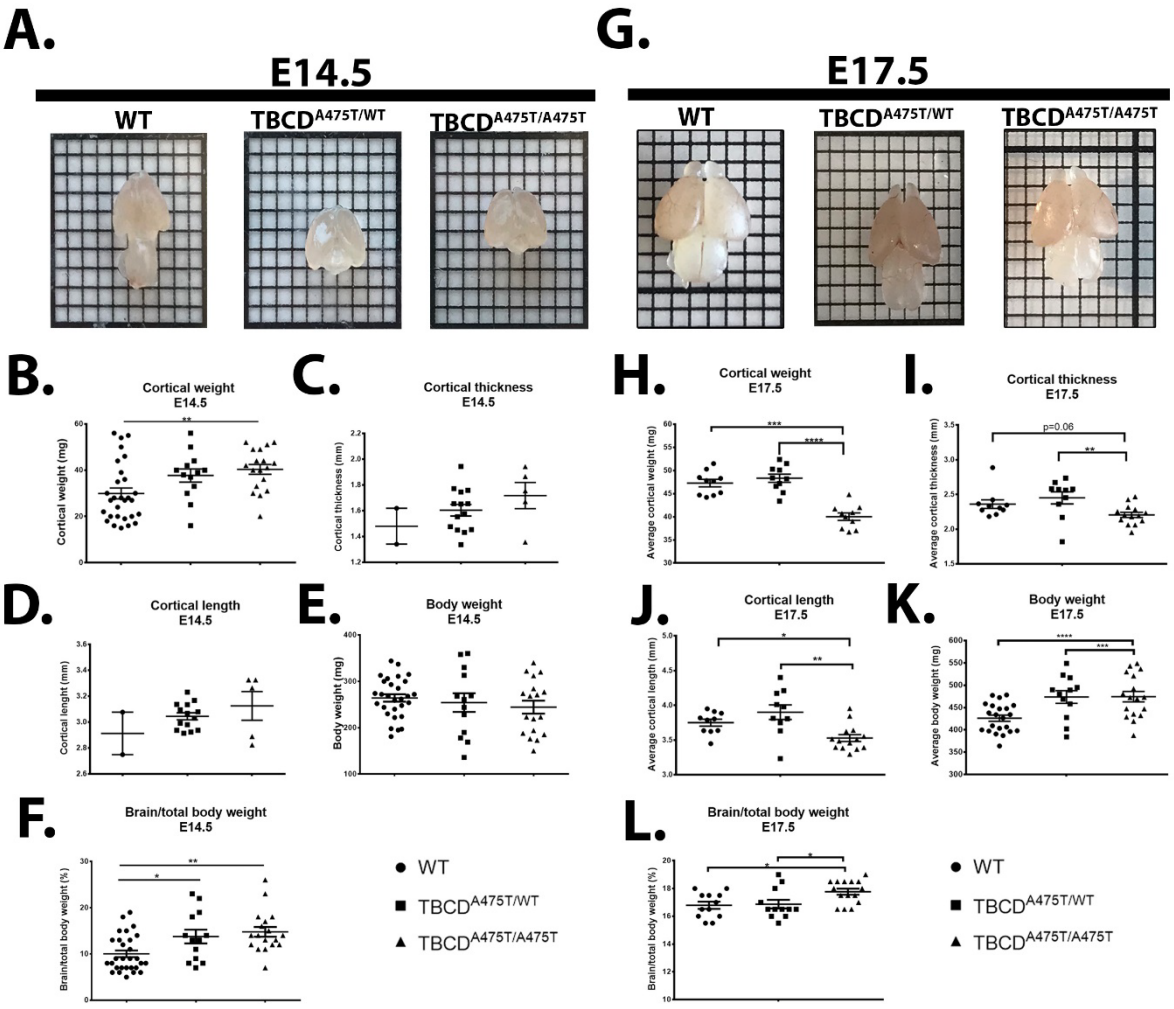

Figure 4.1. TBCD$^{A475T/A475T}$ mice display a perturbed brain anatomy

Gross brain morphology was assessed at embryonic day 14.5 (E14.5) (A-F) and E17.5 (G-L) for wild-type mice and mice carrying the TBCD A475T mutation variant in a heterozygous (TBCD$^{A475T/WT}$) and homozygous fashion (TBCD$^{A475T/A475T}$). (A and G) Representative images of wild-type, heterozygous and homozygous mice brains at E14.5 and E17.5. (B and H) Assessment of cortical weight (mg). (C, D, I and J) Measurements of gross cortical thickness and length at all time points. (E, F, K and L) Assessment body weight (mg) and brain weight (as % of total weight) at E14.5 (E and F) and E17.5 (K and L). Data represents mean ± SEM. n ≥ 2 brains per genotype at E14.5 and n ≥ 5 brains per genotype at E17.5. *P < 0.05, **P < 0.01, ***P < 0.001, ****P < 0.0001.

Cortical weight measurements at embryonic day E14.5 (E14.5), revealed that TBCD$^{A475T/A475T}$ mice had significantly heavier cortices (~40.3 mg) compared to WT mice (~29.9 mg, p <0.01), but not heterozygous TBCD$^{A475T/WT}$ mice (~37.06 mg) (**Fig. 4.1B**). No statistically significant differences were observed between the cortical weight of WT and TBCD$^{A475T/WT}$ mice. Extending these findings, assessment of gross brain morphology at E14.5, showed that TBCD$^{A475T/A475T}$ mice trended towards an increase in both cortical thickness and length (~1.7 mm, and ~3.1 mm, respectively) compared to both WT (~1.4 mm, and ~2.9 mm, respectively), and TBCD$^{A475T/WT}$ littermates (~1.6 mm, and ~3.0 mm, respectively) (**Fig. 4.1C and D**).

At E17.5, TBCD$^{A475T/A475T}$ cortices had a reduced cortical weight, thickness, and length compared to their WT (~15%, $p < 0.001$, ~7%, $p=0.06$, and ~6%, $p < 0.05$, respectively) and TBCD$^{A475T/WT}$ litter mates (17%, $p < 0.0001$~7%, $p < 0.05$, and 7%, $p < 0.05$, respectively) (**Fig. 4.1G-J**). However, when comparing cortical weight relative to total body weight, TBCD$^{A475T/A475T}$ mouse brains were significantly heavier versus WT (~15%, $p < 0.05$) and TBCD$^{A475/WT}$ (13%, $p < 0.05$) at E17.5 (**Fig. 4.1J-L**). To elucidate the impact of the TBCD$^{A475T/A475T}$ mutation on cortical development, 16µm thick coronal cryo-sections of foetal brains at E14.5 and E17.5 were Nissl-stained to assess brain morphology (**Fig. 4.2**).

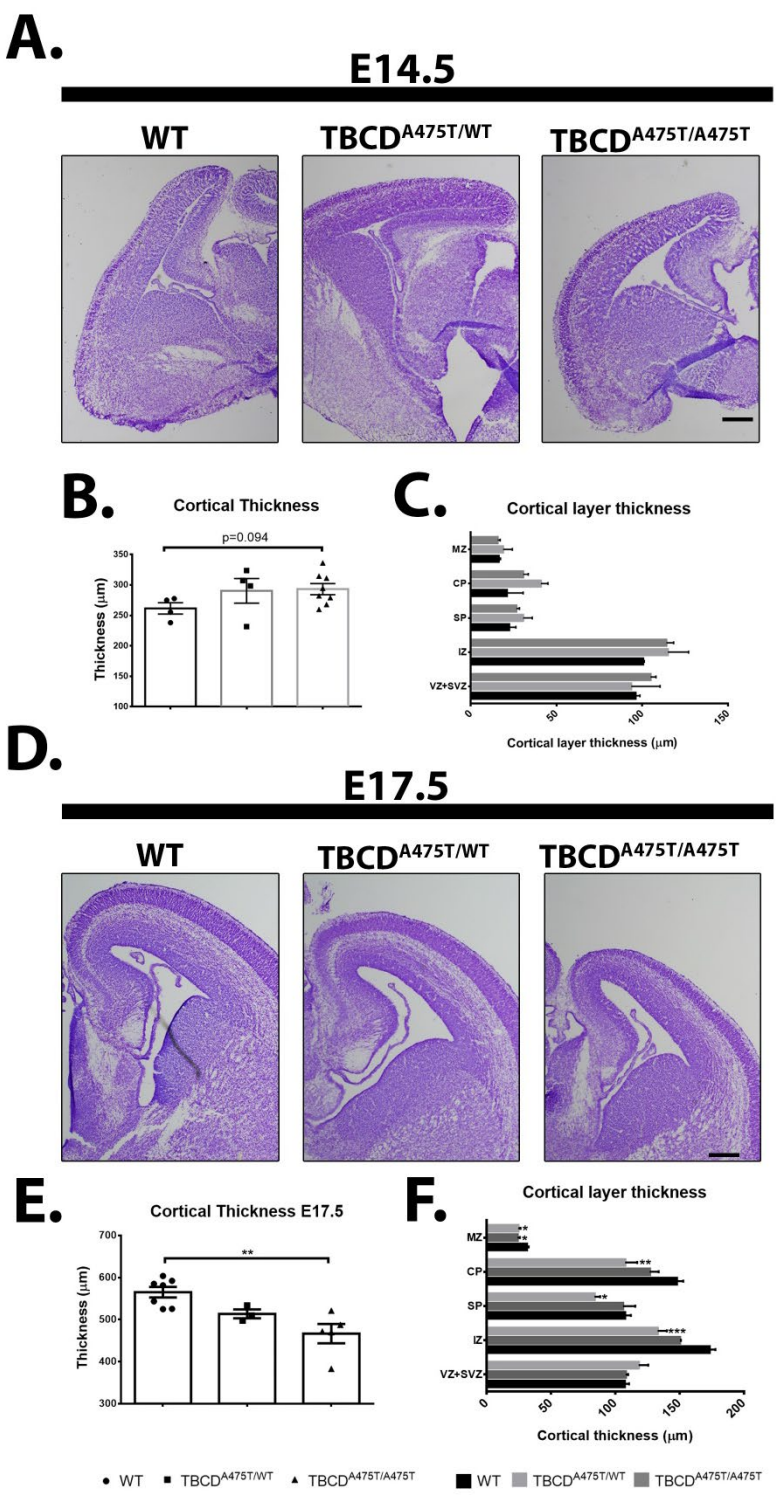

Figure 4.2. Alterations to cortical morphology are observed in TBCD$^{A475T/A475T}$ mice

Representative Nissl staining of coronal sections from WT, TBCD$^{A475T/WT}$ and TBCD$^{A475T/A475T}$ mice at E14.5 (A) and E17.5 (D). (B, C, E and F) Quantification of Nissl stained coronal sections assessing total cortical thickness (B and E) and individual cortical layer thickness of the Ventricular/Sub-ventricular zone (VZ/SVZ), Intermediate zone (IZ), Subplate (SP), and Cortical plate (CP) and Marginal zone (MZ) at all time points. For each brain, a rostral, medial and caudal section for the right and left hemisphere were measured and results averaged. Data represents mean ± SEM. $n \geq 2$ brains per genotype at E14.5 and $n \geq 5$ brains per genotype at E17.5. *$P < 0.05$, **$P < 0.01$, ***$P < 0.001$, ****$P < 0.0001$. Scale bar 200 µm.

4.2.2 Alterations to cortical morphology are observed in TBCD$^{A475T/A475T}$ mice

Nissl-stained coronal sections at E14.5 revealed no significant changes between the groups at E14.5, however, this is most likely due to the small sample size of the WT group at this time point, and would require a larger sample size in order for the differences to be observed, and is further detailed in the discussion. Although no significant differences were observed for Nissl-stained coronal sections at E14.5, a slight increase in total cortical thickness was observed in TBCD$^{A475T/A475T}$ mice (293.3 µm ± SEM 9.16 µm), and to a lesser extent in TBCD$^{A475T/WT}$ brains (290.4 µm ± SEM 20.25 µm), compared to WT (261.66 µm ±SEM 9.28 µm, p= 0.09 and 0.17, respectively) (**Fig. 4.2A and B**). No significant difference was observed in the thickness of individual cortical layers at E14.5 (**Fig. 4.2C**).

At E17.5, TBCD$^{A475T/A475T}$ mouse brains had severely perturbed cortical morphology and laminar organisation (**Fig. 4.2D-F**), with a significant reduction of approximately 20% observed in the total cortical thickness compared to WT ($p < 0.01$) (**Fig. 4.2E**). Whilst the cortical thickness of TBCD$^{A475T/WT}$ foetal brains at E17.5 were smaller and larger compared to WT (~8%) and TBCD$^{A475T/A475T}$ respectively (~10%), this was not significantly different to either group (**Fig. 4.2E**). On closer inspection, and in comparison to WT foetal brains at E17.5, TBCD$^{A475T/A475T}$ had on average an approximate reduction of 23% in thickness of the intermediate zone (IZ) ($p < 0.001$), subplate (SP) ($p < 0.05$), and cortical plate (CP) ($p < 0.01$), whilst a non-significant increase of approximately 10% was observed in the thickness of the ventricular/sub-ventricular zone (VZ/SVZ) (**Fig. 4.2F**). A similar but statistically insignificant decrease was observed in TBCD$^{A475T/A475T}$ mice compared to TBCD$^{A475T/WT}$ in the thickness of the IZ (~12%), SP (~21%, p=0.07) and CP (~16%) (**Fig. 4.2F**). In addition, both TBCD$^{A475T/WT}$ and TBCD$^{A475T/A475T}$ mice had an approximate reduction of 21% in marginal zone (MZ) thickness in comparison to WT littermates ($p < 0.05$ for both) (**Fig. 4.2F**). Taken together, these data indicate that the TBCD clinical mutation A475T results in premature cortical growth and lamination early in embryonic development (E14.5), leading to a progressively reduced brain anatomy at later developmental stages (E17.5).

4.2.3 Reduced TBCD$^{A475T/A475T}$ stability leads to developmental disturbances

Previous studies analysing TBCD clinical mutations have indicated a reduction in mutant TBCD protein expression, attributed to the impact of the mutations on protein structure and function [33-37]. Reduced expression or changes in structure of TBCs severely perturbs the

MT lattice and dynamics, leading to a plethora of neurodegenerative and developmental disorders [9, 24, 25, 44]. Thus, I sought to assess the protein expression of TBCD, total αβ-tubulin, and β-actin in whole brain lysates at E14.5 (**Fig. 4.3**) and E17.5 (**Fig. 4.4**). Similar to previous studies, analyses revealed a significant reduction in expression of mutant TBCD protein levels in $TBCD^{A475T/A475T}$ mice (~20%, $p < 0.0001$) (**Figs. 4.3A and B, and 4.4A and B**) [33-37]. Interestingly, a statistically significant increase in $TBCD^{A475T/A475T}$ foetal brains was observed at E14.5 and E17.5 in the total level of αβ-tubulin (26%, $p < 0.05$ and 31%, $p < 0.05$, respectively), and a similar although non-significant trend towards an increase in β-actin levels (27% and 10%, respectively) compared to WT (**Figs. 4.3A and B 4.4A and B**). No significant changes in protein expression were observed in the $TBCD^{A475T/WT-}$ mice at either time point for any markers assessed. These data are unique in that they differ from those of previous studies, wherein the authors do not assess the total level of αβ-tubulin, rather they report only changes in either α or β-tubulin, and is further detailed in the discussion [33, 34, 36, 37, 52].

To elucidate the role that the TBCD A475T mutation plays in neuronal development, immunofluorescent staining was used to investigate the expression of the early neuronal marker β-III Tubulin (Tuj1), and Pax6 (Paired box protein Pax-6), a homeodomain transcription factor involved in proliferation, lamination and differentiation in the developing cortex(**Fig. 4.3**) [6, 53]. Examination of coronal sections from E14.5 mice revealed that, whilst there was no significant differences in the thickness of either the Tuj1 positive or Pax6 positive immunostained layers, and/or cell number, between any groups, there was a slight increase in the total layer thickness of Tuj1 and Pax6 of approximately 1.27 and 1.20-fold respectively in $TBCD^{A475T/A475T}$ cortices, when compared to WT (**Fig. 4.3C-I**). Additionally, when compared to WT littermates, $TBCD^{A475T/A475T}$ mice brains displayed an increase of approximately 1.15-fold in the total and relative number of Pax6 positive (Pax6+) cells, as well as an approximate 2.5-fold increase in the total and relative number of ectopic Pax6+ cells (**Fig. 4.3F-I**). Similar, but still statistically insignificant increases were observed in Tuj1+ immunostained layer thickness (~1.3-fold), and the number of ectopic Pax6+ cells (~2.5-fold) in $TBCD^{A475T/WT}$ mice when compared to WT (**Fig. 4.3F-I**). No significant changes were observed in either the total or relative number of Pax6+ cells for $TBCD^{A475T/WT}$ cortices in comparison to all other groups (**Fig. 4.3D and E)**.

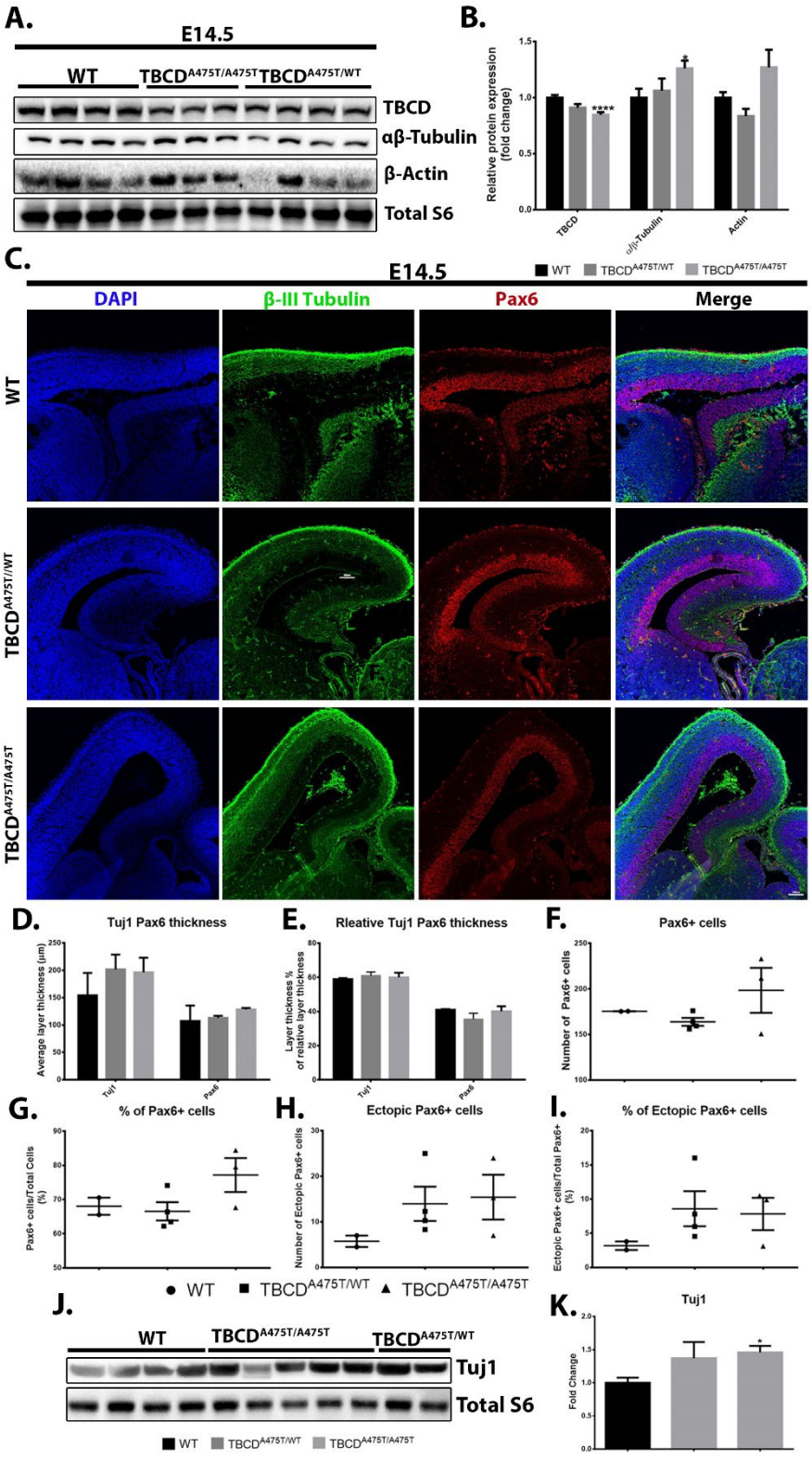

Figure 4.3. Reduced TBCD stability leads to developmental disturbance in TBCD$^{A475T/A475T}$ mice

(A and B) Immunoblot and band densitometry analysis of TBCD, total αβ-Tubulin and β-Actin protein expression levels from wild-type (WT), TBCD$^{A475T/WT}$ and TBCD$^{A475T/A475T}$ mice at E14.5, (B) Representative images of immunostained coronal sections of E14.5 mice for DAPI (blue), Paired box protein Pax-6 (Pax6) (red) and class III β- tubulin (Tuj1) (green). (C-I) Quantification of the Pax6- and Tuj1-positive total and relative immunostained layer thickness (C and D), total DAPI positive (+) cells (E), total Pax6+ cells (F), ectopic Pax6+ cells (G), relative (%) of Pax6+ cells (H) and ectopic Pax6+ cells (I). (J and K) Analysis of Tuj1 protein expression from whole brain lysates. For each brain, a rostral, medial and caudal section were measured and results averaged. Data represents mean ± SEM. n ≥ 2 brains per genotype. *P < 0.05, **P < 0.01, ***P < 0.001, ****P < 0.0001. Scale bar 100µm

Adding to these findings, analysis of whole brain lysates from E14.5, revealed an approximate 1.45-fold increase of Tuj1 protein expression in TBCD$^{A475T/A475T}$ mice compared to WT control ($p < 0.05$), while a similar but non-significant increase was observed in the TBCD$^{A475T/WT}$ brains compared to WT (~1.37-fold) (**Fig. 4.3J and K**).

Extending these early embryonic findings, examination of E17.5 cortices revealed an increase of approximately 22% and 45% in the total and relative Pax6 layer thickness of $TBCD^{A475T/A475T}$ cortices compared to either WT ($p < 0.001$ and $p < 0.0001$, respectively) or $TBCD^{A475T/WT}$ littermates ($p < 0.01$ and $p < 0.001$, respectively) (**Fig. 4.4C-E).** Additionally, the total number of Pax6+ and DAPI+ cells in $TBCD^{A475T/A475T}$ mice were increased by approximately 30%, compared to either WT ($p < 0.05$ and $p < 0.05$, respectively) and 40% versus heterozygous littermates ($p < 0.01$ and $p < 0.01$, respectively) (**Fig. 4.4F and G**). Whilst no differences were observed between any group in the relative number of Pax6+ or DAPI+ cells, $TBCD^{A475T/WT}$ cortices possessed a significant increase in the total and relative number of ectopic Pax6+ cells compared to both WT (~2-fold, $p < 0.05$, and ~3-fold $p < 0.0001$, respectively) and $TBCD^{A475T/A475T}$ mice (~1.4-fold, $p < 0.01$, and ~1.3-fold, $p < 0.0001$, respectively) (**Fig. 4.4G-J**). In contrast to the earlier embryonic findings, the expression of Tuj1 in both tissue sections and protein lysates at E17.5, was significantly decreased in $TBCD^{A475T/A475}$ mice compared to their WT littermates (~20%, $p < 0.0001$, and ~25%, $p < 0.01$, respectively) (**Fig. 4.4A-F**). Pax6 is known to have a dosage dependent control on proliferation, neurogenesis and laminar fate, with both overexpression and under expression leading to neurogenesis at the expense of self-renewal, albeit via distinct mechanisms [6, 7, 10, 53]. Whilst the loss of Pax6 expression leads to reduced expression of cell cycle regulators, and thus premature neurogenesis, enhanced Pax6 expression upregulates key transcription factors, such as T-box brain protein 2 (Tbr2), thereby promoting neurogenesis and basal progenitor genesis (BP, aka intermediate progenitor cells (IPCs) [53-60]. It is thus attractive to hypothesise that in this model, the increased expression of Pax6 in $TBCD^{A475T/A475T}$ mice may result in premature BP genesis at the expense of self-renewal.

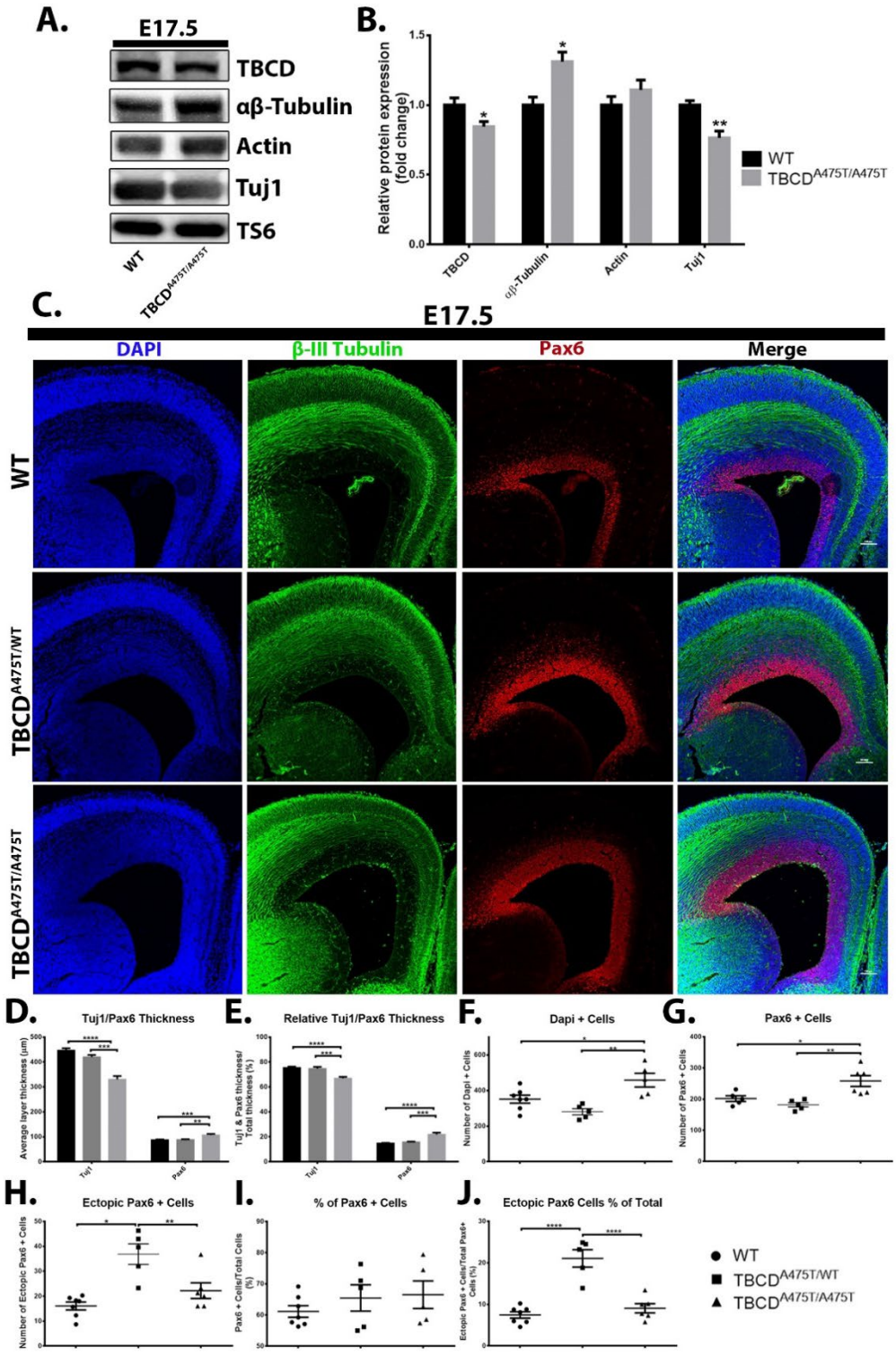

Figure 4.4. Changes in markers of cell proliferation and neuronal maturation in TBCD$^{A457T/A475T}$ mice

(A and B) Assessment of TBCD, total αβ-Tubulin, β-Actin and Tuj1 protein expression levels from whole brain lysates of WT, TBCD$^{A475T/WT}$ and TBCD$^{A475T/A475T}$ mice at E17.5. (C) Representative images of immunostained coronal sections of E17.5 mice for DAPI (blue), Pax6 (red) and Tuj1 (green). (D-J) Quantification of the Pax6- and Tuj1-positive total and relative immunostained layer thickness (D and E), total DAPI positive (+) cells (F), total Pax6+ cells (G), ectopic Pax6+ cells (H), relative (%) of Pax6+ cells (I) and ectopic Pax6+ cells (J). For each brain, a rostral, medial and caudal section were measured and results averaged. Data represents mean ± SEM. n ≥ 5 brains per genotype. *P < 0.05, **P < 0.01, ***P < 0.001, ****P < 0.0001. Scale bar 100µm.

4.2.4 TBCD impacts neuronal identity *in vivo*

Switching of NSCs from symmetric divisions to asymmetric divisions marks the beginning of neurogenesis and results in the generation of two daughter cells. One daughter cell will retain the self-renewal capacity of the mother cell and can be another NSC or a radial glial cell (RGC). Whereas the other daughter will become either an apical RGC (a highly related but distinct NSC type), a BP/IPC or a postmitotic neuron. [6, 61, 62]. Fortunately, a plethora of research examining this coordinated stepwise process has identified a range of neuronal markers that can be sequentially expressed and repressed during neurogenesis, thereby enabling an estimation of their current developmental state [6, 12, 53, 63, 64]. One such example of this, is the sequential expression of Pax6→Tbr2→Tbr1 during the differentiation of RGC to IPC to postmitotic projection neuron respectively. Highly expressed in the VZ/SVZ, Tbr2 (aka Eomes) is upregulated and Pax6 downregulated as cells transition from RG to IPCs/BPs [53, 54, 57-60, 65, 66]. It should be noted however, that in rodents a small proportion of newly differentiating IPCs can co-express Pax6 and Tbr2, whilst many progenitors co-express Pax6 and Tbr2 in primates [6, 53, 54, 67]. Following this, the majority of progenitors will undergo terminal division, and migrate towards the CP. Migration towards the CP is marked by the upregulation of T-box brain protein 1 (Tbr1), a regulator of postmitotic neurons regional and laminar identity, and BAF Chromatin Remodelling Complex Subunit BCL11B (Ctip2), a zinc finger protein essential for proliferation, differentiation and subcortical projection neuron identity [14-16, 53, 65, 66]. Coupling this knowledge with the altered cortical morphology and aberrant Pax6/Tuj1 expression observed in $TBCD^{A475T/A475T}$ embryonic mice, prompted investigation to delineate the impact of the clinical TBCD A475T mutation on cortical lamination and neuronal identity. To achieve this, immunofluorescence staining was conducted to investigate the expression of the neuronal markers; Tbr2, Tbr1, and Ctip2.

Examination of E14.5 cortices revealed no significant differences in the total or relative number of Tbr2+ cells between any groups (**Fig. 4.5A, D-F**). However, $TBCD^{A475T/A475T}$ mice did display a slight increase in total Tbr2 layer thickness, compared to WT (~21%) and $TBCD^{A475T/WT}$ mice (~15%) (**Fig. 4.5A-C**). Extending these findings, $TBCD^{A475T/A475T}$ E14.5 cortices stained with Tbr1 and Ctip2 displayed an approximate increase in relative layer thickness of 40% and 45%, respectively, compared to WT ($p < 0.05$ for both markers), and 20%, for both markers, when compared to $TBCD^{A475T/WT}$ mice (**Fig. 4.5H-J**). No significant

differences were observed in the total number of Tbr1+ and Ctip2+ cells between the groups. However, quantification of the relative number of Tbr1+ and Ctip2+ cells revealed an increase of approximately 26% in TBCD$^{A475T/A475T}$ mice cortices compared to WT ($p < 0.01$ and $p < 0.05$, respectively), and 16% compared to TBCD$^{A475T/WT}$ litter mates ($p < 0.05$ and $p < 0.05$, respectively) (**Fig. 4.5N and O**). Thus, at E14.5, TBCD$^{A475T/A475T}$ mice possess an increased expression of deep layer neuronal markers, compared to WT or TBCD$^{A475T/WT}$ littermates.

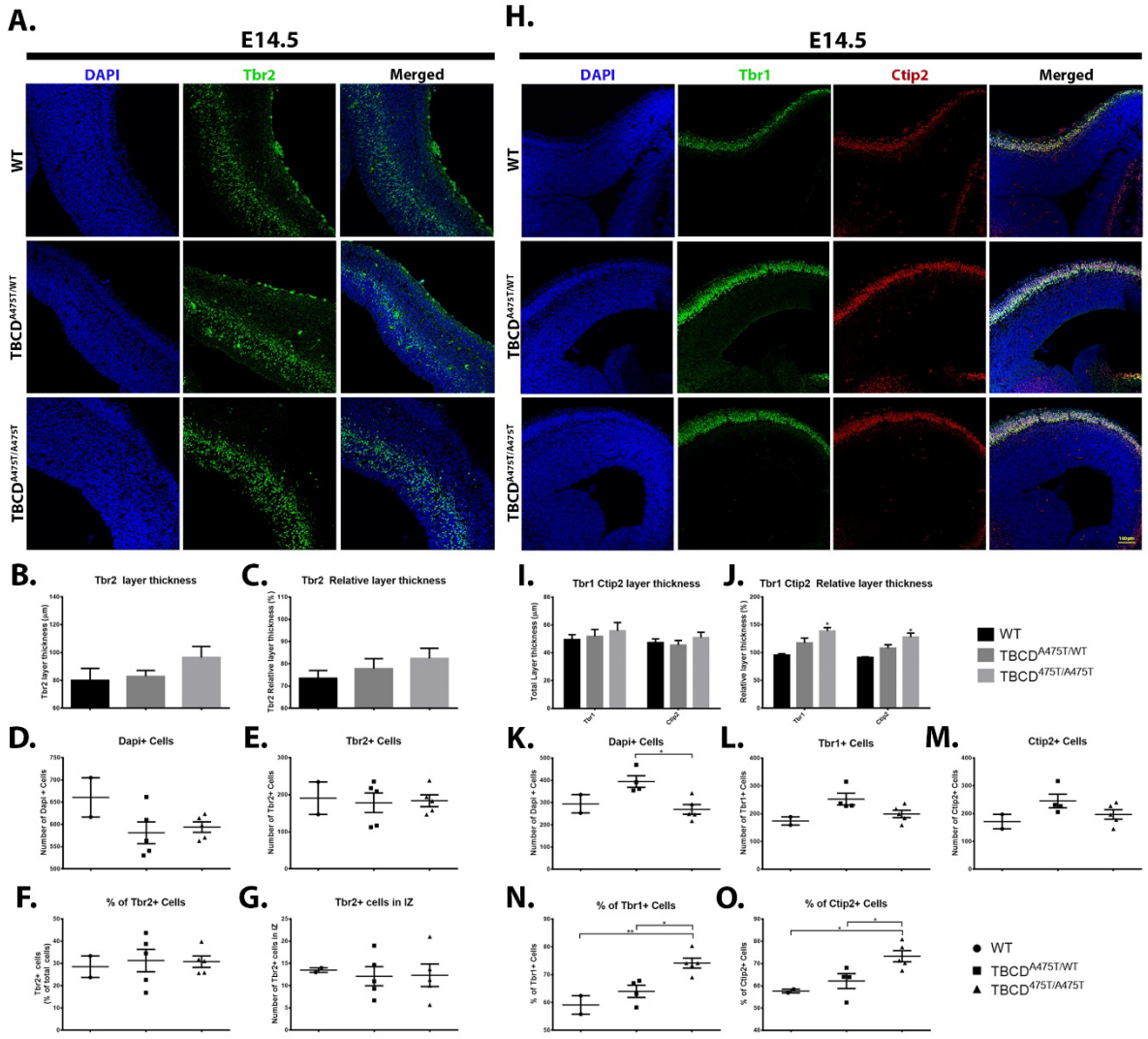

Figure 4.5. TBCD$^{A475T/A475T}$ display altered cortical lamination.

Representative images of E14.5 coronal sections for WT, TBCD$^{A475T/WT}$ and TBCD$^{A475T/A475T}$ embryonic mice. (A-O) Immunostaining and quantification for T-box brain protein 2 (Tbr2) (A-G), and Tbr1 and BAF Chromatin Remodelling Complex Subunit BCL11B (Ctip2) (H-O) (A) Co-staining of Tbr2 (green) and DAPI (blue) stained E14.5 cortices. (B-G) Quantification of total and relative Tbr2+ immunostained thickness (B and C), DAPI + cells (D), total and relative Tbr2+ cells (E and F), and Tbr2+ cells in the IZ (G). (H) Tbr1 (green), Ctip2 (red) and DAPI (blue) stained WT, TBCD$^{A475T/WT}$ and TBCD $^{A547T/A475T}$ brains at E14.5. (I and J) Total and relative Tbr1 and Ctip2 layer thickness, (K) DAPI + cells, total and relative number of Tbr1+ and Ctip2+ cells in the cortical plate (CP) (L-O). For each brain, a rostral, medial and caudal section were measured and results averaged. Data represents mean ± SEM. n ≥ 2 brains per genotype at E14.5 and n ≥ 5 brains per genotype at E17.5. *P < 0.05, **P < 0.01, ***P < 0.001, ****P < 0.0001. Scale bar 100 µm.

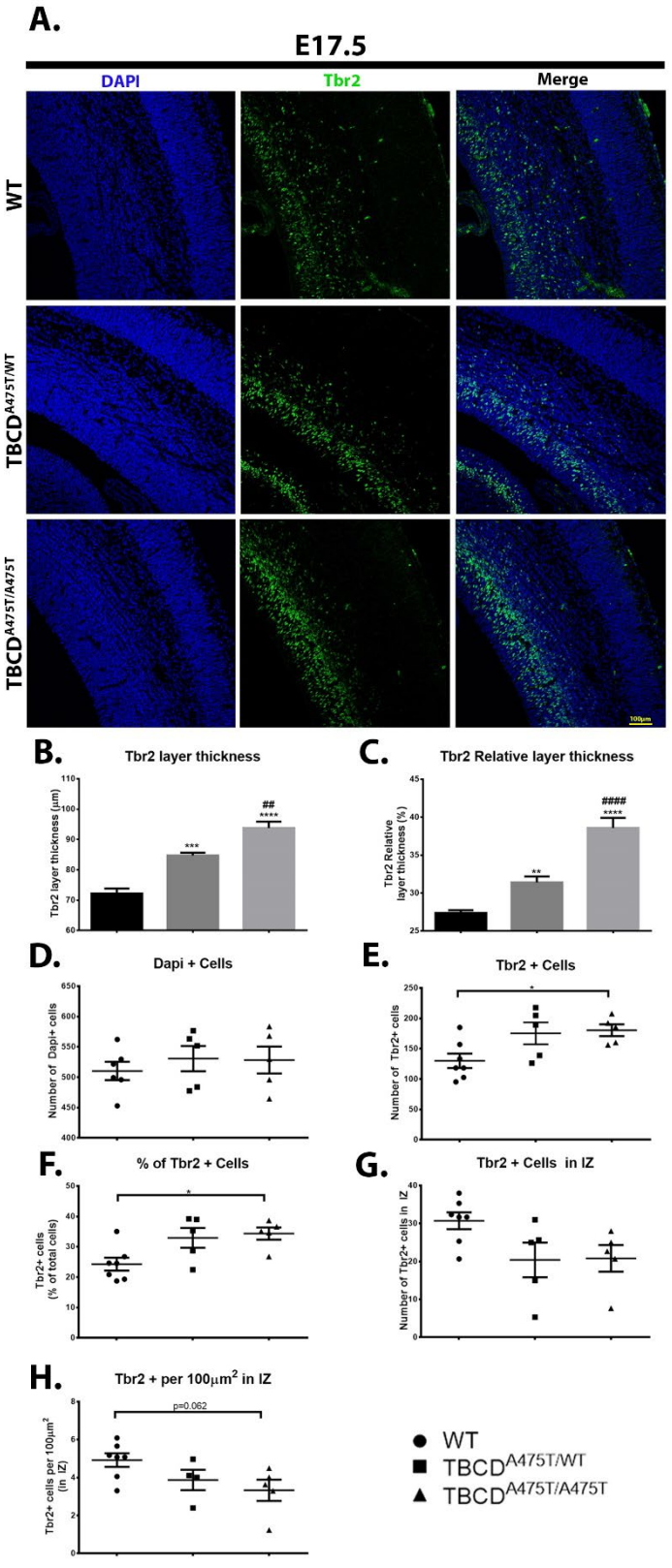

Figure 4.6. Perturbed expression of intermediate progenitor cells in TBCD$^{A475T/A475T}$ mutant cortices.

Coronal sections from E17.5 WT, TBCD$^{A475T/WT}$ and TBCD$^{A475T/A475T}$ embryonic mice assessing Tbr2 expression (A-H). (A) Immunostaining for Tbr2 (green) and Nuclei (DAPI, blue). (B and C)) Quantification of total and relative Tbr2+ immunostained layer thickness, (D) DAPI + cells, (E and F) total and relative Tbr2+ cells, (G), Tbr2+ cells in the IZ and (H) Tbr2+ cells per 100µm^2 in the IZ. For each brain, a rostral, medial and caudal section were measured and results averaged. Data represents mean ± SEM. n ≥ 6 brains per genotype. * represent comparisons against WT littermates. # represents comparisons against heterozygous littermates. *P < 0.05, **P < 0.01, ***P < 0.001, ****P < 0.0001. #P < 0.05, ##P < 0.01, ###P < 0.001. Scale bar 100µm.

Given these observations, it was then assessed whether the changes observed persisted at E17.5 in the TBCD$^{A475T/A475T}$ mice. Immunostaining and analysis of Tbr2 expression showed a significant increase of TBCD$^{A475T/WT}$ against WT mice (~15%, p < 0.001), and in the TBCD$^{A475T/A475T}$ mice compared to both WT and TBCD$^{A475T/WT}$ (~35%, p < 0.0001 and ~20%, p < 0.01, respectively) (**Fig. 4.6A-C**). No other significant differences were observed between TBCD$^{A475T/WT}$ and any other group (**Fig. 4.6B-H**). A significant increase of approximately 40% in both the total and relative number of Tbr2+ cells, in the VZ/SVZ of the TBCD$^{A475T/A475T}$ mice compared to WT counterparts was observed (**Fig. 4.6D-F**). In addition, a decrease in the relative number of Tbr2+ cells in the IZ (ectopic) was observed for the TBCD$^{A475T/A475T}$ mice

compared to both WT (~30%, p=0.062) and to a lesser extent, heterozygous littermates (~15%) (**Fig. 4.6G and H**). Previous studies identifying the ectopic expression of Tbr2, have observed disruptions to laminar positioning and neuronal fate, including, a strong reduction in the expression of the key deep cortical marker Tbr1 [63, 65, 68].

Consistent with these findings, $TBCD^{A475T/A475T}$ mice cortices immunostained with Tbr1 and Ctip2 displayed an approximate decrease of 30% and 25% in their total and relative SP layer thickness, respectively, in comparison to all other groups (**Fig. 4.7A-C**). In contrast, an increase of approximately 35% in the relative, but not total, thickness of Tbr1 and Ctip2 in the CP was observed for $TBCD^{A475T/A475T}$ mice in comparison to WT ($p < 0.01$ and $p < 0.01$, respectively) and $TBCD^{A475T/WT}$ ($p < 0.001$ and $p < 0.05$, respectively) (**Fig. 4.7B and C**). Additionally, the relative number of Tbr1+ and Ctip2+ cells in the SP was significantly decreased in the $TBCD^{A475T/A475T}$ mice (~25%) compared to both WT ($p < 0.01$ and $p < 0.05$, respectively) and $TBCD^{A475T/WT}$ mice ($p < 0.05$ and $p < 0.001$, respectively) (**Fig. 4.7D-H**).

Known to play important roles in the proliferation, migration and maturation of neurons in the developing cortex, loss of Tbr1 and Ctip2 results in neuronal fate switching and severe cortical malformations [14-16, 53, 69, 70]. Coupled with the knowledge that SP neurons are also crucial to the organization of the cerebral cortex [14, 16, 71, 72], the alterations observed in Tbr1/2 and Ctip2 expression may impact neuronal number, identity and laminar fate in the $TBCD^{A475T/A475T}$ mice. Therefore, I sought to examine the DNA-binding protein Special AT-Rich Sequence-Binding Protein 2 (Satb2), which is initially strongly expressed around E14.5/E15.5 and is required for upper layer projection neurons, neuronal migration, and identity [17, 69, 70, 73, 74]. Quantification of Satb2 immunostaining at E17.5, revealed a significantly decreased total and relative number of Satb2+ cells, in $TBCD^{A475T/A475T}$ mice compared to WT (~33%, $p < 0.05$, and 21%, $p < 0.01$, respectively), and $TBCD^{A475T/WT}$ mice (~40%, $p < 0.01$, and 30%, $p < 0.001$, respectively) (**Fig. 4.8A-C**). No differences were observed for $TBCD^{A475T/WT}$ mice when compared against WT for either total or relative Satb2+ cell number.

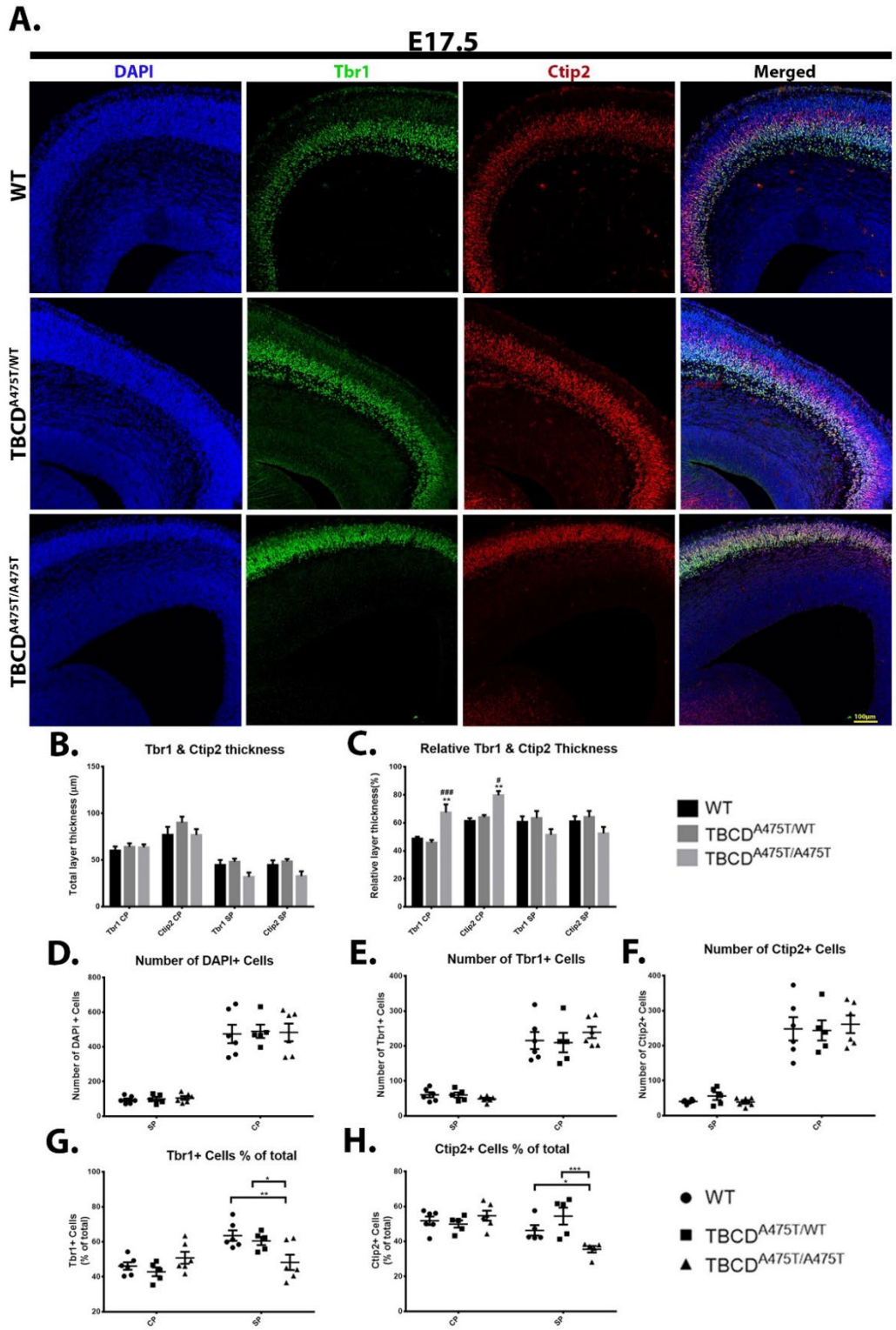

Figure 4.7. TBCD impacts cell cycle and neuronal identity in vivo.

(A) Co-immunostaining for Tbr1 (green), Ctip2 (red) and DAPI (blue) cells from coronal sections of WT, $TBCD^{A475T/WT}$ and $TBCD^{A475T/A475T}$ embryonic mice at E17.5. (B and C) Quantification of relative and total Tbr1 and Ctip2 thickness, (D) number of DAPI+ cells, (E-H) and total and relative number of Tbr1 and Ctip2 cells in the SP and CP. For each brain, a rostral, medial and caudal section were measured and results averaged. Data represents mean ± SEM. n ≥ 6 brains per genotype. * represent comparisons against WT littermates. # represents comparisons against heterozygous littermates. *P < 0.05, **P < 0.01, ***P < 0.001, ****P < 0.0001. #P < 0.05, ##P < 0.01, ###P < 0.001. Scale bar 100µm.

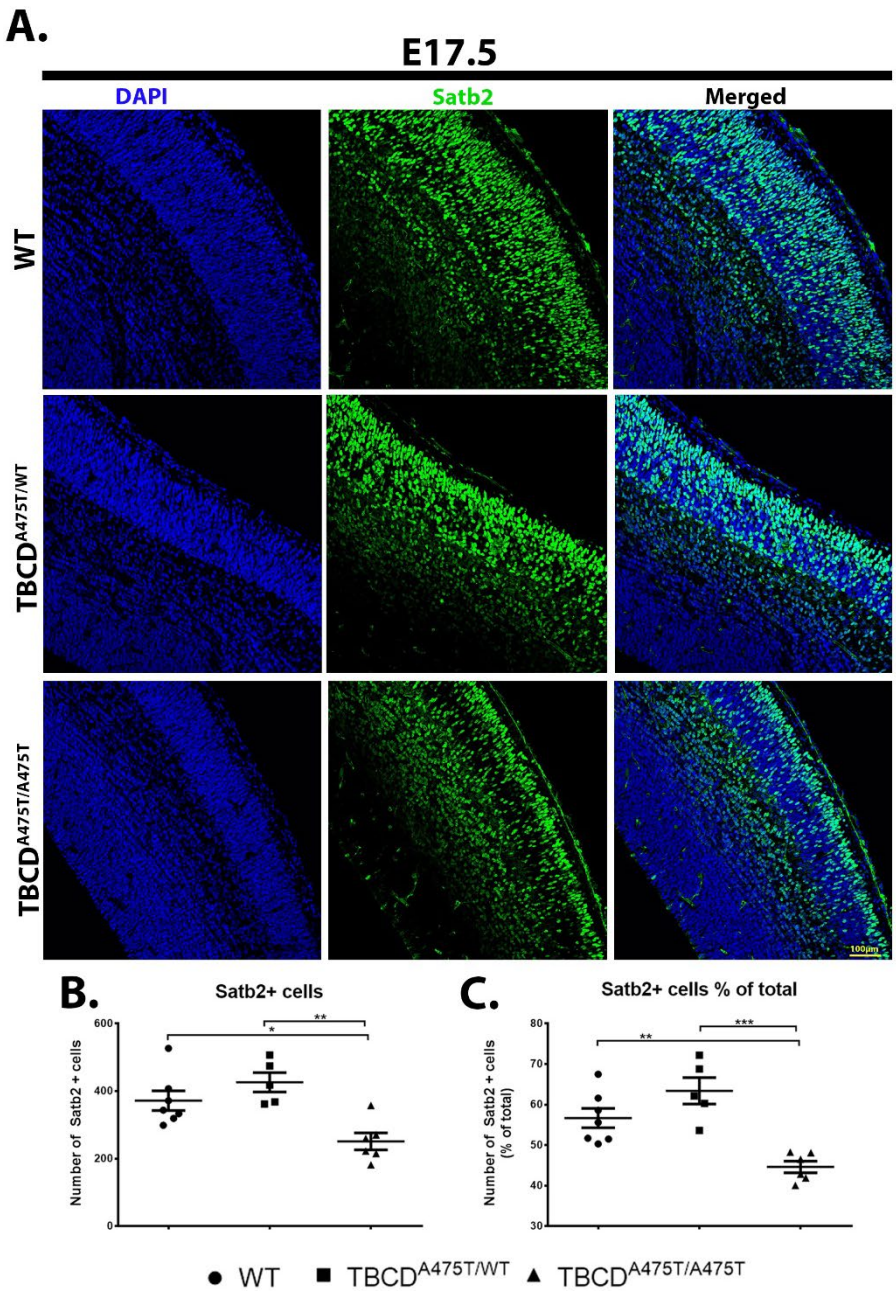

Figure 4.8. TBCD$^{A475T/A475T}$ mice display altered expression of callosal projection neuron regulator

(A-C) Immunostaining and quantification for Special AT-Rich Sequence-Binding Protein 2 (Satb2). (A) Representative images on coronal sections from WT, TBCD$^{A475T/WT}$ and TBCD$^{A475T/A475T}$ embryonic mice at E17.5 co-stained with Satb2 (green) and DAPI (nuclei, blue). (B) Quantification of the total number of Satb2+ cells, and (C) relative number of Satb2+ cells (%).For each brain, a rostral, medial and caudal section were measured and results averaged. Data represents mean ± SEM. n ≥ 6 brains per genotype. *P < 0.05, **P < 0.01, ***P < 0.001, ****P < 0.0001. #P < 0.05. Scale bar 100µm.

Next, immunoblot analysis of whole brain lysates from E14.5 and E17.5 mice was undertaken to assess the protein expression of various mitochondrial, glycolytic and neuronal markers (**Figs. 4.9 and 4.10**). Previous studies assessing the metabolic state of NPCs and postmitotic neurons during embryonic development have reported, that the onset of neurogenesis marks a progressive shift from a primarily glycolytic state in uncommitted Sox2+ NSCs, towards an increased mitochondrial respiration. This metabolic switch is marked by increased mitochondrial mass/activity, increased reactive oxygen species (ROS) presence, and enhanced oxidative phosphorylation (OXPHOS), to meet energy demands [75-77].

Concomitant with this shift to mitochondrial-dependent energy production, a decrease in the expression of the glycolytic enzymes such as Hexokinase 2 (HK2), critical in controlling the amount of glucose entering into glycolysis, and Pyruvate Kinase Isozyme M2 (PKM2), hypothesised to aid in the accumulation of metabolites for biosynthetic pathways, have been reported both *in vivo* and *in vitro* models [78-80]. Contrastingly, a minor increase in the expression of Hexokinase 1 (HK1), which is required to provide sufficient pyruvate for the TCA cycle, and PKM1, which functions to increase oxygen consumption and reduce lactate production, have also been observed during NSC fate commitment [78, 80, 81].

Validating these studies and similar to the increased mitochondrial mass observed in TBCD perturbed P19ECs, expression of the mitochondrial markers succinate dehydrogenase complex subunit A (SDHA), and cytochrome c oxidase subunit 4 (COXIV), two key enzymes in the electron transport chain, were observed to be significantly upregulated in the $TBCD^{A475T/A475T}$ mice compared to WT at E14.5 (∼16%, $p < 0.01$ and ∼35%, $p < 0.01$) (**Fig. 4.9A and B**). $TBCD^{A475T/WT}$ mice did not significantly differ from either WT or $TBCD^{A475T/A475T}$ littermates. Extending these findings, assessment of the various glycolytic markers known to be altered during neuronal differentiation was undertaken. Analysis of whole brain lysates from $TBCD^{A475T/A475T}$ mice at E14.5 revealed a statistically significant increase and decrease in PKM1/2 and HK2, respectively, versus WT littermates (∼14%, $p < 0.05$ and ∼16%, $p < 0.05$, respectively) (**Fig. 4.9C-E**). Consistent with previous studies, it was observed that $TBCD^{A475T/A475T}$ mice at E14.5 had an increased expression of HK1, and a decreased expression PKM2 and GAPDH in comparison to WT mice, only reaching significance in the latter (∼15%, ∼10%, and ∼20%, $p < 0.05$) (**Fig. 4.9C-E**) [78, 80-82]. These shifts in metabolic enzyme expression are in line with a glycolysis to OXPHOS reprogramming, which would be expected from cells undergoing differentiation. Thus, I sought to investigate the impact of the TBCD A475T clinical mutation on the expression of early neuronal differentiation markers [24, 77]. Confirming these findings, protein expression of the neuronal markers Tuj1 (previously mentioned), Neuronal Nuclei (NeuN), and Forkhead Box G1 (FoxG1), was found to be significantly increased in the $TBCD^{A475T/A475T}$ mice compared to WT mice at E14.5 by ∼1.45 ($p < 0.01$), 1.4 ($p < 0.05$), and 2.7-fold ($p < 0.0001$), respectively (**Figs. 4.3J and K, and 4.9F and G**). A similarly significant decrease in the expression of the pluripotency marker sex determining region Y-box 2 (Sox2), and the proliferation marker cyclin D1 (CD1), was also

observed in the TBCD$^{A475T/A475T}$ mice at E14.5 compared to WT mice (~21%, $p < 0.05$ and 31%, $p < 0.001$, respectively) (**Fig. 4.9F and G**). TBCD$^{A475T/WT}$ mice did not display any differences in CD1 or FoxG1 expression, but did show a statistically significant increase in NeuN expression (~48%, $p < 0.05$) and a trend towards a decreased Sox2 expression (~15%), when compared to WT littermates at E14.5 (**Fig. 4.9F and G**). The changes observed in the metabolic, pluripotency, proliferative, and neuronal markers, are strongly indicative that, in comparison to WT mice at E14.5, TBCD$^{A475T/A475T}$ mice possess an increased proportion of NSCs that have begun the transition from NSC to IPC and/or postmitotic neuron [78-80, 83-85].

Similar to the earlier embryonic findings, at E17.5 TBCD$^{A475T/A475T}$ mice displayed an increased expression of the mitochondrial markers SDHA and COXIV (~1.24-fold, $p < 0.05$ and 1.26-fold, $p < 0.05$, respectively) (**Fig. 4.10A and B**). Furthermore, when compared to WT mice, the expression of the glycolytic markers in the TBCD$^{A475T/A475T}$ mice at E17.5 is reminiscent of the expression profile observed at E14.5, with decreased expression of HK2, PKM2, and GAPDH, and increased expression of PKM1/2 and HK1, however this only reached statistical significance for the latter (~1.34-fold, $p < 0.05$) (**Fig. 4.10C and D**). Strikingly, E17.5 TBCD$^{A475T/A475T}$ mice also exhibited a reduction in CD1 (~35%, $p < 0.05$), Tuj1 (~24%, $p < 0.01$), and to a lesser degree in NeuN and FoxG1, whilst Sox2 expression was increased (~40%, $p < 0.05$) in comparison to WT (**Fig. 4.10E and F**). The reduced expression of neuronal markers in the TBCD$^{A475T/A475T}$ mice is consistent with the immunohistochemistry findings, and may be indicative of a reduced prevalence of late-stage neurons. Although the reduced expression of CD1 can be attributed to the increased mitochondrial activity [86-88], the altered glycolytic and mitochondrial metabolic profile, increased expression of Sox2, increased number of Pax6 + cells, and Tbr2 + cells (mitotically active IPCs), is highly suggestive of an increased proportion of actively proliferating cells in the TBCD$^{A475T/A475T}$ cortices at E17.5 [6, 53, 57, 59, 65, 75, 89-93]. Collectively, these data strongly support the notion that disruptions to TBCD *in vivo* affect neuronal development, with serious impacts on cell cycle dynamics, metabolism, and neuronal identity.

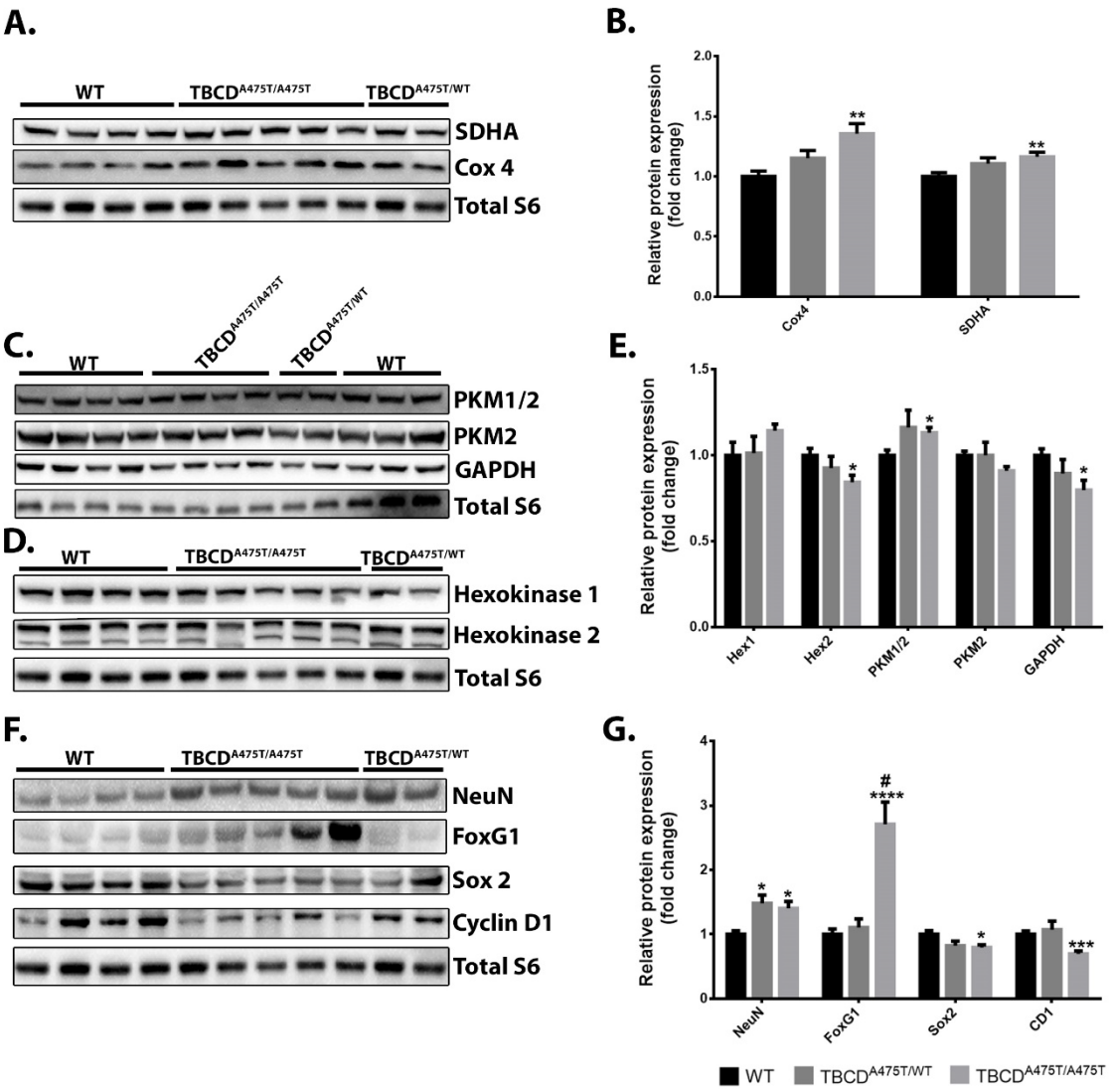

Figure 4.9. Perturbations to TBCD impact neuronal differentiation *in vivo*

Whole brain protein lysates from WT, TBCD$^{A475T/WT}$ and TBCD$^{A475T/A475T}$ mice assessing protein expression of various metabolic, glycolytic and neuronal markers via immunoblot at E14.5. (A and B) Immunoblot and densitometry analysis of the mitochondrial metabolic markers, Succinate dehydrogenase complex subunit A (SDHA), and cytochrome c oxidase subunit 4 (COXIV). (C-E) Assessment of glycolytic markers Hexokinase 1 and 2 (HK1 and HK2), Pyruvate Kinase Isozymes M1/M2 (PKM1/2), PKM2, and Glyceraldehyde 3-phosphate dehydrogenase (GAPDH). (F and G) Similar to above, analysis of the neuronal markers Neuronal nuclei (NeuN), Forkhead Box G1 (FoxG1), the pluripotency marker sex determining region Y-box 2 (Sox2), and the cell cycle marker Cyclin D1 (CD1). Data represents mean ± SEM. n ≥ 6 animals per genotype. * represents comparisons against WT littermates. # represents comparisons against heterozygous littermates. *P < 0.05, **P < 0.01, ***P < 0.001, ****P < 0.0001. #P < 0.05, ##P < 0.01, ###P < 0.001.

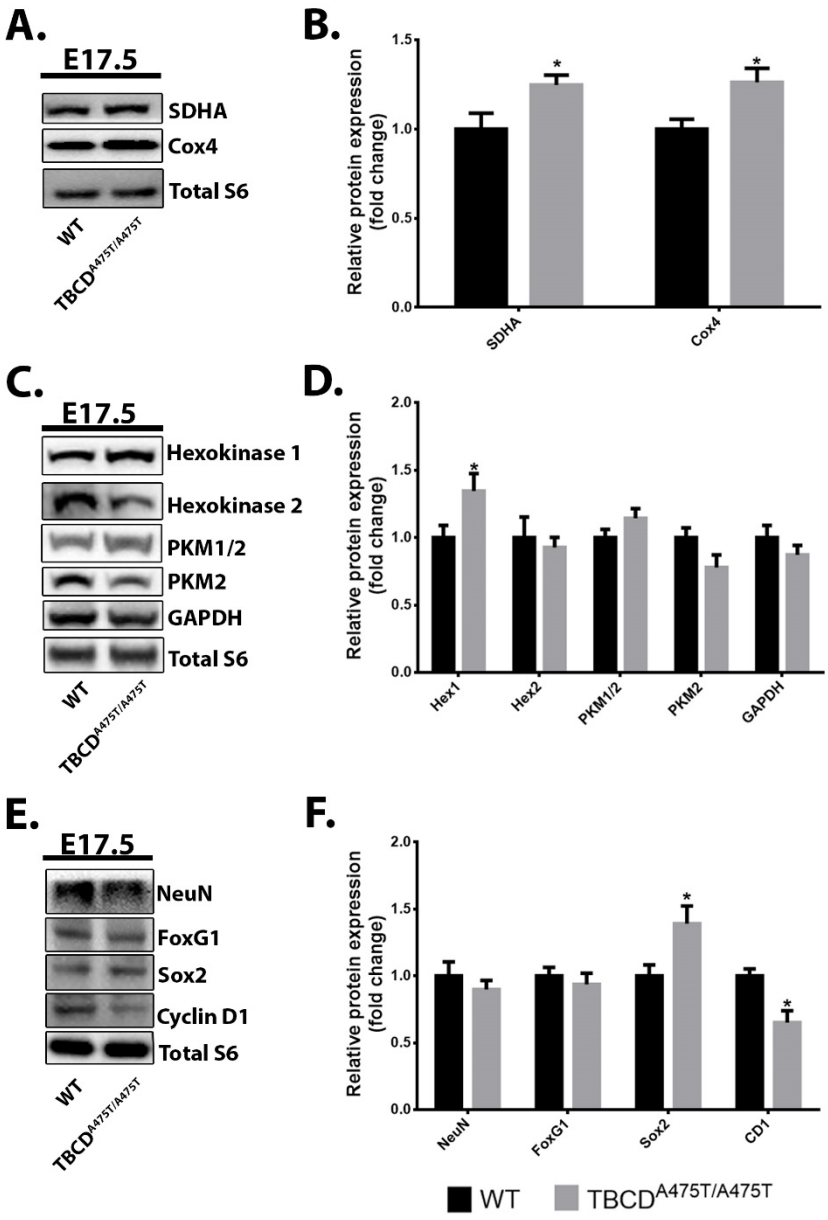

Figure 4.10. TBCD$^{A475T/A475T}$ mutant mice alter metabolism and differentiation *in vivo*

Similar to above, whole brain protein lysates from WT, TBCD$^{A475T/WT}$ and TBCD$^{A475T/A475T}$ mice assessing protein expression of various metabolic, glycolytic and neuronal markers via immunoblot at E17.5. (A and B) Immunoblot and densitometry analysis of the mitochondrial markers, SDHA, and COXIV. (C and D) Assessment of glycolytic markers HK1, HK2, PKM1/2, PKM2, and GAPDH. (E and F) Analysis of the neuronal markers NeuN, and FoxG1, as well as the pluripotency and proliferative markers Sox2 and CD1. Data represents mean ± SEM. n ≥ 6 animals per genotype. *P < 0.05, **P < 0.01, ***P < 0.001, ****P < 0.0001.

4.2.5 Cortical malformations persist postnatally in TBCD$^{A475T/A475T}$ mice

In order to delineate the impact that the A475T clinical mutation has postnatally, a similar array of tests as above were conducted on mice obtained at postnatal day 5 (P5) (**Figs. 4.11-15**). Assessment of the gross brain morphology at P5 revealed a reduction of approximately 9% in the cortical weight, thickness, and length in TBCD$^{A475T/A475T}$ mice compared to WT littermates ($p < 0.05$, $p < 0.05$ and $p < 0.05$, respectively) (**Fig. 4.11A-D**). Although the body weight of TBCD$^{A475T/A475T}$ mice was increased compared to WT (~20%, $p < 0.05$), the relative brain weight was drastically reduced in TBCD$^{A475T/A475T}$ mice (~30%, $p < 0.0001$) (**Fig. 4.11E and**

F). Immunoblot analysis of TBCD, total αβ-tubulin and β-actin protein expression confirmed previous findings of a reduced TBCD abundance and increase to the key cytoskeletal proteins in TBCD$^{A475T/A475T}$ mice brains (~16%, $p < 0.05$, 1.16-fold, $p < 0.05$, and 1.15-fold, respectively) (**Fig 4.12A and B**) [33, 34, 36, 37, 39-41]. No differences were observed between WT and heterozygous mouse, and as such heterozygous mice were not included in further analysis. Following this, assessment of Nissl-stained coronal sections from TBCD$^{A475T/A475T}$ mice revealed significant reductions in both corpus callosum (CC) and cortical thickness compared to WT litter mates (~30%, $p < 0.05$ and 14%, $p < 0.05$, respectively) (**Fig. 4.12C-G**).

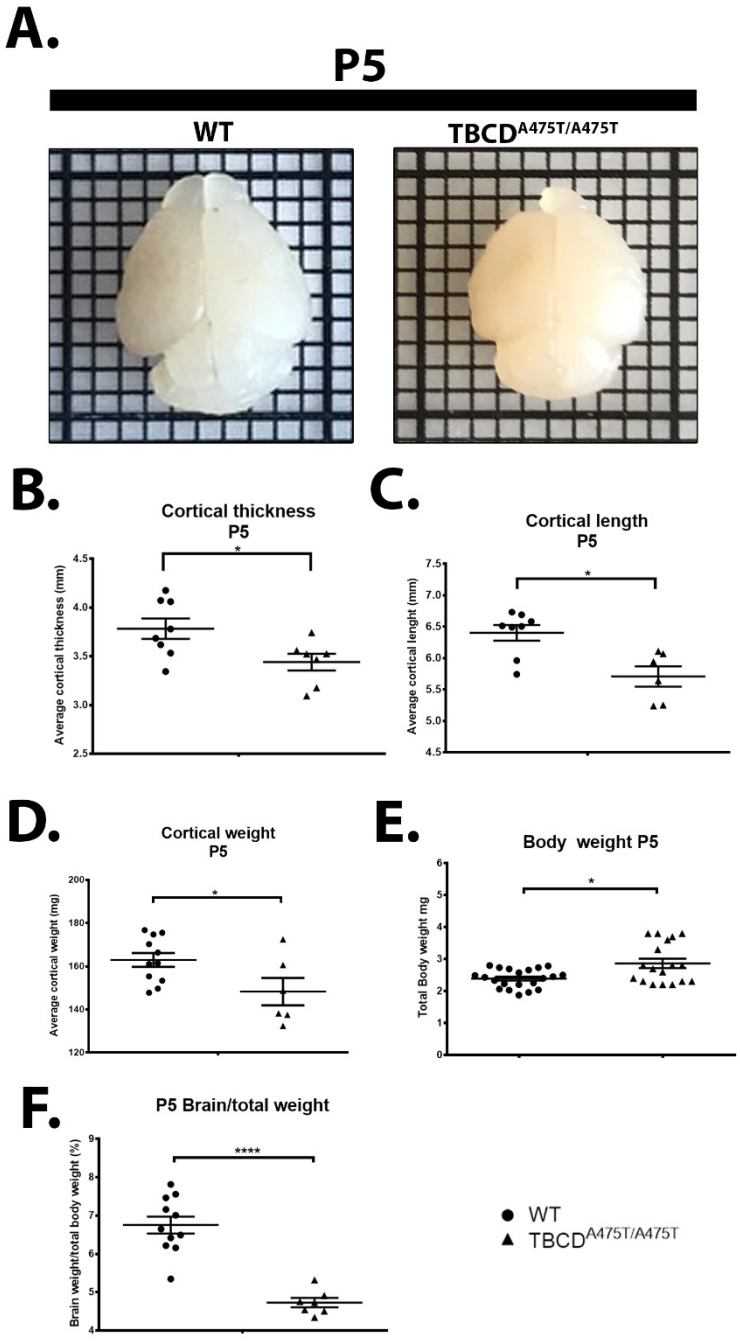

Figure 4.11. Cortical malformations are present in postnatal TBCD$^{A475T/A475T}$ mice

Mice brains were collected at postnatal day 5 and gross morphology assessed as previously described. (A) Representative images of WT and TBCD$^{A475T/A475T}$ brains at P5. (B) Measurements of gross cortical thickness, (C) cortical length, (D) cortical weight, (E) body weight, and (F) relative (%) brain weight. Data represents mean ± SEM. n ≥ 7 brains per genotype. *P < 0.05, **P < 0.01, ***P < 0.001, ****P < 0.0001.

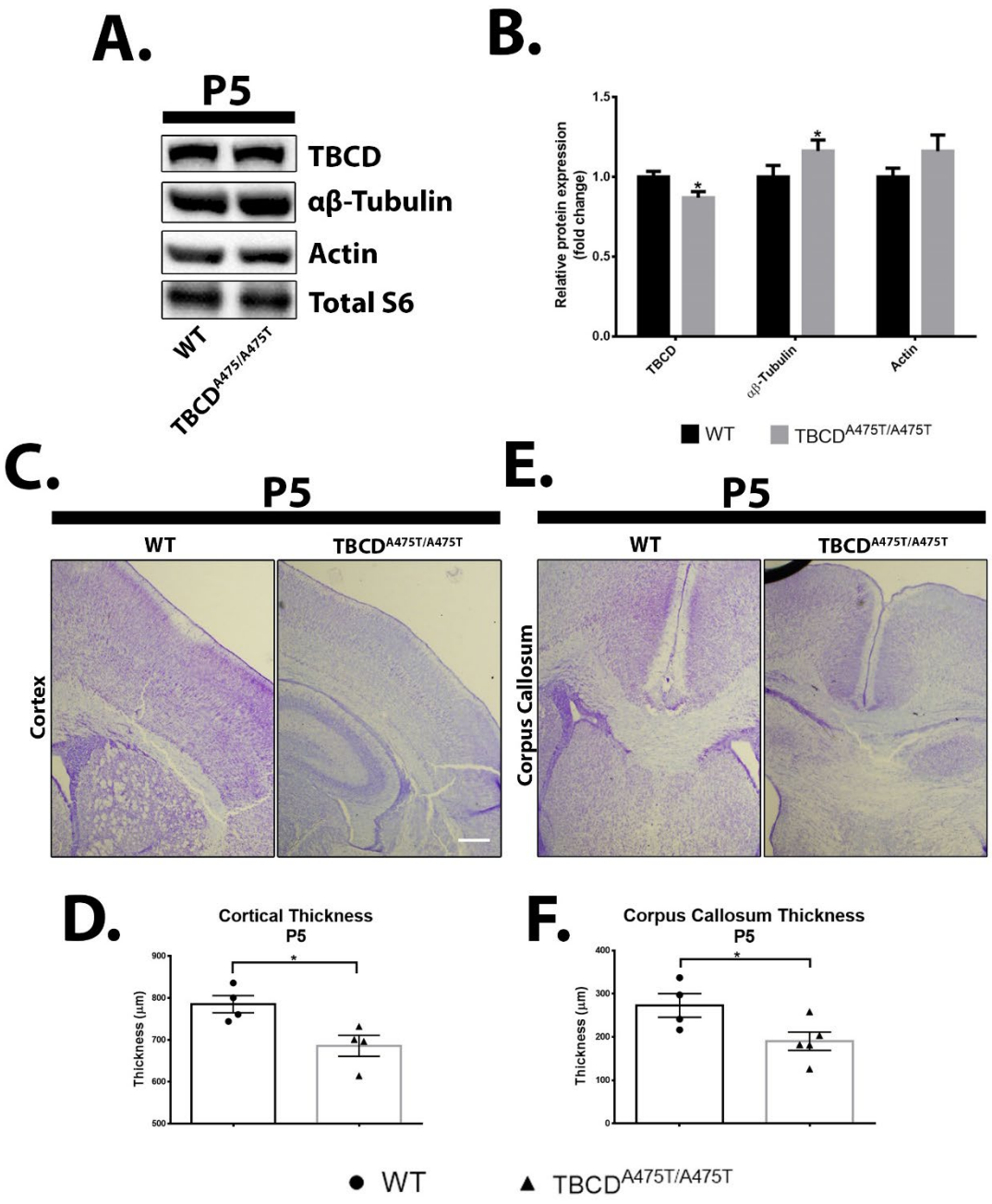

Figure 4.12. TBCD$^{A475T/A475T}$ mice display altered brain anatomy postnatally

(A and B) Band densitometry analysis of TBCD, total αβ-Tubulin, and total Actin protein expression in postnatal day 5 (P5) brains. (C-F) Nissl staining and quantification of coronal sections of WT and TBCD$^{A475T/A475T}$ brains assessing cortical (D) and corpus callosum thickness (F) at P5. For each brain, a rostral, medial and caudal section for the right and left hemisphere were measured and results averaged. Data represents mean ± SEM. n = 4-6 brains per genotype. *P < 0.05, **P < 0.01, ***P < 0.001, ****P < 0.0001. Scale bar 100µm.

Subcortical projections stemming from neurons in layers 5 and 6 can target the spinal cord, midbrain, thalamus and pons. It is therefore essential that the appropriate number of neurons are generated, as perturbed expression to layer 5 and 6 neurons (marked by Ctip2 and Tbr1 specific markers, respectively) may impede specific sensory, motor or multimodal information processing and distribution [14-18]. Therefore, I next sought to assess whether or not the cortical lamination defects observed at the embryonic time points persisted postnatally. To achieve this, immunostaining of Tbr1, Ctip2 and Satb2 was undertaken (**Figs 4.13 and 4.14)**. These data showed that although $TBCD^{A475T/A475T}$ mice trended towards a decrease in Tbr1 and Ctip2 total layer thickness, this was ablated when assessing relative layer thickness (**Fig. 4.13A-C**). Furthermore, whilst there was no difference in the total number of either Tbr1+ or Ctip2+ cells, there was an increase in the relative number of Ctip2+ cells for $TBCD^{A475T/A475T}$ mice compared to WT counterparts (~39%) (**Fig. 4.13D-I**). Following this, I assessed the expression of Satb2, which is known to be critically important in both the adult CNS and developing CNS, wherein it regulates synaptic plasticity and identity of callosal projection neurons through its repression of Ctip2 [69, 70, 73]. Although a significant decrease of Satb2+ cells at E17.5 was observed, no differences were observed in any parameters measured for Satb2 stained sections at P5 (**Fig. 4.14A-C**).

Finally, immunoblot analysis was undertaken of whole brain lysates from P5 mice in order to determine if there were any alterations in the expression of neuronal, mitochondrial, glycolytic, cell cycle or ER stress markers (**Fig. 4.15**). Similar to findings from E17.5, there was a significant increase in the expression of Sox2, SDHA, Cox4, NeuN, and HK1 in $TBCD^{A475T/A475T}$ mice (~1.6-fold, $p < 0.001$, ~1.15-fold, $p < 0.05$, ~1.25-fold, $p < 0.05$, ~1.25-fold, $p<0.001$, and ~1.25-fold, $p < 0.05$, respectively) (**Fig. 4.15A-F**). These increases in the $TBCD^{A475T/A475T}$ mice were paralleled by a decrease in the expression of Synapsin 1 (Syn1) and PKM2, however this only reached significance in the latter (~22%, $p<0.05$, and 12%, $p < 0.05$, respectively) (**Fig. 4.15A-F**). A neuron specific phosphoprotein, Syn1 plays a key role in axonogenesis, synaptogenesis, and neurotransmitter release [94-96]. Perturbation to Syn1 can impair neuronal outgrowth, synaptic vesicle trafficking, and synaptic transmission, leading to seizure development and synaptic depression [94-100]. Given that perturbations to TBCD can impair MT dynamics, which are essential for synaptic plasticity and functioning [94, 101-103], it is plausible that the decreased expression of Syn1 observed in $TBCD^{A475T/A475T}$ mice is an

indication of impaired synaptic functioning and or a reduction in the number of postmitotic neurons. However further studies are required before a definitive conclusion can be drawn.

Strongly expressed at developmental time points that correspond with NPC withdrawal from cell cycle and/or initiation of terminal differentiation, NeuN has recently been recognised as a member of the RNA-binding protein Fox-1 gene family, Fox-3 [104-108].

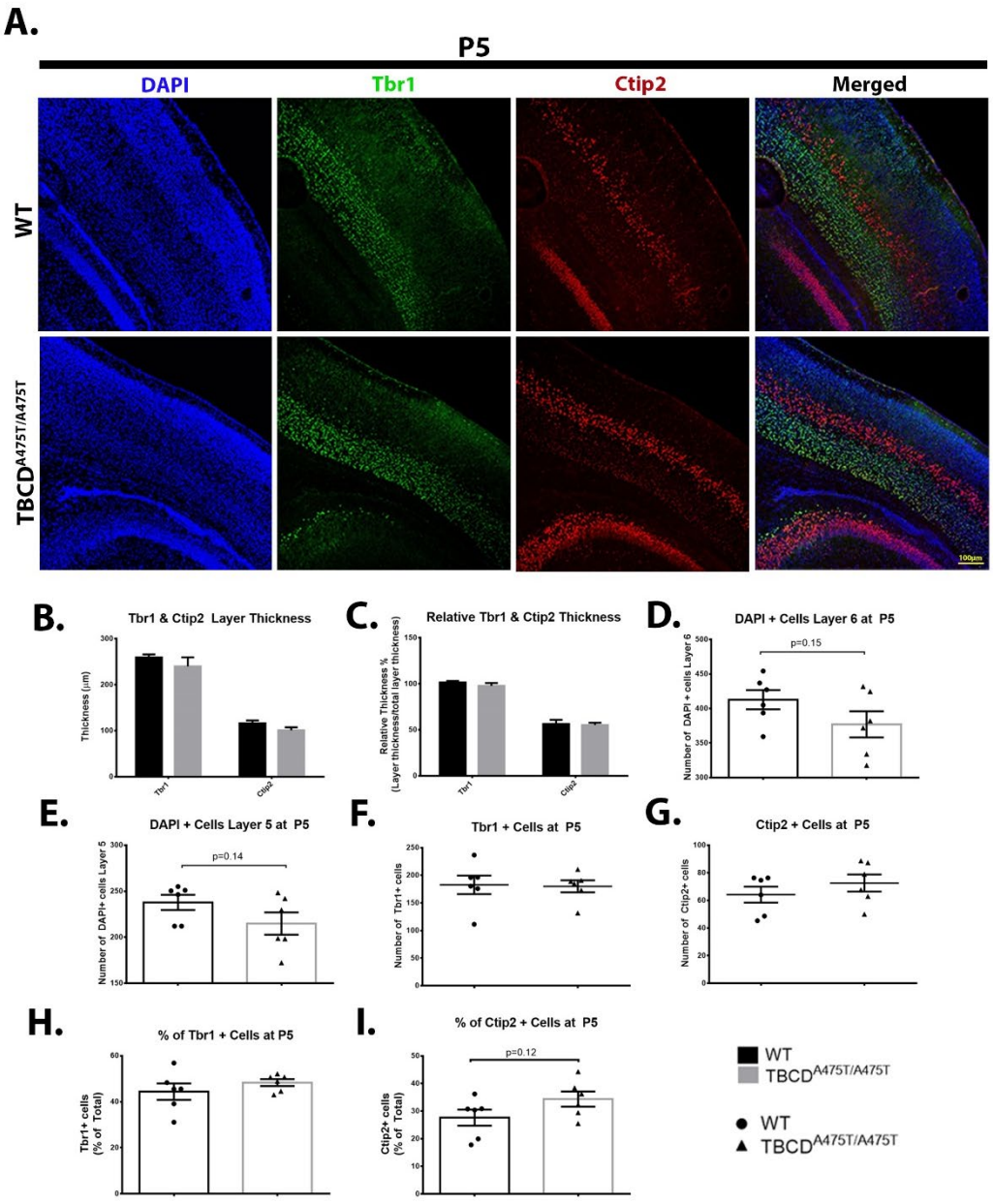

Figure 4.13. Clinical TBCD A475T mutation impacts laminar identity postnatally in mice

Coronal sections from P5 WT and TBCD$^{A475T/A475T}$ mice assessing the deep layer neuronal markers Tbr1 and Ctip2. (A) Immunostaining for Tbr1 (green), Ctip2 (red) and Nuclei (DAPI, blue) on coronal cryosections. (B and C) Quantification of Tbr1 and Ctip2 total and relative layer thickness, (D and E) DAPI+ cells in cortical layer 5 and 6, (F-G) total and relative (%) Tbr1+ and Ctip2+ cells. For each brain, a rostral, medial and caudal section were measured and results averaged. Data represents mean ± SEM. n = 5-6 brains per genotype. *P < 0.05, **P < 0.01, ***P < 0.001, ****P < 0.0001. Scale bar: 100 µm.

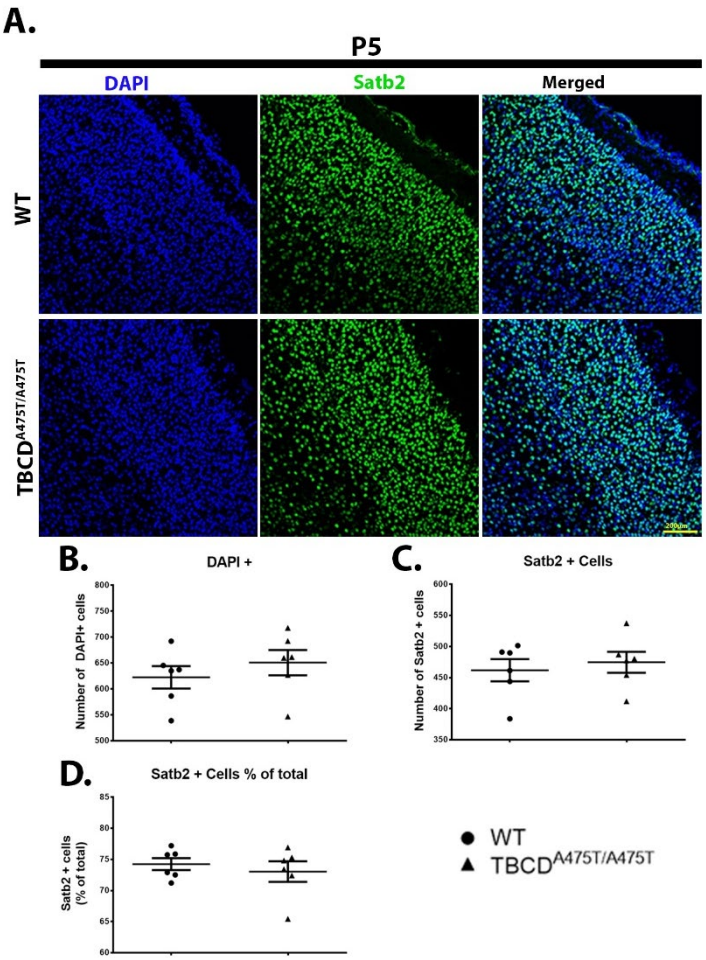

Figure 4.14. Impact of clinical TBCD A475T mutation on laminar identity in postnatal mice

Coronal sections from P5 WT and TBCD$^{A475T/A475T}$ mice assessing the deep layer neuronal marker Satb2. (A) Co-stained cortices positive for Satb2 (green) and DAPI (blue). (B) Quantified number of DAPI+ cells, (C and D) total and relative number of Satb2+ cells. For each brain, a rostral, medial and caudal section were measured and results averaged. Data represents mean ± SEM. n = 5-6 brains per genotype. *P < 0.05, **P < 0.01, ***P < 0.001, ****P < 0.0001. Scale bar: 200 µm.

Additionally, as expression levels of NeuN are believed to correspond to several other factors, including state of differentiation, level of neuronal function, neuritogenesis, axonogenesis and state of polarization, it is difficult to fully interpret the increased expression of NeuN observed in TBCD$^{A475T/A475T}$ mice at P5 [105-109]. However, coupling the increased expression of NeuN, the pluripotency marker Sox2, the metabolic markers HK1, SDHA, and Cox4, with the decreased expression of Syn1, Tuj1 and PKM2, these data are suggestive of an increased pool of mitotically active NPCs and a reduction in postmitotic neurons in the cortex of TBCD$^{A475T/A475T}$ mice.

Furthermore, it was observed that TBCD$^{A475T/A475}$ mice had an increased expression of unfolded protein response (UPR) pathway elements, protein kinase-like endoplasmic reticulum kinase (p-PERK) and Activating Transcription Factor 4 (ATF4), that have previously been reported to be upregulated during neurogenesis, (**Fig. 4.15G and H**) [109-112]. Interestingly, immunoblot analysis of cleaved caspase 3 expression was increased by ~1.3-fold in the TBCD$^{A475T/A475T}$ brains compared to WT ($p < 0.01$) (**Fig. 4.15G and H**). It should be noted however, that caspase 3 IHC and the terminal deoxynucleotidyl transferase dUTP nick end labelling (TUNEL) assay could not be achieved in order to validate this potential increase in cell death. Whilst caspase cleavage events are usually associated with cell death, several

recent studies have identified a role for caspase in cellular differentiation and synaptic plasticity, and is further detailed in the discussion [113-117]. Taken together, these data indicate that homozygous TBCD$^{475T/475T}$ mutant mice display defective cortical development during embryogenesis and in early postnatal (P5) life, with hallmarks of changes to NPCs cortical neurogenesis and cell migration, leading to altered cerebral cortical size and disrupted laminar identity.

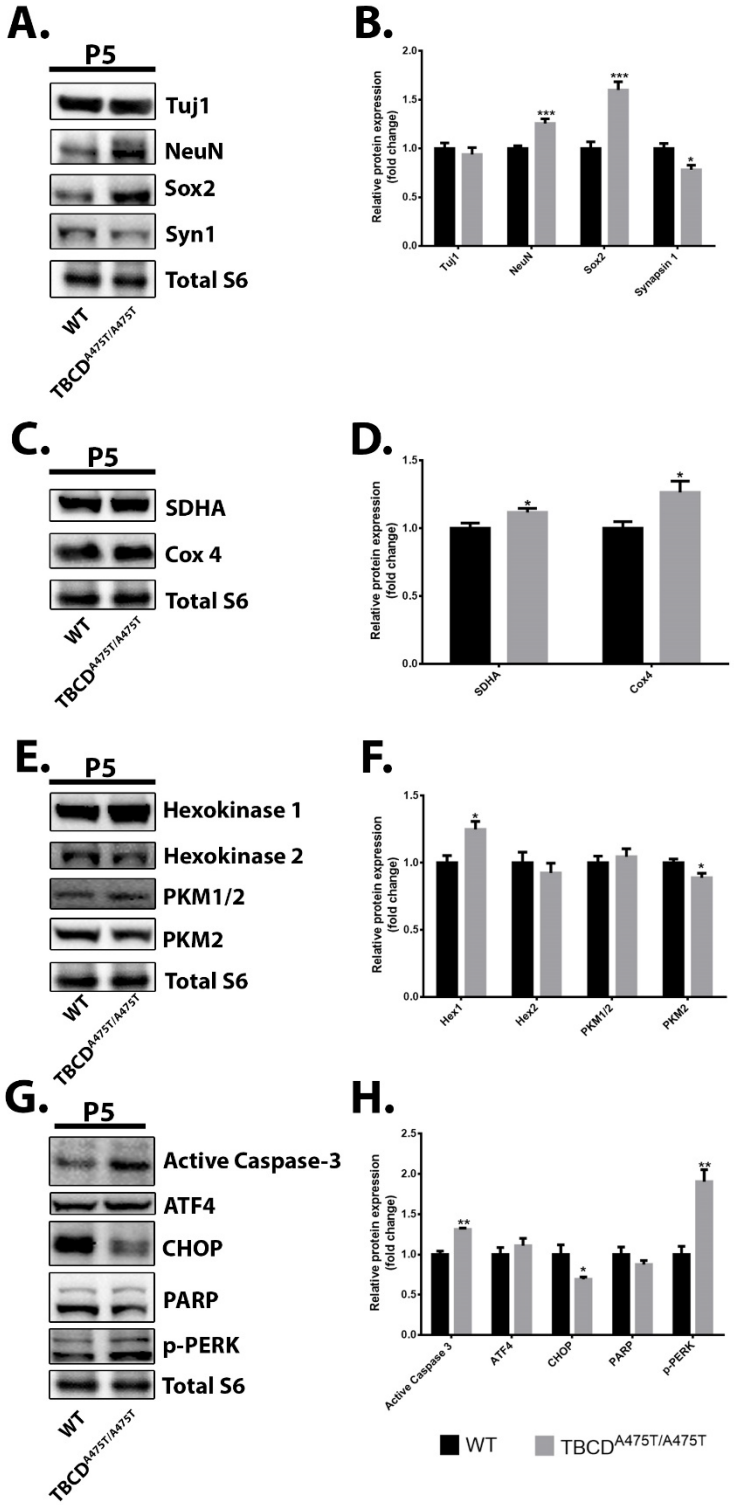

Figure 4.15 Altered metabolic and differentiated state of TBCD$^{A475T/A475T}$ mice is accompanied by increase endoplasmic reticulum stress and death markers postnatally per metabolism and differentiation

P5 whole brain protein lysates from WT and TBCD$^{A475T/A475T}$ mice assessing TBCDs impact across various aspects of cellular function from neuronal identity, to metabolism and through to cell death. (A and B) Immunoblot and band densitometry analysis of neuronal markers-β-III Tubulin (Tuj1), Neuronal nuclei (NeuN), sex determining region Y-box 2 (Sox2), Synapsin I (Syn I), (C and D) mitochondrial markers SDHA and Cox4, (E and F) glycolytic markers Hexokinase 1, Hexokinase 2, Pyruvate Kinase Isozymes M1/M2 (PKM1/2), PKM2 (E and F) and cell death and stress markers, Active (Cleaved) Caspase-3, Activating Transcription Factor 4 (ATF4), and phosphorylated-Protein kinase-like endoplasmic reticulum kinase at Th980 (p-PERK) (G and H). Data represents mean ± SEM. n = 5-6 animals per genotype. *P < 0.05, **P < 0.01, ***P < 0.001, ****P < 0.0001.

4.3 Discussion

The dynamic properties of the neuronal cytoskeleton are essential for the establishment of the neocortex, which relies upon the proliferation, migration and terminal differentiation of neurons. This coordinated stepwise process is achieved through the organisation, assembly and remodelling of the cytoskeletal elements in order to establish the complex neuronal circuitry required for cognitive functioning [6, 9, 24, 25]. Perturbations to these processes can impact neuronal signalling and/or morphology, impeding appropriate development, which can result in cognitive impairment [20, 22]. In support of this notion, recent findings identified mutations in TBCD, a key regulator of MT biosynthesis, to be causative for a severe, early onset neurodegenerative condition in infants [33, 34, 36, 37]. Findings from these studies are unique however, as they attribute the secondary microcephaly reported in patients to disruptions in MT function [33, 37]. Despite being identified over 20 years ago, there is still a gap in knowledge regarding the extensive role of TBCD in MT biosynthesis [118, 119]. Data presented herein exams a novel mouse model carrying the recently reported autosomal recessive clinical TBCD A475T mutation and details the impact of this mutation on neuronal development. These data support and extend the *in vitro* findings from the P19ECs, wherein perturbations to TBCD altered cell cycle dynamics, metabolism and fate commitment. Consistent with clinical findings, the mouse model presented herein displays perturbed cortical morphology and laminar organisation.

Examination of cortices from mice harbouring the clinical A475T mutation at E14.5, revealed significantly heavier, longer and thicker brains in $TBCD^{A475T/A475T}$ mice compared to WT littermates (**Fig. 4.1**). While no significant differences were observed in Nissl-stained cortices at E14.5, with the caveat that a small sample size of the WT group was sampled for this time point. Based on these findings, power analysis calculations were conducted and revealed that for a desired power of 0.80 a sample size of 7 for each group would be required, although this is currently beyond the capability of this work currently. By the end/late stage of cortical development (E17.5) however, the homozygous TBCD mutant mice possessed a severely perturbed morphology, with clear reductions in size, weight and cortical layering compared to their WT and $TBCD^{A475T/WT}$ counterparts (**Figs. 4.1-8**). These perturbations persisted postnatally, with examination of mice at P5 validating the aberrant lamination, size and expression of deep layer neuronal markers (**Figs. 4.13-15**). This phenotype was paralleled, at

all time points, by the expected reduction in TBCD protein expression, attributable to protein instability leading to proteasomal degradation [37], as well as by an unexpected increase in the expression of the total level of αβ-tubulin and β-actin (**Figs. 4.3,4.4 and 4.12**). Previously, studies have only assessed either, the level of β-tubulin, noting a reduced protein expression that was resultant from accelerated degradation, or α-tubulin protein expression, with no identifiable changes, except for a reduction in the soluble pool of tubulin [33, 36, 37]. Interestingly, studies assessing MT stability and tubulin expression have observed that increasing MT stability decreases the soluble pool of tubulin dimers, leading to an upregulation of tubulin mRNA, synthesis and subsequent MT incorporation [120-124]. Taken together with the increased MT stability, resultant from the $TBCD^{A475T/A475T}$ mutation, these data provide a possible explanation for the enhanced tubulin expression observed in this model.

In addition to the enlarged state of the E14.5 cortex in $TBCD^{A475T/A475T}$ mice, a corresponding increase in cortical lamination, enhanced expression of neuronal markers and a decreased expression of proliferation markers was also observed (**Figs. 4.1-3, 4.5 and 4.9**). On the other hand, examination of brains at E17.5 revealed a significant reduction in the expression of the early neuronal marker Tuj1, accompanied by a drastic increase in expression and distribution of the transcription factor Pax6 in the $TBCD^{A475T/A475T}$ mice (**Fig. 4.4**). Consistent between both embryonic time points however, is the downregulation of CD1 (**Figs. 4.9 and 4.11**). Once activated, CD1 binds and activates Cdk4 and Cdk6, thereby enabling G1 entry and progression [125-128]. The observations that CD1 is downregulated at E14.5 and E17.5, are supported by the increased expression of Pax6, which has been reported to bind directly to and repress expression of Cdk4 and Cdk6. By binding and repressing these cell cycle regulators, when overexpressed, Pax6 impairs NPC proliferation and promotes neurogenesis at the expense of self-renewal [54-57, 59, 60]. Systems overexpressing Pax6 promote BP genesis over proliferation, leading to an increase in the BP/IPC marker Tbr2, which is believed to regulate the early steps of fate commitment/differentiation in projection neurons (PNs) [53, 55-57, 59, 60]. Additionally, it has also been shown that Tbr2 is highly expressed in IPCs undergoing the S- and M-phase of cell cycle [53]. Consistent with this notion, and in support of the observed G2/M delay in TBCD perturbed P19ECs, a significant increase in the number of Tbr2+ cells is seen in the $TBCD^{A475T/A475T}$ mouse cortices at E17.5 (**Fig. 4.6**), although no difference was

observed in Tbr2 expression at E14.5 (**Fig. 4.5**). Tbr2 expressing cells are characterised as progenitor cells that divide at positions away from the ventricular surface, non-surface divisions (NS-div), for one or more rounds of symmetric/proliferative division prior to a neurogenic division [6, 53]. This is notable as IPCs are believed to contribute a significant proportion of neurons to most layers, with NS-div cells generating >50% of neuron-producing mitoses during early neurogenesis, and between 32-100% during mid-neurogenesis [53, 129, 130]. Consequently, misexpression of Tbr2 can cause severe neurodevelopmental syndromes by impeding cell cycle progression, forcing differentiation towards an IPC fate, ultimately leading to inappropriate cortical lamination and neuronal fate, [53, 55-57, 59, 60]. Given that both Pax6 and Tbr2 regulate discrete steps in PN differentiation, it is unsurprising that at E14.5 and E17.5 a significant increase and reduction, respectively, is observed in the relative number of Tbr1+ and Ctip2+ cells in TBCD$^{A475T/A475T}$ mice (**Figs. 4.5-7**). Tbr1 and Ctip2+ cells, markers of layer 5 and 6 neurons respectively, play important roles in the developing cortex, as they are required for the specification, migration, and maturation of neurons in the developing cortex, as well as establishing subcortical projections targeting the spinal cord, midbrain, thalamus and pons [14, 15, 18, 53, 131, 132]. Disruptions to the precise spatiotemporal patterning of these markers therefore, deleteriously impacts the appropriate establishment of the cellular architecture, and may impede specific sensory, motor responses and/or multimodal information processing and distribution [14-18]. Future investigations validating this hypothesis would be beneficial given that patients with TBCD mutations display impaired motor control and response to physical and auditory cues [33, 37]. Taken together, the altered expression of neuronal and proliferative markers observed at E14.5 and E17.5, are strongly indicative of perturbed timing of NPC proliferation, terminal cell cycle exit and differentiation in TBCD$^{A475T/A475T}$ mice.

Cells undergoing terminal cell cycle exit and neurogenesis display an increased mitochondrial metabolism and decreased reliance on glycolysis as they differentiate. The shift from glycolysis to OXPHOS and enhanced mitochondrial activity can increase ROS accumulation, which triggers NRF2-mediated retrograde signalling to promote differentiation over self-renewal [9, 77, 133-136]. Therefore, it is perhaps unsurprising that a similar expression profile is observed in the TBCD$^{A475T/A475T}$ mice at E14.5, with increases seen in markers of mitochondrial mass/function, and a decreased expression of certain glycolytic enzymes, such

as HK2, PKM2 and GAPDH compared to WT littermates (**Fig. 4.9**). These findings are further supported by the downregulation of CD1, which when present has been reported to impede mitochondrial function and OXPHOS, as well as decreased expression of the pluripotency marker Sox2 in the TBCD mutant mice brains [87, 88, 126, 128, 137]. Although a similar expression profile of mitochondrial and glycolytic markers is observed in the $TBCD^{A475T/A475T}$ mice at E17.5, this is accompanied by an increase in the expression of Sox2, Pax6 and Tbr2 (**Figs. 4.5 and 4.10**). Furthermore, $TBCD^{A475T/A475T}$ mice at E17.5 display a decrease in Tuj1, NeuN and FoxG1 expression compared to their WT counterparts. Taken together, these findings are strongly indicative that whilst there is a decreased NPC proliferation and increased commitment to neurogenic divisions at E14.5, there is an increased population of mitotically active NPCs in the $TBCD^{A475T/A475T}$ mice compared to their WT littermates at E17.5. Given that appropriate cortical development requires coordinated spatiotemporal NPC proliferation, migration and differentiation, the TBCD induced perturbations to these processes are highly likely to ultimately lead to postnatal cortical malformations.

In support of this hypothesis, examination of $TBCD^{A475T/A475T}$ postnatal brains revealed that P5 mice had a significantly reduced cortical weight, thickness and length compared to WT counterparts (**Figs. 4.11 and 4.12**). Additionally, $TBCD^{A475T/A475T}$ mice were also observed to have a significant reduction in CC thickness (**Fig. 4.11**). Consisting of white matter tracts linking associative areas of the two cerebral hemispheres, the CC functions primarily to integrate, transfer and process motor, sensory and high-level cognitive signals between these two regions [138-140]. Abnormalities in size and development of the CC have been reported in a wide array of neurological disorders [138-143], including patients harbouring the TBCD A475T and A568V clinical mutations [37]. These findings, coupled with the altered cortical size and CC thickness observed in the $TBCD^{A475T/A475T}$ mice, may be indicative of adverse neurodevelopmental outcomes in this mouse model. Although assessment of cognitive deficits is beyond the scope of this study, these data not only highlight future areas for investigation, but also offer strong support for the biological validity of the $TBCD^{A475T/A475T}$ mouse mode. Due to the integral role that layer 5 and 6 neurons also play in establishing subcortical projections and transmitting information between and to different regions of the brain, I next sought to assess the expression of the markers Tbr1 and Ctip2. In contrast to the significant decrease in the relative number Tbr1+ and Ctip2+ cells seen at E17.5,

TBCD$^{A475T/A475T}$ mice at P5 were only observed to trend towards an increase in the relative number of Ctip2+ cells, and a decrease in DAPI+ cells (**Fig. 4.13**). Similarly, immunostaining of Satb2 at P5 revealed that the number of Satb2+ cells did not differ between the groups (**Fig. 4.15**). In light of the partially restored number of Satb2, Tbr1 and Ctip2 cells at P5, it is attractive to hypothesise that this restoration is resultant from the increased population of mitotically active NPCs observed in the TBCD$^{A475T/A475T}$ mice at E17.5 [76, 144-147]. However, this is an avenue for future explanation and is currently beyond the scope of this study. Strikingly though, a significant increase in the expression of active caspase 3- typically a cell death marker, was observed. Whilst immunoblot results from previous time points revealed no significant differences in cell death or stress markers (data not shown), data obtained from P5 mice reveals an increase in active caspase-3 and a slight decrease in CHOP (**Fig. 4.15**). Unfortunately, additional assessment of cell death via immunostaining of caspase-3 and TUNEL assay failed to yield results, and thus leaves this area open for speculation and further investigation. Of note, several previous studies have reported on the non-apoptotic roles for caspase-3 during neuronal development, differentiation and functioning [113-117]. Findings from these *in vivo* and *in vitro* models have shown that caspase-3 is required for facilitating NPC neurogenesis and even has a role in neuroplasticity/synaptic functioning [113-117]. Coupled with upregulation of the UPR arm PERK-eiF2α-ATF4, which is known to be involved in neurogenesis, these data are indicative of a late stage increase in neurogenesis for the TBCD$^{A475T/A475T}$ mice at P5 (**Fig. 4.15**) [109-112]. Furthermore, not only was there a significant increase in the pluripotency marker Sox2, but TBCD$^{A475T/A475T}$ mice also exhibited perturbations to the energy metabolism of the cell at P5, with significant increases in the mitochondrial markers SDHA and CoxIV, as well as the glycolytic enzymes HK I, and a decrease in PKM2 (**Fig. 4.15C-F**). Taken together with the data above, the increased expression of Sox2, active caspase-3, and the metabolic alterations observed at P5 are indicative of an impaired and protracted period of cortical neurogenesis in the TBCD$^{A475T/A475T}$ mice. Given the perturbed metabolic phenotype observed in the P19ECs and the TBCD$^{A475T/A475T}$ mouse model, the recent findings that mitochondrial dynamics can regulate stem cell fate provides a potential avenue for exploration in an effort to mitigate the neuropathological condition and neurodegeneration resultant from TBCD perturbations [148]. This is further emphasised by the knowledge that a metabolic switch from OXPHOS to glycolysis can convert differentiated cells to pluripotent stem cells [82, 149, 150]. Intriguingly, studies have begun

to elucidate the protective and restorative capability of pharmacological or genetic manipulations that can target and alter glycolytic enzymes, enhancing glycolytic flux, glucose uptake and availability [148, 151-153]. Augmentation of these pathways enhances glycolytic production of ATP, alleviating energy defects, increasing redox buffering capacity and alters related signalling pathways [84, 149, 154]. Several recent reports have identified such effects to occur in response to treatment with GLP-1R agonists in multiple tissues, most relevantly, the brain (detailed in chapter 5). Briefly, these studies reveal that in addition to its original purposing as a type 2 diabetic therapy to elevate β-cell glucose metabolism to meet the increasing insulin demand, GLP-1R agonists are able to cross the blood brain barrier and initiate a downstream signalling cascade resulting in neuroprotection, progenitor cell proliferation, and neurogenesis [151, 155-161]. This neuroprotective capacity has been shown to be effective in animal models and has furthermore been implemented in several clinical trials globally to tackle the plethora of emerging neurodegenerative diseases [162-168]. Chronic exposure of long lasting GLP-1R agonist, such as Exendin-4, are known to alter β-cell bioenergetics through a PI3K/mTOR/HIF-1α pathway, resulting in augmented glucose production and upregulation of key glycolytic enzymes [152, 153, 169]. Furthermore, it can upregulate the expression of the insulin like-growth factor receptor 1 (IGF1R), the insulin receptor (INSR) and their associated products, ultimately leading to an autocrine loop [152, 153, 169]. Stimulation of the GLP-1R and its downstream signalling pathways, including IGF1R and INSR, has been reported to impact cell cycle dynamics, proliferation, metabolism, and cytoskeletal re-organisation [120, 170-183]. Coupling these data with the observed metabolic and mitotic perturbations in the model presented herein, it is attractive to hypothesise that GLP-1R agonists, such as Exendin-4, may offer a potential therapeutic avenue of exploration to alleviate the homeostatic imbalance resultant from TBCD induced perturbations. In support of this notion, chronic exposure of P19ECs to Exendin-4 was able to alleviate the TBCD induced homeostatic perturbations, as detailed in Chapter 6, and has provided support for an animal study evaluating the effect of Exendin-4 given to pregnant TBCD$^{A475T/A475T}$ mutant mice in the future.

Consistent with the critical role in heterodimer assembly/disassembly and thus MT dynamics, the findings presented herein show that perturbations to TBCD can deleteriously impact multiple facets of cortical formation. By disrupting the coordinated stepwise process of

proliferation, migration and differentiation, TBCD mutations can prematurely reduce the pool of NPCs, alter NPC fate and lead to abnormal cortical lamination through a multitude of systems. This can impact connectivity and signalling, ultimately leading to severe neurodegenerative phenotypes [10, 22, 184]. Taken together with the findings from the *in vitro* study with P19ECs, the analysis of this *in vivo* model has aided the elucidation of the underpinning molecular mechanisms arising from compromised interactions of TBCD, and its effectors, on the dynamic behaviour of the neuronal cytoskeleton throughout neuronal development. This preclinical animal model may be essential to the development of therapies that counteract the detrimental impact of TBCD perturbations in the nervous system.

4.4 References

1. Hofman, M.A., *Evolution of the human brain: when bigger is better.* Frontiers in neuroanatomy, 2014. **8**: p. 15.
2. Collins, A. and E. Koechlin, *Reasoning, learning, and creativity: frontal lobe function and human decision-making.* PLoS Biol, 2012. **10**(3): p. e1001293.
3. Jung, J., et al., *The structural connectivity of higher order association cortices reflects human functional brain networks.* cortex, 2017. **97**: p. 221-239.
4. Funahashi, S. and J.M. Andreau, *Prefrontal cortex and neural mechanisms of executive function.* Journal of Physiology-Paris, 2013. **107**(6): p. 471-482.
5. Chouinard, P.A. and T. Paus, *The primary motor and premotor areas of the human cerebral cortex.* The neuroscientist, 2006. **12**(2): p. 143-152.
6. Florio, M. and W.B. Huttner, *Neural progenitors, neurogenesis and the evolution of the neocortex.* Development, 2014. **141**(11): p. 2182-2194.
7. Stiles, J. and T.L. Jernigan, *The Basics of Brain Development.* Neuropsychology Review, 2010. **20**(4): p. 327-348.
8. Rakic, P., *Specification of cerebral cortical areas.* Science, 1988. **241**(4862): p. 170.
9. Kapitein, Lukas C. and Casper C. Hoogenraad, *Building the Neuronal Microtubule Cytoskeleton.* Neuron, 2015. **87**(3): p. 492-506.
10. Greig, L.C., et al., *Molecular logic of neocortical projection neuron specification, development and diversity.* Nature Reviews Neuroscience, 2013. **14**(11): p. 755-769.
11. Ayala, R., T. Shu, and L.-H. Tsai, *Trekking across the brain: the journey of neuronal migration.* Cell, 2007. **128**(1): p. 29-43.
12. Métin, C., et al., *Cell and molecular mechanisms involved in the migration of cortical interneurons.* European Journal of Neuroscience, 2006. **23**(4): p. 894-900.
13. Heng, J.I.-T., A. Chariot, and L. Nguyen, *Molecular layers underlying cytoskeletal remodelling during cortical development.* Trends in neurosciences, 2010. **33**(1): p. 38-47.
14. Hevner, R.F., et al., *Tbr1 regulates differentiation of the preplate and layer 6.* Neuron, 2001. **29**(2): p. 353-366.
15. Bedogni, F., et al., *Tbr1 regulates regional and laminar identity of postmitotic neurons in developing neocortex.* Proceedings of the National Academy of Sciences, 2010. **107**(29): p. 13129-13134.

16. Lennon, M.J., et al., *Bcl11b—A Critical Neurodevelopmental Transcription Factor—Roles in Health and Disease.* Frontiers in cellular neuroscience, 2017. **11**: p. 89.
17. Molyneaux, B.J., et al., *Neuronal subtype specification in the cerebral cortex.* Nature reviews neuroscience, 2007. **8**(6): p. 427-437.
18. Arlotta, P., et al., *Ctip2 controls the differentiation of medium spiny neurons and the establishment of the cellular architecture of the striatum.* Journal of Neuroscience, 2008. **28**(3): p. 622-632.
19. Karaca, E., et al., *Genes that Affect Brain Structure and Function Identified by Rare Variant Analyses of Mendelian Neurologic Disease.* Neuron, 2015. **88**(3): p. 499-513.
20. Jaglin, X.H. and J. Chelly, *Tubulin-related cortical dysgeneses: microtubule dysfunction underlying neuronal migration defects.* Trends Genet, 2009. **25**(12): p. 555-66.
21. Hirokawa, N., S. Niwa, and Y. Tanaka, *Molecular motors in neurons: transport mechanisms and roles in brain function, development, and disease.* Neuron, 2010. **68**(4): p. 610-638.
22. Guerrini, R. and E. Parrini, *Neuronal migration disorders.* Neurobiology of Disease, 2010. **38**(2): p. 154-166.
23. Guerrini, R. and W.B. Dobyns, *Malformations of cortical development: clinical features and genetic causes.* The Lancet Neurology, 2014. **13**(7): p. 710-726.
24. Poulain, F.E. and A. Sobel, *The microtubule network and neuronal morphogenesis: Dynamic and coordinated orchestration through multiple players.* Molecular and Cellular Neuroscience, 2010. **43**(1): p. 15-32.
25. Lundin, V.F., M.R. Leroux, and P.C. Stirling, *Quality control of cytoskeletal proteins and human disease.* Trends in biochemical sciences, 2010. **35**(5): p. 288-297.
26. Gilmore, E.C. and C.A. Walsh, *Genetic causes of microcephaly and lessons for neuronal development.* Wiley Interdiscip Rev Dev Biol, 2013. **2**(4): p. 461-78.
27. Valenzuela, I., et al., *Microcephaly with simplified gyral pattern, epilepsy and permanent neonatal diabetes syndrome (MEDS). A new patient and review of the literature.* European Journal of Medical Genetics, 2017.
28. Chang, B.S., *Tubulinopathies and Their Brain Malformation Syndromes: Every TUB on Its Own Bottom.* Epilepsy Currents, 2015. **15**(2): p. 65-67.
29. Breuss, M. and D.A. Keays, *Microtubules and neurodevelopmental disease: the movers and the makers.* Adv Exp Med Biol, 2014. **800**: p. 75-96.
30. Woods, C.G. and A. Parker, *Investigating microcephaly.* Archives of disease in childhood, 2013: p. archdischild-2012-302882.
31. Woods, C.G., *Human microcephaly.* Current opinion in neurobiology, 2004. **14**(1): p. 112-117.
32. Mutch, C.A., et al., *Disorders of microtubule function in neurons: imaging correlates.* American Journal of Neuroradiology, 2016. **37**(3): p. 528-535.
33. Pode-Shakked, B., et al., *Microcephaly, intractable seizures and developmental delay caused by biallelic variants in TBCD: Further delineation of a new chaperone-mediated tubulinopathy.* Clinical genetics, 2016.
34. Miyake, N., et al., *Biallelic TBCD mutations cause early-onset neurodegenerative encephalopathy.* The American Journal of Human Genetics, 2016. **99**(4): p. 950-961.
35. Ikeda, T., et al., *TBCD may be a causal gene in progressive neurodegenerative encephalopathy with atypical infantile spinal muscular atrophy.* J Hum Genet, 2017. **62**(4): p. 473-480.
36. Flex, E., et al., *Biallelic Mutations in TBCD, Encoding the Tubulin Folding Cofactor D, Perturb Microtubule Dynamics and Cause Early-Onset Encephalopathy.* The American Journal of Human Genetics, 2016. **99**(4): p. 962-973.
37. Edvardson, S., et al., *Infantile neurodegenerative disorder associated with mutations in TBCD, an essential gene in the tubulin heterodimer assembly pathway.* Human Molecular Genetics, 2016. **25**(21): p. 4635-4648.
38. Nithianantham, S., et al., *Tubulin cofactors and Arl2 are cage-like chaperones that regulate the soluble αβ-tubulin pool for microtubule dynamics.* Elife, 2015. **4**: p. e08811.

39. Tian, G., S. Thomas, and N.J. Cowan, *Effect of TBCD and its regulatory interactor Arl2 on tubulin and microtubule integrity.* Cytoskeleton, 2010. **67**(11): p. 706-714.
40. Francis, J.W., et al., *A Trimer Consisting of the Tubulin-specific Chaperone D (TBCD), Regulatory GTPase ARL2, and β-Tubulin Is Required for Maintaining the Microtubule Network.* Journal of Biological Chemistry, 2017. **292**(10): p. 4336-4349.
41. Fanarraga, M.L., et al., *TBCD links centriologenesis, spindle microtubule dynamics, and midbody abscission in human cells.* PLoS One, 2010. **5**(1): p. e8846.
42. Francis, J.W., et al., *Nucleotide Binding to ARL2 in the TBCD·ARL2·β-Tubulin Complex Drives Conformational Changes in β-Tubulin.* Journal of Molecular Biology, 2017. **429**(23): p. 3696-3716.
43. Jánosi, I.M., D. Chrétien, and H. Flyvbjerg, *Structural Microtubule Cap: Stability, Catastrophe, Rescue, andThird State.* Biophysical Journal, 2002. **83**(3): p. 1317-1330.
44. Janke, C., *The tubulin code: Molecular components, readout mechanisms, and functions.* The Journal of Cell Biology, 2014. **206**(4): p. 461-472.
45. Chakraborti, S., et al., *The emerging role of the tubulin code: from the tubulin molecule to neuronal function and disease.* Cytoskeleton, 2016. **73**(10): p. 521-550.
46. Fedyanina, O.S., A.J. Book, and E.L. Grishchuk, *Tubulin heterodimers remain functional for one cell cycle after the inactivation of tubulin-folding cofactor D in fission yeast cells.* Yeast, 2009. **26**(4): p. 235-247.
47. Fedyanina, O.S., et al., *Chromosome segregation in fission yeast with mutations in the tubulin folding cofactor D.* Current genetics, 2006. **50**(5): p. 281-294.
48. Okumura, M., et al., *Linking cell surface receptors to microtubules: tubulin folding cofactor D mediates Dscam functions during neuronal morphogenesis.* Journal of Neuroscience, 2015. **35**(5): p. 1979-1990.
49. Steinborn, K., et al., *The Arabidopsis PILZ group genes encode tubulin-folding cofactor orthologs required for cell division but not cell growth.* Genes & development, 2002. **16**(8): p. 959-971.
50. Hirata, D., et al., *Essential role of tubulin-folding cofactor D in microtubule assembly and its association with microtubules in fission yeast.* The EMBO Journal, 1998. **17**(3): p. 658-666.
51. Cunningham, L.A. and R.A. Kahn, *Cofactor D functions as a centrosomal protein and is required for the recruitment of the gamma-tubulin ring complex at centrosomes and organization of the mitotic spindle.* J Biol Chem, 2008. **283**(11): p. 7155-65.
52. Ikeda, T., et al., *TBCD may be a causal gene in progressive neurodegenerative encephalopathy with atypical infantile spinal muscular atrophy.* Journal of Human Genetics, 2016.
53. Englund, C., et al., *Pax6, Tbr2, and Tbr1 are expressed sequentially by radial glia, intermediate progenitor cells, and postmitotic neurons in developing neocortex.* Journal of Neuroscience, 2005. **25**(1): p. 247-251.
54. Manuel, M.N., et al., *Regulation of cerebral cortical neurogenesis by the Pax6 transcription factor.* Frontiers in cellular neuroscience, 2015. **9**: p. 70.
55. Sansom, S.N., et al., *The level of the transcription factor Pax6 is essential for controlling the balance between neural stem cell self-renewal and neurogenesis.* PLoS genetics, 2009. **5**(6).
56. Quinn, J.C., et al., *Pax6 controls cerebral cortical cell number by regulating exit from the cell cycle and specifies cortical cell identity by a cell autonomous mechanism.* Developmental biology, 2007. **302**(1): p. 50-65.
57. Estivill-Torrus, G., et al., *Pax6 is required to regulate the cell cycle and the rate of progression from symmetrical to asymmetrical division in mammalian cortical progenitors.* Development, 2002. **129**(2): p. 455-466.
58. Georgala, P.A., M. Manuel, and D.J. Price, *The generation of superficial cortical layers is regulated by levels of the transcription factor Pax6.* Cerebral Cortex, 2011. **21**(1): p. 81-94.
59. Mi, D., et al., *Pax6 exerts regional control of cortical progenitor proliferation via direct repression of Cdk6 and hypophosphorylation of pRb.* Neuron, 2013. **78**(2): p. 269-284.

60. Berger, J., et al., *Conditional activation of Pax6 in the developing cortex of transgenic mice causes progenitor apoptosis.* Development, 2007. **134**(7): p. 1311-1322.
61. Taverna, E., M. Götz, and W.B. Huttner, *The cell biology of neurogenesis: toward an understanding of the development and evolution of the neocortex.* Annual review of cell and developmental biology, 2014. **30**.
62. Paridaen, J.T. and W.B. Huttner, *Neurogenesis during development of the vertebrate central nervous system.* EMBO reports, 2014. **15**(4): p. 351-364.
63. Penisson, M., et al., *Genes and mechanisms involved in the generation and amplification of basal radial glial cells.* Frontiers in cellular neuroscience, 2019. **13**: p. 381.
64. Noctor, S.C., et al., *Dividing precursor cells of the embryonic cortical ventricular zone have morphological and molecular characteristics of radial glia.* Journal of Neuroscience, 2002. **22**(8): p. 3161-3173.
65. Sessa, A., et al., *Tbr2 directs conversion of radial glia into basal precursors and guides neuronal amplification by indirect neurogenesis in the developing neocortex.* Neuron, 2008. **60**(1): p. 56-69.
66. Mihalas, A.B., et al., *Intermediate progenitor cohorts differentially generate cortical layers and require Tbr2 for timely acquisition of neuronal subtype identity.* Cell reports, 2016. **16**(1): p. 92-105.
67. Betizeau, M., et al., *Precursor diversity and complexity of lineage relationships in the outer subventricular zone of the primate.* Neuron, 2013. **80**(2): p. 442-457.
68. Nomura, T., et al., *The evolution of basal progenitors in the developing non-mammalian brain.* Development, 2016. **143**(1): p. 66-74.
69. Kwan, K.Y., N. Šestan, and E. Anton, *Transcriptional co-regulation of neuronal migration and laminar identity in the neocortex.* Development, 2012. **139**(9): p. 1535-1546.
70. Whitton, L., et al., *Genes regulated by SATB2 during neurodevelopment contribute to schizophrenia and educational attainment.* PLoS genetics, 2018. **14**(7): p. e1007515.
71. Kanold, P.O., *Subplate neurons: crucial regulators of cortical development and plasticity.* Frontiers in neuroanatomy, 2009. **3**: p. 16.
72. McConnell, S.K., A. Ghosh, and C.J. Shatz, *Subplate neurons pioneer the first axon pathway from the cerebral cortex.* Science, 1989. **245**(4921): p. 978-982.
73. Leone, D.P., et al., *The determination of projection neuron identity in the developing cerebral cortex.* Current opinion in neurobiology, 2008. **18**(1): p. 28-35.
74. Hevner, R.F., et al., *Transcription factors in glutamatergic neurogenesis: conserved programs in neocortex, cerebellum, and adult hippocampus.* Neuroscience research, 2006. **55**(3): p. 223-233.
75. Bani-Yaghoub, M., et al., *Role of Sox2 in the development of the mouse neocortex.* Developmental biology, 2006. **295**(1): p. 52-66.
76. Zhang, S. and W. Cui, *Sox2, a key factor in the regulation of pluripotency and neural differentiation.* World Journal of Stem Cells, 2014. **6**(3): p. 305-311.
77. Khacho, M., et al., *Mitochondrial dynamics impacts stem cell identity and fate decisions by regulating a nuclear transcriptional program.* Cell stem cell, 2016. **19**(2): p. 232-247.
78. Zheng, X., et al., *Metabolic reprogramming during neuronal differentiation from aerobic glycolysis to neuronal oxidative phosphorylation.* eLife, 2016. **5**: p. e13374.
79. Vega-Naredo, I., et al., *Mitochondrial metabolism directs stemness and differentiation in P19 embryonal carcinoma stem cells.* Cell Death & Differentiation, 2014. **21**(10): p. 1560-1574.
80. Agostini, M., et al., *Metabolic reprogramming during neuronal differentiation.* Cell death and differentiation, 2016. **23**(9): p. 1502-1514.
81. Lunt, S.Y., et al., *Pyruvate kinase isoform expression alters nucleotide synthesis to impact cell proliferation.* Mol Cell, 2015. **57**(1): p. 95-107.
82. Ito, K. and T. Suda, *Metabolic requirements for the maintenance of self-renewing stem cells.* Nature reviews Molecular cell biology, 2014. **15**(4): p. 243-256.

83. Klepinin, A., et al., *Comparative analysis of some aspects of mitochondrial metabolism in differentiated and undifferentiated neuroblastoma cells.* Journal of bioenergetics and biomembranes, 2014. **46**(1): p. 17-31.
84. Kalucka, J., et al., *Metabolic control of the cell cycle.* Cell cycle (Georgetown, Tex.), 2015. **14**(21): p. 3379-3388.
85. Kranenburg, O., et al., *Inhibition of cyclin-dependent kinase activity triggers neuronal differentiation of mouse neuroblastoma cells.* J Cell Biol, 1995. **131**(1): p. 227-34.
86. Hydbring, P., M. Malumbres, and P. Sicinski, *Non-canonical functions of cell cycle cyclins and cyclin-dependent kinases.* Nature reviews Molecular cell biology, 2016. **17**(5): p. 280-292.
87. Sakamaki, T., et al., *Cyclin D1 determines mitochondrial function in vivo.* Mol Cell Biol, 2006. **26**(14): p. 5449-69.
88. Yang, K., M. Hitomi, and D.W. Stacey, *Variations in cyclin D1 levels through the cell cycle determine the proliferative fate of a cell.* Cell division, 2006. **1**(1): p. 32.
89. Ferri, A.L., et al., *Sox2 deficiency causes neurodegeneration and impaired neurogenesis in the adult mouse brain.* Development, 2004. **131**(15): p. 3805-3819.
90. Candelario, K.M., C.W. Shuttleworth, and L.A. Cunningham, *Neural stem/progenitor cells display a low requirement for oxidative metabolism independent of hypoxia inducible factor-1alpha expression.* Journal of neurochemistry, 2013. **125**(3): p. 420-429.
91. Antico Arciuch, V.G., et al., *Mitochondrial regulation of cell cycle and proliferation.* Antioxidants & redox signaling, 2012. **16**(10): p. 1150-1180.
92. Lv, X., et al., *TBR2 coordinates neurogenesis expansion and precise microcircuit organization via Protocadherin 19 in the mammalian cortex.* Nature communications, 2019. **10**(1): p. 1-15.
93. Hindley, C. and A. Philpott, *Co-ordination of cell cycle and differentiation in the developing nervous system.* Biochemical Journal, 2012. **444**(3): p. 375-382.
94. Chin, L.-S., et al., *Impairment of axonal development and of synaptogenesis in hippocampal neurons of synapsin I-deficient mice.* Proceedings of the National Academy of Sciences, 1995. **92**(20): p. 9230-9234.
95. Fornasiero, E.F., et al., *The role of synapsins in neuronal development.* Cellular and Molecular Life Sciences, 2010. **67**(9): p. 1383-1396.
96. Baldelli, P., et al., *Lack of synapsin I reduces the readily releasable pool of synaptic vesicles at central inhibitory synapses.* Journal of Neuroscience, 2007. **27**(49): p. 13520-13531.
97. Yuan, S.B., et al., *Gp120 in the pathogenesis of human immunodeficiency virus–associated pain.* Annals of neurology, 2014. **75**(6): p. 837-850.
98. Corradi, A., et al., *Synapsin-I-and synapsin-II-null mice display an increased age-dependent cognitive impairment.* Journal of cell science, 2008. **121**(18): p. 3042-3051.
99. Jovanovic, J.N., et al., *Neurotrophins stimulate phosphorylation of synapsin I by MAP kinase and regulate synapsin I-actin interactions.* Proceedings of the National Academy of Sciences, 1996. **93**(8): p. 3679-3683.
100. Qin, S., et al., *Regional alteration of synapsin I in the hippocampal formation of Alzheimer's disease patients.* Acta neuropathologica, 2004. **107**(3): p. 209-215.
101. Li, Z., et al., *The importance of dendritic mitochondria in the morphogenesis and plasticity of spines and synapses.* Cell, 2004. **119**(6): p. 873-887.
102. Merriam, E.B., et al., *Synaptic regulation of microtubule dynamics in dendritic spines by calcium, F-actin, and drebrin.* Journal of Neuroscience, 2013. **33**(42): p. 16471-16482.
103. Jaworski, J., et al., *Dynamic microtubules regulate dendritic spine morphology and synaptic plasticity.* Neuron, 2009. **61**(1): p. 85-100.
104. Mullen, R.J., C.R. Buck, and A.M. Smith, *NeuN, a neuronal specific nuclear protein in vertebrates.* Development, 1992. **116**(1): p. 201-211.
105. Kim, K.K., R.S. Adelstein, and S. Kawamoto, *Identification of neuronal nuclei (NeuN) as Fox-3, a new member of the Fox-1 gene family of splicing factors.* Journal of Biological Chemistry, 2009. **284**(45): p. 31052-31061.

106. Gusel'Nikova, V. and D. Korzhevskiy, *NeuN as a neuronal nuclear antigen and neuron differentiation marker.* Acta Naturae (англоязычная версия), 2015. **7**(2 (25)).
107. Sarnat, H.B., D. Nochlin, and D.E. Born, *Neuronal nuclear antigen (NeuN): a marker of neuronal maturation in the early human fetal nervous system.* Brain and Development, 1998. **20**(2): p. 88-94.
108. Weyer, A. and K. Schilling, *Developmental and cell type-specific expression of the neuronal marker NeuN in the murine cerebellum.* Journal of neuroscience research, 2003. **73**(3): p. 400-409.
109. Cho, Y.M., et al., *Induction of unfolded protein response during neuronal induction of rat bone marrow stromal cells and mouse embryonic stem cells.* Experimental & molecular medicine, 2009. **41**(6): p. 440-452.
110. Godin, J.D., et al., *Emerging roles for the unfolded protein response in the developing nervous system.* Trends in neurosciences, 2016. **39**(6): p. 394-404.
111. Kawada, K., et al., *Aberrant neuronal differentiation and inhibition of dendrite outgrowth resulting from endoplasmic reticulum stress.* Journal of neuroscience research, 2014. **92**(9): p. 1122-1133.
112. Laguesse, S., et al., *A dynamic unfolded protein response contributes to the control of cortical neurogenesis.* Developmental cell, 2015. **35**(5): p. 553-567.
113. Williams, D.W., et al., *Local caspase activity directs engulfment of dendrites during pruning.* Nature neuroscience, 2006. **9**(10): p. 1234-1236.
114. Fernando, P., S. Brunette, and L.A. Megeney, *Neural stem cell differentiation is dependent upon endogenous caspase-3 activity.* The FASEB journal, 2005. **19**(12): p. 1671-1673.
115. Lossi, L., C. Castagna, and A. Merighi, *Caspase-3 mediated cell death in the normal development of the mammalian cerebellum.* International journal of molecular sciences, 2018. **19**(12): p. 3999.
116. Tzeng, T.-T., et al., *Caspase 3 involves in neuroplasticity, microglial activation and neurogenesis in the mice hippocampus after intracerebral injection of kainic acid.* Journal of biomedical science, 2013. **20**(1): p. 1-16.
117. D'amelio, M., V. Cavallucci, and F. Cecconi, *Neuronal caspase-3 signaling: not only cell death.* Cell Death & Differentiation, 2010. **17**(7): p. 1104-1114.
118. Zabala, J.C. and N.J. Cowan, *Tubulin dimer formation via the release of alpha- and beta-tubulin monomers from multimolecular complexes.* Cell Motil Cytoskeleton, 1992. **23**(3): p. 222-30.
119. Tian, G. and N.J. Cowan, *Tubulin-specific chaperones: components of a molecular machine that assembles the alpha/beta heterodimer.* Methods Cell Biol, 2013. **115**: p. 155-71.
120. Gasic, I., S.A. Boswell, and T.J. Mitchison, *Tubulin mRNA stability is sensitive to change in microtubule dynamics caused by multiple physiological and toxic cues.* PLoS biology, 2019. **17**(4): p. e3000225.
121. Cleveland, D., *Autoregulated control of tubilin synthesis in animal cells.* Current opinion in cell biology, 1989. **1**(1): p. 10-14.
122. Yen, T., et al., *Autoregulated changes in stability of polyribosome-bound beta-tubulin mRNAs are specified by the first 13 translated nucleotides.* Molecular and Cellular Biology, 1988. **8**(3): p. 1224-1235.
123. Pachter, J.S., T.J. Yen, and D.W. Cleveland, *Autoregulation of tubulin expression is achieved through specific degradation of polysomal tubulin mRNAs.* Cell, 1987. **51**(2): p. 283-92.
124. Yen, T.J., P.S. Machlin, and D.W. Cleveland, *Autoregulated instability of β-tubulin mRNAs by recognition of the nascent amino terminus of βtubulin.* Nature, 1988. **334**(6183): p. 580-585.
125. Malumbres, M., *Cyclin-dependent kinases.* Genome biology, 2014. **15**(6): p. 1-10.
126. Stacey, D.W., *Cyclin D1 serves as a cell cycle regulatory switch in actively proliferating cells.* Current Opinion in Cell Biology, 2003. **15**(2): p. 158-163.
127. Topacio, B.R., et al., *Cyclin D-Cdk4, 6 drives cell-cycle progression via the retinoblastoma protein's C-terminal helix.* Molecular cell, 2019. **74**(4): p. 758-770. e4.

128. Lange, C., W.B. Huttner, and F. Calegari, *Cdk4/cyclinD1 overexpression in neural stem cells shortens G1, delays neurogenesis, and promotes the generation and expansion of basal progenitors.* Cell stem cell, 2009. **5**(3): p. 320-331.
129. Miyata, T., et al., *Asymmetric production of surface-dividing and non-surface-dividing cortical progenitor cells.* Development, 2004. **131**(13): p. 3133-3145.
130. Haubensak, W., et al., *Neurons arise in the basal neuroepithelium of the early mammalian telencephalon: a major site of neurogenesis.* Proceedings of the National Academy of Sciences, 2004. **101**(9): p. 3196-3201.
131. Simon, R., et al., *A dual function of Bcl11b/Ctip2 in hippocampal neurogenesis.* The EMBO journal, 2012. **31**(13): p. 2922-2936.
132. Zhang, L.-j., et al., *Ctip2 is a dynamic regulator of epidermal proliferation and differentiation by integrating EGFR and Notch signaling.* Journal of cell science, 2012. **125**(23): p. 5733-5744.
133. Garone, C., et al., *Mitochondrial dynamics: overview of molecular mechanisms.* Essays in biochemistry, 2018. **62**(3): p. 341-360.
134. Lee, S., et al., *Cell cycle-dependent mitochondrial biogenesis and dynamics in mammalian cells.* Biochemical and biophysical research communications, 2007. **357**(1): p. 111-117.
135. Horbay, R. and R. Bilyy, *Mitochondrial dynamics during cell cycling.* Apoptosis, 2016. **21**(12): p. 1327-1335.
136. Mishra, P. and D.C. Chan, *Mitochondrial dynamics and inheritance during cell division, development and disease.* Nature reviews Molecular cell biology, 2014. **15**(10): p. 634-646.
137. Ratineau, C., et al., *Cyclin D1 represses the basic helix-loop-helix transcription factor, BETA2/NeuroD.* Journal of Biological Chemistry, 2002. **277**(11): p. 8847-8853.
138. Bloom, J.S. and G.W. Hynd, *The role of the corpus callosum in interhemispheric transfer of information: excitation or inhibition?* Neuropsychology review, 2005. **15**(2): p. 59-71.
139. Goldstein, A., et al., *Neuroanatomy, corpus callosum.* 2017.
140. Paul, L.K., *Developmental malformation of the corpus callosum: a review of typical callosal development and examples of developmental disorders with callosal involvement.* Journal of neurodevelopmental disorders, 2011. **3**(1): p. 3-27.
141. Thompson, D.K., et al., *Corpus callosum alterations in very preterm infants: perinatal correlates and 2 year neurodevelopmental outcomes.* Neuroimage, 2012. **59**(4): p. 3571-3581.
142. D'Antonio, F., et al., *Outcomes associated with isolated agenesis of the corpus callosum: a meta-analysis.* Pediatrics, 2016. **138**(3).
143. Egaas, B., E. Courchesne, and O. Saitoh, *Reduced size of corpus callosum in autism.* Archives of neurology, 1995. **52**(8): p. 794-801.
144. Hutton, S.R. and L.H. Pevny, *SOX2 expression levels distinguish between neural progenitor populations of the developing dorsal telencephalon.* Developmental biology, 2011. **352**(1): p. 40-47.
145. Manuel, M.N., et al., *The transcription factor Foxg1 regulates telencephalic progenitor proliferation cell autonomously, in part by controlling Pax6 expression levels.* Neural development, 2011. **6**(1): p. 1-12.
146. Hanashima, C., et al., *Foxg1 suppresses early cortical cell fate.* Science, 2004. **303**(5654): p. 56-59.
147. Pancrazi, L., et al., *Foxg1 localizes to mitochondria and coordinates cell differentiation and bioenergetics.* Proceedings of the National Academy of Sciences, 2015. **112**(45): p. 13910-13915.
148. Tang, B.L., *Glucose, glycolysis, and neurodegenerative diseases.* Journal of Cellular Physiology, 2020.
149. Folmes, C.D., et al., *Somatic oxidative bioenergetics transitions into pluripotency-dependent glycolysis to facilitate nuclear reprogramming.* Cell metabolism, 2011. **14**(2): p. 264-271.
150. Shyh-Chang, N., et al., *Influence of threonine metabolism on S-adenosylmethionine and histone methylation.* Science, 2013. **339**(6116): p. 222-226.

151. Rowlands, J., et al., *Pleiotropic Effects of GLP-1 and Analogs on Cell Signaling, Metabolism, and Function.* Frontiers in Endocrinology, 2018. **9**(672).
152. Rowlands, J., et al., *Insulin and IGF-1 receptor autocrine loops are not required for Exendin-4 induced changes to pancreatic β-cell bioenergetic parameters and metabolism in BRIN-BD11 cells.* Peptides, 2018. **100**: p. 140-149.
153. Carlessi, R., et al., *GLP-1 receptor signalling promotes beta-cell glucose metabolism via mTOR-dependent HIF-1alpha activation.* Sci Rep, 2017. **7**(1): p. 2661.
154. Kondoh, H., et al., *A high glycolytic flux supports the proliferative potential of murine embryonic stem cells.* Antioxidants & redox signaling, 2007. **9**(3): p. 293-299.
155. Li, Y., et al., *GLP-1 receptor stimulation preserves primary cortical and dopaminergic neurons in cellular and rodent models of stroke and Parkinsonism.* Proc Natl Acad Sci U S A, 2009. **106**(4): p. 1285-90.
156. McGovern, S.F., K. Hunter, and C. Hölscher, *Effects of the glucagon-like polypeptide-1 analogue (Val8) GLP-1 on learning, progenitor cell proliferation and neurogenesis in the C57B/16 mouse brain.* Brain research, 2012. **1473**: p. 204-213.
157. Li, Y., et al., *GLP-1 receptor stimulation preserves primary cortical and dopaminergic neurons in cellular and rodent models of stroke and Parkinsonism.* Proceedings of the National Academy of Sciences, 2009. **106**(4): p. 1285-1290.
158. Hölscher, C., *Central effects of GLP-1: new opportunities for treatments of neurodegenerative diseases.* Journal of Endocrinology, 2014. **221**(1): p. T31-T41.
159. Hölscher, C., *Potential role of glucagon-like peptide-1 (GLP-1) in neuroprotection.* CNS drugs, 2012. **26**(10): p. 871-882.
160. Holscher, C., *The role of GLP-1 in neuronal activity and neurodegeneration.* Vitam Horm, 2010. **84**: p. 331-54.
161. Farr, O.M., et al., *GLP-1 receptors exist in the parietal cortex, hypothalamus and medulla of human brains and the GLP-1 analogue liraglutide alters brain activity related to highly desirable food cues in individuals with diabetes: a crossover, randomised, placebo-controlled trial.* Diabetologia, 2016. **59**(5): p. 954-65.
162. Butler, P.C., et al., *A Critical Analysis of the Clinical Use of Incretin-Based Therapies: Are the GLP-1 Therapies Safe?: How safe are the GLP-1–based therapies?* Diabetes care, 2013: p. DC_122713.
163. Holst, J.J., *Pharmacology of GLP-1-based therapies.* The British Journal of Diabetes & Vascular Disease, 2008. **8**(2_suppl): p. S10-S18.
164. Trujillo, J.M., W. Nuffer, and S.L. Ellis, *GLP-1 receptor agonists: a review of head-to-head clinical studies.* Therapeutic Advances in Endocrinology and Metabolism, 2015. **6**(1): p. 19-28.
165. Holt, M.K. and S. Trapp, *The physiological role of the brain GLP-1 system in stress.* Cogent Biology, 2016. **2**(1): p. 1229086.
166. Gejl, M., et al., *In Alzheimer's Disease, 6-Month Treatment with GLP-1 Analog Prevents Decline of Brain Glucose Metabolism: Randomized, Placebo-Controlled, Double-Blind Clinical Trial.* Front Aging Neurosci, 2016. **8**: p. 108.
167. Cantini, G., E. Mannucci, and M. Luconi, *Perspectives in GLP-1 research: new targets, new receptors.* Trends in Endocrinology & Metabolism, 2016. **27**(6): p. 427-438.
168. Cabou, C. and R. Burcelin, *GLP-1, the Gut-Brain, and Brain-Periphery Axes.* The Review of Diabetic Studies : RDS, 2011. **8**(3): p. 418-431.
169. Cornu, M., et al., *Glucagon-like peptide-1 protects beta-cells against apoptosis by increasing the activity of an IGF-2/IGF-1 receptor autocrine loop.* Diabetes, 2009. **58**(8): p. 1816-25.
170. Kadowaki, T., et al., *Insulin-like growth factors, insulin, and epidermal growth factor cause rapid cytoskeletal reorganization in KB cells. Clarification of the roles of type I insulin-like growth factor receptors and insulin receptors.* Journal of Biological Chemistry, 1986. **261**(34): p. 16141-16147.

171. Bassil, F., et al., *Insulin, IGF-1 and GLP-1 signaling in neurodegenerative disorders: targets for disease modification?* Progress in neurobiology, 2014. **118**: p. 1-18.
172. Mill, J.F., M.V. Chao, and D.N. Ishii, *Insulin, insulin-like growth factor II, and nerve growth factor effects on tubulin mRNA levels and neurite formation.* Proceedings of the National Academy of Sciences, 1985. **82**(20): p. 7126-7130.
173. Fernyhough, P., et al., *Stabilization of tubulin mRNAs by insulin and insulin-like growth factor I during neurite formation.* Molecular Brain Research, 1989. **6**(2-3): p. 109-120.
174. Lara-Diaz, V., et al., *IGF-1 modulates gene expression of proteins involved in inflammation, cytoskeleton, and liver architecture.* Journal of physiology and biochemistry, 2017. **73**(2): p. 245-258.
175. Hakuno, F. and S.-I. Takahashi, *40 years of IGF1: IGF1 receptor signaling pathways.* Journal of molecular endocrinology, 2018. **61**(1): p. T69-T86.
176. Brooker, G.J., et al., *Endogenous IGF-1 regulates the neuronal differentiation of adult stem cells.* Journal of neuroscience research, 2000. **59**(3): p. 332-341.
177. Fellows, A.D., et al., *IGF 1R regulates retrograde axonal transport of signalling endosomes in motor neurons.* EMBO reports, 2020. **21**(3): p. e49129.
178. Cahill, A.L. and R.L. Perlman, *Activation of a Microtubule-Associated Protein-2 Kinase by Insulin-Like Growth Factor-I in Bovine Chromaffin Cells.* Journal of neurochemistry, 1991. **57**(6): p. 1832-1839.
179. Duenas, M., et al., *Interaction of insulin-like growth factor-I and estradiol signaling pathways on hypothalamic neuronal differentiation.* Neuroscience, 1996. **74**(2): p. 531-539.
180. Chesik, D., N. Wilczak, and J. De Keyser, *Insulin-like growth factor binding protein-4 interacts with centrosomes and microtubules in primary astrocytes.* Neuroscience, 2004. **125**(2): p. 381-390.
181. Chen, J., et al., *Liraglutide activates autophagy via GLP-1R to improve functional recovery after spinal cord injury.* Oncotarget, 2017. **8**(49): p. 85949.
182. Roscioni, S.S., C.R. Elzinga, and M. Schmidt, *Epac: effectors and biological functions.* Naunyn-Schmiedeberg's archives of pharmacology, 2008. **377**(4-6): p. 345-357.
183. Luciani, P., et al., *Differentiating effects of the glucagon-like peptide-1 analogue exendin-4 in a human neuronal cell model.* Cellular and molecular life sciences, 2010. **67**(21): p. 3711-3723.
184. Gilmore, E.C. and C.A. Walsh, *Genetic causes of microcephaly and lessons for neuronal development.* Wiley Interdisciplinary Reviews: Developmental Biology, 2013. **2**(4): p. 461-478.

Chapter 5 Pleiotropic Effects of GLP-1 and Analogs on Cell Signaling, Metabolism, and Function

Jordan Rowlands, Julian Heng, Philip Newsholme, Rodrigo Carlessi

School of Pharmacy and Biomedical Sciences, Curtin Health Innovation Research Institute, Perth, Western Australia 6845.

Key words: GLP-1 receptor signalling promotes β-cell glucose metabolism via mTOR-dependent HIF-1α activation (2017)

Corresponding Authors:

Philip Newsholme, School of Pharmacy and Biomedical Sciences, Curtin University Bldg 305 Rm 135, CHIRI, Kent St, Bentley, WA, 6102. +61892667425, philip.newsholme@curtin.edu.au

Rodrigo Carlessi, School of Pharmacy and Biomedical Sciences, Curtin University, Bldg 308, Rm 113 – CHIRI, Kent St, Bentley, WA, 6102. +61475299969, rodrigo.carlessi@curtin.edu.au

Rowlands, J., Heng, J., Newsholme, P., & Carlessi, R. (2018). Pleiotropic effects of GLP-1 and analogs on cell signaling, metabolism, and function. Frontiers in endocrinology, 9, 672.

doi:10.3389/fendo.2018.00672

Content is removed due to copyright restrictions

Chapter 6 GLP-1R agonism, a potential therapeutic avenue to alleviate the effects of TBCD mutations

6.1 Introduction

Disruptions to the neuronal cytoskeleton to lead to a multitude of deleterious phenotypes, with recent reports segregating genetic mutations in the gene of the MT biosynthesis enzyme, tubulin binding co-factor D (TBCD), with the novel severe neurodegenerative condition observed in infants [1-8]. Originally identified by Edvardson and colleagues in 2016 [8], the *TBCD* homozygous missense mutations, A475T and A586V, were reported to lead to a functional deficiency in the MT biosynthesis pathway, impairing MT dynamics, which in turn contributed to secondary microcephaly. Of the two mutations reported, the TBCD A475T mutation was observed to lead to greater biological deficits than the A586V mutation in all systems observed, however the underlying molecular mechanisms for these severe phenotypes remained elusive Edvardson, Tian [8]. Utilising both *in vivo* and *in vitro* approaches, I was able to identify a potential mode of action to address this gap in knowledge, wherein the expression of the mutant TBCDs altered cell cycle dynamics, leading to a loss of pluripotency accompanied by metabolic reprogramming, finally accumulating in premature cell fate acquisition (discussed in chapter 4). Whilst these results strongly align with various studies detailing MTs and TBCDs role [5, 8], they also provide a unique and novel insight into the essential role of the tubulin co-factors and their impact on cellular mechanics.

More importantly, delineating the molecular mechanisms underpinning these mutations has enabled the identification of potential therapeutic targets that may be explored to alleviate the deleterious mutational effects. One such target of interest is the incretin peptide glucagon-like peptide-1 (GLP-1). Although it was originally appropriated for use as a type 2 diabetes (T2D) therapy, a plethora of physiological effects have been observed in a variety of tissues from both acute and chronic GLP-1 receptor (GLP-1R) activation (detailed in chapter 5) [9-11].

Secreted from either the enteroendocrine L-cells, pancreatic α-cells or the preproglucagon (PPG) neurons in the brain stem, GLP-1 can then bind to the GLP-1R initiating a cascade of signalling events beginning with the activation of membrane bound Adenyl Cyclase (AC) and

consequent production of cyclic adenosine monophosphate (cAMP) [12]. Following this, cAMP leads to the activation of the cAMP effectors, exchange protein directly activated by cAMP (EPAC) and Protein kinase A (PKA) [12-15]. Downstream of these two main pathways is the activation and inducement of the extracellular-signal related kinases (ERK) 1 and 2, cAMP responsive element binding (CREB) signalling, transcriptional induction of insulin receptor substrate (IRS)-2, and activation of the phosphatidylinositol 3-kinase (PI3K)/Akt pathway [12, 16]. In addition, it has recently been demonstrated that the acute stimulation of the GLP-1R results in the secretion of insulin like growth factor 1/2 (IGF-1/2) and insulin, whilst prolonged GLP-1R activation promotes the expression of the Insulin-like growth factor 1 receptor (IGF1R) and, to a lesser extent, the insulin receptor (INSR) [12]. Activation of these two growth factor receptors can trigger a variety of downstream signals including IRS phosphorylation, AKT/PKB, and ERK activation [17, 18]. In the brain, activation of these pathways has been shown to promote progenitor cell proliferation, reduce oxidative stress, reduce inflammation, inhibit apoptosis, promote neurogenesis, as well as aid mitochondrial function and bioenergetics [12, 19]. Notably, several studies have also highlighted that both IGF1R and INSR signalling pathways are able to interact with the cytoskeleton and its various elements, increasing MT dynamics, triggering cytoskeletal reorganisation, and even stabilizing tubulin mRNA [12, 20]. These studies, coupled with the previous observations that perturbations to TBCD can disrupt cell cycle dynamics, enhance mitochondrial metabolism, increase reactive oxygen species (ROS), and increase differentiation, offer a potential mechanism to alleviate the issues arising from the clinical TBCD mutations.

Here, the potential therapeutic benefit of chronic GLP-1R activation on perturbations arising from the TBCD silencing, and the clinical TBCD A475T mutation, as well as the involvement of IGF1R and IR in this process, was investigated. Through TBCD shRNA knockdown (KD) and rescue experiments it was demonstrated, that chronic exposure to Exendin-4, a long lasting GLP-1 analogue, alleviates the G2 cycle delay, promotes bioenergetics reprogramming and alters the enhanced cell fate commitment resultant from the clinical TBCD A475T mutation. In addition, knock outs (KO) of the Igf1r and Insr in P19 embryonic carcinoma cells (P19ECs) via CRISPR-CAS9 was performed, following which TBCD shRNA silencing and rescue experiments were conducted in the presence or absence of Exendin-4 for 18 h. Exendin-4 effects were completely lost in Igf1r KO P19ECs, but unchanged in Insr KO P19ECs. This

demonstrated that GLP-1Rs restorative abilities were dependent on IGF1R but no INSR. These data highlight that Exendin-4 acts via an IGF1R dependent mechanism to alleviate TBCD induced perturbations to cell cycle dynamics. These results suggest that GLP-1R agonism may be an effective therapeutic treatment for the cellular pathologies that arise form TBCD missense mutations.

6.2 Results

6.2.1 Ex-4 alleviates cell cycle delay

GLP-1R agonists have been reported in several studies to increase both proliferation and differentiation of neuronal stem/progenitor cells (NSC/NPC) [21-32]. Therefore, the impact of GLP-1R signalling in the context of TBCD perturbations was investigated. In order to achieve this, P19ECs were co-transfected with either the previously generated and characterized GFP positive (GFP+) TBCD targeting short hairpin RNA (shRNA) or scrambled shRNA, in a balanced stoichiometry with mammalian expression vectors containing either wild-type human TBCD (WT), the A475T or the A586V TBCD mutation, as previously described [12, 22, 33-36]. After 30 h of transfection, cells were treated or not, with the long lasting GLP-1 analogue Exendin-4, and incubated for an additional 18 h. Following this FxCycle PI/RNAse staining solution and flow cytometry to assess cell cycle dynamics in GFP+ sorted cells was utilised, as previously outlined (**Fig. 6.1**). Data obtained from cell cycle analysis revealed a significant decrease in the percent of TBCD silenced and A475T rescued cells in G1 compared to control (~30%, $p < 0.05$ and ~40%, $p < 0.001$ respectively) (**Fig. 6.1A**). No significant differences were observed for either TBCD silenced or TBCD A475T rescued cells in S phase compared to control (**Fig. 6.1B**). Confirming the previous observations, assessment of cells in G2 revealed a significant increase of approximately 1.8-fold for both TBCD silenced and A475T rescued cells in comparison to control ($p < 0.001$) (**Fig. 6.1C**). Next, the impact of Exendin-4 on cell cycle dynamics was explored. Interestingly, compared with corresponding control cells, treatment with Exendin-4 led to an increased percentage of G1 cells in scrambled control cells (~1.5-fold, $p < 0.0001$), TBCD silenced cells (~1.5-fold, $p < 0.001$) and to a lesser extent in TBCD

A475T rescued cells (~1.3-fold); restoring the latter two to a level similar to that of control (**Fig. 6.1A**).

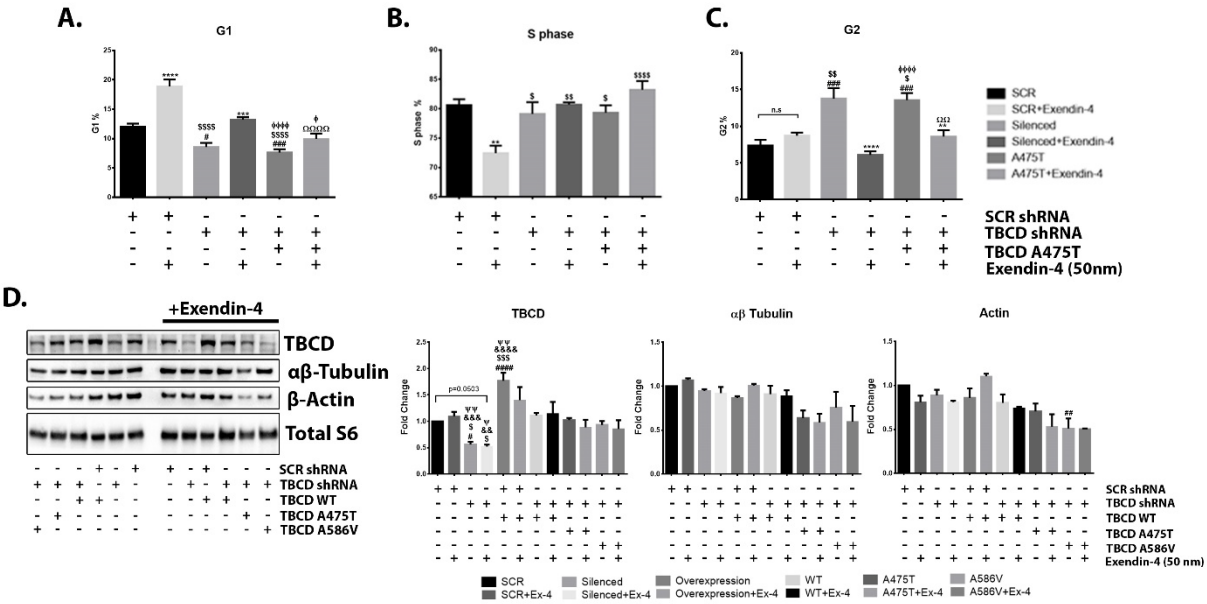

Figure 6.4. GLP-1R agonism mitigates cell cycle delay

As previously described P19ECs were co-transfected with shRNA vectors and TBCD expression constructs, as indicated, and incubated for 30 h, followed by addition, or not of 50nm Ex-4 for an additional 18 h. Following transfection GFP+ cells were sorted and processed for cell cycle analysis (A-C), or immunoblot assay of TBCD, total αβ-tubulin, and total actin expression levels (D). (A-C) Cells stained with FxCycle PI/RNAse staining solution, and a minimum of $1.0x10^4$ GFP+ cells were collected by flow cytometry and analysed using the Dean-Jett Fox algorithm model. Cell cycle analysis indicates that the TBCD induced G2 arrest is mitigated in cells treated with Ex-4 (A-C). (D) Band densitometry analysis indicated alterations to TBCD actin and tubulin are not altered by administration of Ex-4. Data represents mean ± SEM. n ≥ 5 independent experiments. * represents pairwise comparisons against own Exendin-4 untreated control. # represents comparisons against scrambled control cells. $ represents comparisons against Exendin-4 treated scrambled control cells. & represents comparisons against WT cells. Ψ represents comparisons against Exendin-4 treated WT cells. Ω represents comparisons against TBCD silenced cells. ϕ represents comparisons against Exendin-4 treated TBCD silenced cells. *P < 0.05, **P < 0.01, ***P < 0.001, ****P < 0.0001. #P < 0.05, ##P < 0.01, ###P < 0.001. $P < 0.05, $$P < 0.01, $$$P < 0.001. &P <0.05, &&P < 0.01, &&&P < 0.001, &&&&P < 0.0001. ΨP <0.05, ΨΨP < 0.01, ΨΨΨP < 0.001, ΨΨΨΨP < 0.0001. ΩP <0.05, ΩΩP < 0.01, ΩΩΩP < 0.001, ΩΩΩΩP < 0.0001. ϕP <0.05, ϕϕP < 0.01, ϕϕϕP < 0.001, ϕϕϕϕP < 0.0001.

No significant differences were observed in S phase between control cells, TBCD A475T rescued, TBCD silenced, or TBCD silenced cells in the presence of Exendin-4 (**Fig. 6.1B**). However, control cells and TBCD A475T rescued cells incubated with Exendin-4 displayed a decrease and increase in S phase cells respectively, compared to their own untreated controls (~11%, p < 0.01, and ~5% respectively) (**Fig. 6.1B**). Whilst the presence of Exendin-4 did not significantly alter the number of control cells in G2, the G2 cycle arrest observed in TBCD silenced and A475T rescued cells was ablated in the presence of Exendin-4 (~50%, p < 0.0001

and ~45%, $p < 0.01$ respectively), restoring the number of cells in these groups to a level similar to that of the control (**Fig. 6.1C**). Following this, transfected cells in the presence or absence of Exendin-4 were GFP+ sorted and subject to immunoblot assay and protein expression analysis of TBCD, total αβ-Tubulin and total actin. Band densitometry analysis validated the previously observed results, confirming TBCD silencing, overexpression, and rescue (**Fig. 6.1D**). Chronic exposure to Exendin-4 however, did not significantly alter either TBCD protein expression levels or the expression of the cytoskeletal elements αβ-Tubulin and β-Actin (**Fig. 6.1D**).

6.2.2 Chronic GLP-1R receptor stimulation rescues TBCD perturbation effects, promotes metabolic reprogramming and protein expression associated with stemness

Cell cycle entry and progression requires coordinated interaction of the cytoskeleton and metabolic machinery in order to synthesise and segregate a large number of cellular components [8]. Highly proliferative NPCs are primarily glycolytic, requiring fast glucose turnover to efficiently generate the precursors needed for synthesis and division [37-41]. During cell cycle however, NPCs will initially adapt their mitochondrial network into a more polarized tubular network, ultimately increasing mitochondrial OXPHOS and generation of ATP. This high level of OXPHOS is maintained until mitotic exit, when mitochondria become fragmented and dispersed, which is believed to be resultant from Cdk1 phosphorylation of the mitochondrial respiration chain complex I [40, 42]. Sustaining high levels of mitochondrial activity, however, can impact stem cell fate decision by acting as an upstream regulator of developmental gene expression and physiological reactive oxygen species (ROS) levels [40, 43]. Increased ROS can lead to the stabilisation of the master redox regulator, nuclear respiratory factor 2 (NRF2), which once stabilised translocates to the nucleus and mediates the transcriptional up-regulation of genes required to suppress self-renewal and activate differentiation [44, 45]. Interestingly, this metabolic induced cell fate switch has been demonstrated to act in reverse, with the switch from OXPHOS to glycolysis driving somatic cell reprogramming, as well as in the generation of induced pluripotent stem cells [45-47]. Recent findings from the Newsholme lab have demonstrated that chronic GLP-1R stimulation enacts a bioenergetic reprograming and augmentation of glycolytic flux through mTOR/ *Hypoxia-inducible factor 1α* (HIF-1α) pathway [48-51]. Coupling these findings with the enhanced mitochondrial respiration observed in TBCD altered cells, the crucial role of

mitochondria in cell cycle and the normally high glycolytic metabolism of stem cells, the ability of chronic GLP-1R activation to revert or alleviate the metabolic alterations observed in TBCD perturbed cells was thus assessed [18, 52].

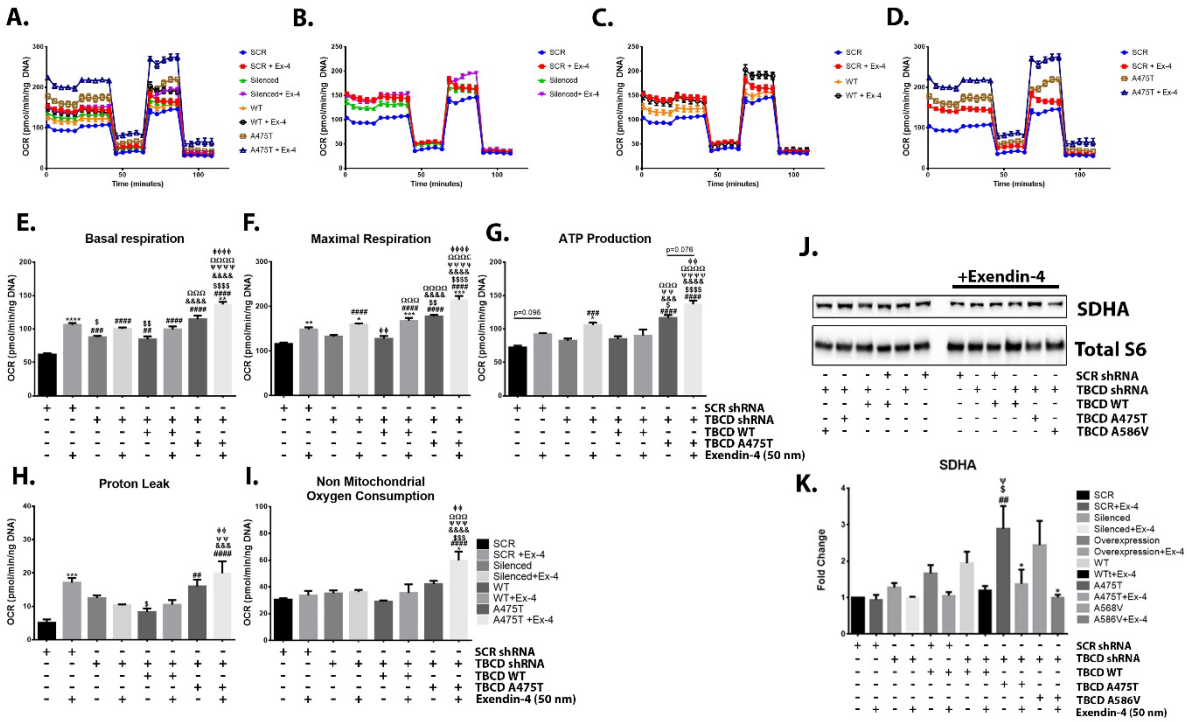

Figure 6.2. Bioenergetics is altered by chronic exposure to Exendin-4

Similar to above, cells co-transfected with TBCD shRNA and expression vectors for 30 h, with or without treatment of 50nm Ex-4 for 18 h and were GFP+ sorted. Cells were then subject to extracellular flux analysis using Seahorse Biosciences XF^{e}96 Flux Analyser. (A-I) Mitochondrial parameters were measured by subsequent injections of 25mM glucose, 2µM of oligomycin, 0.3µM FCCP and 1µM each of rotenone and antimycin A, which enabled the generation of an Oxygen consumption rate (OCR)/mitochondrial stress test profile (A-D). (E-I) Basal respiration, maximal respiration, ATP production, Proton leak and non-mitochondrial oxygen consumption were calculated from OCR measurements. (J and K) Immunoblot and band densitometry analysis of succinate dehydrogenase complex, subunit A (SDHA). Data represents mean ± SEM. n ≥ 3 independent experiments. Each point, n=5 technical replicates. * represents pairwise comparisons against own Exendin-4 untreated control. # represents comparisons against scrambled control cells. $ represents comparisons against Exendin-4 treated scrambled control cells. & represents comparisons against WT cells. Ψ represents comparisons against Exendin-4 treated WT cells. Ω represents comparisons against TBCD silenced cells. $^{\phi}$ represents comparisons against Exendin-4 treated TBCD silenced cells. *P < 0.05, **P < 0.01, ***P < 0.001, ****P < 0.0001. #P < 0.05, ##P < 0.01, ###P < 0.001, ####P < 0.0001. $P <0.05, $$P < 0.01, $$$P < 0.001, $$$$P < 0.0001. &P <0.05, &&P < 0.01, &&&P < 0.001, &&&&P < 0.0001. ΨP <0.05, ΨΨP < 0.01, ΨΨΨP < 0.001, ΨΨΨΨP < 0.0001. ΩP <0.05, ΩΩP < 0.01, ΩΩΩP < 0.001, ΩΩΩΩP < 0.0001. $^{\phi}$P <0.05, $^{\phi\phi}$P < 0.01, $^{\phi\phi\phi}$P < 0.001, $^{\phi\phi\phi\phi}$P < 0.0001.

Similar to above, cells were transfected, treated or not with Exendin-4 for 18 h, GFP+ sorted, then subject to oxygen consumption rate (OCR) measurements and immunoblot assessment of mitochondrial protein expression (**Fig. 6.2**). Initially, OCR measurements were conducted, as previously described, to determine the impact of TBCD alterations on mitochondrial

respiration with or without 18 h of Exendin-4 treatment. In these experiments, TBCD A475T rescued cells displayed increases in basal respiration, maximal respiration, ATP

production, proton leak and non-mitochondrial oxygen consumption compared to all other groups, reaching significance in all measurements except for non-mitochondrial oxygen consumption (**Fig. 6.2A-I**). TBCD silenced and WT rescue cells did not significantly differ from control cells in any parameter except basal respiration (**Fig. 6.2E**). Following chronic receptor stimulation however, it was observed that control cells in the presence of Exendin-4 had an increase in basal respiration (~1.7-fold, $p < 0.0001$), maximal respiratory capacity (~1.3-fold, $p < 0.01$), ATP production (~1.25-fold, $p=0.096$) and proton leak (~3-fold, $p < 0.001$) when compared to untreated control (**Fig. 6.2A and E-H**). Similarly, TBCD silenced cells in the presence of Exendin-4 had significant increases in maximal respiration and ATP production compared to its own untreated control (~1.2-fold, $p < 0.05$ and 1.3-fold, $p < 0.05$ respectively). Exendin-4 treated TBCD silenced cells also displayed an increase in maximal respiration when compared to TBCD WT rescue cells (~1.25-fold, $p < 0.01$), and in ATP production, basal, and maximal respiration compared to untreated control cells (~1.45-fold, $p < 0.001$, 1.4-fold, $p < 0.0001$ and 1.6-fold, $p < 0.0001$ respectively) (**Fig. 6.2B and E-H**). TBCD WT cells treated with Exendin-4, whilst trending towards an increase in basal respiration and ATP production, only reached a significant increase in maximal respiratory versus its own control (~1.3-fold, $p < 0.001$) (**Fig. 6.2C and E-G**). Additionally, it was observed that TBCD WT rescued cells in the presence of Exendin-4, possessed a significantly increased maximal and basal respiration compared to control cells (~1.45-fold, $p < 0.0001$, and ~1.6-fold, $p < 0.0001$ respectively), and maximal respiration compared to TBCD silenced cells (~1.15-fold, $p < 0.001$) (**Fig. 6.2E and F**). Basal respiration, maximal respiration, ATP production and interestingly, non-mitochondrial oxygen consumption were all increased in TBCD A475T rescued cells in the presence of Exendin-4 by approximately 1.25-fold compared to its own untreated control ($p < 0.01$, $p < 0.001$, $p=0.076$, and $p < 0.05$ respectively) (**Fig. 6.2D-I**). Furthermore, TBCD A475T rescued cells incubated with Exendin-4 displayed an increase in all parameters measured, except proton leak, of approximately 2, 1.4, 1.6, 1.3, 1.6, and 1.4-fold against control ($p < 0.0001$), control plus Exendin-4($p < 0.0001$), TBCD silenced($p < 0.0001$), TBCD silenced plus Exendin-4 ($p < 0.0001$), TBCD WT ($p < 0.0001$), and TBCD WT plus Exendin-4 ($p < 0.0001$) respectively (**Fig. 6.2A-I**). Finally, a significantly increased proton leak in control cells plus Exendin-4, TBCD

A475T rescued, and TBCD A475T rescued cells plus Exendin-4 was observed when compared to control cells (~3.4-fold, $p < 0.001$, ~3.2-fold, $p < 0.01$, and ~3.8-fold, $p < 0.0001$ respectively).

In light of these increases in various mitochondrial parameters, an assessment of the protein expression of the mitochondrial marker succinate dehydrogenase complex, subunit A (SDHA) was conducted so as to elucidate whether Exendin-4 was altering mitochondrial function or mass (**Fig. 6.2J and K**). Interestingly, immunoblot analysis revealed that following treatment with Exendin-4, the increased expression of SDHA observed in TBCD A475T was reduced by ~50%, restoring SDHA expression to a level similar to control cells. A similar restoration to control levels was seen in the TBCD silenced, A568V and WT rescued cells in the presence of Exendin-4 (**Fig. 6.2J and K**). Coupling these data with the observed effects in the OCR parameters above, it is attractive to hypothesise that chronic GLP-1R activation is driving the cell towards an increase in glycolysis and consequent flux of substrates into the Krebs cycle.

In order to confirm whether chronic GLP-1R activation was altering glycolytic metabolism tests for Extracellular Flux glycolytic stress, glycolytic rate tests, as well as an assessment of panel of glycolytic proteins via immunoblot assay was conducted (**Figs. 6.3-5**). As shown, TBCD A475T rescued cells displayed an average increase of approximately 1.4-fold in glycolysis, glycolytic capacity and glycolytic reserve when compared to all other groups ($p \leq 0.001$) (**Fig. 6.3A-G**). A significant increase in glycolysis was also observed for TBCD silenced cells compared to control (~1.3-fold, $p < 0.001$) and in glycolytic capacity when compared to TBCD WT rescued cells (~1.3-fold, $p < 0.05$) (**Fig. 6.3A-G**). No significant differences were observed for TBCD WT rescued cells compared to control (**Fig. 6.3A-G**). Reminiscent of data from OCR measurements, control cells and TBCD WT rescued cells pre-conditioned with Exendin-4 trended towards an approximately increase of 10% in glycolysis, glycolytic capacity and glycolytic reserve compared to their own control (**Fig. 6.3A-G**). TBCD silenced and A475T rescued cells pre-conditioned with Exendin-4 however, were observed to increase glycolysis (~5% and ~7% respectively), glycolytic capacity (~14%, $p=0.0543$, and ~15%, $p < 0.001$ respectively), and glycolytic reserve (~22%, and ~21%, $p < 0.05$ respectively) compared to their own untreated controls (**Fig. 6.3A-G**). Additionally, it was determined that TBCD silenced cells in the presence of Exendin-4 possessed a significantly increased rate of glycolysis when comparted to both Exendin-4 un-treated and treated control cells (~1.4-fold, $p < 0.001$, and

~1.25-fold, $p < 0.0001$ respectively). TBCD silenced cells plus Exendin-4 were also observed to have an increased glycolytic capacity compared to both control and TBCD WT rescue cells with or without Exendin-4 (~1.3-fold, $p < 0.0001$, and ~1.2-fold, $p < 0.01$ for both groups and measurements respectively) (**Fig. 6.3E and F**). Furthermore, TBCD A475T rescued cells in the presence of Exendin-4 displayed a significantly increased glycolysis, glycolytic capacity and reserved when compared to either, control, TBCD silenced, or TBCD WT rescued cells with or without Exendin-4 (~1.7 ±0.2-fold, $p < 0.0001$ for all groups and measurements) (**Fig. 6.3A-G**). Of note, it was also observed that in the presence of Exendin-4 all groups trended towards an increase in non-glycolytic acidification compared to their untreated counterparts, although this was most pronounced in the control, TBCD WT and A475T rescued cells (**Fig. 6.3H**).

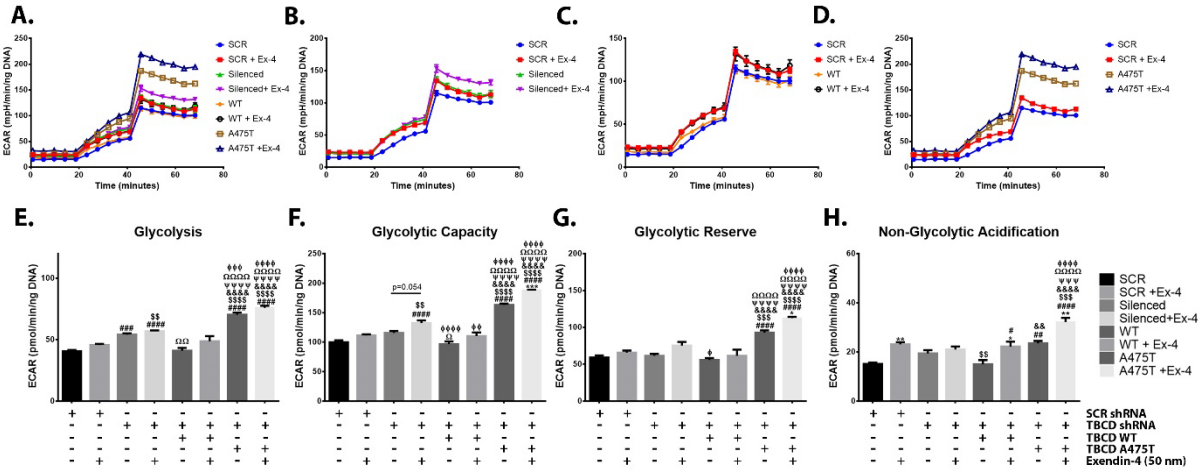

Figure 6.3. GLP-1R signalling enhances bioenergetics despite TBCD perturbations

Glycolytic capacity of the P19 cell line was assessed following transfection and cell sorting as previously outlined. (A-H) Extracellular acidification rate (ECAR) profiles were generated after sequential injection of 25mM glucose and 2µM oligomycin for GFP+ sorted cells. (E) Glycolysis, (F) glycolytic capacity, (G) glycolytic reserve and (H) non-glycolytic acidification were calculated from the ECAR profile as described in the methods section. Data represents mean ± SEM. n ≥ 3 independent experiments. Each point, n=5 technical replicates. * represents pairwise comparisons against own Exendin-4 untreated control. # represents comparisons against scrambled control cells. $ represents comparisons against Exendin-4 treated scrambled control cells. & represents comparisons against WT cells. Ψ represents comparisons against Exendin-4 treated WT cells. Ω represents comparisons against TBCD silenced cells. ϕ represents comparisons against Exendin-4 treated TBCD silenced cells. *P < 0.05, **P < 0.01, ***P < 0.001, ****P < 0.0001. #P < 0.05, ##P < 0.01, ###P < 0.001, ####P < 0.0001. $P <0.05, $$P < 0.01, $$$P < 0.001, $$$$P < 0.0001. &P <0.05, &&P < 0.01, &&&P < 0.001, &&&&P < 0.0001. ΨP <0.05, ΨΨP < 0.01, ΨΨΨP < 0.001, ΨΨΨΨP < 0.0001. ΩP <0.05, ΩΩP < 0.01, ΩΩΩP < 0.001, ΩΩΩΩP < 0.0001. ϕP <0.05, ϕϕP < 0.01, ϕϕϕP < 0.001, ϕϕϕϕP < 0.0001.

To further analyse glycolysis in these treatment groups, the Agilent Glycolytic Rate Assay (Agilent Technologies, USA) was applied to ascertain the contribution of mitochondrial/TCA cycle derived CO_2 extracellular acidification [43, 45, 47, 53-56]. Similar to previous findings,

glycolytic rate measurements obtained from the glycolytic-derived proton efflux rate (PER) profiles showed that when compared to control cells, TBCD A475T rescued cells, and to a lesser extent TBCD silenced and WT rescued cells, had an increase in basal glycolysis (~1.4, $p < 0.05$, ~1.2, and ~1.1-fold respectively) and basal PER (~1.4, $p < 0.05$, ~1.2, and ~1.1-fold respectively) (**Fig. 6.4A-I**). However, it was observed that each of these groups, when compared to control, had an approximate 3% decrease in the % of PER from glycolysis, and 20% increase in acidification from mitochondrial-derived CO_2 (**Fig. 6.4A-I**). Following this, it was found that in the presence of Exendin-4, control-treated cells had an increased basal glycolysis (~1.25-fold), compensatory glycolysis (~1.2-fold, $p < 0.05$), and basal PER (~1.3-fold, $p=0.063$), compared to untreated control (**Fig. 6.4A-I**). Interestingly, it was also observed that control cells treated with Exendin-4 had an approximate 1.3-fold increase in mitOCR/glycoPER, and a 4% decrease in the % of PER derived from glycolysis compared to their untreated control (**Fig. 6.4I**). These changes are suggestive that chronic exposure to Exendin-4 is increasing mitochondrial derived CO_2 acidification. However, coupling these data with the observed Exendin-4 induced increase in maximal mitochondrial respiration, these changes are most likely attributable to GLP-1's ability to increase glycolysis, augmenting the flux of glycolytic derived pyruvate into the Krebs cycle, and consequently to the mitochondrial electron transport [57].

Similar to above, TBCD WT rescued cells treated with Exendin-4 were observed to have an approximately 1.18-fold increase in basal glycolysis and PER, as well as a significant increase in compensatory glycolysis (~1.16-fold, $p < 0.05$) when compared to its untreated control cells (**Fig. 6.4A-I**). No changes in mitoOCR/glycoPER were observed when comparing the presence or absence of Exendin-4 in TBCD WT rescued cells. Additionally, when compared to control cells, TBCD silenced and A475T cells exposed to Exendin-4 displayed a significant increase in basal glycolysis (~1.4-fold, $p < 0.05$, and 1.6-fold, $p < 0.0001$), PER (~1.4-fold, $p < 0.01$, and 1.6-fold, $p < 0.0001$), compensatory glycolysis (~1.4-fold, $p < 0.001$, and 1.6-fold, $p < 0.0001$), and in the percent of PER from glycolysis (~1% and 2% respectively) (**Fig. 6.4A-H**). Furthermore, when compared to their own controls, TBCD silenced and A475T rescued cells in the presence of Exendin-4 possessed an approximate 15% increase in basal glycolysis, basal PER, compensatory glycolysis, a 2% increase in the % of PER from glycolysis, and a decrease of approximately 21% in mitoOCR/glycoPER (**Fig. 6.4 I**). As the Glycolytic Rate Assay test relies

on lactate secretion in order to estimate glycolytic parameters, these data indicate that TBCD silenced and A475T rescued cells in the presence of Exendin-4 have an increased accumulation of glycolytic derived extracellular lactate [52, 58]. Therefore, the increased ECAR and PER measured in the TBCD silenced and A475T rescued cells likely reflects a decreased reliance on mitochondrial OXPHOS and increased rate of glycolysis to meet their energetic demands. In support of this notion, previous observations have shown that GLP-1R signalling enhances glycolytic flux through the transcriptional activation and expression of glycolytic genes via PI3K/mTOR/HIF-1α pathway [58]. Notably, activation of this pathway has been shown to upregulate protein expression of enzymes Hexokinase 1 (HK1), HK2, Pyruvate kinase isozymes 1/2 (PKM1/2), and PKM2 [12, 18, 52, 59]. Thus, I sought to investigate whether GLP-1R signalling was also able to mitigate the perturbed expression of glycolytic enzymes previously observed in TBCD silencing and A475T rescued cells (detailed in chapter 4) [18, 52].

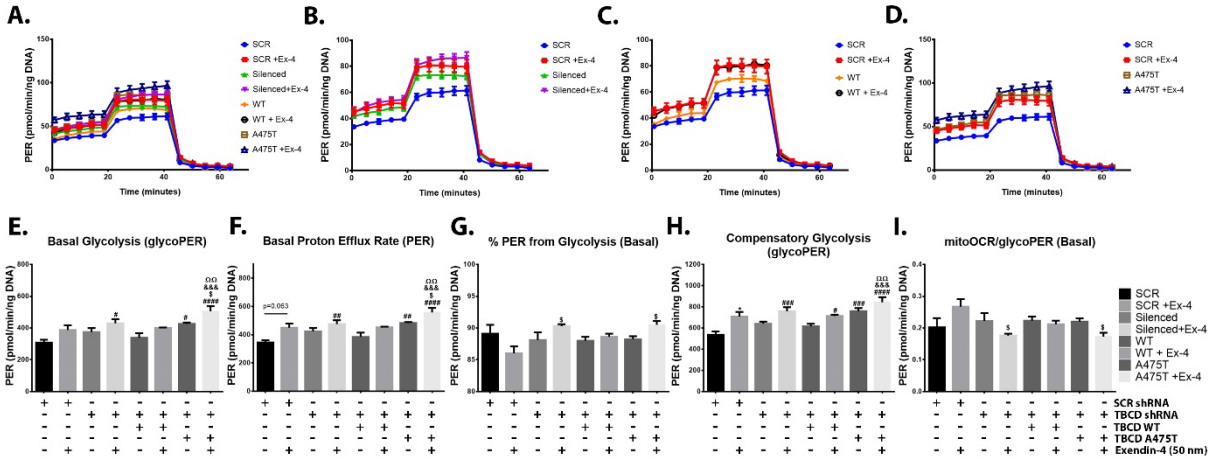

Figure 6.4. GLP-1R signalling enhances glycolytic parameters despite TBCD perturbations

Glycolytic-derived proton efflux rate (PER) profiles of transfected cells were generated following transfection and cell sorting as previously outlined. (A-D) PER profiles were generated after sequential injection of 1 µM each of rotenone and antimycin A and 2-Deoxy-D-glucose (2-DG) (100 mM) and determination of bioenergetics parameters was generated using Agilent Seahorse XF report generator. Calculation of (E) basal glycolysis, (F) basal PER, (G) % of PER from glycolysis, (H) compensatory glycolysis, and (I) the rate of acidification due to mitochondrial metabolism (mitoOCR/glycoPER) from PER profiles. Data represents mean ± SEM. n ≥ 3 independent experiments. Each point, n=5 technical replicates. * represents pairwise comparisons against own Exendin-4 untreated control. # represents comparisons against scrambled control cells. $ represents comparisons against Exendin-4 treated scrambled control cells. & represents comparisons against WT cells. Ψ represents comparisons against Exendin-4 treated WT cells. Ω represents comparisons against TBCD silenced cells. ϕ represents comparisons against Exendin-4 treated TBCD silenced cells. *P < 0.05, **P < 0.01, ***P < 0.001, ****P < 0.0001. #P < 0.05, ##P < 0.01, ###P < 0.001, ####P < 0.0001. $P <0.05, $$P < 0.01, $$$P < 0.001, $$$$P < 0.0001. &P <0.05, &&P < 0.01, &&&P < 0.001, &&&&P < 0.0001. ΨP <0.05, ΨΨP < 0.01, ΨΨΨP < 0.001, ΨΨΨΨP < 0.0001. ΩP <0.05, ΩΩP < 0.01, ΩΩΩP < 0.001, ΩΩΩΩP < 0.0001. ϕP <0.05, ϕϕP < 0.01, ϕϕϕP < 0.001, ϕϕϕϕP < 0.0001.

Validating the previous observations, an increased expression of HK1 and PKM 1/2, paralleled by a decrease in HK2, and PKM2 in TBCD silenced, overexpressed, A475T and A586V rescued groups when compared to control (**Fig. 6.5A and B**). No significant changes were observed in TBCD WT rescued cells compared to control. Chronic exposure of control cells to Exendin-4 however, led to an approximate 1.2-fold increase in the protein expression all glycolytic enzymes, except for PKM1/2, in comparison to its own control (**Fig. 6.5A and B**). Similarly, TBCD WT cells incubated with Exendin-4 displayed an approximate 1.3-fold increased expression of HK2 and PKM2, as well as a 20% decrease in the expression of PKM1/2 and HK1 (**Fig. 6.5A and B**).

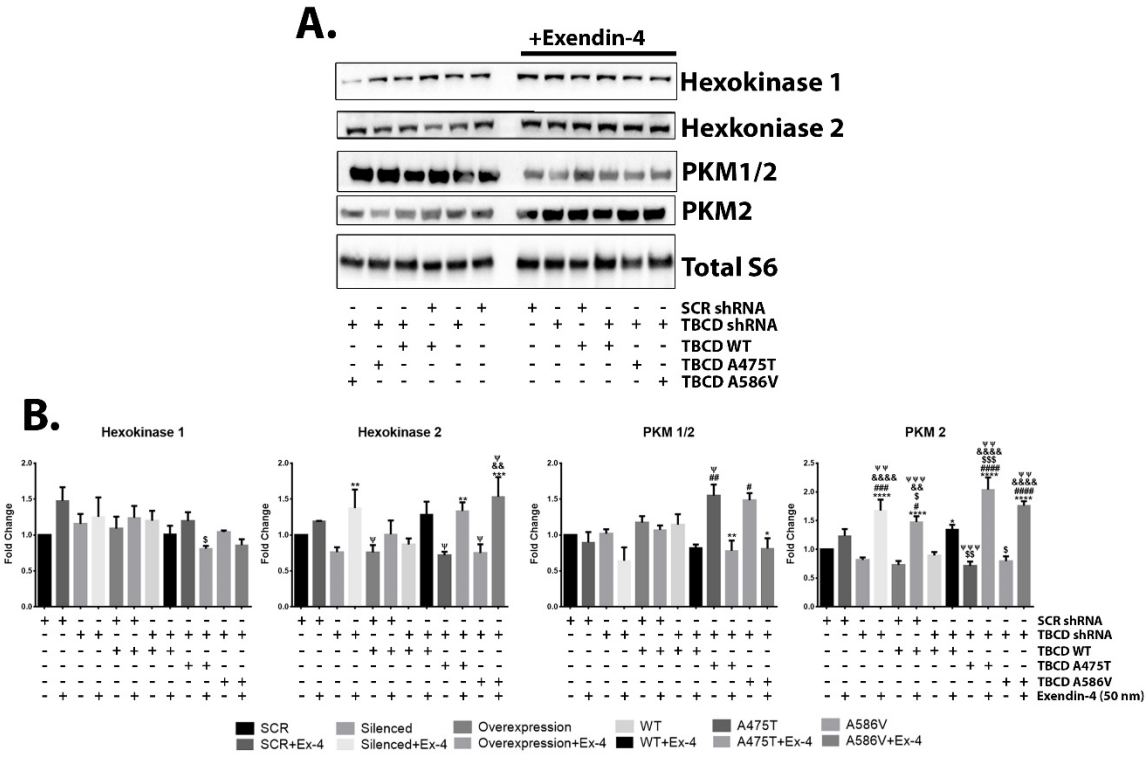

Figure 6.5. Exendin-4 treatment enhances glycolytic enzymes

P19ECs were transfected, treated with or without Ex-4 for 18 h and GFP+ sorted. (A and B) Immunoblot and band densitometry analysis of glycolytic markers Hexokinase 1, Hexokinase 2, Pyruvate kinase isozymes 1/2 (PKM1/2), PKM2. (C and D). Data represents mean ± SEM. n ≥ 3. * represents comparisons of absence or presence of Ex-4 within each shRNA treatment group. *P < 0.05, **P < 0.01, ***P < 0.001, ****P < 0.0001. Data represents mean ± SEM. n ≥ 3. * represents pairwise comparisons against own Exendin-4 untreated control. # represents comparisons against scrambled control cells. $ represents comparisons against Exendin-4 treated scrambled control cells. & represents comparisons against WT cells. Ψ represents comparisons against Exendin-4 treated WT cells. Ω represents comparisons against TBCD silenced cells. $^{\phi}$ represents comparisons against Exendin-4 treated TBCD silenced cells. *P < 0.05, **P < 0.01, ***P < 0.001, ****P < 0.0001. #P < 0.05, ##P < 0.01, ###P < 0.001, ####P < 0.0001. $P <0.05, $$P < 0.01, $$$P < 0.001, $$$$P < 0.0001. &P <0.05, &&P < 0.01, &&&P < 0.001, &&&&P < 0.0001. ΨP <0.05, ΨΨP < 0.01, ΨΨΨP < 0.001, ΨΨΨΨP < 0.0001. ΩP <0.05, ΩΩP < 0.01, ΩΩΩP < 0.001, ΩΩΩΩP < 0.0001. $^{\phi}$P <0.05, $^{\phi\phi}$P < 0.01, $^{\phi\phi\phi}$P < 0.001, $^{\phi\phi\phi\phi}$P < 0.0001.

In TBCD silenced, overexpressed, A475T and A586V rescued cells the presence of Exendin-4 was noted to increase and decrease the expression of PKM2, HK2, and HK1, PKM1/2 respectively, restoring them to a similar level to that of control (**Fig. 6.5A and B**). Whilst these data support previous findings that chronic GLP-1R activation induces the expression of glycolytic enzymes [12, 45, 56, 60], they also provide novel evidence that in TBCD perturbed cells, GLP-1R signalling impacts mitochondrial mass/function, and promoting metabolic reprogramming. Recently, studies have highlighted the importance of the cells metabolic state in cell fate decisions and neuronal reprogramming [18, 52]. Notably, a metabolic switch from aerobic glycolysis to OXPHOS has been demonstrated to be sufficient to lead to the loss of stemness and induction of differentiation. Interestingly, it has also been highlighted that an inverse metabolic switch from OXPHOS to glycolysis is sufficient to promote dedifferentiation [48, 56, 60]. Thus, the expression of neuronal markers associated with cell differentiation, Tuj1 (β-III tubulin), Neuronal Nuclei (NeuN), Forkhead Box G1 (FoxG1), and the pluripotency marker Sex determining region Y-box 2 (Sox2) was investigated. As shown, in the case of TBCD A475T-, as well as A586V-rescued cells, and to a lesser extent TBCD silenced and overexpressed cells, steady-state levels of the pluripotency marker Sox2 were reduced, while signals for neuronal differentiation markers NeuN and FoxG1 increased compared with control (**Fig. 6.6A and B**). Thus, the application of Exendin-4 to the TBCD perturbed cells may elevate Sox2 levels, and decreased the expression of FoxG1, NeuN and Tuj1, restoring the expression of the former three to a similar level to that of control (**Fig. 6.6A and B**). It should be noted however, that in control cells treated with Exendin-4 there was an increase in FoxG1 and NeuN, along with a decrease in Sox2. Coupled with the enhanced mitochondrial metabolism, these data suggest Exendin-4 treatment induces neuronal differentiation, a finding that is reminiscent of the activity of Exendin-4 in other cell types [48-51, 56, 60, 61]. Taken together, these findings suggest that chronic GLP-1R activation in TBCD perturbed cells promotes glycolytic metabolism, cell proliferation and suppresses markers of neuronal differentiation.

GLP-1 activation can lead to a variety of downstream signalling cascades, promoting energy homeostasis/metabolism, proliferation, neurogenesis, and anti-apoptotic/pro-survival properties [20, 22, 62]. Although several studies have proposed a pathway or pathways responsible for these GLP-1 mediated effects in neuronal cells [12], the molecular

mechanisms underpinning GLP-1s mode of action require further elucidation. Recently however, chronic GLP-1R activation has been shown to upregulate the Insulin-Like Growth Factor 1 Receptor (IGF1R) and the Insulin Receptor (INSR). Whilst induction of both these pathways stimulate a downstream signalling cascade impacting cytoskeletal organisation, proliferation, and pro-survival signalling [12, 34, 52], they are not required for the GLP-1R induced metabolic reprogramming [12, 15, 17, 18, 30, 63-65]. Thus, I thus sought to assess whether the restorative effects of chronic Exendin-4 treatment were mediated via either an IGF1R or INSR autocrine loop.

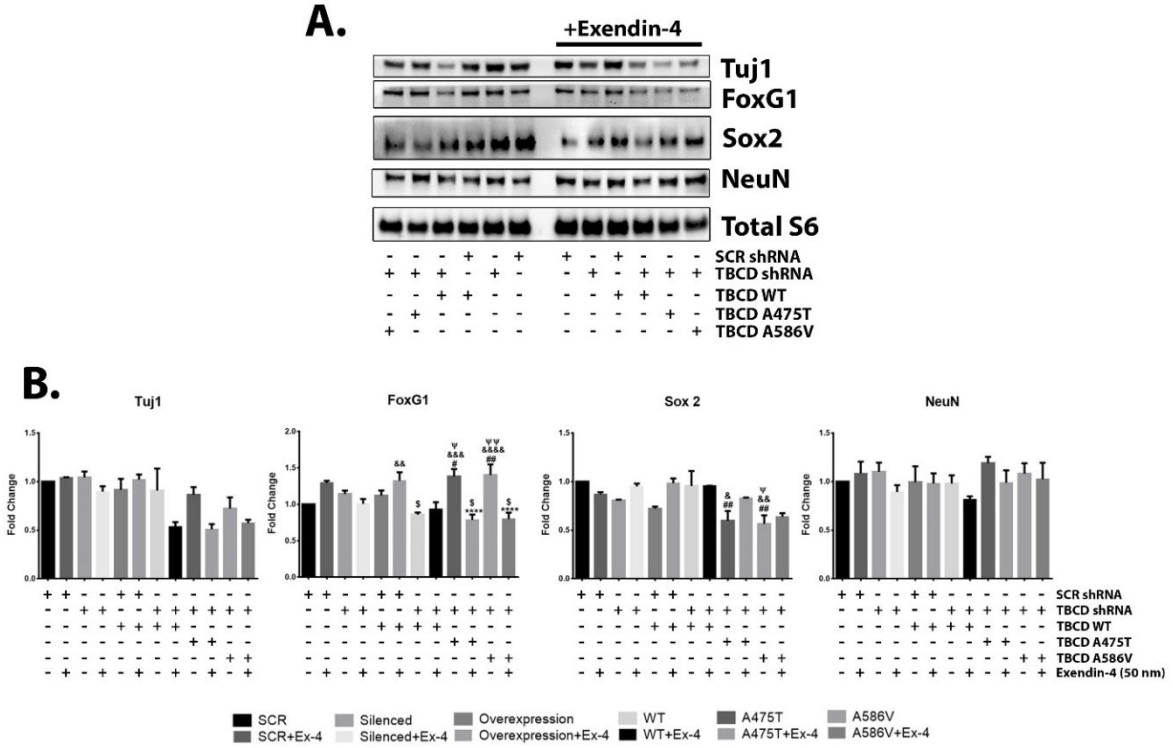

Figure 6.6. Aberrant expression of neuronal markers rescued following Exendin-4 treatment

P19ECs were transfected, treated with or without Ex-4 for 18 h and GFP+ sorted. (A and B). Immunoblot and band densitometry analysis of various differentiation markers, Tuj1 (β-III tubulin), Forkhead Box G1 (FoxG1), Sex determining region Y-box 2 (Sox2), and Neuronal Nuclei (NeuN) in P19ECs transfected cell lysates. Data represents mean ± SEM. n ≥ 3. * represents comparisons of absence or presence of Ex-4 within each shRNA treatment group. *P < 0.05, **P < 0.01, ***P < 0.001, ****P < 0.0001. Data represents mean ± SEM. n ≥ 3 independent experiments. * represents pairwise comparisons against own Exendin-4 untreated control. # represents comparisons against scrambled control cells. $ represents comparisons against Exendin-4 treated scrambled control cells. & represents comparisons against WT cells. Ψ represents comparisons against Exendin-4 treated WT cells. Ω represents comparisons against TBCD silenced cells. $^{\phi}$ represents comparisons against Exendin-4 treated TBCD silenced cells. *P < 0.05, **P < 0.01, ***P < 0.001, ****P < 0.0001. #P < 0.05, ##P < 0.01, ###P < 0.001, ####P < 0.0001. $P <0.05, $$P < 0.01, $$$P < 0.001, $$$$P < 0.0001. &P <0.05, &&P < 0.01, &&&P < 0.001, &&&&P < 0.0001. ΨP <0.05, ΨΨP < 0.01, ΨΨΨP < 0.001, ΨΨΨΨP < 0.0001. ΩP <0.05, ΩΩP < 0.01, ΩΩΩP < 0.001, ΩΩΩΩP < 0.0001. $^{\phi}$P <0.05, $^{\phi\phi}$P < 0.01, $^{\phi\phi\phi}$P < 0.001, $^{\phi\phi\phi\phi}$P < 0.0001.

6.2.4 Loss of IGF1R but not INSR ablates Exendin-4's G2 rescue

To elucidate the molecular mechanisms underlying GLP-1R signalling's restorative abilities, CRISPR-CAS9 was utilised to generate stable IGF1R or an INSR knockout (KO) P19ECs for cell cycle analysis. Initially, single colony sorted cells were assessed for the presence or absence of the IGF1R or INSR. In confirmation, immunoblot analysis revealed a complete ablation of IGF1R protein expression in 3 out of 3 targeted cell groups, whilst INSR protein expression was ablated in 2 out of 3 groups compared to blank and control plasmid sorted cells (**Fig. 6.7A**). Following this, plasmid control, IGF1R and INSR KO cells were subject to TBCD shRNA silencing and rescue experiments, in the presence or absence of 50 nM Exendin-4 for 18 h prior to cell cycle analysis, as previously described. Assessment of cell cycle dynamics by flow cytometry revealed that in all treatments and groups, except the IGF1R KO group, there was a trend towards an increase in the percent of G1 phase cells for Exendin-4 treated cells compared to their own untreated control (**Fig. 6.7B-D**). A significant reduction of approximately 10% for cells in S phase was observed in the plasmid control group for both TBCD silenced and A475T rescued cells in comparison to Exendin-4 treated scrambled control ($p < 0.05$) (**Fig. 6.7E**). However, in the plasmid control group, treatment of TBCD silenced and TBCD A475T rescued cells with Exendin-4 was able to increase percent of cells in S phase(~6%, $p < 0.01$ and 15%, $p < 0.05$ respectively), reaching a similar level to that of control (**Fig. 6.7E**). No differences were observed for any transfection in IGF1R KO cells in the S phase, whilst INSR KO cells displayed a similar profile to that observed in the plasmid control group, with Exendin-4 treatment increasing the percent of S phase cells in TBCD silenced and A475T rescued cells (~1.15-fold for both) (**Fig. 6.7F and G**). A small but non-significant reduction was observed in the INSR KO group, with exposure of control cells to Exendin-4 decreasing the percent of S phase cells by approximately 10% compared to untreated control (**Fig. 6.7E and G**).

Extending these observations, both TBCD silenced and A475T rescued cells increased the percent of cells in G2 compared to control cells in the plasmid control group (~1.7-fold, $p < 0.0001$ and ~1.75-fold, $p < 0.0001$ respectively), IGF1R KO group (~1.15-fold, $p=0.08$ and 1.35-fold, $p < 0.05$ respectively) and INSR KO group (~1.5-fold, $p < 0.0001$ and ~1.7-fold, $p < 0.0001$ (**Fig. 6.7H-J**).

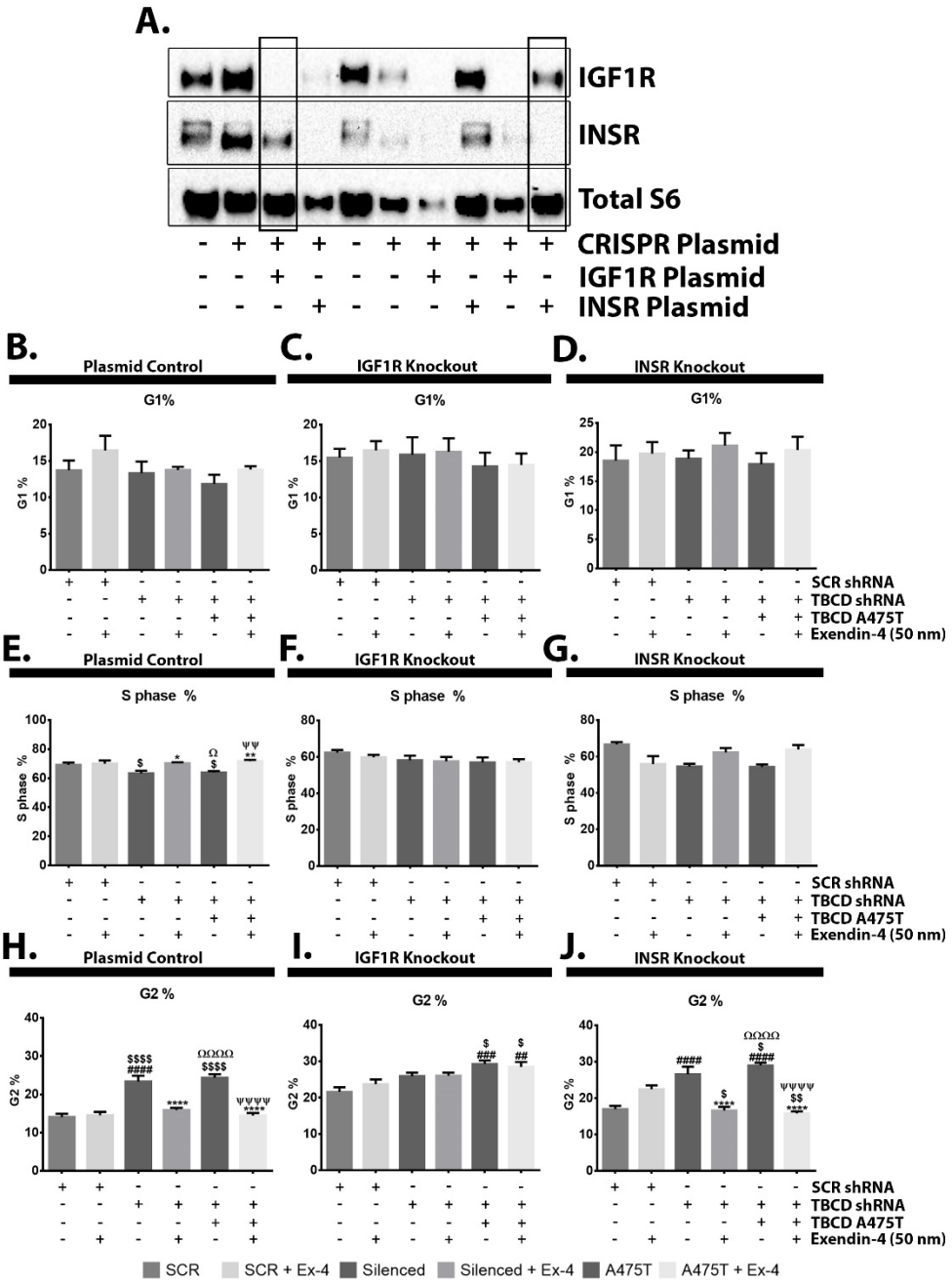

Figure 6.7. Loss of IGF1R but not INSR ablates Exendin-4's G2 rescue

Knockout (KO) of the Insulin-Like Growth Factor 1 Receptor (IGF1R) or Insulin Receptor (INSR) in P19ECs was performed as previously described. (A) Protein expression of IGF1R or INSR P19ECs in comparison to un-transfected and Cas9 Plasmid control, with chosen populations (highlighted by boxes) subject to further analysis. Control, IGF1R and INSR P19ECs were co-transfected, as previously described with shRNA vectors and TBCD expression constructs, as indicated, and incubated for 30 h, followed by addition or not of 50nm Exendin-4 for an additional 18 h. (B-J) Cells were then prepared for cell cycle analysis, by Flow cytometry. (B-D) Percent of cells in G1 phase, (E-G) percent of cells in S phase, (H-J) percent of cells in G2 phase of cell cycle. Data represents mean ± SEM. n ≥ 3 independent experiments. * represents comparisons of absence or presence of Exendin-4 within each shRNA treatment group. # represents comparisons against scrambled cells. $ represents comparison against scrambled cells in the presence of Exendin-4. Ψ represents comparisons against TBCD silenced cells. Ω represent comparisons against TBCD silenced cells in the presence of Exendin-4. *P < 0.05, **P < 0.01, ***P < 0.001, ****P < 0.0001. #P < 0.05, ##P < 0.01, ###P < 0.001. $P < 0.05, $$P < 0.01, $$$P < 0.001. ΨP <0.05, ΨΨP < 0.01, ΨΨΨP < 0.001, ΨΨΨΨP < 0.0001. ΩP <0.05, ΩΩP < 0.01, ΩΩΩP < 0.001, ΩΩΩΩP < 0.0001.

In the plasmid control group the percentage of G2 cells in TBCD silenced and TBCD A475T rescued cells was significantly reduced when treated with Exendin-4 (~30%, $p < 0.0001$, and ~40%, $p < 0.0001$ respectively) being restored to a level similar to scrambled control (**Fig. 6.7H**). This result is consistent with findings form the separate experiments presented in **Figure 6.1**. Similarly, a reduction and restoration of the G2 delay was observed for TBCD silenced and TBCD A475T rescued cells treated with Exendin-4 in the INSR KO group (~40%, $p < 0.0001$ and ~45%, $p < 0.0001$ respectively) (**Fig. 6.7J**). In the IGF1R KO group however, Exendin-4 was unable to rescue the G2 cycle arrest in either TBCD silenced or TBCD A475T rescued cells (**Fig. 6.7I**). Taken together, these data strongly support the notion that the IGF1R autocrine loop is required for the G2 rescue effect of Exendin-4. However, it would be beneficial for future studies to assess the full range of impacts that may occur in Exendin-4 treated IGF1R KO cells.

6.3 Discussion

Neurodegenerative diseases share several pathological features, including but not limited to, chronic inflammation, synaptic loss and failure, reduced neurogenesis, altered energy homeostasis, enhanced free radical production, and cell death [18, 52]. Recently, several studies have reported on a novel severe neurodegenerative condition observed in infants that is attributable to genetic mutations in the gene of the MT biosynthesis enzyme TBCD [66-69]. Through a detailed analysis of the homozygous missense mutations, A475T and A586V, originally identified by Edvardson, Tian and colleagues, [8], and again by Pode-Shakked et al. in 2016 [5], data from this thesis identifies a potential mode of action was identified wherein, the expression of the mutant TBCDs alter cell cycle dynamics and cell metabolism, leading to changes in cell proliferation and cell fate acquisition. Furthermore, this work identifies GLP-1R agonism as a potential therapeutic approach to alleviate the deleterious cellular impact of TBCD mutations.

Expressed throughout the brain, the GLP-1R, once bound by its ligand, undergoes conformational changes leading to the activation of AC, production of cAMP, and subsequent activation of the two main effectors EPAC and PKA [8]. Downstream of PKA and EPAC several signal transduction pathways can be initiated, with both acute and chronic effects resulting

in pro-survival signalling, improved cognitive functioning, augmented energy metabolism, reduced neural tissue inflammation, progenitor cell proliferation and, neurogenesis [12]. Additionally, GLP-1R activation promotes the secretion and expression of IGF-1/2, insulin, and the upregulation of their associated receptors, which ultimately leads to the generation of an autocrine loop [12, 66, 70-73]. These signalling pathways have been shown to interact with the cytoskeleton and its regulatory elements by increasing the stability of tubulin mRNA, increasing MT dynamics, and promoting cytoskeletal reorganisation [17, 18]. Working in concert, these GLP-1R induced signalling pathways can lead to the modulation of ion channel activity, energy metabolism and growth factor signalling, ultimately aiding in homeostatic restoration [19, 27-33, 74-80].

Taking into account the established mechanisms of GLP-1R activation and growth factor signalling, with the observed perturbations arising from the TBCD mutations, it is tantalizing to speculate that chronic GLP-1R activation alleviates the homeostatic imbalance resulting from the clinical TBCD mutations, possibly through the IGF1R/INSR signalling pathway. Data presented herein, provide evidence that chronic exposure to the GLP-1R agonist, Exendin-4, alleviates the cell cycle delay resultant from TBCD perturbations and induces a robust metabolic adaptation in the P19ECs. Furthermore, the restorative effects of Exendin-4 on cell cycle dynamics is dependent is dependent upon IGF1R expression, and not INSR expression.

In the model presented, prolonged GLP-1R activation rescued the G2 cycle arrest observed in TBCD silenced or A475T rescued cells, as well as promoting G1 entry and progression into S phase. Additionally, it was observed that in control cells chronic exposure to Exendin-4 lead to a significant increase of G1 phase cells, paralleled by a decrease in S phase (**Fig. 6.1**). G2 exit, cell cycle re-entry, and G1 progression requires the concerted actions of the cytoskeleton, metabolic machinery, and the cell cycle regulators [12, 18, 81-85]. Initially activated by mitogens and growth factors during cell cycle initiation, the cell cycle regulator cyclin D (cyclin D1, D2, and D3 in mammals) will activate and complex with Cdk4/Cdk6, which are required for G1 progression. CD1 expression then persists until the G1/S transition, following which it is then downregulated during S phase, and if conditions are conducive for proliferation, subsequently upregulated by the Ras/ERK pathway during late G2 for re-entry into G1 [42, 61, 86-88]. Taken together, these results suggest that the Exendin-4 induced G2

cycle rescue is attributable to its intracellular signal transduction cascades accumulating in activation of the Ras/ERK pathway, leading to upregulation of CD1 [87, 89-91].

Although NPCs are primarily glycolytic, they will adapt their mitochondrial activities by increasing the rates of mitochondrial fission and or fusion, in order to meet the energetic demands of the cell [12, 92-95]. This is seen throughout each stage of the cell cycle, with multiple individual mitochondrial organelles spaced throughout the cell in the G2/M phase, which upon re-entry into G1 are observed to partially regain their elongated structure [38, 39, 43, 53]. During the G1-S transition however, mitochondria travel along the MT cytoskeleton in order to form a hyper fused giant tubular network required to stimulate OXPHOS and meet the cells metabolic demands [96-98]. In addition to their role in cell cycle progression, cyclins and Cdks have also been reported to directly regulate the metabolic activity of the cell during cell cycle. Notably, CD1 can inhibit OXPHOS, whilst Cdk1, which is expressed during the G2/M phase, can increase mitochondrial respiration [38, 99, 100]. Due to the G2 rescue observed in this model and GLP-1's pleiotropic effects on bioenergetics, this thesis assessed whether Exendin-4 was able to restore the TBCD induced metabolic perturbations [40, 88, 101].

Using the Seahorse XF flux analyser and immunoblot assay, it was confirmed that prior to treatment with Exendin-4, TBCD perturbed cells possessed an increased OCR, an increased mitochondrial function and mass, a decreased rate of glycolysis, and altered protein expression of glycolytic enzymes (**Figs. 6.2-5**). Following this, it was determined that whilst all cells treated Exendin-4 possessed an enhanced OCR profile and increased ATP levels, in TBCD perturbed cells treated with Exendin-4, the increase in OCR was paralleled by a significantly increased non-mitochondrial oxygen consumption and decreased mitochondrial mass/function (as evidenced by expression of SDHA) (**Fig. 6.2**). This phenotype was accompanied by an increased rate of glycolysis in all groups treated with Exendin-4, although this was most prominent in the TBCD silenced and A475T rescued cells (**Fig. 6.3**). Extending these findings, it was determined through the use of the Agilent Glycolytic Rate assay, that control cells treated with Exendin-4 possessed an increase in mitochondrial derived CO_2 production, and subsequently extracellular acidification, thereby contributing to the observed increase in the rate of glycolysis. However, in TBCD silenced and A475T rescued cells, chronic exposure to Exendin-4 led to a decreased mitochondrial derived CO_2 production

(**Fig. 6.4A and B**). This suggests that in the TBCD silenced and A475T rescued cells, chronic GLP-1R activation is able to increase glycolytic metabolism and is accompanied by a decreased mitochondrial/TCA cycle activity (as evidenced by mitochondrial derived CO_2 production). In support of this notion, previous observations have shown that prolonged exposure to GLP-1R agonists can enhance glycolysis and flux of substrates into the Krebs cycle through the activity of the PI3K/mTOR/HIF-1α axis [12, 38, 54, 101, 102]. Activation of this pathway induces the transcriptional up-regulation of glycolytic genes such as, HK1, HK2, PKM1/2 and PKM2 [18, 52, 59]. In agreement with these findings, in the context of TBCD disruption, as well as TBCD A475T and A586V rescued cells, treatment with Exendin-4 was able to reduce the expression of HK1 and PKM1/2, whilst increasing the expression of HK2 and PKM2, restoring them to a similar level to that of control (**Fig. 6.5**). Findings from both *in vivo* and *in vitro* studies have shown that ESC and NSCs undergoing terminal cell cycle exit and differentiation undergo a metabolic switch from glycolysis to OXPHOS, marked by an increase in mitochondrial morphology and activity. These changes are paralleled by a decreased expression of HK2, an increased expression of HK1, and an isoform shift from PKM2 to PKM1 [18, 52, 59]. Of note, upon mitogenic stimulation PKM2, has been reported to translocate to the nucleus, wherein its phosphorylation of histone H3 leads to the removal of histone deactylase 3 from regulatory DNA sequences, and consequently inducing CD1 expression [42, 45, 48, 55, 56, 61, 103]. Furthermore, PKM2 and ERK1/2 are able to phosphorylate and activate each other, resulting in a positive feedback loop whose sustained activity is necessary for cell proliferation, however this has not been recorded *in vivo* [42, 104, 105]. Interestingly, whilst a metabolic switch from OXPHOS to glycolysis has been demonstrated to be sufficient to lead to the loss of stemness and initiation of differentiation, a metabolic switch from OXPHOS to glycolysis has also been shown to be able to convert differentiated cells to pluripotent stem cells [104-107].

Consistent with a role in influencing cell proliferation versus neurodifferentiation in cultured cells, it was determined that chronic exposure to Exendin-4 reduced the expression of the neuronal differentiation markers Tuj1, FoxG1 and NeuN, whilst increasing the expression of the pluripotency marker Sox2 [51, 61, 108] (**Fig. 6.6**). A key transcription factor that is highly expressed in ESCs and NSCs, Sox2 functions to maintain the self-renewal of cells *in vivo* and *in vitro*, but is downregulated upon differentiation to glial cells and post-mitotic neurons. In

NSCs, reduced expression of Sox2 not only inhibits proliferation and self-renewal, but promotes early cell cycle exit and terminal differentiation [60, 109-112]. Thus, the increased expression of Sox2, coupled with the reduction in Tuj1, NeuN and FoxG1, fit a model whereby Exendin-4 treatment promotes proliferation, and reduces differentiation in TBCD perturbed cells. It is important to note however, that there was also an increase in HK1, HK2, PKM2, FoxG1 and NeuN in Exendin-4 treated control cells, as well as a decreased expression of the pluripotency marker Sox2 (**Figs. 6.5 and 6.6**). Whilst in contrast to the results observed in TBCD silenced, overexpressed, A475T and A586V rescued cells, these divergent results are most likely attributable to GLP-1's ability to promote differentiation and proliferation in a physiological dependent context [110, 111, 113-115]. Taken together, these data demonstrate that in this model, Exendin-4 induces a metabolic switch towards a highly glycolytic phenotype, paralleled by an increased rate of proliferation, and decreased rate of differentiation.

Due to the highly interconnected nature of cell cycle and metabolism it is difficult to identify if the homeostatic restoration of Exendin-4 is resultant from its ability to promote cell cycle progression, its role in bioenergetics reprogramming, or the concerted effects of both [12, 21, 22]. However, several studies have demonstrated GLP-1R stimulation can promote IGF1R and INSR expression and signalling, both of which play important roles in cellular protection, proliferation and differentiation [12, 40, 42, 43, 109, 116]. Furthermore, recent work by the Newsholme lab demonstrated that whilst Exendin-4 can promote expression of IGF1R and INSR, it acts via an IGF1R and INSR independent mechanism to promote bioenergetic reprograming and augmentation of glycolytic pathways [17-19, 63, 77, 117, 118]. Coupled with the data presented herein, these findings offer a potential avenue to elucidate the molecular mechanisms underpinning Exendin-4's beneficial effects. In order to better understand the beneficial effects resultant from Exendin-4 treatment, work in this thesis applied CRIPSR-Cas9 to generate IGF1R and INSR KO cell lines to study the impact of Exendin-4 and TBCD disruptions, on cell cycle dynamics. Consistent with the role of IGF1R and INSR signalling in the regulation of cyclins and cell cycle dynamics [18, 52], it was observed that in the absence of the IGF1R, but not INSR, Exendin-4 was unable to restore the G2 cycle arrest in TBCD silenced and A475T rescued cells (**Fig. 6.7**). This suggests that GLP-1R stimulation requires IGF1R induced signalling, but not INSR, to restore the perturbed TBCD cell cycle

dynamics. Given that GLP-1's bioenergetics effects are independent of the IGF1R autocrine loop, it is attractive to hypothesise that the restoration of cell cycle dynamics is independent of chronic GLP-1R induced bioenergetic reprograming [19, 27, 28, 74, 77, 78, 118]. However, further investigations are necessary before a definitive conclusion can be drawn. Similarly, whether the restorative ability arising from GLP-1R induced IGF1R signalling is due to their mitogenic properties, cytoskeletal interactions, or a combination of both, requires further investigation before a complete mechanistic model can be established. Taken together, these data suggest that GLP-1 analogues may be effective in alleviating the homeostatic perturbations arising from clinically-relevant TBCD mutations, on cell cycle dynamics and respiration.

6.4 References

1. Kapitein, Lukas C. and Casper C. Hoogenraad, *Building the Neuronal Microtubule Cytoskeleton.* Neuron, 2015. **87**(3): p. 492-506.
2. Breuss, M. and D.A. Keays, *Microtubules and neurodevelopmental disease: the movers and the makers.* Adv Exp Med Biol, 2014. **800**: p. 75-96.
3. Ayala, R., T. Shu, and L.-H. Tsai, *Trekking across the brain: the journey of neuronal migration.* Cell, 2007. **128**(1): p. 29-43.
4. Amos, L.A. and D. Schlieper, *Microtubules and maps.* Advances in protein chemistry, 2005. **71**: p. 257-298.
5. Pode-Shakked, B., et al., *Microcephaly, intractable seizures and developmental delay caused by biallelic variants in TBCD: Further delineation of a new chaperone-mediated tubulinopathy.* Clinical genetics, 2016.
6. Miyake, N., et al., *Biallelic TBCD mutations cause early-onset neurodegenerative encephalopathy.* The American Journal of Human Genetics, 2016. **99**(4): p. 950-961.
7. Flex, E., et al., *Biallelic Mutations in TBCD, Encoding the Tubulin Folding Cofactor D, Perturb Microtubule Dynamics and Cause Early-Onset Encephalopathy.* The American Journal of Human Genetics, 2016. **99**(4): p. 962-973.
8. Edvardson, S., et al., *Infantile neurodegenerative disorder associated with mutations in TBCD, an essential gene in the tubulin heterodimer assembly pathway.* Human Molecular Genetics, 2016. **25**(21): p. 4635-4648.
9. Lundin, V.F., M.R. Leroux, and P.C. Stirling, *Quality control of cytoskeletal proteins and human disease.* Trends in biochemical sciences, 2010. **35**(5): p. 288-297.
10. Jaglin, X.H. and J. Chelly, *Tubulin-related cortical dysgeneses: microtubule dysfunction underlying neuronal migration defects.* Trends Genet, 2009. **25**(12): p. 555-66.
11. Fanarraga, M.L., et al., *TBCD links centriologenesis, spindle microtubule dynamics, and midbody abscission in human cells.* PLoS One, 2010. **5**(1): p. e8846.
12. Rowlands, J., et al., *Pleiotropic Effects of GLP-1 and Analogs on Cell Signaling, Metabolism, and Function.* Frontiers in Endocrinology, 2018. **9**(672).

13. Portha, B., C. Tourrel-Cuzin, and J. Movassat, *Activation of the GLP-1 receptor signalling pathway: a relevant strategy to repair a deficient beta-cell mass.* Exp Diabetes Res, 2011. **2011**: p. 376509.
14. Li, Y., et al., *GLP-1 receptor stimulation preserves primary cortical and dopaminergic neurons in cellular and rodent models of stroke and Parkinsonism.* Proc Natl Acad Sci U S A, 2009. **106**(4): p. 1285-90.
15. Candeias, E., et al., *Brain GLP-1/IGF-1 Signaling and Autophagy Mediate Exendin-4 Protection Against Apoptosis in Type 2 Diabetic Rats.* Molecular Neurobiology, 2017.
16. Fletcher, Madeleine M., et al., *The complexity of signalling mediated by the glucagon-like peptide-1 receptor.* Biochemical Society Transactions, 2016. **44**(2): p. 582-588.
17. Cornu, M., et al., *Glucagon-like peptide-1 increases beta-cell glucose competence and proliferation by translational induction of insulin-like growth factor-1 receptor expression.* J Biol Chem, 2010. **285**(14): p. 10538-45.
18. Rowlands, J., et al., *Insulin and IGF-1 receptor autocrine loops are not required for Exendin-4 induced changes to pancreatic β-cell bioenergetic parameters and metabolism in BRIN-BD11 cells.* Peptides, 2018. **100**: p. 140-149.
19. Bassil, F., et al., *Insulin, IGF-1 and GLP-1 signaling in neurodegenerative disorders: targets for disease modification?* Progress in neurobiology, 2014. **118**: p. 1-18.
20. Li, H., et al., *Chronic treatment of exendin-4 affects cell proliferation and neuroblast differentiation in the adult mouse hippocampal dentate gyrus.* Neurosci Lett, 2010. **486**(1): p. 38-42.
21. Li, H., et al., *Chronic treatment of exendin-4 affects cell proliferation and neuroblast differentiation in the adult mouse hippocampal dentate gyrus.* Neuroscience letters, 2010. **486**(1): p. 38-42.
22. Parthsarathy, V. and C. Hölscher, *Chronic treatment with the GLP1 analogue liraglutide increases cell proliferation and differentiation into neurons in an AD mouse model.* PloS one, 2013. **8**(3): p. e58784.
23. Grieco, M., et al., *Glucagon-like peptide-1: a focus on neurodegenerative diseases.* Frontiers in neuroscience, 2019. **13**: p. 1112.
24. During, M.J., et al., *Glucagon-like peptide-1 receptor is involved in learning and neuroprotection.* Nature medicine, 2003. **9**(9): p. 1173.
25. Bae, C.S. and J. Song, *The Role of Glucagon-Like Peptide 1 (GLP1) in Type 3 Diabetes: GLP-1 Controls Insulin Resistance, Neuroinflammation and Neurogenesis in the Brain.* International Journal of Molecular Sciences, 2017. **18**(11): p. 2493.
26. Athauda, D. and T. Foltynie, *The glucagon-like peptide 1 (GLP) receptor as a therapeutic target in Parkinson's disease: mechanisms of action.* Drug Discovery Today, 2016. **21**(5): p. 802-818.
27. Mill, J.F., M.V. Chao, and D.N. Ishii, *Insulin, insulin-like growth factor II, and nerve growth factor effects on tubulin mRNA levels and neurite formation.* Proceedings of the National Academy of Sciences, 1985. **82**(20): p. 7126-7130.
28. Fernyhough, P., et al., *Stabilization of tubulin mRNAs by insulin and insulin-like growth factor I during neurite formation.* Molecular Brain Research, 1989. **6**(2-3): p. 109-120.
29. Lara-Diaz, V., et al., *IGF-1 modulates gene expression of proteins involved in inflammation, cytoskeleton, and liver architecture.* Journal of physiology and biochemistry, 2017. **73**(2): p. 245-258.
30. Brooker, G.J., et al., *Endogenous IGF-1 regulates the neuronal differentiation of adult stem cells.* Journal of neuroscience research, 2000. **59**(3): p. 332-341.
31. Fellows, A.D., et al., *IGF 1R regulates retrograde axonal transport of signalling endosomes in motor neurons.* EMBO reports, 2020. **21**(3): p. e49129.
32. Gasic, I., S.A. Boswell, and T.J. Mitchison, *Tubulin mRNA stability is sensitive to change in microtubule dynamics caused by multiple physiological and toxic cues.* PLoS biology, 2019. **17**(4): p. e3000225.

33. Chen, J., et al., *Liraglutide activates autophagy via GLP-1R to improve functional recovery after spinal cord injury.* Oncotarget, 2017. **8**(49): p. 85949.
34. Sisley, S., et al., *Neuronal GLP1R mediates liraglutide's anorectic but not glucose-lowering effect.* The Journal of clinical investigation, 2014. **124**(6): p. 2456-2463.
35. McGovern, S.F., K. Hunter, and C. Hölscher, *Effects of the glucagon-like polypeptide-1 analogue (Val8) GLP-1 on learning, progenitor cell proliferation and neurogenesis in the C57B/16 mouse brain.* Brain research, 2012. **1473**: p. 204-213.
36. Li, Y., et al., *GLP-1 receptor stimulation preserves primary cortical and dopaminergic neurons in cellular and rodent models of stroke and Parkinsonism.* Proceedings of the National Academy of Sciences, 2009. **106**(4): p. 1285-1290.
37. Bartolák-Suki, E., et al., *Regulation of mitochondrial structure and dynamics by the cytoskeleton and mechanical factors.* International journal of molecular sciences, 2017. **18**(8): p. 1812.
38. Liu, X., et al., *Mitochondrial 'kiss-and-run': interplay between mitochondrial motility and fusion–fission dynamics.* The EMBO journal, 2009. **28**(20): p. 3074-3089.
39. Moore, A.S. and E.L. Holzbaur, *Mitochondrial-cytoskeletal interactions: dynamic associations that facilitate network function and remodeling.* Current opinion in physiology, 2018. **3**: p. 94-100.
40. Salazar-Roa, M. and M. Malumbres, *Fueling the Cell Division Cycle.* Trends Cell Biol, 2017. **27**(1): p. 69-81.
41. Syred, H.M., et al., *Cell cycle regulation of microtubule interactomes: multi-layered regulation is critical for the interphase/mitosis transition.* Molecular & Cellular Proteomics, 2013. **12**(11): p. 3135-3147.
42. Kalucka, J., et al., *Metabolic control of the cell cycle.* Cell cycle (Georgetown, Tex.), 2015. **14**(21): p. 3379-3388.
43. Lopez-Mejia, I.C. and L. Fajas, *Cell cycle regulation of mitochondrial function.* Current opinion in cell biology, 2015. **33**: p. 19-25.
44. Khacho, M., et al., *Mitochondrial Dynamics Impacts Stem Cell Identity and Fate Decisions by Regulating a Nuclear Transcriptional Program.* Cell Stem Cell, 2016. **19**(2): p. 232-247.
45. Vega-Naredo, I., et al., *Mitochondrial metabolism directs stemness and differentiation in P19 embryonal carcinoma stem cells.* Cell Death & Differentiation, 2014. **21**(10): p. 1560-1574.
46. Khacho, M., et al., *Mitochondrial dysfunction underlies cognitive defects as a result of neural stem cell depletion and impaired neurogenesis.* Human molecular genetics, 2017. **26**(17): p. 3327-3341.
47. Khacho, M., et al., *Mitochondrial dynamics impacts stem cell identity and fate decisions by regulating a nuclear transcriptional program.* Cell stem cell, 2016. **19**(2): p. 232-247.
48. Cliff, T.S. and S. Dalton, *Metabolic switching and cell fate decisions: implications for pluripotency, reprogramming and development.* Current opinion in genetics & development, 2017. **46**: p. 44-49.
49. Gascón, S., et al., *Identification and successful negotiation of a metabolic checkpoint in direct neuronal reprogramming.* Cell stem cell, 2016. **18**(3): p. 396-409.
50. Gascón, S., et al., *Direct neuronal reprogramming: achievements, hurdles, and new roads to success.* Cell stem cell, 2017. **21**(1): p. 18-34.
51. Folmes, C.D., et al., *Somatic oxidative bioenergetics transitions into pluripotency-dependent glycolysis to facilitate nuclear reprogramming.* Cell metabolism, 2011. **14**(2): p. 264-271.
52. Carlessi, R., et al., *GLP-1 receptor signalling promotes beta-cell glucose metabolism via mTOR-dependent HIF-1alpha activation.* Sci Rep, 2017. **7**(1): p. 2661.
53. Lee, S., et al., *Cell cycle-dependent mitochondrial biogenesis and dynamics in mammalian cells.* Biochemical and biophysical research communications, 2007. **357**(1): p. 111-117.
54. Horbay, R. and R. Bilyy, *Mitochondrial dynamics during cell cycling.* Apoptosis, 2016. **21**(12): p. 1327-1335.

55. Beckervordersandforth, R., et al., *Role of mitochondrial metabolism in the control of early lineage progression and aging phenotypes in adult hippocampal neurogenesis.* Neuron, 2017. **93**(3): p. 560-573. e6.
56. Agostini, M., et al., *Metabolic reprogramming during neuronal differentiation.* Cell death and differentiation, 2016. **23**(9): p. 1502-1514.
57. Carlessi, R., et al., *Glutamine deprivation induces metabolic adaptations associated with beta cell dysfunction and exacerbate lipotoxicity.* Molecular and cellular endocrinology, 2019. **491**: p. 110433.
58. TeSlaa, T. and M.A. Teitell, *Techniques to Monitor Glycolysis.* Methods in enzymology, 2014. **542**: p. 91-114.
59. Van de Velde, S., M.F. Hogan, and M. Montminy, *mTOR links incretin signaling to HIF induction in pancreatic beta cells.* Proc Natl Acad Sci U S A, 2011. **108**(41): p. 16876-82.
60. Zheng, X., et al., *Metabolic reprogramming during neuronal differentiation from aerobic glycolysis to neuronal oxidative phosphorylation.* eLife, 2016. **5**: p. e13374.
61. Ito, K. and T. Suda, *Metabolic requirements for the maintenance of self-renewing stem cells.* Nature reviews Molecular cell biology, 2014. **15**(4): p. 243-256.
62. Drucker, D.J., *Glucagon-like peptides: regulators of cell proliferation, differentiation, and apoptosis.* Molecular endocrinology, 2003. **17**(2): p. 161-171.
63. Cornu, M., et al., *Glucagon-like peptide-1 protects beta-cells against apoptosis by increasing the activity of an IGF-2/IGF-1 receptor autocrine loop.* Diabetes, 2009. **58**(8): p. 1816-25.
64. Modi, H., M. Cornu, and B. Thorens, *Glutamine Stimulates Biosynthesis and Secretion of Insulin-like Growth Factor 2 (IGF2), an Autocrine Regulator of Beta Cell Mass and Function.* The Journal of Biological Chemistry, 2014. **289**(46): p. 31972-31982.
65. Poulain, F.E. and A. Sobel, *The microtubule network and neuronal morphogenesis: Dynamic and coordinated orchestration through multiple players.* Molecular and Cellular Neuroscience, 2010. **43**(1): p. 15-32.
66. Hölscher, C., *Potential role of glucagon-like peptide-1 (GLP-1) in neuroprotection.* CNS drugs, 2012. **26**(10): p. 871-882.
67. Ziabreva, I., et al., *Altered neurogenesis in Alzheimer's disease.* Journal of psychosomatic research, 2006. **61**(3): p. 311-316.
68. Holmes, C., et al., *Proinflammatory cytokines, sickness behavior, and Alzheimer disease.* Neurology, 2011. **77**(3): p. 212-218.
69. Chen, S.-Y., et al., *Sequence variants of interleukin 6 (IL-6) are significantly associated with a decreased risk of late-onset Alzheimer's disease.* Journal of neuroinflammation, 2012. **9**(1): p. 21.
70. Katsurada, K. and T. Yada, *Neural effects of gut- and brain-derived glucagon-like peptide-1 and its receptor agonist.* J Diabetes Investig, 2016. **7 Suppl 1**: p. 64-9.
71. Holt, M.K. and S. Trapp, *The physiological role of the brain GLP-1 system in stress.* Cogent Biology, 2016. **2**(1): p. 1229086.
72. Hölscher, C., *Central effects of GLP-1: new opportunities for treatments of neurodegenerative diseases.* Journal of Endocrinology, 2014. **221**(1): p. T31-T41.
73. Holscher, C., *The role of GLP-1 in neuronal activity and neurodegeneration.* Vitam Horm, 2010. **84**: p. 331-54.
74. Kadowaki, T., et al., *Insulin-like growth factors, insulin, and epidermal growth factor cause rapid cytoskeletal reorganization in KB cells. Clarification of the roles of type I insulin-like growth factor receptors and insulin receptors.* Journal of Biological Chemistry, 1986. **261**(34): p. 16141-16147.
75. Hakuno, F. and S.-I. Takahashi, *40 years of IGF1: IGF1 receptor signaling pathways.* Journal of molecular endocrinology, 2018. **61**(1): p. T69-T86.

76. Cahill, A.L. and R.L. Perlman, *Activation of a Microtubule-Associated Protein-2 Kinase by Insulin-Like Growth Factor-I in Bovine Chromaffin Cells.* Journal of neurochemistry, 1991. **57**(6): p. 1832-1839.
77. Duenas, M., et al., *Interaction of insulin-like growth factor-I and estradiol signaling pathways on hypothalamic neuronal differentiation.* Neuroscience, 1996. **74**(2): p. 531-539.
78. Chesik, D., N. Wilczak, and J. De Keyser, *Insulin-like growth factor binding protein-4 interacts with centrosomes and microtubules in primary astrocytes.* Neuroscience, 2004. **125**(2): p. 381-390.
79. Roscioni, S.S., C.R. Elzinga, and M. Schmidt, *Epac: effectors and biological functions.* Naunyn-Schmiedeberg's archives of pharmacology, 2008. **377**(4-6): p. 345-357.
80. Luciani, P., et al., *Differentiating effects of the glucagon-like peptide-1 analogue exendin-4 in a human neuronal cell model.* Cellular and molecular life sciences, 2010. **67**(21): p. 3711-3723.
81. Gekel, I. and E. Neher, *Application of an Epac activator enhances neurotransmitter release at excitatory central synapses.* Journal of Neuroscience, 2008. **28**(32): p. 7991-8002.
82. Zhong, N. and R.S. Zucker, *cAMP acts on exchange protein activated by cAMP/cAMP-regulated guanine nucleotide exchange protein to regulate transmitter release at the crayfish neuromuscular junction.* Journal of Neuroscience, 2005. **25**(1): p. 208-214.
83. Sakaba, T. and E. Neher, *Direct modulation of synaptic vesicle priming by GABA B receptor activation at a glutamatergic synapse.* Nature, 2003. **424**(6950): p. 775-778.
84. Laurent, A.-C., et al., *Role of Epac in brain and heart*. 2012, Portland Press Ltd.
85. Ster, J., et al., *Exchange protein activated by cAMP (Epac) mediates cAMP activation of p38 MAPK and modulation of Ca2+-dependent K+ channels in cerebellar neurons.* Proceedings of the National Academy of Sciences, 2007. **104**(7): p. 2519-2524.
86. Malumbres, M., *Cyclin-dependent kinases.* Genome biology, 2014. **15**(6): p. 1-10.
87. Stacey, D.W., *Cyclin D1 serves as a cell cycle regulatory switch in actively proliferating cells.* Current Opinion in Cell Biology, 2003. **15**(2): p. 158-163.
88. Wang, Z., et al., *Cyclin B1/Cdk1 coordinates mitochondrial respiration for cell-cycle G2/M progression.* Developmental cell, 2014. **29**(2): p. 217-232.
89. Hitomi, M. and D.W. Stacey, *Ras-dependent cell cycle commitment during G2 phase.* FEBS Letters, 2001. **490**(3): p. 123-131.
90. Lange, C., W.B. Huttner, and F. Calegari, *Cdk4/cyclinD1 overexpression in neural stem cells shortens G1, delays neurogenesis, and promotes the generation and expansion of basal progenitors.* Cell stem cell, 2009. **5**(3): p. 320-331.
91. Yang, K., M. Hitomi, and D.W. Stacey, *Variations in cyclin D1 levels through the cell cycle determine the proliferative fate of a cell.* Cell division, 2006. **1**(1): p. 32.
92. Chambard, J.-C., et al., *ERK implication in cell cycle regulation.* Biochimica et Biophysica Acta (BBA) - Molecular Cell Research, 2007. **1773**(8): p. 1299-1310.
93. Costes, S., et al., *ERK1/2 control phosphorylation and protein level of cAMP-responsive element-binding protein: a key role in glucose-mediated pancreatic beta-cell survival.* Diabetes, 2006. **55**(8): p. 2220-30.
94. Liu, X., et al., *Extracellular signal-regulated Kinases (ERKs) phosphorylate Lin28a protein to modulate P19 cell proliferation and differentiation.* Journal of Biological Chemistry, 2017. **292**(10): p. 3970-3976.
95. Quoyer, J., et al., *GLP-1 mediates antiapoptotic effect by phosphorylating Bad through a beta-arrestin 1-mediated ERK1/2 activation in pancreatic beta-cells.* J Biol Chem, 2010. **285**(3): p. 1989-2002.
96. Lawrence, E.J. and C.A. Mandato, *Mitochondria localize to the cleavage furrow in mammalian cytokinesis.* PLoS One, 2013. **8**(8): p. e72886.
97. Sauer, H., M. Wartenberg, and J. Hescheler, *Reactive oxygen species as intracellular messengers during cell growth and differentiation.* Cellular physiology and biochemistry, 2001. **11**(4): p. 173-186.

98. Katajisto, P., et al., *Asymmetric apportioning of aged mitochondria between daughter cells is required for stemness.* Science, 2015. **348**(6232): p. 340-343.
99. Garone, C., et al., *Mitochondrial dynamics: overview of molecular mechanisms.* Essays in biochemistry, 2018. **62**(3): p. 341-360.
100. Westermann, B., *Bioenergetic role of mitochondrial fusion and fission.* Biochimica et Biophysica Acta (BBA)-Bioenergetics, 2012. **1817**(10): p. 1833-1838.
101. Hydbring, P., M. Malumbres, and P. Sicinski, *Non-canonical functions of cell cycle cyclins and cyclin-dependent kinases.* Nature reviews Molecular cell biology, 2016. **17**(5): p. 280-292.
102. Bienvenu, F., et al., *Transcriptional role of cyclin D1 in development revealed by a genetic–proteomic screen.* Nature, 2010. **463**(7279): p. 374-378.
103. Knobloch, M. and S. Jessberger, *Metabolism and neurogenesis.* Current opinion in neurobiology, 2017. **42**: p. 45-52.
104. Keller, K.E., et al., *SAICAR induces protein kinase activity of PKM2 that is necessary for sustained proliferative signaling of cancer cells.* Molecular cell, 2014. **53**(5): p. 700-709.
105. Mazurek, S., *Pyruvate kinase type M2: a key regulator of the metabolic budget system in tumor cells.* The international journal of biochemistry & cell biology, 2011. **43**(7): p. 969-980.
106. Lv, L., et al., *Mitogenic and oncogenic stimulation of K433 acetylation promotes PKM2 protein kinase activity and nuclear localization.* Molecular cell, 2013. **52**(3): p. 340-352.
107. Yang, W., et al., *PKM2 phosphorylates histone H3 and promotes gene transcription and tumorigenesis.* Cell, 2012. **150**(4): p. 685-696.
108. Shyh-Chang, N., et al., *Influence of threonine metabolism on S-adenosylmethionine and histone methylation.* Science, 2013. **339**(6116): p. 222-226.
109. Ruijtenberg, S. and S. van den Heuvel, *Coordinating cell proliferation and differentiation: Antagonism between cell cycle regulators and cell type-specific gene expression.* Cell cycle, 2016. **15**(2): p. 196-212.
110. Bani-Yaghoub, M., et al., *Role of Sox2 in the development of the mouse neocortex.* Developmental biology, 2006. **295**(1): p. 52-66.
111. Sikorska, M., et al., *Epigenetic modifications of SOX2 enhancers, SRR1 and SRR2, correlate with in vitro neural differentiation.* Journal of neuroscience research, 2008. **86**(8): p. 1680-1693.
112. Florio, M. and W.B. Huttner, *Neural progenitors, neurogenesis and the evolution of the neocortex.* Development, 2014. **141**(11): p. 2182-2194.
113. Ferri, A.L., et al., *Sox2 deficiency causes neurodegeneration and impaired neurogenesis in the adult mouse brain.* Development, 2004. **131**(15): p. 3805-3819.
114. Hutton, S.R. and L.H. Pevny, *SOX2 expression levels distinguish between neural progenitor populations of the developing dorsal telencephalon.* Developmental biology, 2011. **352**(1): p. 40-47.
115. Zhang, S. and W. Cui, *Sox2, a key factor in the regulation of pluripotency and neural differentiation.* World Journal of Stem Cells, 2014. **6**(3): p. 305-311.
116. Hardwick, L.J.A., et al., *Cell cycle regulation of proliferation versus differentiation in the central nervous system.* Cell and Tissue Research, 2015. **359**: p. 187-200.
117. Peyot, M.L., et al., *Glucagon-like peptide-1 induced signaling and insulin secretion do not drive fuel and energy metabolism in primary rodent pancreatic beta-cells.* PLoS One, 2009. **4**(7): p. e6221.
118. Lewitt, M.S. and G.W. Boyd, *The Role of Insulin-Like Growth Factors and Insulin-Like Growth Factor–Binding Proteins in the Nervous System.* Biochemistry insights, 2019. **12**: p. 1178626419842176.

Chapter 7 Conclusion

The microtubule (MT) cytoskeleton is an essential element of the neuronal cytoskeleton, as it is highly dynamic and adaptive, in order to meet various cellular needs. In addition to its role in cell signalling, mitochondrial dynamics, and thus metabolism, the MT cytoskeleton is required for the segregation of chromosomes, organelles, orientation of the mitotic spindle, and plane of orientation [1-7]. A precise equilibrium of these processes is required for appropriate nervous system development, and their functions are underpinned by the efficient production of MTs by biosynthetic machinery, including co-factors such as TBCD. Perturbations to MTs and their biosynthetic machinery can lead to a plethora of cortical malformations [3, 8-14]. This has been evidenced most recently with several studies reporting *TBCD* mutations that cause a severe neuronal infantile neurodegenerative disorder [15-18]. Recognised as early as 1992 [19-23], TBCD has since been reported to play roles in cell cycle, mitosis and metabolism [3, 6, 11, 23-32]. In this thesis, a detailed analysis of TBCD and its disease-associated missense variants and the underlying molecular mechanisms responsible for neuronal development and homeostasis was undertaken.

With the rationale that TBCD processes impact MT dynamics, and that MT dynamics are crucial for cell cycle dynamics and proliferation [4, 6, 26, 33-38], this thesis has established that disruptions to TBCD expression levels, and or its structure/function *in vitro*, impede cell cycle progression, with cells accumulating in a G2 cycle arrest. These cell cycle perturbations were paralleled by an augmented mitochondrial metabolism, mitochondrial mass/function, and ROS presence, as well as an altered glycolytic metabolism, which is reminiscent of a more differentiated neuronal phenotype [39-44]. Consistent with this, cells expressing the disease-associated TBCD missense variants A475T and A586V, and to a lesser extent TBCD silenced and overexpressed cells, displayed hallmarks of an increased expression of differentiation markers, as well as a decreased expression of proliferation and pluripotency markers. Recent reports that metabolism can direct stemness and differentiation *in vitro* and *in vivo* [40-45], and that cell cycle is strongly linked to cell fate and lineage commitment [46-51], support these novel findings and provide evidence for the notion that the altered cell cycle dynamics and metabolic state of TBCD perturbed P19ECs are acting in concert to direct cell fate and stemness (**Fig. 7.1**).

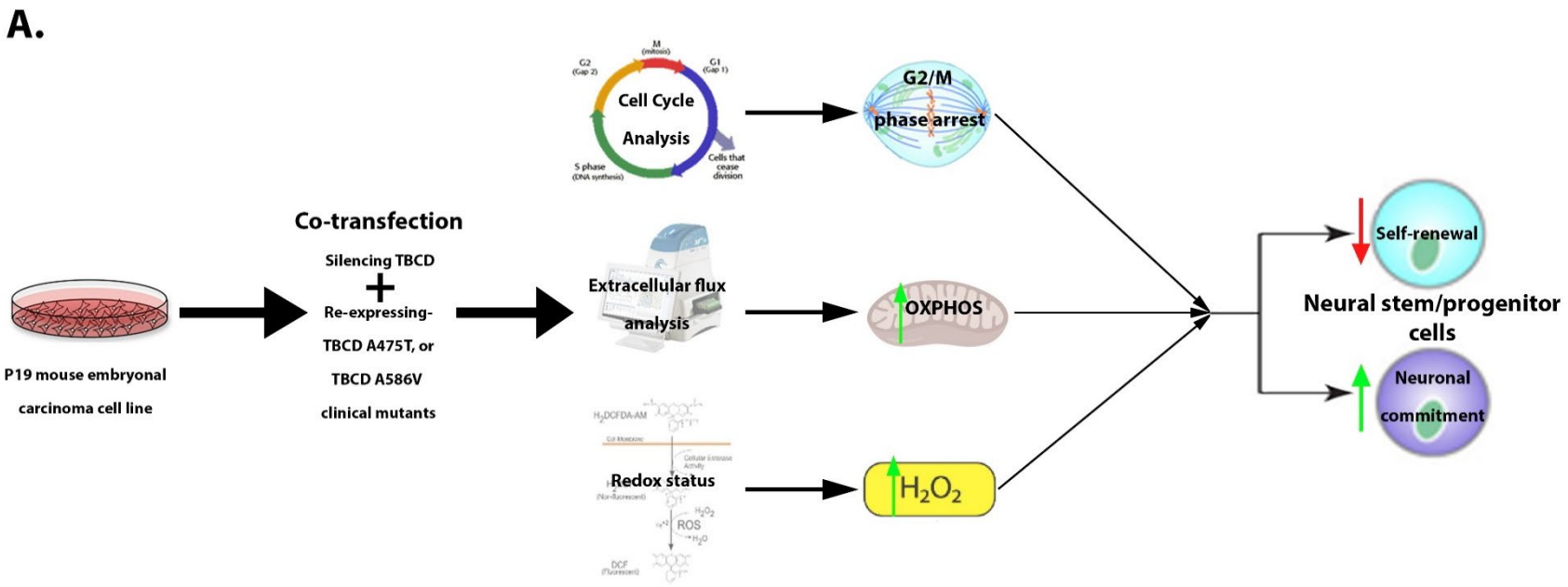

Figure 7.1. TBCD mutations mice alter NPC proliferation and metabolism impacting cell fate

Schematic diagram outlining experimental procedures and a summary of findings. (A) P19 embryonic carcinoma cells co-incubated with shRNA silencing TBCD, and a mammalian expression vector for either of the clinically-relevant mutants TBCD A475T, or TBCD A586V. Cells were subject to cell cycle analysis, extracellular flux analysis, and redox status tests, which revealed that the presence of these mutants lead to a G2/M phase arrest, increased oxidative phosphorylation (OXPHOS), and an increase in reactive oxygen species (ROS, AKA H_2O_2). These changes to metabolism, cell cycle and redox status resulted in a decrease in proliferative divisions, or self-renewal, and an increase in cell fate and neuronal lineage commitment.

Given the *in vitro* findings for TBCD in neural cell proliferation and differentiation, this thesis investigated mice harbouring the homozygous recessive TBCD A475T clinically-relevant mutation, investigating the potential neurodevelopment impact of such a mutation in embryonic and postnatal brains. The brains of $TBCD^{A475T/A475T}$ mice were significantly different to WT littermates in terms of size, thickness, weight, and cortical lamination. Detailed evaluation of these mice revealed a phenotype congruent with the observed homeostatic imbalances reported for the *in vitro* findings. $TBCD^{A475T/A475T}$ mice from embryonic day 14.5 (E14.5), were observed to possess a significantly enlarged cortex, with a decreased expression of proliferation and pluripotency markers, altered expression of glycolytic enzymes, as well as an increased expression of markers of mitochondrial mass/function, and post mitotic neuronal markers. Whilst these results indicate a prematurely advanced state of neuronal development at E14.5, an inverse effect is seen at E17.5, with $TBCD^{A475T/A475T}$ mice possessing a significantly reduced cortical weight, size, thickness, and perturbed lamination. These cortical malformations are accompanied by a reduced expression of post mitotic neuronal markers, increased expression of pluripotency and proliferative markers and mitochondrial markers, as well as an altered expression of glycolytic markers. This phenotype persisted postnatally at P5, and was paralleled by an increase in active caspase-3, although an increase in cell death could not be confirmed. Whilst typically a marker of cell death, caspase-3 has non-apoptotic roles that include, facilitating both NPC neurogenesis and neuroplasticity/synaptic functioning [52-54]. Coupled with the increased expression of Sox2, mitochondrial markers, and the altered glycolytic enzymes, these data are suggestive of an increase in mitotically active NPCs that are still undergoing differentiation in the $TBCD^{A475T/A475T}$ mice cortices at P5 (**Fig. 7.2**). Taken together, these results are consistent with findings in P19EC that show defective cell cycling, as well as hallmarks of altered differentiation in the context of TBCD perturbations (Chapter 3). Given that changes in brain volume has been reported in humans with homozygous A475T mutations [15-18], the mouse model reported in this thesis will be informative to understand the progression of neurodevelopmental disease.

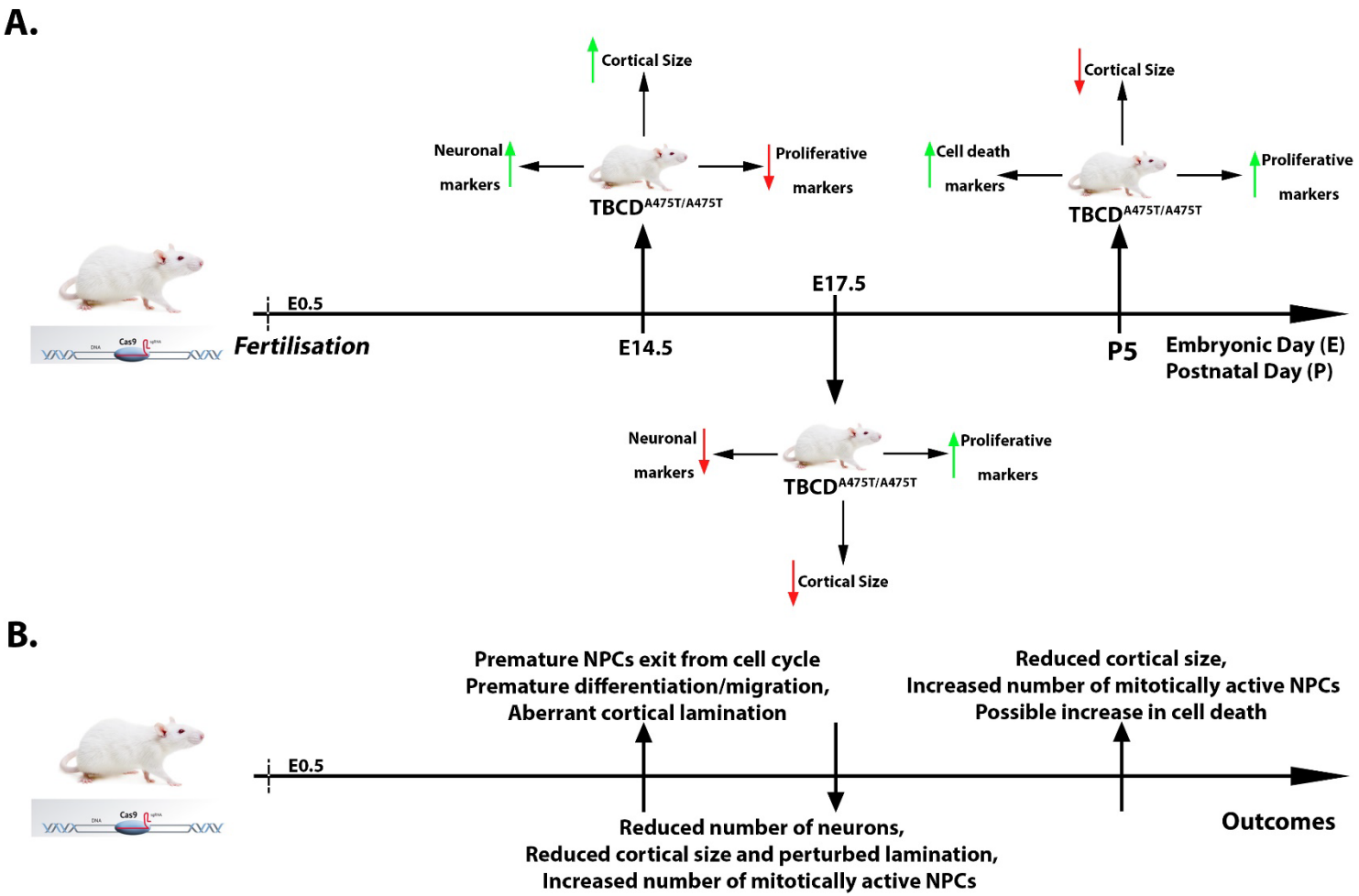

Figure 7.2. TBCD$^{A475T/A475T}$ mice display cortical malformations embryonically and postnatally

Schematic diagram outlining the examination, experimental procedures and findings from TBCD$^{A475T/A475T}$ mice compared to WT littermates at embryonic day 14.5 (E14.5), E17.5, and postnatal day 5 (P5). (A) Examination of phenotype from mice harbouring the TBCD$^{A475T/A475T}$ mutation over time. (B) Interpretation and outcomes from examination of mice harbouring the TBCD$^{A475T/A475T}$ mutation at each time point.

In addition to these findings, an *in silico* model of TBCD in complex with its physiologically relevant interactors was developed to address the current lack of a crystallographic structure of TBCD. It was observed that TUBB2A and TUBB2B had the most energetically favourable interactions with the TBC-DEG complex, whilst TUBB, TUBB4A and TUBB8 exhibited less favourable binding. These results suggest that TBCD shows preference for binding to distinct β-tubulin isoforms. Therefore, future work will address the impact of disease-associated TBCD missense variants on binding the various β-tubulins and other protein partners that may be relevant to their pathogenic mechanisms of action in cells.

The findings from this thesis support previously reported roles for TBCD in cell cycle progress and neurodevelopment. These findings have also revealed a previously unreported effect wherein TBCD disruptions can induce a G2 delay, alter cellular metabolism and direct cell fate. Furthermore, by detailing the molecular mechanisms underpinning TBCD mode of action, this work has enabled the identification of a potential therapeutic target to alleviate the TBCD induced homeostatic perturbations. Incubation of TBCD perturb cells with the long lasting GLP-1R analogue Exendin-4 was observed to alleviate the G2 delay, promote metabolic reprogramming towards a more glycolytic phenotype, and restore the aberrant expression of markers of neuronal differentiation and pluripotency (**Figure 7.3**). Furthermore, it was determined that the loss of the IGF1R, but not the INSR, was responsible for the ability of Exendin-4 to restore the TBCD induced G2 cycle deficit. Although neither the IGF1R nor INSR autocrine loops are believed to be required for chronic GLP-1R induced metabolic reprogramming [55-57], it would be interesting to determine if loss of these receptors impacted the ability of Exendin-4 to restore the aberrant expression of neuronal differentiation markers, and whether this was dependent or independent of metabolic state of the cells. After exploring the effects of chronic GLP-1R activation in cell lines, it would be beneficial to assess the therapeutic application of GLP-1R signalling *in vivo* in the context of TBCD mutations.

Whilst these results help to delineate TBCDs underlying molecular mechanisms in neurodevelopment and homeostasis, they also open up several other avenues for future exploration. One such area for exploration is the interaction and impact of differentiation signals, developmental stage, and the different phases of the cell cycle on NPC commitment to different cell fates [46, 58]. Cell fate commitment has been reported to be determined not

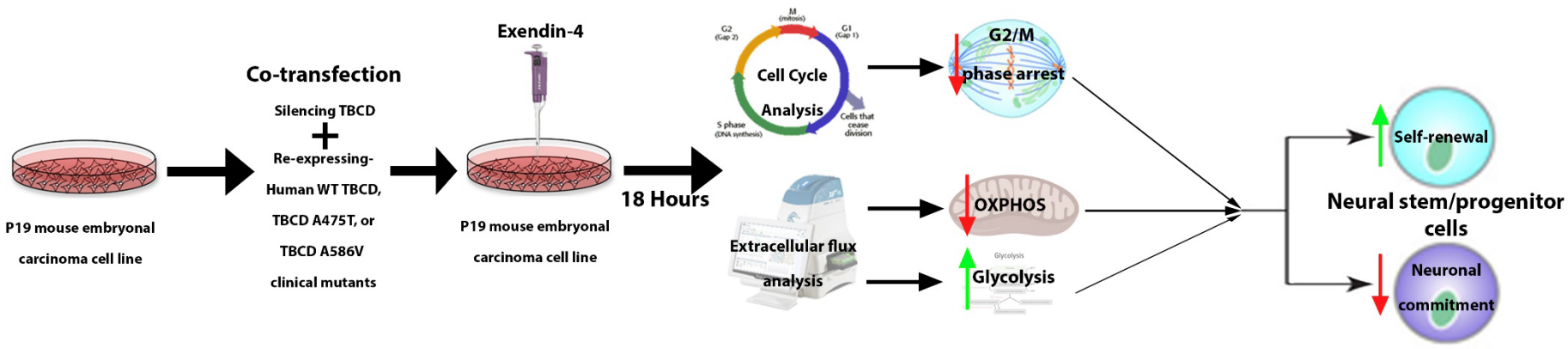

Figure 7.3. Chronic treatment with GLP-1 analog, Exendin-4, alleviates TBCD included homeostatic imbalance

Schematic diagram outlining experimental procedures and a summary of findings. (A) P19 embryonic carcinoma cells co-incubated with shRNA silencing TBCD, and a mammalian expression vector for either of the clinically-relevant mutants TBCD A475T, or TBCD A586V were incubated in the presence or absence of 50nM Exendin-4 for 18 hours. Cells were then subject to cell cycle analysis and extracellular flux analysis. Analysis revealed that Exendin-4 rescued the TBCD mutants' induced G2/M phase arrest, reduced oxidative phosphorylation (OXPHOS), and an increased the rate of glycolysis. These changes to metabolism and cell cycle resulted in an increased number of proliferative divisions, or self-renewal, and a decreased commitment to neurogenic divisions.

only on the previous round of division [58-60], but by the exposure of the cell to different signalling cues during certain cell cycle phases [49, 61-63]. Therefore, taken in the context of cortical development, the cell cycle arrest observed in TBCD perturbed cells *in vitro*, coupled with the altered expression of proliferation and pluripotency markers *in vivo*, may indicate that the exposure of NPCs to differentiation signals is impacted, thereby altering cell fate and lineage, and thus warrants further investigation [64-68]. It is also important to consider that during neuronal development it is not only cell cycle and metabolism that influences cell fate and lineage commitment, but the mode of division, be it the proliferative symmetric divisions or neurogenic asymmetric divisions [45, 69, 70]. Disruptions to the mode of division can impact the number of neurons, their laminar location, cortical connections, and ultimately, the size of the brain [71-74]. Studies have previously demonstrated that the orientation of the mitotic spindle is essential in cell fate decisions as its orientation determines the axis of cell division and thus the symmetric or asymmetric division of the cell [75-78]. Given that TBCD is required for the organisation of the mitotic spindle, as well as spindle MT dynamics [2, 5, 6], the phenotype observed in the $TBCD^{A475T/A475T}$ mice may be resultant from disruptions to spindle orientation, and thus mode of division, thereby impacting NPC proliferation and differentiation [1, 4, 79, 80]. It would therefore be beneficial to stain MTs and the mitotic spindle, in order to evaluate spindle orientation in relation to the VZ wall, and thus determine mode of division, during embryonic development. Although this is currently beyond the scope of this work, it does provide interesting and diverse questions for future elucidation.

Altogether, this thesis illuminates the vast and interconnected molecular mechanisms through which TBCD and its clinically-relevant mutations influence cell cycle, metabolism and differentiation. Furthermore, this thesis has identified GLP-1R, and IGF1R, signalling as a potential molecular pathway through which the cellular effects of TBCD perturbations may be ameliorated. Altogether, work from this thesis has improved our understanding of TBCD in neuronal development and homeostasis, and identified potential molecular pathways for therapeutic intervention for the treatment of clinically-relevant TBCD mutations.

References

1. Lancaster, M.A. and J.A. Knoblich, *Spindle orientation in mammalian cerebral cortical development.* Current opinion in neurobiology, 2012. **22**(5): p. 737-746.
2. Mishima, M., S. Kaitna, and M. Glotzer, *Central spindle assembly and cytokinesis require a kinesin-like protein/RhoGAP complex with microtubule bundling activity.* Developmental cell, 2002. **2**(1): p. 41-54.
3. Poulain, F.E. and A. Sobel, *The microtubule network and neuronal morphogenesis: Dynamic and coordinated orchestration through multiple players.* Molecular and Cellular Neuroscience, 2010. **43**(1): p. 15-32.
4. Wittmann, T., A. Hyman, and A. Desai, *The spindle: a dynamic assembly of microtubules and motors.* Nat Cell Biol, 2001. **3**(1): p. E28-34.
5. Glotzer, M., *The 3Ms of central spindle assembly: microtubules, motors and MAPs.* Nat Rev Mol Cell Biol, 2009. **10**(1): p. 9-20.
6. Fanarraga, M.L., et al., *TBCD links centriologenesis, spindle microtubule dynamics, and midbody abscission in human cells.* PLoS One, 2010. **5**(1): p. e8846.
7. Stiles, J. and T.L. Jernigan, *The Basics of Brain Development.* Neuropsychology Review, 2010. **20**(4): p. 327-348.
8. Gilmore, E.C. and C.A. Walsh, *Genetic causes of microcephaly and lessons for neuronal development.* Wiley Interdisciplinary Reviews: Developmental Biology, 2013. **2**(4): p. 461-478.
9. Rees, M., et al., *Tubulinopathies in malformations of the cerebral cortex.* Journal of Neurology, Neurosurgery & Psychiatry, 2014. **85**(10): p. e4-e4.
10. Karaca, E., et al., *Genes that Affect Brain Structure and Function Identified by Rare Variant Analyses of Mendelian Neurologic Disease.* Neuron, 2015. **88**(3): p. 499-513.
11. Jaglin, X.H. and J. Chelly, *Tubulin-related cortical dysgeneses: microtubule dysfunction underlying neuronal migration defects.* Trends Genet, 2009. **25**(12): p. 555-66.
12. Guerrini, R. and E. Parrini, *Neuronal migration disorders.* Neurobiology of Disease, 2010. **38**(2): p. 154-166.
13. Guerrini, R. and W.B. Dobyns, *Malformations of cortical development: clinical features and genetic causes.* The Lancet Neurology, 2014. **13**(7): p. 710-726.
14. Breuss, M. and D.A. Keays, *Microtubules and neurodevelopmental disease: the movers and the makers.* Adv Exp Med Biol, 2014. **800**: p. 75-96.
15. Pode-Shakked, B., et al., *Microcephaly, intractable seizures and developmental delay caused by biallelic variants in TBCD: Further delineation of a new chaperone-mediated tubulinopathy.* Clinical genetics, 2016.
16. Miyake, N., et al., *Biallelic TBCD mutations cause early-onset neurodegenerative encephalopathy.* The American Journal of Human Genetics, 2016. **99**(4): p. 950-961.
17. Flex, E., et al., *Biallelic Mutations in TBCD, Encoding the Tubulin Folding Cofactor D, Perturb Microtubule Dynamics and Cause Early-Onset Encephalopathy.* The American Journal of Human Genetics, 2016. **99**(4): p. 962-973.
18. Edvardson, S., et al., *Infantile neurodegenerative disorder associated with mutations in TBCD, an essential gene in the tubulin heterodimer assembly pathway.* Human Molecular Genetics, 2016. **25**(21): p. 4635-4648.
19. Gao, Y., et al., *Two cofactors and cytoplasmic chaperonin are required for the folding of alpha- and beta-tubulin.* Molecular and Cellular Biology, 1993. **13**(4): p. 2478-2485.
20. Tian, G., et al., *Tubulin subunits exist in an activated conformational state generated and maintained by protein cofactors.* J Cell Biol, 1997. **138**(4): p. 821-32.
21. Tian, G., et al., *Pathway Leading to Correctly Folded β-Tubulin.* Cell, 1996. **86**(2): p. 287-296.

22. Martín, L., et al., *Tubulin folding cofactor D is a microtubule destabilizing protein.* FEBS letters, 2000. **470**(1): p. 93-95.
23. Hirata, D., et al., *Essential role of tubulin-folding cofactor D in microtubule assembly and its association with microtubules in fission yeast.* The EMBO Journal, 1998. **17**(3): p. 658-666.
24. Fedyanina, O.S., A.J. Book, and E.L. Grishchuk, *Tubulin heterodimers remain functional for one cell cycle after the inactivation of tubulin-folding cofactor D in fission yeast cells.* Yeast, 2009. **26**(4): p. 235-247.
25. Fedyanina, O.S., et al., *Chromosome segregation in fission yeast with mutations in the tubulin folding cofactor D.* Current genetics, 2006. **50**(5): p. 281-294.
26. Okumura, M., et al., *Linking cell surface receptors to microtubules: tubulin folding cofactor D mediates Dscam functions during neuronal morphogenesis.* Journal of Neuroscience, 2015. **35**(5): p. 1979-1990.
27. Hage-Sleiman, R., et al., *Silencing of tubulin binding cofactor C modifies microtubule dynamics and cell cycle distribution and enhances sensitivity to gemcitabine in breast cancer cells.* Molecular cancer therapeutics, 2011. **10**(2): p. 303-312.
28. Tian, G. and N.J. Cowan, *Tubulin-specific chaperones: components of a molecular machine that assembles the α/β heterodimer.* Methods in cell biology, 2013. **115**: p. 155.
29. Kapitein, Lukas C. and Casper C. Hoogenraad, *Building the Neuronal Microtubule Cytoskeleton.* Neuron, 2015. **87**(3): p. 492-506.
30. Cunningham, L.A. and R.A. Kahn, *Cofactor D functions as a centrosomal protein and is required for the recruitment of the gamma-tubulin ring complex at centrosomes and organization of the mitotic spindle.* J Biol Chem, 2008. **283**(11): p. 7155-65.
31. Ayala, R., T. Shu, and L.-H. Tsai, *Trekking across the brain: the journey of neuronal migration.* Cell, 2007. **128**(1): p. 29-43.
32. Al-Bassam, J., *Revisiting the tubulin cofactors and Arl2 in the regulation of soluble αβ-tubulin pools and their effect on microtubule dynamics.* Molecular Biology of the Cell, 2017. **28**(3): p. 359-363.
33. Tian, G., S. Thomas, and N.J. Cowan, *Effect of TBCD and its regulatory interactor Arl2 on tubulin and microtubule integrity.* Cytoskeleton, 2010. **67**(11): p. 706-714.
34. Alsop, G.B. and D. Zhang, *Microtubules are the only structural constituent of the spindle apparatus required for induction of cell cleavage.* The Journal of cell biology, 2003. **162**(3): p. 383-390.
35. Murthy, K. and P. Wadsworth, *Dual role for microtubules in regulating cortical contractility during cytokinesis.* Journal of cell science, 2008. **121**(14): p. 2350-2359.
36. Somers, W.G. and R. Saint, *A RhoGEF and Rho family GTPase-activating protein complex links the contractile ring to cortical microtubules at the onset of cytokinesis.* Developmental cell, 2003. **4**(1): p. 29-39.
37. Zhai, Y., et al., *Microtubule dynamics at the G2/M transition: abrupt breakdown of cytoplasmic microtubules at nuclear envelope breakdown and implications for spindle morphogenesis.* The Journal of Cell Biology, 1996. **135**(1): p. 201-214.
38. Mora-Bermúdez, F. and W.B. Huttner, *Novel insights into mammalian embryonic neural stem cell division: focus on microtubules.* Molecular Biology of the Cell, 2015. **26**(24): p. 4302-4306.
39. Karsten, S.L., et al., *Global analysis of gene expression in neural progenitors reveals specific cell-cycle, signaling, and metabolic networks.* Developmental biology, 2003. **261**(1): p. 165-182.
40. Beckervordersandforth, R., et al., *Role of mitochondrial metabolism in the control of early lineage progression and aging phenotypes in adult hippocampal neurogenesis.* Neuron, 2017. **93**(3): p. 560-573. e6.
41. Vega-Naredo, I., et al., *Mitochondrial metabolism directs stemness and differentiation in P19 embryonal carcinoma stem cells.* Cell Death & Differentiation, 2014. **21**(10): p. 1560-1574.

42. Kalucka, J., et al., *Metabolic control of the cell cycle.* Cell cycle (Georgetown, Tex.), 2015. **14**(21): p. 3379-3388.
43. Agostini, M., et al., *Metabolic reprogramming during neuronal differentiation.* Cell death and differentiation, 2016. **23**(9): p. 1502-1514.
44. Zheng, X., et al., *Metabolic reprogramming during neuronal differentiation from aerobic glycolysis to neuronal oxidative phosphorylation.* eLife, 2016. **5**: p. e13374.
45. Knobloch, M. and S. Jessberger, *Metabolism and neurogenesis.* Current opinion in neurobiology, 2017. **42**: p. 45-52.
46. Soufi, A. and S. Dalton, *Cycling through developmental decisions: how cell cycle dynamics control pluripotency, differentiation and reprogramming.* Development, 2016. **143**(23): p. 4301-4311.
47. Ruijtenberg, S. and S. van den Heuvel, *Coordinating cell proliferation and differentiation: Antagonism between cell cycle regulators and cell type-specific gene expression.* Cell cycle, 2016. **15**(2): p. 196-212.
48. Hindley, C. and A. Philpott, *Co-ordination of cell cycle and differentiation in the developing nervous system.* Biochemical Journal, 2012. **444**(3): p. 375-382.
49. Cremisi, F., A. Philpott, and S.-i. Ohnuma, *Cell cycle and cell fate interactions in neural development.* Current opinion in neurobiology, 2003. **13**(1): p. 26-33.
50. Quinn, J.C., et al., *Pax6 controls cerebral cortical cell number by regulating exit from the cell cycle and specifies cortical cell identity by a cell autonomous mechanism.* Developmental biology, 2007. **302**(1): p. 50-65.
51. Hardwick, L.J.A., et al., *Cell cycle regulation of proliferation versus differentiation in the central nervous system.* Cell and Tissue Research, 2015. **359**: p. 187-200.
52. Fernando, P., S. Brunette, and L.A. Megeney, *Neural stem cell differentiation is dependent upon endogenous caspase-3 activity.* The FASEB journal, 2005. **19**(12): p. 1671-1673.
53. Tzeng, T.-T., et al., *Caspase 3 involves in neuroplasticity, microglial activation and neurogenesis in the mice hippocampus after intracerebral injection of kainic acid.* Journal of biomedical science, 2013. **20**(1): p. 1-16.
54. D'amelio, M., V. Cavallucci, and F. Cecconi, *Neuronal caspase-3 signaling: not only cell death.* Cell Death & Differentiation, 2010. **17**(7): p. 1104-1114.
55. Cornu, M., et al., *Glucagon-like peptide-1 protects beta-cells against apoptosis by increasing the activity of an IGF-2/IGF-1 receptor autocrine loop.* Diabetes, 2009. **58**(8): p. 1816-25.
56. Cornu, M., et al., *Glucagon-like peptide-1 increases beta-cell glucose competence and proliferation by translational induction of insulin-like growth factor-1 receptor expression.* J Biol Chem, 2010. **285**(14): p. 10538-45.
57. Rowlands, J., et al., *Insulin and IGF-1 receptor autocrine loops are not required for Exendin-4 induced changes to pancreatic β-cell bioenergetic parameters and metabolism in BRIN-BD11 cells.* Peptides, 2018. **100**: p. 140-149.
58. Pauklin, S. and L. Vallier, *The cell-cycle state of stem cells determines cell fate propensity.* Cell, 2013. **155**(1): p. 135-147.
59. Florio, M. and W.B. Huttner, *Neural progenitors, neurogenesis and the evolution of the neocortex.* Development, 2014. **141**(11): p. 2182-2194.
60. Yang, K., M. Hitomi, and D.W. Stacey, *Variations in cyclin D1 levels through the cell cycle determine the proliferative fate of a cell.* Cell division, 2006. **1**(1): p. 32.
61. Stancik, E.K., et al., *Heterogeneity in ventricular zone neural precursors contributes to neuronal fate diversity in the postnatal neocortex.* Journal of Neuroscience, 2010. **30**(20): p. 7028-7036.
62. Mione, M.C., et al., *Cell fate specification and symmetrical/asymmetrical divisions in the developing cerebral cortex.* Journal of Neuroscience, 1997. **17**(6): p. 2018-2029.
63. Greig, L.C., et al., *Molecular logic of neocortical projection neuron specification, development and diversity.* Nature Reviews Neuroscience, 2013. **14**(11): p. 755-769.

64. Duenas, M., et al., *Interaction of insulin-like growth factor-I and estradiol signaling pathways on hypothalamic neuronal differentiation.* Neuroscience, 1996. **74**(2): p. 531-539.
65. Soppa, U., et al., *The Down syndrome-related protein kinase DYRK1A phosphorylates p27Kip1 and Cyclin D1 and induces cell cycle exit and neuronal differentiation.* Cell cycle, 2014. **13**(13): p. 2084-2100.
66. Kawada, K., et al., *Aberrant neuronal differentiation and inhibition of dendrite outgrowth resulting from endoplasmic reticulum stress.* Journal of neuroscience research, 2014. **92**(9): p. 1122-1133.
67. Hardwick, L.J. and A. Philpott, *Nervous decision-making: to divide or differentiate.* Trends in Genetics, 2014. **30**(6): p. 254-261.
68. Zhang, L.-j., et al., *Ctip2 is a dynamic regulator of epidermal proliferation and differentiation by integrating EGFR and Notch signaling.* Journal of cell science, 2012. **125**(23): p. 5733-5744.
69. Khacho, M., et al., *Mitochondrial dysfunction underlies cognitive defects as a result of neural stem cell depletion and impaired neurogenesis.* Human molecular genetics, 2017. **26**(17): p. 3327-3341.
70. Manuel, M.N., et al., *Regulation of cerebral cortical neurogenesis by the Pax6 transcription factor.* Frontiers in cellular neuroscience, 2015. **9**: p. 70.
71. Knoblich, J.A., *Mechanisms of asymmetric stem cell division.* Cell, 2008. **132**(4): p. 583-597.
72. Noctor, S.C., V. Martínez-Cerdeño, and A.R. Kriegstein, *Distinct behaviors of neural stem and progenitor cells underlie cortical neurogenesis.* Journal of Comparative Neurology, 2008. **508**(1): p. 28-44.
73. Gómez-López, S., R.G. Lerner, and C. Petritsch, *Asymmetric cell division of stem and progenitor cells during homeostasis and cancer.* Cellular and Molecular Life Sciences, 2014. **71**(4): p. 575-597.
74. Matsuzaki, F. and A. Shitamukai, *Cell division modes and cleavage planes of neural progenitors during mammalian cortical development.* Cold Spring Harbor perspectives in biology, 2015. **7**(9): p. a015719.
75. Laan, L., et al., *Cortical dynein controls microtubule dynamics to generate pulling forces that position microtubule asters.* Cell, 2012. **148**(3): p. 502-514.
76. Good, M.C., et al., *Cytoplasmic volume modulates spindle size during embryogenesis.* Science, 2013. **342**(6160): p. 856-860.
77. Théry, M., et al., *Experimental and theoretical study of mitotic spindle orientation.* Nature, 2007. **447**(7143): p. 493-496.
78. di Pietro, F., A. Echard, and X. Morin, *Regulation of mitotic spindle orientation: an integrated view.* EMBO reports, 2016: p. e201642292.
79. Mora-Bermúdez, F., F. Matsuzaki, and W.B. Huttner, *Specific polar subpopulations of astral microtubules control spindle orientation and symmetric neural stem cell division.* eLife, 2014. **3**: p. e02875.
80. Haren, L., et al., *NEDD1-dependent recruitment of the γ-tubulin ring complex to the centrosome is necessary for centriole duplication and spindle assembly.* The Journal of Cell Biology, 2006. **172**(4): p. 505-515.

Supplementary Material

Table S1. Primary Antibody list

Primary Antibodies								
Target Protein	**Cat#**	**Company**	**Source**	**Dilution Factor**	**Mwt (kDa)**	**Cross Species Reactivity**	**Applications**	**Storage**
α/β-Tubulin	2148S	Cell Signalling	Rabbit	1:1000	55	H, M, R, Mk	WB, IHC, IF, FC	-20˚C
ATF4	11815S	Cell Signalling	Rabbit	1:1000	49	H, M, R	WB	-20˚C
β-Actin	4970	Cell Signalling	Rabbit	1:1000	45	H, M, R	WB, IHC, IF, FC	-20˚C
Bip	3183	Cell Signalling	Rabbit	1:1000	78	H, M, R	WB	-20˚C
Cleaved Cas-3	9664	Cell Signalling	Rabbit	1:1000	17, 19	H, M, R	WB, IP, IHC, IF, FC	-20˚C
CHOP	5554	Cell Signalling	Rabbit	1:1000	27	M	WB, IP	-20˚C
CHOP	2895	Cell Signalling	Mouse	1:1000	27	H, M, R	WB, IP, IF	-20˚C
Ctip2	AB18465	Abcam	Rat	1:300	95-120	H, M, R	WB, IP, IHC, IF, FC	-20˚C
COXIV	4850	Cell Signalling	Rabbit	1:300	17	H, R	WB, IP, IHC, IF, FC	-20˚C
Cyclin D1	2922	Cell Signalling	Rabbit	1:1000	36	H, M, R	WB, IP	-20˚C
FOXG1	AB18259	Abcam	Rabbit	1:1000	50	H, M, R	WB, IF, IHC	-20˚C
GADPH	5174	Cell Signalling	Rabbit	1:1000	37	H, M, R	WB, IHC, IF	-20˚C
Hexokinase-1	2024	Cell Signalling	Rabbit	1:1000	102	H, M	WB, IP, IHC, IF	-20˚C
Hexokinase-2	2867	Cell Signalling	Rabbit	1:1000	102	H, M, R	WB	-20˚C
HSP70	4872	Cell Signalling	Rabbit	1:1000	72	H, M, R	WB, IHC	-20˚C
IGF-1-R β	3027	Cell Signalling	Rabbit	1:1000	95	H, M, R	WB, IP, IHC	-20˚C
IR-β	3025	Cell Signalling	Rabbit	1:1000	95	H, M, R	WB, IP	-20˚C

NeuN	MAB377	Merck	Mouse	1:500	46-48, 60	H, M, R	WB, IP, IHC, IF, FC	-20˚C
Phospho-Histone H3 (Ser 10)	06-570	Merck	Rabbit	1:400	17	H, M	WB, ICC, IP	-20˚C
Phosphate vimentin	AB22651	Abcam	Mouse	1:1000	54-57	H, M, R	WB, IP, IHC, IF, FC	-20˚C
P-mTOR s2448	5536	Cell Signalling	Rabbit	1:1000	289	H, M, R	WB, IP, IF	-20˚C
p38 MAPK	8690	Cell Signalling	Rabbit	1:1000	40	H, M, R	WB, IHC, IF, FC	-20˚C
P-p38 MAPK	4511	Cell Signalling	Rabbit	1:1000	43	H, M, R	WB, IP, IHC, IF, FC	-20˚C
p42/44 MAPK ERK1/2	4695	Cell Signalling	Rabbit	1:1000	42, 44	H, M, R	WB, IP, IHC, IF, FC	-20˚C
P-p42/44 MAPK ERK1/2	4370	Cell Signalling	Rabbit	1:1000	42, 44	H, M, R	WB, IP, IHC, IF, FC	-20˚C
PARP	9542	Cell Signalling	Rabbit	1:1000	89, 116	H, M, R	WB	-20˚C
PAX-6	901301	Biolegend	Rabbit	1:500	47	H, M, R	WB, IHC, IF	-20˚C
PERK	3192	Cell Signalling	Rabbit	1:1000	140	H, M, R	WB	-20˚C
P-PERK T980	3179	Cell Signalling	Rabbit	1:1000	170	R	WB	-20˚C
PKM1/2	3190	Cell Signalling	Rabbit	1:1000	60	H, M, R	WB, IF	-20˚C
PKM2	4053	Cell Signalling	Rabbit	1:1000	60	H, M, R	WB, IP, IHC, IF, FC	-20˚C
Satb2	AB1502	Abcam	Mouse	1:400	81	H, M	WB, ICC, IP	-20˚C
Synapsin	AB1543	Merck	Rabbit	1:500-1000	77, 80	H, M, R	WB, IHC, IP	-20˚C
S6 Ribosomal	2217	Cell Signalling	Rabbit	1:1000	32	H, M, R	WB, IHC, IF	-20˚C
SOX2	AB5603	Abcam	Rabbit	1:1000	32-34	H,M	WB, IHC, iCC, IF	-20˚C
SIRT1	8469	Cell Signalling	Mouse	1:1000	120	H, M, R	WB, IP, IF	-20˚C
TBCD	14867-1-AP	Proteintech	Rabbit	1:500-1000	130	H, M, R	WB, IP, IF	-20˚C
Tbr1	AB31940	Abcam	Rabbit	1:200	74	H, M, R	WB, IP, IHC, IF, FC	-20˚C
Tbr2	AB23345	Abcam	Rabbit	1:500	85	H, M, R	WB, IP, IHC, IF, FC	-20˚C
Tuj1	MMS-435P	Covance/Biolegend	Mouse	1:1000	50	H, M, R	WB, IHC, FC	-20˚C

WB= Western Blot

IP= Immunoprecipitation

H= Human

IHC= Immunohisto-chemistry

M= Mouse

IF= Immunofluorescence

R= Rat

FC= Flow Cytometry

Mk= Monkey

AF= Alexa Fluoro Conjugated

Hm= Hamster

PE= PE Conjugated

ICC= Immunocytochemistry

Table S2. Secondary Antibody list

Secondary Antibodies				
Target	**Cat#**	**Company**	**Dilution Factor**	**Storage**
Rabbit	P0448	Dako	1:2000	4˚C
Mouse	P0447	Dako	1:2000	4˚C
Rabbit (488)	A21206	Invitrogen	1:800	4˚C
Goat (568)	A11057	Molecular Probe	1:800	4˚C
DAPI	D1306	ThermoFisher	1:10000	4˚C

Table S3. CRISPR gRNA sequences

CRISPR oligo name	CRISPR gRNA sequence 5’-3’
Igf1r CRISPR Guide RNA or crRNA 1	ATGGCGGATCTTCACGTAGC
Igf1r CRISPR Guide RNA or crRNA 2	AGCAGAAGTCACCGAATCGA
Insr CRISPR Guide RNA or crRNA 1	TATAGCCAGACGGGCACTCG
Insr CRISPR Guide RNA or crRNA 2	TATCGACTGGTCCCGTATCC

```
             10        20        30        40        50        60
              |         |         |         |         |         |
Conf: 9877798789983677774898999999415699999998987430786437899999
Pred: CCCCCCCCCCCCCHHHHHHHHHHHHHHHHHHCCCHHHHHHHHHHHHHCCCCHHHHHHHH
  AA: MALSDEPAAGGPEEEAEDETLAFGAALEAFGESAETRALLGRLREVHGGGAEREVALERF

             70        80        90       100       110       120
              |         |         |         |         |         |
Conf: 9998885119111438899999999999803999579999999999999997558258997
Pred: HHHHHHHHCCCCCCCHHHHHHHHHHHHHHHCCCCCHHHHHHHHHHHHHHHHHCCCHHHHH
  AA: RVIMDKYQEQPHLLDPHLEWMMNLLLDIVQDQTSPASLVHLAFKFLYIITKVRGYKTFLR

            130       140       150       160       170       180
              |         |         |         |         |         |
Conf: 5872126741004366531857742899999999999967504568542788766897 43
Pred: HCCCCCCCCCCCCEEEEEECCCCCCCHHHHHHHHHHHHHHHHHHCCCCHHHCCCCCCCCCH
  AA: LFPHEVADVEPVLDLVTIQNPKDHEAWETRYMLLLWLSVTCLIPFDFSRLDGNLLTQPGQ

            190       200       210       220       230       240
              |         |         |         |         |         |
Conf: 7688999999999842204248899999998662392525267899874999999964 3
Pred: HHHHHHHHHHHHHHHHHHHCCHHHHHHHHHHHHHHCCCCCCHHHHHHHHCHHHHHHHHHH
  AA: ARMSIMDRILQIAESYLIVSDKARDAAAVLVSRFITRPDVKQSKMAEFLDWSLCNLARSS

            250       260       270       280       290       300
              |         |         |         |         |         |
Conf: 0102345524449999999998187534177899999980168899403899999818 99
Pred: HCCCCEEECCCHHHHHHHHHHHCCCHHHCHHHHHHHHHHHCCCCCCCHHHHHHHHHHHHH
  AA: FQTMQGVITMDGTLQALAQIFKHGKREDCLPYAATVLRCLDGCRLPESNQTLLRKLGVKL

            310       320       330       340       350       360
              |         |         |         |         |         |
Conf: 9995871136649999978567899999899866887589955316999999965589 99
Pred: HHHHCCCCCCHHHHHHHHHHHHHHHHHHHHHHHCCCCCCCCCEEEECCCCCCCCCCHHHHH
  AA: VQRLGLTFLKPKVAAWRYQRGCRSLAANLQLLTQGQSEQKPLILTEDDDEDDDVPEGVER

            370       380       390       400       410       420
              |         |         |         |         |         |
Conf: 9999964377845318889651277870220189872266668626043236751128 79
Pred: HHHHHHHCCCCCCCCHHHHHHHCHHHHCCCCHHHHHHHHHHHHHHHHCCCCCCCCCCCHHH
  AA: VIEQLLVGLKDKDTVVRWSAAKGIGRMAGRLPRALADDVVGSVLDCFSFQETDKAWHGGC

            430       440       450       460       470       480
              |         |         |         |         |         |
Conf: 9999945447558278999999999985565237986679957999999999999514 94
Pred: HHHHHHHHCCCCCCHHHHHHHHHHHHHCCCCCCCCCCCCCCCHHHHHHHHHHHHHHCCC
  AA: LALAELGRRGLLLPSRLVDVVAVILKALTYDEKRGACSVGTNVRDAACYVCWAFARAYEP

            490       500       510       520       530       540
              |         |         |         |         |         |
Conf: 1228999999899999999447856178999999941236788888510202366643 47
Pred: HHHHHHHHHHHHHHHHHHHHHCCCCCHHHHHHHHHHHHCCCCCCCCCCCCCCCCCCCEEECC
  AA: QELKPFVTAISSALVIAAVFDRDINCRRAASAAFQENVGRQGTFPHGIDILTTADYFAVG

            550       560       570       580       590       600
              |         |         |         |         |         |
Conf: 7133067887414479003052878988731350788999999999999997096665 86
Pred: CCCCEEEEEEEHHCCCCHHHHHHHHHHHHHCHHCHHHHHHHHHHHHHHHHHHCCCCCHH
  AA: NRSNCFLVISVFIAGFPEYTQPMIDHLVTMKISHWDGVIRELAARALHNLAQQAPEFSAT

            610       620       630       640       650       660
```

```
               |         |         |         |         |         |
Conf: 488999974269884310443899999999999997608998843529999999999999
Pred: HHHHHHHHCCCCCCCCCCCCHHHHHHHHHHHHHHHHHHCCCCCCCCCCHHHHHHHHHHHH
  AA: QVFPRLLSMTLSPDLHMRHGSILACAEVAYALYKLAAQENRPVTDHLDEQAVQGLKQIHQ

             670       680       690       700       710       720
               |         |         |         |         |         |
Conf: 999457662110599999999998751015999998155315999888889999974114
Pred: HHHHHHHHHHCCHHHHHHHHHHHHHHHHCCCCCCCCCCCEEECCHHHHHHHHHHHHHHCCC
  AA: QLYDRQLYRGLGGQLMRQAVCVLIEKLSLSKMPFRGDTVIDGWQWLINDTLRHLHLISSH

             730       740       750       760       770       780
               |         |         |         |         |         |
Conf: 588999999999999999860599889999999999999945998981651998962
Pred: CHHHHHHHHHHHHHHHHHHHHHCCCCCCCHHHHHHHHHHHHHHHCCHHHHHHHCHHHHHC
  AA: SRQQMKDAAVSALAALCSEYYMKEPGEADPAIQEELITQYLAELRNPEEMTRCGFSLALG

             790       800       810       820       830       840
               |         |         |         |         |         |
Conf: 474147788899999853550389998824667836889999999999684589996001
Pred: CCCCHHHHHHHHHHHHHHHHHCCCCHHHCCHHHHHHHHHHHHHHHHHHHHCCCCCCCCCCC
  AA: ALPGFLLKGRLQQVLTGLRAVTHTSPEDVSFAESRRDGLKAIARICQTVGVKAGAPDEAV

             850       860       870       880       890       900
               |         |         |         |         |         |
Conf: 676789999999863131457898834899999998789999999993398899841654
Pred: CCCCHHHHHHHHHCCCCCCCCCCCCCCHHHHHHHHHHHHHHHHHHHHHHCCHHHHHHCCCC
  AA: CGENVSQIYCALLGCMDDYTTDSRGDVGTWVRKAAMTSLMDLTLLLARSQPELIEAHTCE

             910       920       930       940       950       960
               |         |         |         |         |         |
Conf: 488999998888689999999999999756999999999962687744624033256 99
Pred: HHHHHHHHHHHHHHHHHHHHHHHHHHHHHHCCCCCCCCCCCCCCCCHHHHHCCCCCCCCCCCC
  AA: RIMCCVAQQASEKIDRFRAHAASVFLTLLHFDSPPIPHVPHRGELEKLFPRSDVASVNWS

             970       980       990      1000      1010      1020
               |         |         |         |         |         |
Conf: 910175799999599658899999999963788788988889999999850167976772
Pred: CHHHHHHHHHHHHCCCHHHHHHHHHHHHHHCCCCCHHHHHHHHHHHHHHHCCCCCHHHHH
  AA: APSQAFPRITQLLGLPTYRYHVLLGLVVSLGGLTESTIRHSTQSLFEYMKGIQSDPQALG

            1030      1040      1050      1060      1070      1080
               |         |         |         |         |         |
Conf: 211078999884443645552189757899962721332388878789999999678861
Pred: CCCHHHHHHHHHCCCCCCCCHHHHHHHHHHHHCCCCCCCCCCCCCCHHHHHHHHHHHHHC
  AA: SFSGTLLQIFEDNLLNERVSVPLLKTLDHVLTHGCFDIFTTEEDHPFAVKLLALCKKEIK

            1090      1100      1110      1120      1130      1140
               |         |         |         |         |         |
Conf: 768899999988999977159933999999999999973053613358989999983122
Pred: CCHHHHHHHHHHHHHHHHHCCCHHHHHHHHHHHHHHHHHHCHHCCCCCHHHHHHHHHCHH
  AA: NSKDIQKLLSGIAVFCEMVQFPGDVRRQALLQLCLLLCHRFPLIRKTTASQVYETLLTYS

            1150      1160      1170      1180      1190
               |         |         |         |         |
Conf: 251867898887664044231889999999985689869997322899999 9
Pred: HHCCHHHHHHHHHHHHCCCCHHHHHHHHHHHHHHHHHHCCCCCCCCCCCCCCC
  AA: DVVGADVLDEVVTVLSDTAWDAELAVVREQRNRLCDLLGVPRPQLVPQPGAC
```

Supplementary Figure 1. Secondary structure of human TBCD predicted by PSIPRED.

Guide to symbols/abbreviations: Conf – confidence of prediction (lowest=0, highest=9); Pred – predicted secondary structure (H=Helix; C=Coil; E=Strand)

Table S4. Overlapping TBCD sequence fragments used to prepare models by C-QUARK

TBCD fragment	Residues in TBCD protein
1	1-389
2	50-432
3	93-479
4	141-520
5	201-595
6	246-645
7	288-687
8	353-746
9	390-783
10	433-832
11	480-855
12	555-932
13	596-991
14	646-1037
15	697-1080
16	747-1125
17	803-1192

```
TBCE       ATVRFAG~VVPPVAGPWLGVEWDNPERGKHDGSHEGTVYFKCRHPTGGSFIRPNKV
4B6M_A     GSVRFVGRVASLKPGYWVGVEFDEP~VGKGDGTVKGTRVFQCQ~PNYGGFLRPDQV
            :*** * *     * *:***:* *  ** **: :**  *:*: *  * *:**::*
```

Supplementary Figure 2. Alignment of TBCE CAP-Gly domain (residues 21-75) to template from PDB4B6M

```
SP|Q9BVA1|TBB2B_HUMAN -MREIVHIQAGQCGNQIGAKFWEVISDEHGIDPTGSYHGDSDLQLERINVYYNEATGNKY 59
SP|Q13885|TBB2A_HUMAN -MREIVHIQAGQCGNQIGAKFWEVISDEHGIDPTGSYHGDSDLQLERINVYYNEAAGNKY 59
SP|P04350|TBB4A_HUMAN -MREIVHLQAGQCGNQIGAKFWEVISDEHGIDPTGTYHGDSDLQLERINVYYNEATGGNY 59
SP|P68371|TBB4B_HUMAN -MREIVHLQAGQCGNQIGAKFWEVISDEHGIDPTGTYHGDSDLQLERINVYYNEATGGKY 59
SP|Q13509|TBB3_HUMAN  -MREIVHIQAGQCGNQIGAKFWEVISDEHGIDPSGNYVGDSDLQLERISVYYNEASSHKY 59
SP|P07437|TBB5_HUMAN  -MREIVHIQAGQCGNQIGAKFWEVISDEHGIDPTGTYHGDSDLQLDRISVYYNEATGGKY 59
SP|Q9H4B7|TBB1_HUMAN  -MREIVHIQIGQCGNQIGAKFWEMIGEEHGIDLAGSDRGASALQLERISVYYNEAYGRKY 59
SP|Q9BUF5|TBB6_HUMAN  -MREIVHIQAGQCGNQIGTKFWEVISDEHGIDPAGGYVGDSALQLERINVYYNESSSQKY 59
SP|Q3ZCM7|TBB8_HUMAN  -MREIVLTQIGQCGNQIGAKFWEVISDEHAIDSAGTYHGDSHLQLERINVYYNEASGGRY 59
SP|P23258|TBG1_HUMAN  MPREIITLQLGQCGNQIGFEFWKQLCAEHGISPEGIVEEFATEGTDRKDVFFYQADDEHY 60
SP|Q6B856|TBB2B_BOVIN -MREIVHIQAGQCGNQIGAKFWEVISDEHGIDPTGSYHGDSDLQLERINVYYNEATGNKY 59
                        ***:  * ******** :**: :  **.*.  *     :    :* .*:: :: . .*

SP|Q9BVA1|TBB2B_HUMAN VPRAILVDLEPGTMDSVRSGPFGQIFRPDNFVFGQ--SGAGNNWAKGHYTEGAELVDSVL 117
SP|Q13885|TBB2A_HUMAN VPRAILVDLEPGTMDSVRSGPFGQIFRPDNFVFGQ--SGAGNNWAKGHYTEGAELVDSVL 117
SP|P04350|TBB4A_HUMAN VPRAVLVDLEPGTMDSVRSGPFGQIFRPDNFVFGQ--SGAGNNWAKGHYTEGAELVDAVL 117
SP|P68371|TBB4B_HUMAN VPRAVLVDLEPGTMDSVRSGPFGQIFRPDNFVFGQ--SGAGNNWAKGHYTEGAELVDSVL 117
SP|Q13509|TBB3_HUMAN  VPRAILVDLEPGTMDSVRSGAFGHLFRPDNFIFGQ--SGAGNNWAKGHYTEGAELVDSVL 117
SP|P07437|TBB5_HUMAN  VPRAILVDLEPGTMDSVRSGPFGQIFRPDNFVFGQ--SGAGNNWAKGHYTEGAELVDSVL 117
SP|Q9H4B7|TBB1_HUMAN  VPRAVLVDLEPGTMDSIRSSKLGALFQPDSFVHGN--SGAGNNWAKGHYTEGAELIENVL 117
SP|Q9BUF5|TBB6_HUMAN  VPRAALVDLEPGTMDSVRSGPFGQLFRPDNFIFGQ--TGAGNNWAKGHYTEGAELVDAVL 117
SP|Q3ZCM7|TBB8_HUMAN  VPRAVLVDLEPGTMDSVRSGPFGQVFRPDNFIFGQ--CGAGNNWAKGHYTEGAELMESVM 117
SP|P23258|TBG1_HUMAN  IPRAVLLDLEPRVIHSILNSPYAKLYNPENIYLSEHGGGAGNNWASG-FSQGEKIHEDIF 119
SP|Q6B856|TBB2B_BOVIN VPRAILVDLEPGTMDSVRSGPFGQIFRPDNFVFGQ--SGAGNNWAKGHYTEGAELVDSVL 117
                       :*** *:**** .:.*: ..  . ::.*:.:  .:   *******.* :::* :: : ::

SP|Q9BVA1|TBB2B_HUMAN DVVRKESESCDCLQGFQLTHSLGGGTGSGMGTLLISKIREEYPDRIMNTFSVMPSP-KVS 176
SP|Q13885|TBB2A_HUMAN DVVRKESESCDCLQGFQLTHSLGGGTGSGMGTLLISKIREEYPDRIMNTFSVMPSP-KVS 176
SP|P04350|TBB4A_HUMAN DVVRKEAESCDCLQGFQLTHSLGGGTGSGMGTLLISKIREEFPDRIMNTFSVVPSP-KVS 176
SP|P68371|TBB4B_HUMAN DVVRKEAESCDCLQGFQLTHSLGGGTGSGMGTLLISKIREEYPDRIMNTFSVVPSP-KVS 176
SP|Q13509|TBB3_HUMAN  DVVRKECENCDCLQGFQLTHSLGGGTGSGMGTLLISKVREEYPDRIMNTFSVVPSP-KVS 176
SP|P07437|TBB5_HUMAN  DVVRKEAESCDCLQGFQLTHSLGGGTGSGMGTLLISKIREEYPDRIMNTFSVVPSP-KVS 176
SP|Q9H4B7|TBB1_HUMAN  EVVRHESESCDCLQGFQIVHSLGGGTGSGMGTLLMNKIREEYPDRIMNSFSVMPSP-KVS 176
SP|Q9BUF5|TBB6_HUMAN  DVVRKECEHCDCLQGFQLTHSLGGGTGSGMGTLLISKIREEFPDRIMNTFSVMPSP-KVS 176
SP|Q3ZCM7|TBB8_HUMAN  DVVRKEAESCDCLQGFQLTHSLGGGTGSGMGTLLLSKIREEYPDRIINTFSILPSP-KVS 176
SP|P23258|TBG1_HUMAN  DIIDREADGSDSLEGFVLCHSIAGGTGSGLGSYLLERLNDRYPKKLVQTYSVFPNQDEMS 179
SP|Q6B856|TBB2B_BOVIN DVVRKESESCDCLQGFQLTHSLGGGTGSGMGTLLISKIREEYPDRIMNTFSVMPSP-KVS 176
```

```
                    ::: :*.: .*.*:** : **:.******:*: *:.::.:.:*.:::::::*:.*.  ::*

SP|Q9BVA1|TBB2B_HUMAN DTVVEPYNATLSVHQLVENTDETYCIDNEALYDICFRTLKLTTPTYGDLNHLVSATMSGV 236
SP|Q13885|TBB2A_HUMAN DTVVEPYNATLSVHQLVENTDETYSIDNEALYDICFRTLKLTTPTYGDLNHLVSATMSGV 236
SP|P04350|TBB4A_HUMAN DTVVEPYNATLSVHQLVENTDETYCIDNEALYDICFRTLKLTTPTYGDLNHLVSATMSGV 236
SP|P68371|TBB4B_HUMAN DTVVEPYNATLSVHQLVENTDETYCIDNEALYDICFRTLKLTTPTYGDLNHLVSATMSGV 236
SP|Q13509|TBB3_HUMAN  DTVVEPYNATLSIHQLVENTDETYCIDNEALYDICFRTLKLATPTYGDLNHLVSATMSGV 236
SP|P07437|TBB5_HUMAN  DTVVEPYNATLSVHQLVENTDETYCIDNEALYDICFRTLKLTTPTYGDLNHLVSATMSGV 236
SP|Q9H4B7|TBB1_HUMAN  DTVVEPYNAVLSIHQLIENADACFCIDNEALYDICFRTLKLTTPTYGDLNHLVSLTMSGI 236
SP|Q9BUF5|TBB6_HUMAN  DTVVEPYNATLSVHQLVENTDETYCIDNEALYDICFRTLKLTTPTYGDLNHLVSATMSGV 236
SP|Q3ZCM7|TBB8_HUMAN  DTVVEPYNATLSVHQLIENADETFCIDNEALYDICSKTLKLPTPTYGDLNHLVSATMSGV 236
SP|P23258|TBG1_HUMAN  DVVVQPYNSLLTLKRLTQNADCVVVLDNTALNRIATDRLHIQNPSFSQINQLVSTIMSAS 239
SP|Q6B856|TBB2B_BOVIN DTVVEPYNATLSVHQLVENTDETYCIDNEALYDICFRTLKLTTPTYGDLNHLVSATMSGV 236
                    *.**:***: *::::* :*:*    :** **  *.   *:: .*::.::*:***  **.

SP|Q9BVA1|TBB2B_HUMAN TTCLRFPGQLNADLRKLAVNMVPFPRLHFFMPGFAPLTSRGSQ-QYRALTVPELTQQMFD 295
SP|Q13885|TBB2A_HUMAN TTCLRFPGQLNADLRKLAVNMVPFPRLHFFMPGFAPLTSRGSQ-QYRALTVPELTQQMFD 295
SP|P04350|TBB4A_HUMAN TTCLRFPGQLNADLRKLAVNMVPFPRLHFFMPGFAPLTSRGSQ-QYRALTVPELTQQMFD 295
SP|P68371|TBB4B_HUMAN TTCLRFPGQLNADLRKLAVNMVPFPRLHFFMPGFAPLTSRGSQ-QYRALTVPELTQQMFD 295
SP|Q13509|TBB3_HUMAN  TTSLRFPGQLNADLRKLAVNMVPFPRLHFFMPGFAPLTARGSQ-QYRALTVPELTQQMFD 295
SP|P07437|TBB5_HUMAN  TTCLRFPGQLNADLRKLAVNMVPFPRLHFFMPGFAPLTSRGSQ-QYRALTVPELTQQVFD 295
SP|Q9H4B7|TBB1_HUMAN  TTSLRFPGQLNADLRKLAVNMVPFPRLHFFMPGFAPLTAQGSQ-QYRALSVAELTQQMFD 295
SP|Q9BUF5|TBB6_HUMAN  TTSLRFPGQLNADLRKLAVNMVPFPRLHFFMPGFAPLTSRGSQ-QYRALTVPELTQQMFD 295
SP|Q3ZCM7|TBB8_HUMAN  TTCLRFPGQLNADLRKLAVNMVPFPRLHFFMPGFAPLTSRGSQ-QYRALTVAELTQQMFD 295
SP|P23258|TBG1_HUMAN  TTTLRYPGYMNNDLIGLIASLIPTPRLHFLMTGYTPLTTDQSVASVRKTTVLDVMRRLLQ 299
SP|Q6B856|TBB2B_BOVIN TTCLRFPGQLNADLRKLAVNMVPFPRLHFFMPGFAPLTSRGSQ-QYRALTVPELTQQMFD 295
                    ** **:** :* **  * ..::* *****:* *::***:  *  . *  :* :: :::::

SP|Q9BVA1|TBB2B_HUMAN SKNMMAACDP---RHGRYLTVAAIFRGRMSMKEVDEQMLNVQNKNSSYFVEWIPNNVKTA 352
SP|Q13885|TBB2A_HUMAN SKNMMAACDP---RHGRYLTVAAIFRGRMSMKEVDEQMLNVQNKNSSYFVEWIPNNVKTA 352
SP|P04350|TBB4A_HUMAN AKNMMAACDP---RHGRYLTVAAVFRGRMSMKEVDEQMLSVQSKNSSYFVEWIPNNVKTA 352
SP|P68371|TBB4B_HUMAN AKNMMAACDP---RHGRYLTVAAVFRGRMSMKEVDEQMLNVQNKNSSYFVEWIPNNVKTA 352
SP|Q13509|TBB3_HUMAN  AKNMMAACDP---RHGRYLTVATVFRGRMSMKEVDEQMLAIQSKNSSYFVEWIPNNVKVA 352
SP|P07437|TBB5_HUMAN  AKNMMAACDP---RHGRYLTVAAVFRGRMSMKEVDEQMLNVQNKNSSYFVEWIPNNVKTA 352
SP|Q9H4B7|TBB1_HUMAN  ARNTMAACDL---RRGRYLTVACIFRGKMSTKEVDQQLLSVQTRNSSCFVEWIPNNVKVA 352
SP|Q9BUF5|TBB6_HUMAN  ARNMMAACDP---RHGRYLTVATVFRGPMSMKEVDEQMLAIQSKNSSYFVEWIPNNVKVA 352
```

```
SP|Q3ZCM7|TBB8_HUMAN  AKNMMAACDP---RHGRYLTAAAIFRGRMPMREVDEQMFNIQDKNSSYFADWLPNNVKTA 352
SP|P23258|TBG1_HUMAN  PKNVMVSTGRDRQTNHCYIAILNIIQGEVDPTQVHKSLQRIRERKLANFIPWGPASIQVA 359
SP|Q6B856|TBB2B_BOVIN SKNMMAACDP---RHGRYLTVAAIFRGRMSMKEVDEQMLNVQNKNSSYFVEWIPNNVKTA 352
                       :* *.: .     .  *::   :::* :   :*.:.:  :: :: : *  * * .::.*

SP|Q9BVA1|TBB2B_HUMAN VCDIP---PRGLKMSATFIGNSTAIQELFKRISEQFTAMFRRKAFLHWYTGEGMDEMEFT 409
SP|Q13885|TBB2A_HUMAN VCDIP---PRGLKMSATFIGNSTAIQELFKRISEQFTAMFRRKAFLHWYTGEGMDEMEFT 409
SP|P04350|TBB4A_HUMAN VCDIP---PRGLKMAATFIGNSTAIQELFKRISEQFTAMFRRKAFLHWYTGEGMDEMEFT 409
SP|P68371|TBB4B_HUMAN VCDIP---PRGLKMSATFIGNSTAIQELFKRISEQFTAMFRRKAFLHWYTGEGMDEMEFT 409
SP|Q13509|TBB3_HUMAN  VCDIP---PRGLKMSSTFIGNSTAIQELFKRISEQFTAMFRRKAFLHWYTGEGMDEMEFT 409
SP|P07437|TBB5_HUMAN  VCDIP---PRGLKMAVTFIGNSTAIQELFKRISEQFTAMFRRKAFLHWYTGEGMDEMEFT 409
SP|Q9H4B7|TBB1_HUMAN  VCDIP---PRGLSMAATFIGNNTAIQEIFNRVSEHFSAMFKRKAFVHWYTSEGMDINEFG 409
SP|Q9BUF5|TBB6_HUMAN  VCDIP---PRGLKMASTFIGNSTAIQELFKRISEQFSAMFRRKAFLHWFTGEGMDEMEFT 409
SP|Q3ZCM7|TBB8_HUMAN  VCDIP---PRGLKMSATFIGNNTAIQELFKRVSEQFTAMFRRKAFLHWYTGEGMDEMEFT 409
SP|P23258|TBG1_HUMAN  LSRKSPYLPSAHRVSGLMMANHTSISSLFERTCRQYDKLRKREAFLEQFRKEDMFKDNFD 419
SP|Q6B856|TBB2B_BOVIN VCDIP---PRGLKMSATFIGNSTAIQELFKRISEQFTAMFRRKAFLHWYTGEGMDEMEFT 409
                       :.      * .  ::  ::.* *:*..:*:* ..::  : :*:**:. :  *.*   :*

SP|Q9BVA1|TBB2B_HUMAN EAESNM---NDLVSEYQQYQDATADEQGEFEEEEGEDEA------               445
SP|Q13885|TBB2A_HUMAN EAESNM---NDLVSEYQQYQDATADEQGEFEEEEGEDEA------               445
SP|P04350|TBB4A_HUMAN EAESNM---NDLVSEYQQYQDATAE-EGEFEEEAEEEVA------               444
SP|P68371|TBB4B_HUMAN EAESNM---NDLVSEYQQYQDATAEEEGEFEEEAEEEVA------               445
SP|Q13509|TBB3_HUMAN  EAESNM---NDLVSEYQQYQDATAEEEGEMYEDDEEESEAQGPK-               450
SP|P07437|TBB5_HUMAN  EAESNM---NDLVSEYQQYQDATAEEEEDFGEEAEEEA-------               444
SP|Q9H4B7|TBB1_HUMAN  EAENNI---HDLVSEYQQFQDAKAVLEEDEEVTEEAEMEPEDKGH               451
SP|Q9BUF5|TBB6_HUMAN  EAESNM---NDLVSEYQQYQDATANDGEEAFEDEEEEIDG-----               446
SP|Q3ZCM7|TBB8_HUMAN  EAESNM---NDLVSEYQQYQDATAEEEEDEEYAEEEVA-------               444
SP|P23258|TBG1_HUMAN  EMDTSREIVQQLIDEYHAATRPDYISWGTQEQ-------------               451
SP|Q6B856|TBB2B_BOVIN EAESNM---NDLVSEYQQYQDATADEQGEFEEEEGEDEA------               445
                      * :..    ::*:.**:
```

Supplementary Figure 3. Alignment of β-tubulin isotypes against 1Z5V and 4I4T.

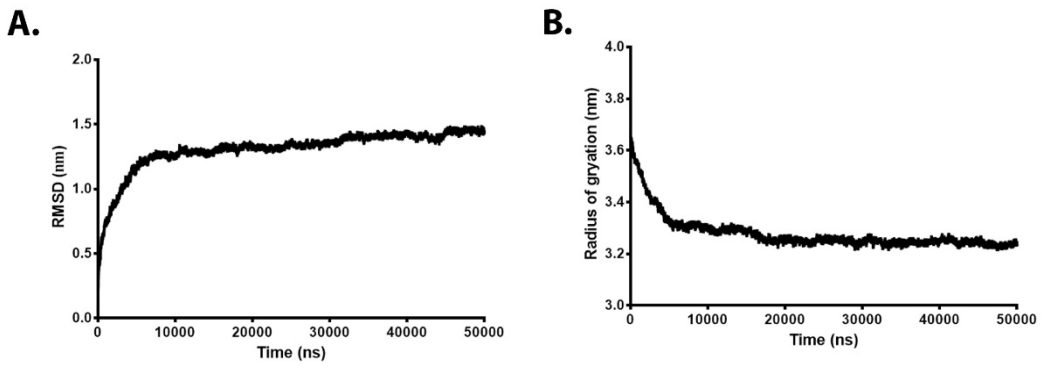

Supplementary Figure 4. Initial equilibration of TBCD-Arl2 complex.

(A) RMSD over time for radius of gryration biasing using adiabatic biased molecular dynamics (ABMD) examining a portion of TBCD (residues 1-837) and the complete Arl2. (B) Radius of gyration over time in nanometres for the portion of TBCD (residues 1-837) and the complete Arl2.

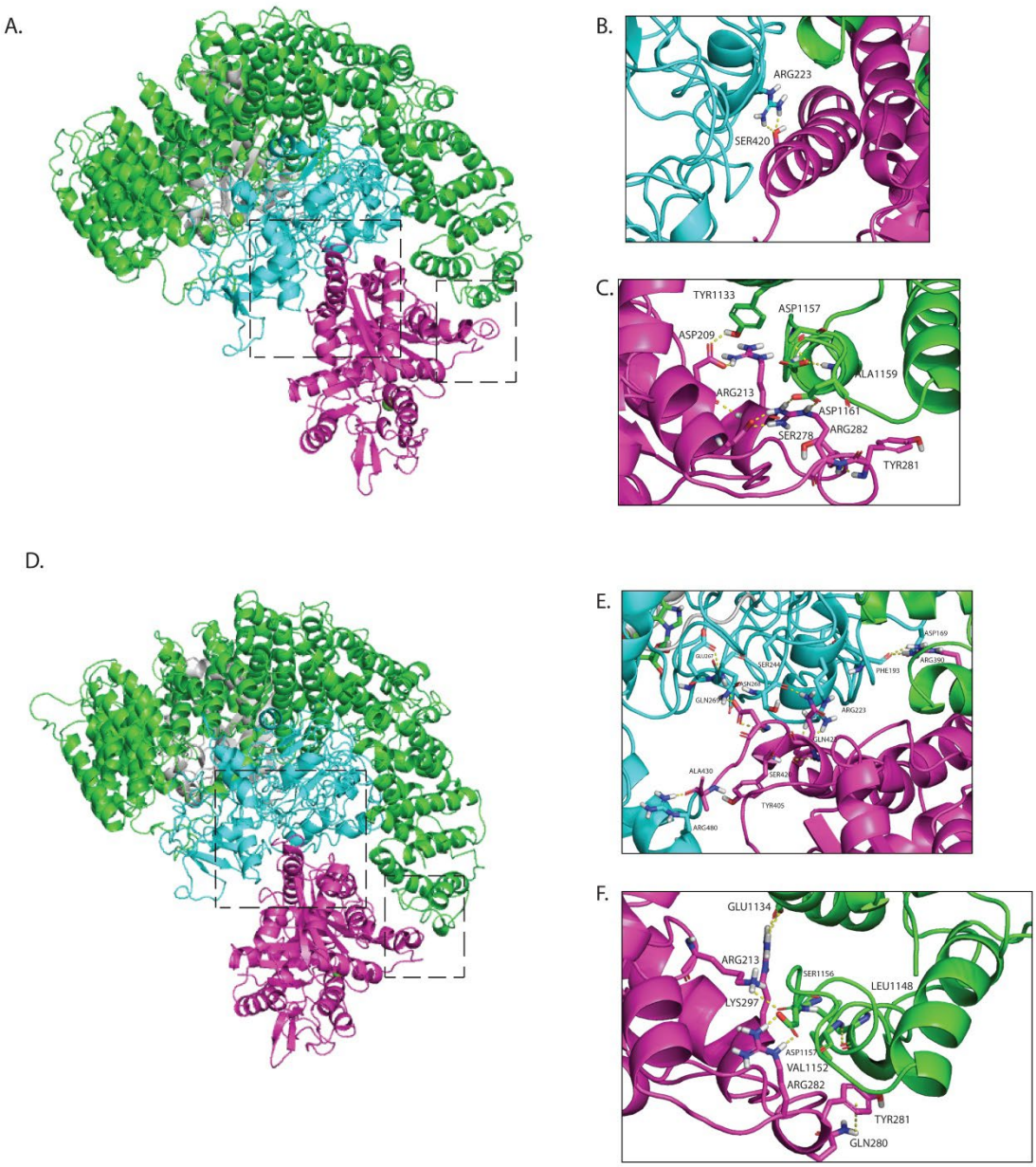

Supplementary Figure 5. Model of TBC-DEG interactions with β-tubulin isoforms TUBB1 and TUBB2A

Representative images of TBC-DEG complex docked with the β-tubulin isoforms TUBB1 and TUBB2A. (A-C) Representative images of close up views for each TBC-DEG complex highlighting energetic contribution of selected residues between TUBB1 and TBCE (B), and TBCD (C). (D-F) Similar to above, highlighting energetic contribution of selected residues between TUBB2A and TBCE (E) and TBCD (F). Favourable intermolecular interactions are represented as dashed yellow lines. In all models, the proteins are coloured as follows TBCD- green; TBCE- cyan; ARL2- grey; β-tubulin- magenta; magnesium- green sphere.

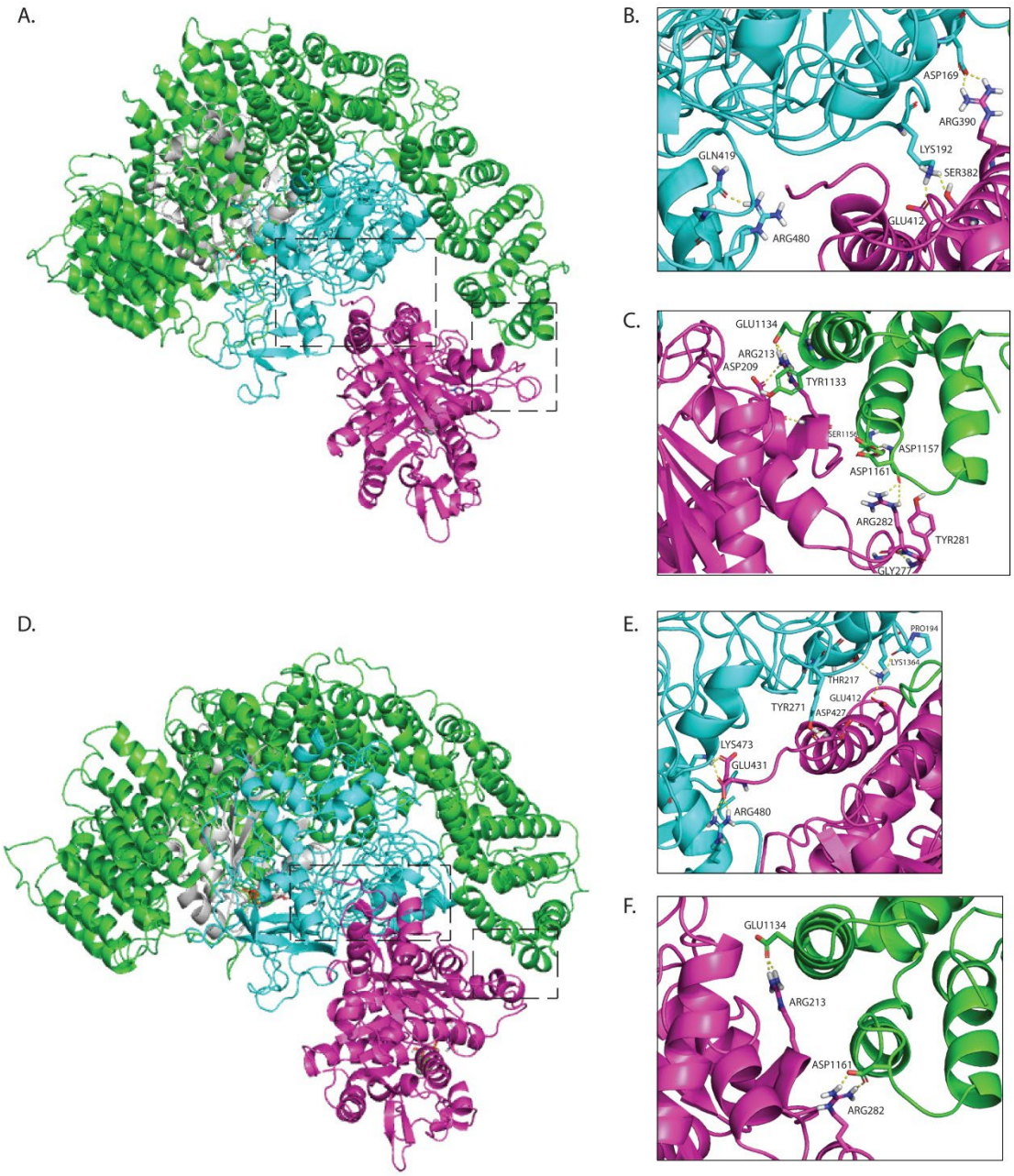

Supplementary Figure 6. Model of TBC-DEG interactions with β-tubulin isoforms TUBB4A and TUBB4B

Representative images of TBC-DEG complex docked with the β-tubulin isoforms TUBB4A and TUBB4B. (A-C) Representative images of close up views for each TBC-DEG complex highlighting energetic contribution of selected residues between TUBB4A and TBCE (B), and TBCD (C). (D-F) Similar to above, highlighting energetic contribution of selected residues between TUBB4B and TBCE (E) and TBCD (F). Favourable intermolecular interactions are represented as dashed yellow lines. In all models, the proteins are coloured as follows TBCD- green; TBCE- cyan; ARL2- grey; β-tubulin- magenta; magnesium-green sphere.

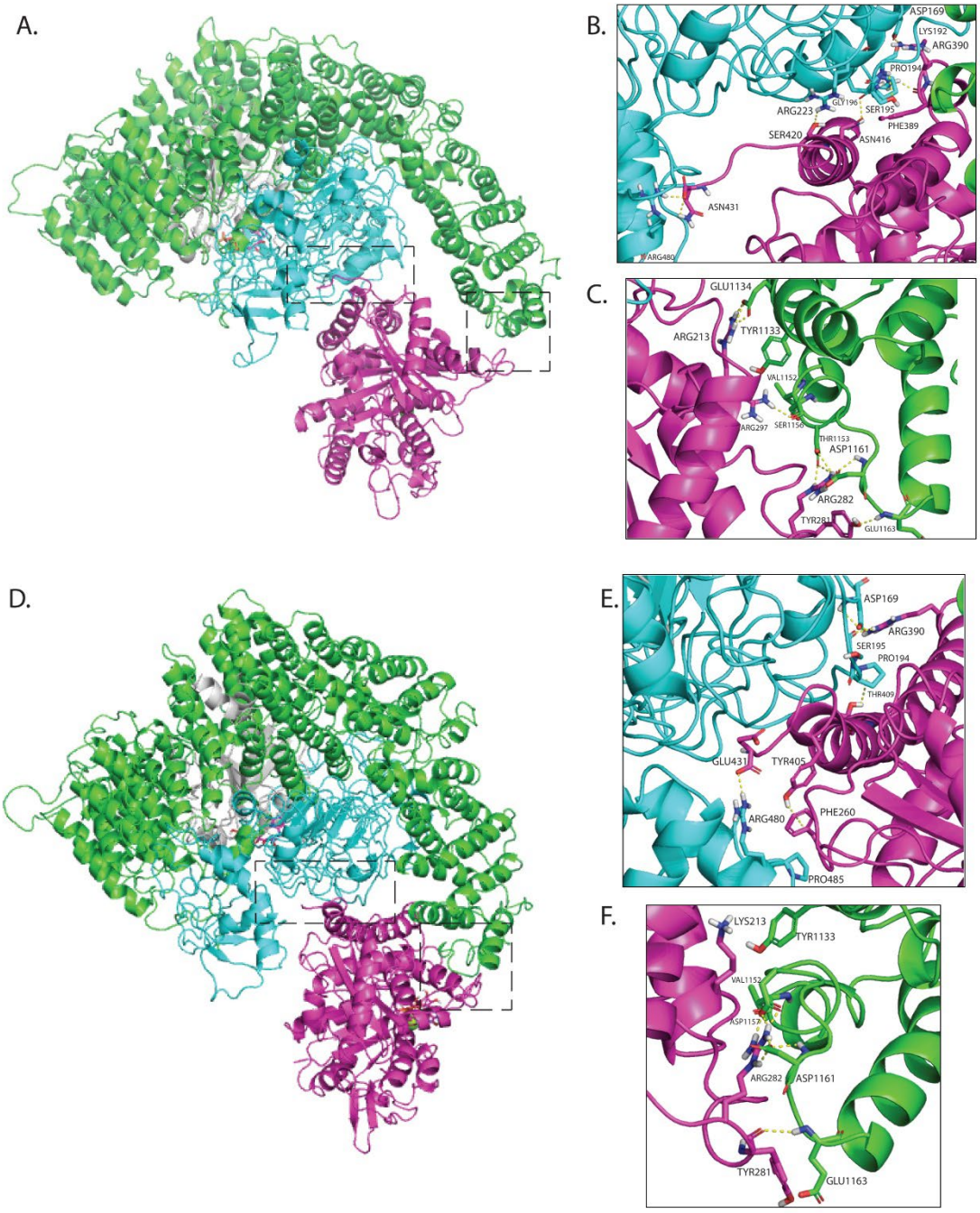

Supplementary Figure 7. Model of TBC-DEG interactions with β-tubulin isoforms TUBB6 and TUBB8

Representative images of TBC-DEG complex docked with the β-tubulin isoforms TUBB6 and TUBB8. (A-C) Representative images of close up views for each TBC-DEG complex highlighting energetic contribution of selected residues between TUBB6 and TBCE (B), and TBCD (C). (D-F) Similar to above, highlighting energetic contribution of selected residues between TUBB8 and TBCE (E) and TBCD (F). Favourable intermolecular interactions are represented as dashed yellow lines. In all models, the proteins are coloured as follows TBCD- green; TBCE- cyan; ARL2- grey; β-tubulin- magenta; magnesium- green sphere.

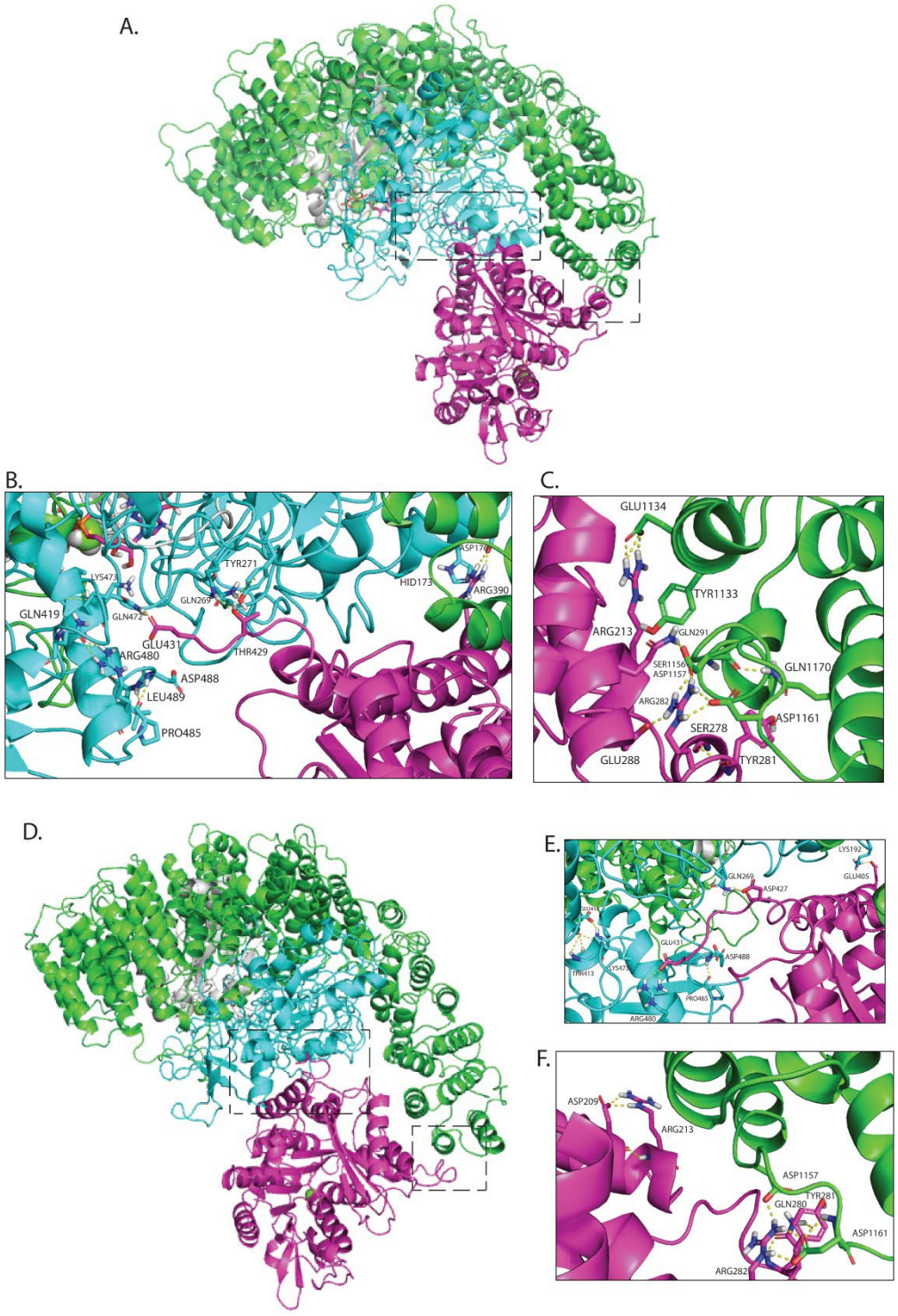

Supplementary Figure 8. Model of TBC-DEG interactions with β-tubulin isoforms TUBB and TUBB3

Representative images of TBC-DEG complex docked with the β-tubulin isoforms TUBB and TUBB3. (A-C) Representative images of close up views for each TBC-DEG complex highlighting energetic contribution of selected residues between TUBB and TBCE (B), and TBCD (C). (D-E) Similar to above highlighting energetic contribution of selected residues between TUBB3 and TBCE (B), and TBCD (C). Favourable intermolecular interactions are represented as dashed yellow lines. In all models, the proteins are coloured as follows TBCD- green; TBCE- cyan; ARL2- grey; β-tubulin- magenta; magnesium- green sphere.

Appendix

Content is removed due to copyright restrictions

Rowlands, J., Cruzat, V., Carlessi, R., & Newsholme, P. (2018). Insulin and IGF-1 receptor autocrine loops are not required for Exendin-4 induced changes to pancreatic β-cell bioenergetic parameters and metabolism in BRIN-BD11 cells. Peptides, 100, 140-149. DOI: 10.1016/j.peptides.2017.11.015

Content is removed due to copyright restrictions

Rowlands, J., Walz, N., Rowles, J. E., Keane, K. N., Carlessi, R., & Newsholme, P. (2019). Method Protocols for Metabolic and Functional Analysis of the BRIN-BD11 β-Cell Line: A Preclinical Model for Type 2 Diabetes. In P. C. Guest (Ed.), Pre-Clinical Models: Techniques and Protocols (pp. 329-340). New York, NY: Springer New York.